GFRP REINFORCED CONCRETE: ENVIRONMENTAL AND MOVEMENT CHARACTERISTICS

by

Sultan Al-Salem

(B.Sc. M.Sc.)

Thesis submitted in accordance with the requirement

For the degree of Doctor of Philosophy

The University of Leeds

School of Civil Engineering

April 2004

The candidate confirms that the work submitted is his own and that appropriate credit has been given where reference has been made to the works of others

ABSTRACT

For the last few decades, research has been conducted in order to come over the problem of corrosion in steel reinforced concrete. Consequently, methods such as cathodic protection, epoxy coatings, concrete additives, etc., have been tried. Unfortunately, non of these methods has totally solved the corrosion problem. The outstanding characteristics of fibre reinforced plastic (FRP) suggest that these materials may be the solution to the problem of steel corrosion. It is believed that the widespread application of glass fibre reinforced plastic (GFRP) reinforcement faces some challenges such as lack of design codes, brittle behaviour of FRP resulting in reduced structural ductility, low bond capacity to concrete, and lack of knowledge of durability issues and long-term behaviour of concrete reinforced with composite reinforcement.

In this investigation, some properties of GFRP rebars were investigated, namely flexural and compressive characteristics, bond strength with concrete with different concrete strengths, and micro-structural features such as porosity and pore size distribution using mercury intrusion porosimetry (MIP), together with observations of the micro-structure of the material under the scanning electron microscopy (SEM). Moreover, monitoring of changes in both the flexural characteristics and the micro-structure of the material under high alkalinity and salinity solutions at high and moderate temperatures for different periods of aging up to 270 days were carried out. The results suggested that bond strength increased with high concrete strength, and alkalinity at high temperature (i.e. 60°C) was the most damaging medium.

Furthermore, the influence of GFRP and steel rebars with different reinforcement ratios on elastic modulus and creep in compression, and drying shrinkage of concrete with and without SRA were considered and compared to concrete specimens with no reinforcement. Finally, a comparison between theoretical values and experimental measurements of elastic modulus, creep and drying shrinkage was made. The use of GFRP reduced the movement restraint due to low stiffness. Therefore, movements are greater for GFRP reinforced concrete than for steel reinforced concrete. Also SRA reduced compressive strength, creep, drying shrinkage and elastic modulus. Hence, concrete cracking is either avoided or delayed and reduced.

ACKNOWLEDGMENT

The author would like to express his sincere gratitude to his supervisors, Dr. J. J. Brooks, Dr. J. Forth and for their great patience in guiding him and for their useful advice during the various stages of the research.

The author also likes to express his appreciation to the Civil Engineering Department, Leeds University, for the facilities and the practical assistance that the department had made available to him. Thanks are especially due to the technical staff in the department for their cooperation during the period of experimental works. Sincere gratitude and thanks to Fibre Force for supplying the GFRP rebars.

Special acknowledgment is due to the Higher Education Ministry in the Kingdom of Saudi Arabia for their financial support. I wish also to express my sincere gratitude and thanks to the Saudi Arabian Cultural Attach to London Mr. Abdullah Al-Nassir for his unforgettable hospitality and great advice.

I would like to extend my gratitude to my wonderful parents and my wife for their enormous patience and support that made this work finally done.

I Wish to Present This Work With All My Love

To

My Parents

Also To

My Wife Areej And Daughter Sara

To Whom I Will Be Indebted For

The Rest Of My Life

TABLE OF CONTENTS

LIST OF TABLES

LIST OF FIGURES

LIST OF PLATES

ABBREVIATIONS

γ	surface tension of mercury (Hg) in N/m
θ	contact angle of Hg with the pore wall
ε_{cr}	drying shrinkage for reinforced concrete specimens
ε_{cs}	drying shrinkage for non-reinforced concrete specimens
a	distance between the applied load on one block and the support in joint-beams
A_b	cross-sectional area of bar in mm^2
A_c	area of concrete in mm^2
ACI	American concrete institute
A_o	total area of the composite (reinforced concrete) specimen in mm^2
APD	average pore diameter
A_r	area of reinforcement in mm^2
ASTM	American standard for testing of materials
b	width of specimen in mm
BS	British standard
C	resultant compressive force in the concrete in N, or distance from centroid to extremities (the outer fibres) in mm
c	cement content in kg/m^3
C'	days of accelerated exposure at certain temperature
CH	calcium hydroxide
C_s	specific creep for reinforced concrete specimens
C_{sc}	specific creep for non-reinforced concrete specimens
C-S-H	calcium-silicate-hydrate
d_b	bar diameter in mm
E	Modulus of elasticity in GPa
E_f	guaranteed modulus of elasticity of FRP defined as the mean modulus of a sample of test specimens minus three times the standard deviation in MPa
E_s	modulus of elasticity of steel in MPa
E_{ea}	effective (reduced)modulus of elasticity in GPa
EM	effective modulus method
E_o, E_c and E_r	elastic moduli for reinforced concrete , non-reinforced concrete and

reinforcement, respectively

f_{fu} design tensile strength of FRP, considering reductions for service environment in MPa.

fb modulus of rupture or flexural strength in N/mm^2

f_f tensile stress in the reinforcement in MPa

FRP fibre reinforced plastic

GFRP glass fibres reinforced plastic

h height of specimen in mm

h_e 2×area/perimeter(m), maximum 0.6m

j age at loading in days

j_m hardening time in days

k_c coefficient depends on the composition of the concrete

k_e coefficient depends on the effective thickness of the member

k_j coefficient defines the development of shrinkage as a function of time

k_L coefficient depends on the environment

l embedment length in mm

L support span or length of specimen in mm

L_{dh} development length in mm

L' tail length in mm

LVDT linear variable displacement transducer

M moment resulting from the applied load in N mm

m modular ratio between the reinforcement and the concrete (E_R/E_c)

MIP mercury intrusion porosimetery

MPD median pore diameter by pore volume

OPC ordinary Portland cement

P applied load in kN

p pressure required to intrude a pore hole in MPa

pH a measure of acidity and alkalinity based on the fact that the concentration of hydrogen ions (acidity) times hydroxyl ions (alkalinity) is 10^{-14} moles/l in aqueous solution

r bend radius in mm, or relative humidity as a decimal

SEM scanning electron microscopy

SF pore shape factor, for cylindrical pore SF = 4

S_o , S_c and S_r shrinkage for reinforced concrete , non-reinforced concrete and reinforcement, respectively

SRA shrinkage-reduction-admixture

T resultant tensile force in the reinforcement in N

t duration of loading in days

T' conditioning temperature in °F or °C

TB Trost-Bazant method

T_g glass transition temperature

TIV total intrusion volume

TPA total pore (surface) area

w water content in liters/m^3

w/c water/cement ratio

Y maximum deflection at load increment in mm

z lever arm between the resultant forces T and C

χ aging coefficient

ε strain in mm/mm

ϕ *creep coefficient* or *characteristic creep*

μ average bond strength in MPa

μ_o , μ_c and μ_r Poisson's ratio for reinforced concrete, non-reinforced concrete and reinforcement, respectively

ρ ratio of reinforcement area to total section area

ρ_n net ration of reinforcement area to concrete area

σ_c compressive strength in MPa

σ_c stress of concrete in MPa

σ_{ct} tensile stress in MPa

σ_o total stress of the composite (reinforced concrete) specimen in MPa

σ_r stress of reinforcement in MPa

Chapter One: Introduction

1.1 General view of concrete

Nowadays, concrete is considered the most worldwide used construction material, which commonly consists of Portland cement alongside with sand, gravel and water. In addition, additives and admixtures are added some times to meet the required performance of the concrete. In many countries the ratio of concrete consumption to that of steel exceeds ten to one. Recently it is believed that the consumption of concrete in the world is in excess of 5 billion tons every year. It is enough to know that water is the only other material that is consumed in such huge quantities (Winter and Nilson, 1979; and Mehta, and Monteiro, 1993).

Unlike other construction materials, for instance wood and ordinary steel, the ability of concrete to tolerate the action of water without serious deterioration makes it a good material for building structures where a great deal of water is involved, such as buildings to control, store, and transport water. Moreover, the durability of concrete to some aggressive waters (e.g., seawater, domestic and industrial wastewater, etc.) is responsible for the fact that its use has been extended to be in direct contact with a variety of industrial and domestic environments. Another advantage of concrete is that the structural concrete elements can be formed into different shapes and sizes quite easily. Last but not least, when cost and availability of material are considered, it is found that the cheapest and most readily produced material in this business is concrete. That is because, the ingredients for producing concrete (i.e., cement, water, fine aggregate, coarse aggregate either crushed stone or gravel, air, and often other admixtures) are relatively cheap, compared with other building materials, and access to this material is common across the world. In addition, large amounts of many industrial wastes can be recycled as a substitute for the cementations material or aggregates in concrete, Mehta, and Monteiro, (1993).

Although plain concrete has high compressive strength, its tensile and flexural strengths are only of the order of 10 and 15 percent, respectively, of the compressive strength.

Materials that fail in tension at relatively low values of strain, such as concrete, are classified as brittle materials. Consequently, tensile and shear reinforcement in the tensile regions of sections, and sometimes compression regions as well, must be provided to compensate for the weak regions in the reinforced concrete element. This can be achieved by application of embedment of steel rebars in concrete (Winter and Nilson, 1979; and Neville, 1998).

1.2 State of the problem

Corrosion of steel represents a major concern in concrete construction. Embedded steel is generally very durable, as it is protected from corrosion by the alkaline environment that concrete provides. The high alkalinity of concrete is actually due to the presence of the microscopic pores with high concentrations of soluble calcium, sodium, and potassium oxides. These oxides form hydroxides when water is added, maintaining a high level of alkalinity (i.e., pH value is between 12 and 13).

Nevertheless, highly aggressive environments, such as structures in direct contact with seawater, chemical plants, water and wastewater treatment stations, bridges when de-icing salts are used, or even structures exposed to air-borne, which is very fine droplets of seawater raised from the sea by turbulence and carried by wind, may cause early deterioration when the protection given by the concrete is insufficient. The steel therefore does corrode, which is a problem for civil engineers (Neville, 1998; Ehsani, 1993).

Rehabilitation costs for the parking structures in Canada have been estimated to be in the order of 4-6 billion dollars in Canadian funds and for the highway structures in the US to be around 50 billion dollars.

According to the Highways Agency in UK more than 75 % of the motorways and trunk road bridges in England and Wales are subject to salt induced-corrosion damage which cost over 600 million pounds sterling (Wallbank, 1989).

In the Middle East, the harsh environment (i.e., warm marine climate with saline ground water) accelerates all corrosion problems (Rasheeduzzafar *et al.*, 1992). Broomfield

(1997) indicated that corrosion of steel in the infrastructure is without doubt the largest problem facing industrialized countries.

In some countries like the Kingdom of Saudi Arabia, reinforced concrete is the first and most common construction materials. Furthermore, many construction works are located in both eastern and western coasts, for instance, petroleum, and saline water conversion works, 70% of potable water nationwide is provided by seawater desalination.

In addition, the climate of the coasts makes it one of the world's most severe environments for reinforced concrete.

The concrete mix ingredients may contain chloride, and the environment around structures is more likely to be contaminated with salts, both under and above ground level. High temperature also promotes rapid rate of corrosion. Consequently, reinforced concrete structures crack and spall due to reinforcement corrosion showing early signs of deterioration.

As a result, researchers have been studying different approaches to overcome this problem. There are three common ways of preventing or retarding the corrosion of reinforcing steel in concrete: by using inhibitors in the mix (e.g., use of calcium nitrite), coating on the rebar (e.g., fusion bonded epoxy coated rebar, polyvinyl, and butyl coated rebar), or treating the external surface of concrete (e.g., polysilicate, and epoxy based paints).

In fact, all these measures prevent or control corrosion but on limited scale and usually their performance decreases with time (Broomfield, 1997; Neville, 1998; and Mehta, and Monteiro, 1993).

As an alternative and radical approach to overcome this problem (i.e., corrosion of steel in concrete), Fibre Reinforced Plastic rebars (FRP) have been considered to reinforce concrete instead.

The main criteria for engineers to use any material to satisfy the requirements of a project are durability, corrosion resistance, cost, weight, material properties, and ease of construction.

There are many reasons to consider using FRP composites in civil engineering applications. In addition to its corrosion resistance, it offers electro magnetic neutrality, high strength to weight ratio, and ease of handling.

In the light of the above, the obvious uses for FRP bars are in areas where seawater, corrosion agents and de-icing salts are in use. Justification of using FRP bars instead of steel would be in structures such as, retaining walls, foundations, wastewater treatment plants, seawater desalination plants, piles, paper mills, mining process tanks, sea front structures and nuclear power plants. Other potential uses are in applications affected by electrical currents, such as some medical activities and military installations that must be hidden from radar.

1.3 Introduction to FRP composites

A structural composite is a material system consisting of two or more phases that are designed to have superior properties and mechanical performance to those constituent materials behaving independently. One of the phases should be stiffer and stronger and therefore is considered as reinforcement (in this case fibre), whereas the weaker phase is called resin matrix. Sometimes, due to chemical interactions or other processing effects, an additional phase results, which is fibre/matrix interface, and located between the first two phases.

The first fibre reinforced composites emerged in the 1930s (Jones, 1998). The idea of using glass in reinforcing or prestressing concrete structures was first actually introduced to structures in the 1950s (Rubinsky and Rubinsky, 1954). In the 1970s, some other fields such as aerospace, shipbuilding etc. had the greatest contributions on the improvement of the new material. As a result, commercial application started in the late 1970s. In Europe a programme called EUROCRETE which is a European collaborative research project, has seen the development of fibre composite reinforcing bars made from glass or carbon or containing aramid fibres. The project partly funded

under the EUREKA scheme with partners from the UK, France, Netherlands, and Norway.

Nowadays FRP takes a variety of forms, cables, bars with circular, square, or even rectangular cross sections, sheets, tubes, stirrups, plates, I-beams, angles, channels. Moreover, some Japanese companies produce spiral reinforcement and two or three dimentional grids. In general the maximum diameter produced is 32 mm bars, (Clarke, 1999; Ehsani, 1993).

The FRP composites are produced by different processes such as hand lay-up, pultrusion, injection moulding, etc. However, pultrusion is the common way of manufacturing the bars, due to its fast speed of operation, good quality control, and cost-effective process. In addition, pultruded composites exhibit all of the features found in products produced by other processes, such as high strength-to-weight ratio, corrosion resistance and dimensional stability. A less obvious process advantage is the ability to use the widest variety of reinforcement types, forms and styles with a broad selection resins and fillers. Reinforcement can be placed precisely where it is needed for mechanical strength and consistency.

This automated process is for producing continuous and constant cross-section composite profiles. It was developed in the early 1950s, and gained a market and technical position of prominence in the 1980s and is now recognised as one of the most versatile of the composite production methods. Pultrusion refers to both the final product and the process.

In the pultrusion process, the continuous fibres are wetted with uncured resin and pulled through a heated die, with a secondary process to produce an appropriate surface deformation pattern to the bar, and hence provide good bond when used as reinforcement in concrete (ASTM D 3918; Faza and GangaRao, 1993; and Sumerak and Martin, 2001) as the detailed schematic diagram is shown in Fig. 1.1. The term pultrusion was used to differentiate the process from extrusion where plastics or metals are pushed through a die opining. In pultrusion, the average line speed is about one to five linear feet per minute.

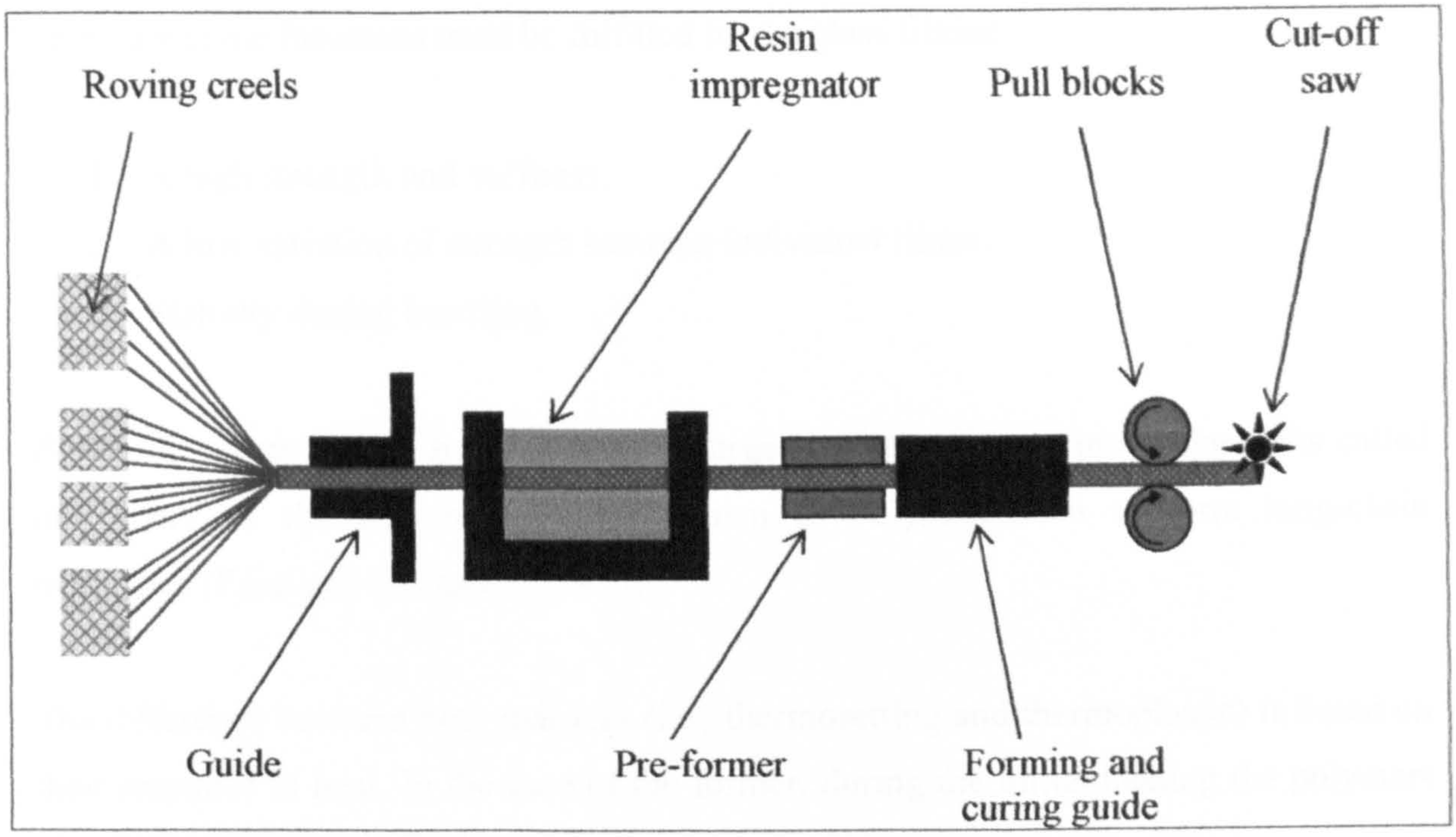

Figure 1.1: Continuous pultrusion process

While for traditional construction materials (e.g. concrete and steel) standard tests have been established to determine their properties, unfortunately the same cannot be said for composite materials.

According to the state-of-the-art report on fibre reinforced plastics (FRP) reinforcement for concrete structures (ACI committee 440R-96) composite materials (i.e., in this study it means FRP composites) are defined as "a polymer matrix, either thermosetting (e.g. polyester, vinyl ester, epoxy, phenolic) or thermoplastic (e.g. nylon, PET) that is reinforced by fibres (e.g. glass, aramid, carbon)".

Glass fibres: are manufactured by continuous drawing of molten glass at high speed through small holes in electrically heated bushings; these bushings form the individual filaments. The filaments cool from the liquid state, at a temperature of about 1200 degree centigrade to room temperature in a very short time. The filaments are gathered into groups or bundles called strands, and bonded to one another by a lubricant. This process is known as sizing, and it aims to protect the filaments from rubbing each other, to reduce the damage of fibres during mechanical handling, and to facilitate the molding process (Faza and GangaRao, 1993).

There are some functions must be fulfilled by the glass fibres:

1 A high strength and stiffness.
2 A low variation of strength between individual fibres.
3 Stability during handling.

Polymers: are produced by combining a large number of small molecular units called monomers by the chemical process known as polymerisation to form long-chain molecules (Faza and GangaRao, 1993).

The difference between both matrices (i.e., thermosetting and thermoplastic) is based on their response to heat. In the case of the former, during the initial heating the polymers are cured; thereafter, sharp bends similar to the standard 90^{o} and 180^{o} hooks cannot be performed. However, FRP bars can be manufactured in any shape in the plant while the resin has not cured. In other words, the thermoset polymers melt only the first time they are heated; from then on, if they are reheated, they degrade because they are highly cross-linked and reheating them would lead to decomposition of the resin, thus a loss of strength in the FRP. In contrary, the thermoplastic resins such as polyethylene, polypropylene and polyvinyl chloride melt on heating and solidify on cooling, the cycle of cooling and heating can be applied several times without harming the properties. Thus, warming and reshaping in the field is possible, but unfortunately thermoplastics have significantly weaker mechanical properties than thermosetting resins (for example, stiffness values of thermoplastics are very low, in the range of 0.15 to 3.5 GPa, in comparison with 1.3 to 8 GPa for thermosettings at room temperature) (Ehsani, 1993 and Kumar and Gupta, 1998).

Yet it should not be forgotten that, as the bar is bent weaker reinforcement is likely to result because of the misalignment of the fibres. In addition, thermoplastic is more expensive than thermosetting (Clarke, 1998).

According to ACI 440.1R-01 (2001) the definitions of both thermoplastics and thermosets are as follows:

Thermoplastic: a resin that is not cross-linked; it generally can be remelted and recycled.

Thermoset: a resin that is formed by cross-linking polymer chains. Note: a thermoset cannot be melted and recycled, because the polymer chains form a three-dimensional network.

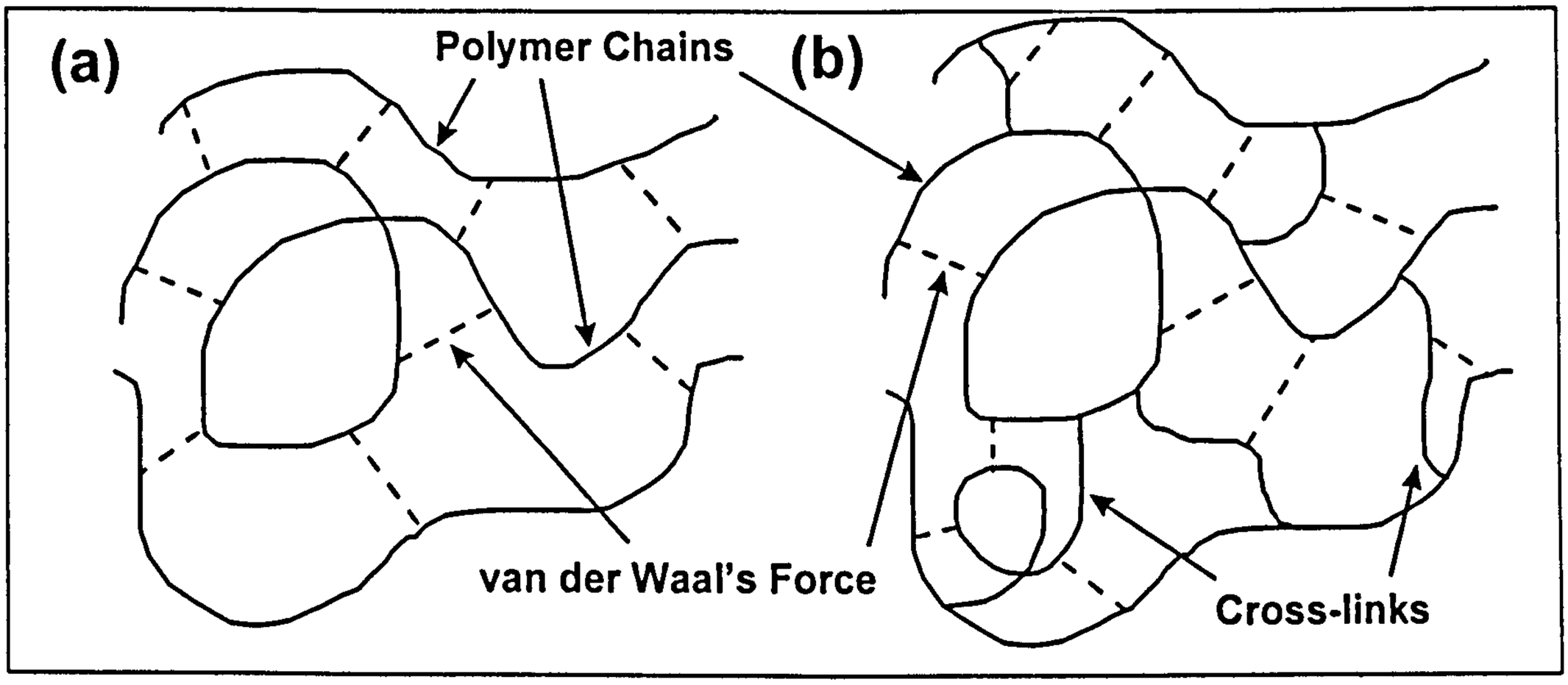

Figure 1.2: Difference between (a) Termoplastics and (b) Thermosets

Cross-link is defined according to ACI 440.1R-01 (2001) as a chemical bond between polymer molecules. Note: an increased number of cross-links per polymer molecule increases strength and modulus at the expense of ductility.

There is, of course, another classification way of polymers based on molecular structure (Kumar and Gupta, 1998), which is rarely mentioned in the literature of FRP construction application.

There are some functions must be fulfilled by the matrix:

1 To bind the fibres together and to provide protection to their surface from damage during the surface life of the composite.
2 To distribute the fibres and to separate them.
3 To be thermally and chemically compatible with the fibres.

4 To transfer stresses from concrete to the fibres efficiently by adhesion and/or friction.

Clarke (1998) stated that both the resin and the fibre determine the durability, while the mechanical properties of FRPs are function of the amount and type of fibre. That is mentioned in (ACI 440R-96) as well. Moreover, the roles that polymer matrix plays are first of all, it is responsible for transferring stresses between the reinforcing fibres and the surrounding structure because it binds and orients the former. Secondly, it provides protection for the fibres from mechanical, including handling, and environmental damage. Thirdly, it acts against fibre buckling under compression loading. Fourthly, it is, once again, considered as a binder that gives the material a structural shape. Last but not least, its properties strongly influence interlaminar shear, and in-plain shear (ACI 440R-96). However, the matrix is probably considered a weak link in the composite, since it could suffer from physical damage and chemical attack during its service.

The initial cost of FRP is higher than ordinary reinforcement. One can argue, however, that the high initial cost of using unconventional reinforcement might be compromised by cheaper long-term costs, namely longer service life and less maintenance, especially if structures are designed to make optimum use of the composites rather than using the existing design with steel (Burgoyne, 1997).

When talking about glass fibre reinforced plastics (GFRP), in particular, despite the fact that they cost between two and four times as much as uncoated steel bars, they are regarded the cheapest among other composite reinforcements.

In recent years, FRP composites have been used in some countries in small projects and some multi-million dollar projects for strengthening parking garages, multi-purpose convention centres, sea walls, chemical plants, concrete tanks, hospital MRI facilities, electrical sub-stations, and office buildings (Benmokrane *et al.*, 1995, Nanni, 2001; Burgoyne and Head, 1993).

The use of externally bonded FRP laminates or near surface mounted (NSM) bars to strengthen and upgrade shear and flexural behaviour of concrete members for

applications in bridges and buildings, and FRP bars as reinforcement embedded in concrete to replace conventional steel rebars primarily to provide a permanent solution to reinforcement corrosion problems. Examples of projects where FRP composites have been used are shown in Plates 1.1-1.3.

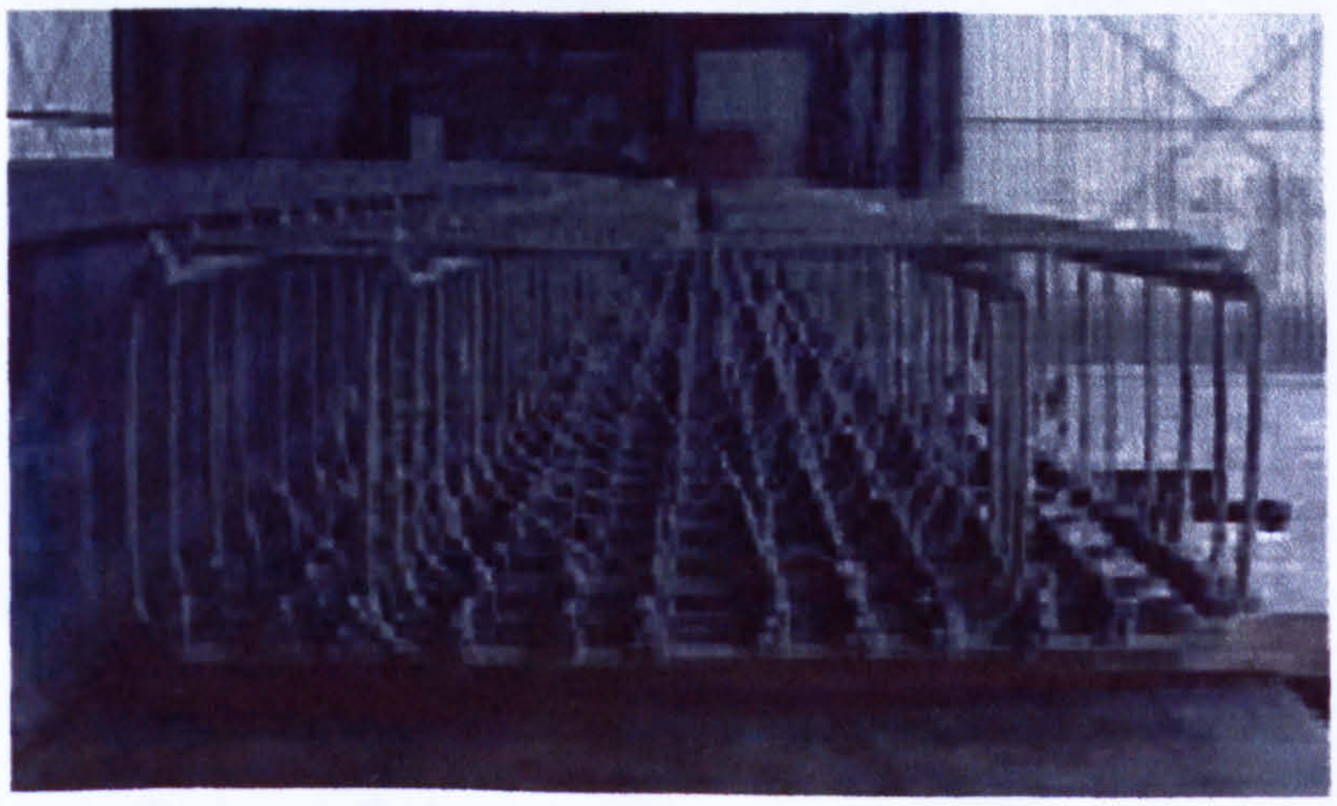

Plate 1.1: FRP cage of the Walters Street Bridge, St. James, Missouri, USA. Both GFRP and CFRP are used (After Nanni, 2001)

Plate 1.2 FRP laminates installed to improve the bridge's flexural strength, after corrosion of steel and deterioration of concrete, Missouri, USA (After Nanni, 2001)

Plate 1.3 The Aberfeldy golfers' motorised bridge. Example of a structure made entirely from composites, Aberfeldy, Scotland, UK (After Burgoyne and Head, 1993)

To sum up, among the fibres that are commercially used, the most suitable one for civil engineering constructions may be glass, with its diversity of types such as alkali resistance (AR-glass); general purpose (E-glass); high strength (S-glass) (ACI 440R-96). That is because of its mechanical and physical properties, as well as its relatively low cost with respect to dimensional stability, and corrosion resistance (Jones, 1998). Nevertheless, others including carbon and aramid are used, in special applications, for their higher strength or better modulus properties. Consequently, the focus of this study is on Glass Fibre Reinforced Plastic (GFRP) rebars.

1.4 Objectives

This research focuses on three aspects regarding GFRP composite. Firstly, some mechanical properties of the GFRP rebar and, secondly, durability in aggressive environments, to be precise brine and alkali, including studying the characteristics in terms of porosity and pore size distribution. Thirdly, shrinkage and creep characteristics of concrete reinforced with the GFRP rebars.The influence of concrete strength on bond capacity between concrete and GFRP rebars was required with concrete of relatively high compressive strength (i.e., 80MPa) as opposed to lower strengths as used by most other researchers. In addition, flexural and compression strengths and micro-structural

the nature of the micro-structure of the material under scanning electron microscopy (SEM).

The second objective involved examining the durability of 8 mm square GFRP rebars by monitoring changes of flexural properties, micro-structural characteristics, pore size distribution and porosity, when the material is subject to hostile solutions (brine and alkali) at different temperatures (i.e., 20°C and 60°C). The micro-structural aspects were to be investigated by mercury intrusion porosimetry (MIP) technique.

Details of the third objective consisted of considering the effects, both experimentally and theoretically, of GFRP reinforcing bars on drying shrinkage of reinforced concrete. Moreover, creep under compression of concrete reinforced with rebars was to be determined. In addition, tests using similar specimens with a shrinkage reducing admixture (SRA) were to be included. Finally, the comparison between shrinkage and creep behaviour of concrete reinforced with GFRP and steel rebars of similar cross-sections was required.

1.5 Hazard identification

It is extremely important to mention the possible hazards when dealing with GFRP bars. Splinters of glass fibres can be generated when the bar is broken, dust also will be generated when the bar is machined. In addition, in case of fire, carbon dioxide, carbon monoxide and smoke will be generated by the destruction of the resin matrix. Last but not least, splinters from a broken bar should be attended to immediately while the splinter is visible as GFRP does not show on an X-ray.

1.6 Thesis presentation

This thesis consists of eight chapters which are summarised below.

Following the general introduction in the present chapter, chapter two gives a brief background of some chief characteristics of GFRP composites. This is followed by a survey of previous research related to this investigation.

In chapter three, information of the instrumentations and materials used in this study is presented including details of their sources and properties. Description of method used for the concrete mix design, and concrete specimen preparation, specimen curing conditions and mechanical properties of hardened concrete are offered.

In chapter four, durability monitoring is presented through examining the changes in flexural strength, the manner in which pores are distributed with respect to pore size and structure. In addition, introductory examinations were made including bond between the reinforcements and concrete as well as flexural and compressive characteristics and micro-structural aspects of the GFRP rebars. Finally, details of test specimens, instruments and testing programmes are mentioned.

In chapter five, experimental and theoretical observations of time-dependent deformations of plain (non-reinforced) and reinforced concrete with steel and GFRP rebars are presented. In addition, details of test specimens, instruments and testing programmes are mentioned.

Chapter six consists of the presentation and discussion of results obtained from tests mentioned in chapter four, while chapter seven presents and discusses the results obtained from tests mentioned in chapter five.

In chapter eight, the results of this investigation and the conclusions reached are summarised, in addition to suggestions for further research.

Tables, figures, and plates for illustration relating to each chapter are included. S.I. units are used throughout the presentation.

Chapter Two Review of Literature

2.1 Introduction

This chapter briefly provides some information on the mechanical and physical properties of FRP rebars. A comparison between these composite materials and ordinary steel reinforcement is also given. Some mechanical properties, serviceability, durability, creep, and shrinkage are covered in the review of literature.

2.2 Physical and mechanical properties of FRPs

Unlike steel, the mechanical properties of FRPs vary from one another depending upon the manufacturer. The characteristics of the products are greatly influenced by factors such as volume and type of fibre and resin, etc. Moreover, the mechanical properties of the bars are affected by some factors such as temperature and moisture.

In fact, these mechanical and physical properties are mentioned in the (ACI 440R-96), some of them will be considered below.

2.2.1 Specific gravity

FRP bars have a specific gravity between 1.5 and 2.0; while in steel is around 7.9, indicating that FRP bars are almost four times lighter than steel bars. That shows how easy it is to deal with this material in the site.

2.2.2 Thermal expansion

It is of a great importance for concrete and the reinforcement material to share similar behaviour under thermal stresses so that the differential deformations of both of them are minimised. The coefficient of thermal expansion of GFRP bar is in the order of 9.9 $\times 10^{-6}$/C and that of concrete is between 6 and 11 $\times 10^{-6}$/C. From those figures it appears that there should not be a problem regarding the thermal expansion of both materials.

2.2.3 Tensile strength

FRP rebars reach their ultimate tensile strength before any yielding takes place. Tensile strength of GFRP rebars is in the range of 517 to 1207MPa, which is relatively high in comparison to that of steel (i.e., steel tensile strength is 483-690MPa).

It should be noted though, as the diameter of FRP bars increase, their strength and efficiency decrease, due to shear lag and less stress for the fibres located away from the outer surface of the bar cross section.

2.2.4 Tensile Elastic Modulus

The typical elastic modulus of GFRP bars is 41-55 GPa, which is about 25% of that of steel. As a result, a smaller transformed moment of inertia for flexural members reinforced with GFRP bars will occur. Therefore, not only is deflection and cracking of members reinforced by FRP higher than those reinforced by steel (Brown and Bartholomew, 1993), but also may control the design of flexural members, except pre-stressed and post-tensioned bars (Ehsani, 1993). There are, however, three ways to counteract this problem namely by adding more reinforcement, making the member (beam or slab) deeper or thicker, and shortening the span's length.

2.2.5 Shear Strength

In general, shear strength of GFRP bars is very low (Ehsani, 1993; and Kalvar, 1995), and this has consequences when the reinforcement is used in structure or tested in tension.

2.2.6 Creep

A material shows creep when its deformation (strain) increases with time under a constant stress due to viscous flow, shortly after the elastic strain. When the stress is removed after a period of time, the elastic deformation is immediately recovered, but the deformation caused by the viscous flow recovers slowly to an asymptotic value, called the recovery strain, Fig. 2.1, illustrates creep behaviour.

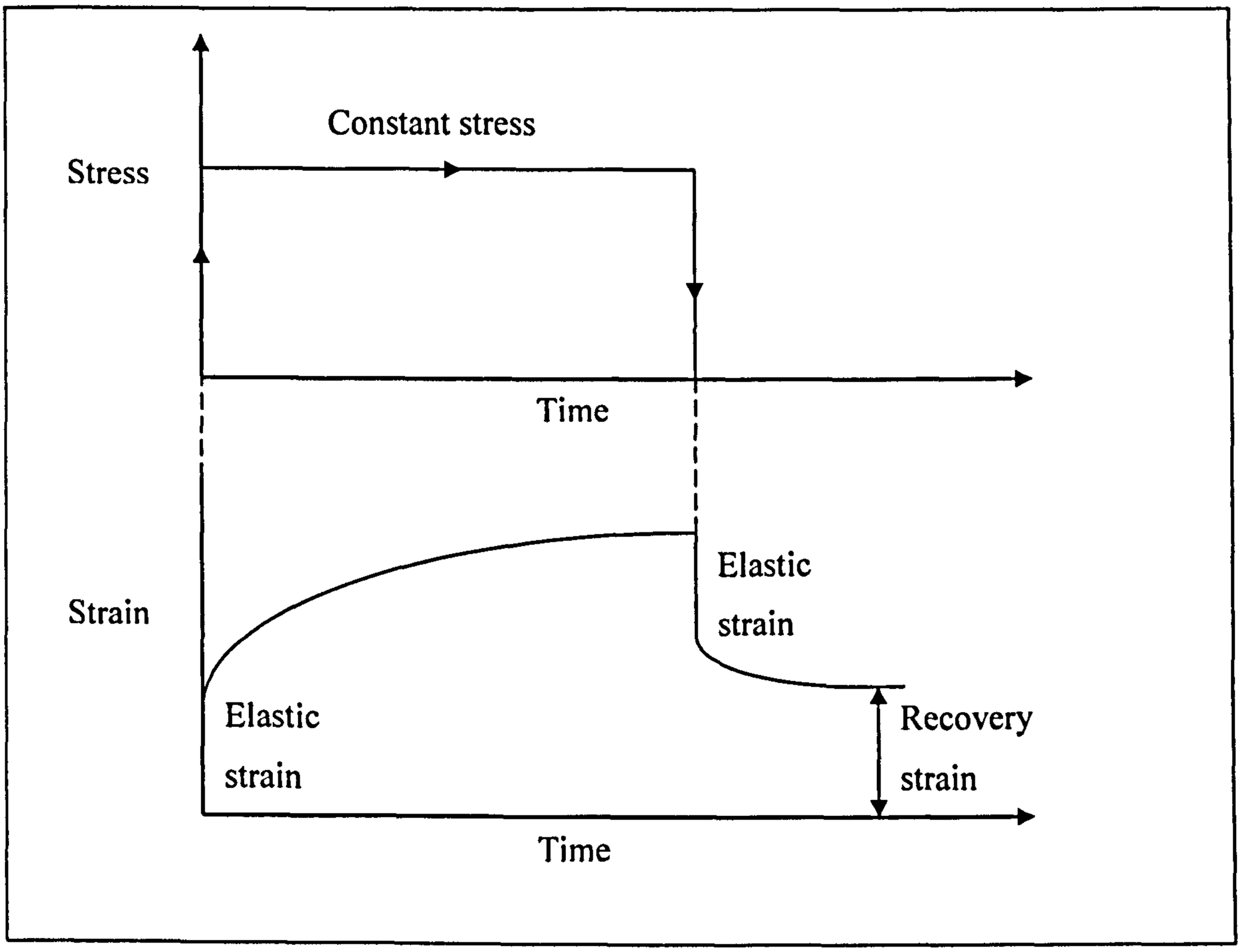

Figure 2.1: Schematic of the strain vs. time curve (with the corresponded stress), for a creep/recovery behaviour

Many materials exhibit creep, yet concrete is a particular material subject to creep at normal levels of stresses under normal conditions of temperature and humidity.

Creep, thus, depends largely on three variables: stress level, temperature, and time. Designers have always been concerned with long-term deflections in concrete structures. This problem is more of a concern in FRP reinforced concrete due to the lack of information on long-term behaviour of FRP bars. Therefore studies specifically related to long-term performance of FRP bars under sustained loads need to be conducted.

Creep is usually measured by the length changes involved and is expressed quantitatively by the corresponding strain, $\Delta l/l_o$ (Gere and Timoshenko, 1992; and Soroka, 1993). Δl: is the change in length between two reference points, and l_o: is the original length between the two reference points.

Ehsani (1993) reported that fibres such as glass and carbon, normally, do not exhibit much creep, while that is not true for most resins. In the light of the above, because of the different constituent materials (fibre and resin) significantly different creep behaviour can be observed for different FRP materials.

2.2.7 Bond Strength

Bond between concrete and its reinforcement is of a great importance, because it is actually responsible for transferring loads to the reinforcing bars to be carried if the concrete cannot stand them. To improve this situation, deformed steel bars are now universally used. With such bars, the shoulders of the projecting ribs bear on the surrounding concrete and result in greatly increased bond strength. In addition, cracks widths and deflections are reduced. Similar things can be expected in the case of deformed or surface-treated FRP reinforcing bars.

The bond stress depends on chemical adhesion and mechanical interlock before bond failure and friction thereafter. The mode of failure (Park and Paulay, 1975) for the specimens included:

1. Splitting failure of concrete due to small concrete cover.
2. Rebar pull-out failure due to inadequate embedment length.
3. Rebar fracture failure when the rebar tensile stress reaches its ultimate strength.

As mentioned above bond failure could be caused by tensile splitting of the concrete along the straight portion of the rebar. Thus, the tensile strength of concrete, which is approximately proportional to the square root of its compressive strength, is considered a key parameter in bond behaviour at least in the case of steel rebars (ACI Committee 408,1992).

Bond behaviour between concrete and the reinforcement is divided into two categories, (i.e., bond of straight and hooked bars). Since both categories have different behaviours, many researchers have studied both of them individually. In general, the tensile force applied to the reinforcing bar is transferred to the concrete along:

1. The straight embedment length.
2. The hook (if existing).
3. The partial tail length near the hook bend (if existing).

Nevertheless, the mechanism of bond transfer changes with the replacement of steel by FRP bars. This is, actually, caused by anisotropy of FRP materials (i.e., longitudinal properties are dominated by the fibres and shear and transverse properties are dominated by the resin). Therefore, a major reason limiting the use of FRP bars is lack of information on the bond behaviour.

In fact there is a practical difficulty when measuring bond, because the nominal bond strength obtained from pullout tests, which are fairly easy to carry out, does not reflect the actual conditions take place in flexural reinforced concrete members, and some tests overestimate the nominal bond strength obtained from reinforcing bars under flexural tension. Because in pullout testing, the concrete surrounding the reinforcing bars is under compression, consequently reducing the possibility of cracking and increasing the bond strength due to Poisson's effect. However, in concrete beams, the concrete surrounding the reinforcing bars is simulating the reality in actual life (i.e., the concrete is under tension). Thus, allowing for cracking at lower stresses and reducing friction (Ehsani *et al.*, 1995). To avoid this difficulty, a technique of splitting beam can be used as performed in the RILEM specifications for testing beams (RILEM, 1978). Having mentioned that, measuring creep in bond for FRP is more likely not possible by this way, due to low bond capacity of FRP with concrete, and another way should be developed.

If FRP rebars are unbonded to concrete, therefore it will be assumed that the reinforcement is attached to the concrete at the ends of the beam. The strain in the reinforcement, hence, is not affected by local strains in the concrete, but it must be the strain of the concrete adjacent to the reinforcement, averaged over the whole length of the beam. Therefore, if the beam is loaded to its ultimate strength and hinges are formed, the reinforcement will not see local peak strain at those regions similar to those generated in concrete, instead it will continue to be subjected to the average value (i.e.,

10% to 25% of the maximum value) and therefore snapping of FRP rebars is hopefully avoided (Burgoyne, 1993).

Finally, bond capacity can be used as a function of durability. It is strongly believed that regardless the fibre type used in the FRP reinforcing bars, it is the resin matrix that plays the major role in transferring forces from the surrounding concrete into the reinforcing bar, and this resin matrix is potentially susceptible to degradation at the concrete interface. Therefore, bond strength is more likely to deteriorate under long-term service loading, especially in aggressive environment, than anything else.

2.2.8 Durability

According to the ACI Committee 201, durability of concrete is defined as "its ability to resist weathering action, chemical attack, abrasion, or other process of deterioration; that is durable concrete will retain its original form, quality, and serviceability when exposed to its environment". When talking about durability of reinforced concrete, two things are actually considered: durability of concrete itself, and durability of reinforcement.

Any problems in durability of concrete must be due to some external or internal actions, and both of them can be mechanical, chemical, or physical. Apart from the mechanical attacks, all concrete durability problems are caused by transporting fluids, water and gases, through the concrete. In fact, there are three fluids can enter concrete and reduce its durability: water, some times containing aggressive ions, carbon dioxide, and oxygen. In addition, concrete in seafronts is continuously attacked by physical and chemical actions. Examples of the chemical attack are, chloride attack, and salt weathering. Generally speaking, the problem of chemical action of sea water on concrete is due to the presence of dissolved salts. The total salinity is typically 35,000 ppm. However, it varies from one sea to another, for instance, 40,000 ppm in the Red Sea (Neville, 1998). Furthermore, sea water can diminish pH down to 12 sometimes, (Gjorv and Vennesland, 1976). In fact, physical actions arise from the existence of frost, and the variation of thermal coefficients between aggregate and cement paste (Neville and Brooks, 1998).

One major reason to replace steel reinforcing bars by fibre reinforced plastic rebars is to achieve a radical solution of corrosion. The increasing use of fibre-reinforced composites requires a thorough understanding of the durability of such materials. It is believed that the resin matrix, regardless of the fibre used in the FRP reinforcing bar, plays the major role in transferring forces from the surrounding concrete into the reinforcing bar. Because the surface of the resin matrix, which is in contact with concrete, is susceptible to degradation, therefore bond capacity can be reduced or even, in sever cases, lost completely. Furthermore, if the reinforcing fibres are exposed to attack, this will lead to loss of the longitudinal strength and stiffness of the reinforcement. Therefore, it is important to know the reasons behind degradation of the bars. It is believed that the primary cause of deterioration of FRPs is the diffusion of moisture and other corrosive solutions into the matrix, which can damage the matrix as well as the fibres depending on the rate and depth of penetration of contaminants. Diffusion is defined according to (Crank, 1986) as "the process by which matter is transported by one part of a system to another as a result of random molecular motion". Moisture absorption of a composite can be defined in terms of two parameters:

1. Maximum moisture content or saturation moisture (M_m).
2. Mass diffusion coefficient (D).

M_m is dependent on material type and temperature and type of the surrounding environment. D is dependent on the material type, moisture content within the composite, and the type and temperature of the surrounding environment.

In the event of glass exposure to solution, the attack begins immediately and Na is leached from the glass to find its way to dissolve in solution, e.g. water. Consequently pH of the solution goes up. Moreover, the hydroxide ions OH^- in an alkaline environment, attack the primary component of glass (silica or SiO_2) and cause a breakdown in the Si-O-Si single bond that forms the glass molecular structure. This results in: glass fibre corrosion, a reduction in the cross-sectional area of the fibre, and loss of strength.

Nevertheless, on one hand a special GFRP bars called "alkali-resistant" can be used so the zirconia (ZrO_2) content of AR-glass could potentially improve its behaviour in this sort of environment by forming a thin stable and passive layer on the surface of the bars. On the other hand, unfortunately, if the pH value is very high, then the alkali-resistant glass fibres are attacked by hydroxyl ions in the pore fluids of hydrated cement paste and the Si-O bonds in AR once again will be broken, but this time the degradation of FRP will be with a lower rate.

2.3 Previous research

2.3.1 General

Composite materials can be viewed, tested and analysed at different levels and on different scales. At the constituent level the scale of consideration is on the order of fibre diameter, or matrix interstices between fibres this level is called the microscopic level, the material in this case is regarded as isotropic meaning: it has identical mechanical, thermal, physical and electrical properties in every direction. Another level is known as macroscopic level it deals with a larger scale as a unidirectional anisotropic material with its own average stiffness and strength properties in different directions. Finally the structural level, where it should be dealt with as one composite material (Daniel and Ishai, 1994 and Vinson and Sierakowski, 1986).

2.3.2 Concrete shrinkage and creep

When concrete is subjected to sustained loading, strain increases with time, i.e. creep. Moreover, whether or not subjected to loading, concrete contracts on drying, i.e. shrinkage.

In general shrinkage takes place when water is lost from the concrete by evaporation (drying shrinkage) or by hydration of cement (autogenous shrinkage), and also by carbonation (various cement hydration products are carbonated in the present of CO_2). It is normally measured as a linear micro-strain. Its unit is thus in mm per mm usually expressed in $\times 10^{-6}$.

The amount of water loss upon drying is not equal to the change in the volume of drying concrete. Because the loss of free water in capillaries, which takes place first, causes little if any shrinkage. As drying proceeds, adsorbed water is removed and, in unrestrained hydrated cement paste, shrinkage would be clear.

In actual structures, movement of concrete due to shrinkage may be restrained in any way. Any restraint of shrinkage induces tensile stress which may lead to cracking when this stress exceeds the tensile strength of concrete.

Restraint of any movement of concrete can be categorised into two forms, namely external and internal. The external restraint takes place when movement of a section in a concrete member is fully or partially prevented by external adjacent member. It can also be provided by differential shrinkage between the repair material and an existing structure in a concrete patch repair system or new and old structures in concrete overlays. While internal restraint exists when there are temperature and moisture gradients within the cross section. For example, an un-insulated concrete mass in which heat develops due to hydration of cement. The heat is dissipated from the surface of the concrete so that a temperature gradient exists across the section. Finally, it is possible to have a combination of external and internal at the same time.

The possibility of controlling shrinkage cracking in concrete for a given environment depends on the following factors: the amount of un-restrained (free) shrinkage, tensile strength of concrete, degree of restraint, modulus of elasticity, and creep in tension. Thus, the amount of shrinkage is only one factor governing the cracking. As far as cracking is concerned, a low modulus of elasticity and high creep characteristic of concrete are desirable since they reduce the magnitude of tensile stress. Therefore, to minimise cracking, the concrete should have low shrinkage characteristic and a high degree of extensibility (i.e. low modulus of elasticity and high creep) as well as high tensile strength.

It is important to understand that the induced stresses are modified by relaxation, which may prevent the development or at least delay the development of cracking. The schematic pattern of crack development when tensile stress due to restrained shrinkage

is relieved by creep is illustrated in Fig. 2.2. As can be shown cracking can be avoided only if the tensile stress induced by the shrinkage strain and reduced by creep is at all times smaller than the tensile strength of the concrete. However, because relaxation occurs only slowly, it may prevent cracking when shrinkage develops slowly, but the same magnitude of shrinkage is occurring rapidly and therefore it may well induce cracking (Neville, 1998).

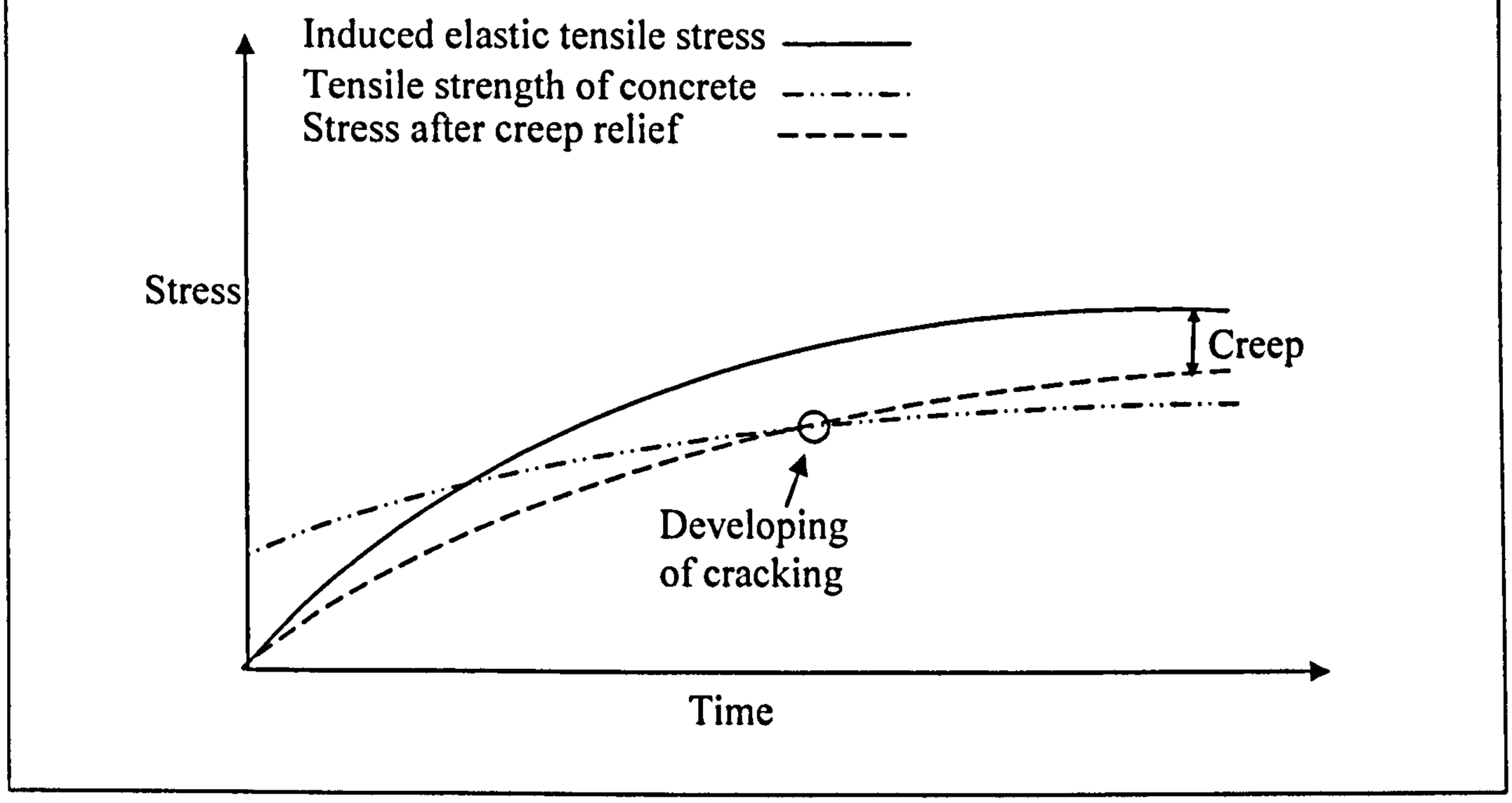

Figure 2.2: Schematic pattern of crack development when tensile stress due to restrained shrinkage is relieved by creep (After Neville, 1998)

Shrinkage cracking can be reduced in several ways, some are as follows:

1. A common way to reduce the risk of shrinkage cracking is to provide a secondary reinforcement. This does not influence any of the factors listed above, however reinforcement can keep cracks from widening.

2. The addition of fibre reinforcement is known to reduce noticeably crack widths resulting from restrained shrinkage cracking. It acts in a similar way of the secondary reinforcement, but since fibres are uniformly distributed across the concrete section, they can prevent microcracks from opening before they become macrocracks.

3. The use of expansive cement. It is worth making it clear that expansive cement does not prevent the development of shrinkage, instead it produces expansion in cement during hydration. Thus, concrete containing such expansive cement, expands in the first few days of its life. If this expansion is restrained by reinforcement bars, the reinforcement is put in tension and concrete in compression, which can counteract the tensile stress in concrete produced by restrained shrinkage.

4. The use of expansive admixture. It is an admixture when mixed with cement and water, produces ettringite or calcium hydroxide by hydration reaction to expand the concrete. The expansion balances the shrinkage in a way similar to the use of expansive cement (Nagataki and Gomi, 1998).

5. The use of shrinkage reducing admixture (SRA) to reduce drying shrinkage. This, in turn, reduces the possibility of concrete cracking (Kristiawan, 2002).

While shrinkage is directly proportional to the water and cement contents, it is adversely proportional to the rigidity of aggregate and its content. Moreover, cracking of concrete due to shrinkage is enhanced in hot and dry environments; this is because drying process is more intensive and rapid (Soroka, 1993).

Not all initial drying shrinkage is reversible, even after a prolonged submerging in water. The absence of full recovery behaviour is probably due to the introduction of additional bonds within the gel during the period of drying, when closer contacts between the gel particles is established.

Creep is defined according to (Mehta and Monteiro, 1993) "the phenomenon of a gradual increase in strain with time under a given level of sustained stress". Creep effects may also be viewed from another standpoint called stress relaxation Fig. 2.2, which is once again defined by Mehta, and Monteiro, (1993), "as the phenomenon of a gradual decrease in stress with time under a given level of sustained strain".

Some researchers (Neville and Brooks, 1998; Soroka, 1993; and Neville, 1959) reported that the source of creep in concrete containing normal weight aggregate is the hardened

cement paste. As normal weight aggregates do not creep at the level of stress existing in concrete, hence their presence in concrete is important in order to resist the creep of the paste. Therefore, the higher the rigidity of aggregate the lower the creep of concrete contains this aggregate. In addition, other factors such as high temperature and wind speed, and lower ambient humidity will increase creep.

Neville and Brooks, (1998) highlighted the importance of water/cement ratio as a factor influences porosity and therefore strength of concrete. In the light of that, the lower the water/cement ratio the lower the creep of concrete, and creep is inversely proportional to strength of concrete.

It is well known that the increase in creep after 20 years under load is small. Neville and Brooks (1998) stated that:

About 25 % of the 20-year creep occurs in a couple of weeks.
About 50 % of the 20-year creep occurs in three months.
About 75 % of the 20-year creep occurs in a year.

Elastic deformation of concrete decreases with time, unlike creep and shrinkage, due to the increase in modulus of elasticity, which reflects the increase in concrete strength with time.

Pickett (1942) reported that in the case of concrete in which only basic creep (i.e., no moisture exchange during loading is involved) occurs, the more evaporable water it contains, the more it creeps. And of course, it creeps even more when the concrete dries during loading.

Under compression of drying concrete (simultaneous creep and shrinkage), the total time-dependent strain is equal to the sum of separate strains of free-load concrete exposed to shrinkage, of loaded concrete prevented from drying, and of extra strain known as drying creep (Neville and Brooks, 1998, Mehta, and Monteiro, 1993, Pickett 1942).

Many of the physical models (Wittmann and Roelfstra, 1980) explained the drying creep in concrete by micro-cracking only. However, Bazant and Xi (1994) found that drying creep has two different sources, which are micro-cracking and stress-induced shrinkage.

Most research on drying creep of concrete has been carried out under compression, and therefore, the drying creep strain coincides by sign with the direction of load application. However, when concrete is under both tensile loading and drying, which produces deformations of the opposite sign, the resulting drying creep strain might not coincide in direction with the load. Furthermore, the direction could change with time. Therefore, the abnormal behaviour of drying creep takes place when concrete is under tension. Because the observed drying creep strain is negative at initial period (as shrinkage) and positive thereafter (as creep).

Kovler (1995) performed a study to resolve the nature of drying creep under axial tension. He concluded that:

Firstly, the extra deformation of concrete under drying creep is the sum of two components, which are creep-induced shrinkage and shrinkage-induced creep. It seems that the second component behaves as an ordinary creep in spite the fact that it is linearly proportional to free shrinkage (i.e., varies linearly with stress). The first component depends on intensity of shrinkage process in the material, even though it is linearly proportional to basic creep.

Secondly, the test of drying concrete under axial tension revealed that in the initial period (up to1.5 or 2 days), creep-induced shrinkage dominates and the total time-dependent strain is less than the sum of basic creep and free shrinkage because drying creep is contrary to load direction, unlike the compression case. Later when shrinkage-induced creep starts to be dominant, the total strain becomes larger than the sum mentioned earlier, i.e., similar to the compression case.

In progressive study Kovler (1999) revised the phenomenological approach describing drying creep of concrete as the sum of creep-induced shrinkage and shrinkage-induced creep, and corrected it. He also concluded that the abnormal behaviour of drying creep

strain in the initial period of drying (i.e., the drying creep strain is contrary to load direction) is caused by swelling of the sealed concrete element in basic creep tests. Such a swelling deformation should be subtracted from the basic creep strain measured in sealed specimens, so that the abnormal character of the curve of drying creep is converted into the regular drying creep curve, which is positive across the whole duration of load, including the early period, as in the compression case. Therefore, the right basic creep strain can be obtained.

Neville (1998) attributed the difference between measured creep in laboratory and creep under normal weather conditions to the wet-dry cycle, i.e., the wet-dry cycles increase the magnitude of creep, therefore the results obtained from laboratory tests underestimate the creep under normal weather conditions.

Neville (1970) reported that there are three stages of creep, i.e., primary, secondary, and tertiary creep. At the beginning, the primary creep takes place with decreasing rate with time until a minimum creep rate is reached, then the secondary creep range starts with a steady state creep, and this one is also increasing with time in a decreasing rate. The tertiary creep could exist, depending on whether or not there is an increase in stress. For example, in concrete this may occur from an increase in micro cracking at high stresses.

Poh (1998) presented an equation that can be formulated for general representation of creep. It considers all three stages of creep (i.e., primary, secondary, and tertiary). Moreover, it expresses creep strain in terms of real time in a single smooth, continuous curve. It is unlike other formulae, which face many shortcomings, such as, being single-curvature functions, which cannot represent the entire three-stage curve. In addition, a comparison with experimental results shows that the equation closely fits the creep curves of steel at various temperatures and stress levels.

Soroka (1993) reported that creep increases with an increase in ambient relative humidity, which in turn, increases the moisture content of the paste.

Neville (1998) reported that for simplicity of calculation it can be assumed that the 30-year creep represents the ultimate creep, which is about 36% in excess of the first year

creep. In fact, 30-years was chosen because it could be the longest period creep had been recorded.

Brooks and Neville (1978 and 1975) viewed the possibility and developed formulae to predict long-term creep and shrinkage from short-term tests under load.

2.3.3 FRP time-dependent behaviour

Ehsani (1993) reported that fibres such as glass and carbon, normally, do not exhibit much creep, while that is not true for most resins. In the light of the above, because of the different constituent materials (fibre and resin) significantly different creep behaviour can be observed for different FRP materials.

Nevertheless, Iyer and Anigol, (1991) conducted work to investigate strain under long term sustained load. They indicated that for vinyl ester fibre glass cables tested for 200 days, there was no creep. They also concluded with other researchers (Gilbert and Gowripalan, 1993) that creep in FRP rebars is negligible if load is limited to 60% of short term strength, which is within the expected service load levels.

Concrete shallow beams reinforced by GFRP and steel bars were tested under different levels of sustained load for eight months by Hall and Ghali (2000). They concluded that beams reinforced with GFRP had a long-term deflection 1.7 times greater than those of steel reinforced beams due to creep and shrinkage.

Some experiments were performed to investigate the creep properties of FRP bars. Mallick (1988), carried out tensile creep tests for vinyl ester glass FRP composites at various stress levels, and indicated that the creep in longitudinal direction (parallel to the fibre direction) is negligible. However, at other fibre orientation angles creep strain could be significant. Thus, it is important in polymer composite design to recognise the influence of creep when the stresses are significantly large with off-axis of fibre orientation. Yamaguchi, *et al.* (1997), performed a number of tests on both 6mm FRP bars and fibres used in the FRP bars, in order to investigate the creep behaviour. The creep stress applied on GFRP bars varied from 60 to 85% of tensile strength (i.e.,

1656MPa). They concluded a linear relationship between creep rupture time and level of loading for the bars. Moreover, each type of FRP bars exhibited a unique behaviour of creep failure depending on the degree of loading and the characteristic of the fibres, namely aramid, glass or carbon, which is in agreement with (Ehsani, 1993, Uomoto *et al.* 1995, and Glaster, *et al.* 1983, and 1984). For example, in the case of GFRP bars, creep strain increases step by step at some instant in the loading time, also glass and aramid fibres over a long period of time exhibit failure by stress rupture, yet carbon fibres are relatively less prone to stress rupture.

Seki, *et al.* (1997), obtained a linear relationship between the ratios of loading (i.e., creep tensile load / maximum tensile load) and creep rupture time, after testing 2.4mm GFRP bars. From the straight line of the relationship, one million hours creep-rupture strength of GFRP bars was found. Furthermore, and in agreement with Nishimura and Uomoto (1995), it was realised that the increase of creep strain shortly after the loading was negligible. However, creep increased for many specimens afterwards, and increased suddenly before a creep-rupture.

An experimental study by Zhang (1999) on the creep fracture of a unidirectional carbon fibre reinforced epoxy composite with notches was carried out and monitored by scanning electron microscopy (SEM); the crack initiation and variation of the crack length with time were observed. It was found that under constant load, the crack initiates from the root of a notch and grows parallel to the fibres with time continuously. Moreover, it was concluded that matrix cracking and interfacial de-bonding are the main fracture mechanisms of creep fracture. However, there are occasions that when crack splits the fibres in the longitudinal direction.

The effects of the GFRP bars on shrinkage and thermal stresses in concrete were studied theoretically by Chen and Choi (2002). The results indicated that the lower the Young's modulus of reinforcement, the lower the reinforcement to restrain concrete shrinkage and therefore the lower the development of concrete tensile stress level and, in turn, the fewer the cracks.

2.3.4 Prediction of modulus of elasticity, shrinkage and creep coefficient

There are several methods available for estimating modulus of elasticity, shrinkage, and creep coefficient. Among them are ACI Committee 209 recommendations (1992), CEB-FIP Model Code (1990), RILEM Model B3 (1996), Gardener and Zhao (1993), BS 5400-4 (1990), and BS 8110-2 (2001).

Brooks and Neville (1975, and 1978) concluded that long term deformation, as long as five years, can be predicted from values measured at 28 days.

Based on a survey of published experimental data, equations were developed by Gardener and Zhao (1993) to calculate modulus of elasticity, shrinkage, and creep coefficient in terms of developed concrete strength. Moreover, the proposed equations together with those recommended by ACI Committee 209-82 (1982), CEB Model Code (1990) were compared to the published data.

Gardener and Zhao (1993) concluded that, the 1990 CEB Model Code underestimates shrinkage strains by approximately a factor of two, and ACI 209-82 overestimates shrinkage at early ages and underestimates it at later ages. Furthermore, total deformation, shrinkage and creep at 30 % strength, is well represented by the proposed expression by Gardener and Zhao (1993), but underestimated by 1990 CEB Model Code and ACI 209-82.

2.3.5 Bond behaviour

In a reinforced concrete flexural member, the tension force carried by the reinforcement balances the compression force in the concrete. The tension force is transferred to the reinforcement through the bond between the reinforcement and the surrounding concrete. In other words, the stress at the surface of the bar resulting from the force component in the direction of the bar can be considered the bond stress between the reinforcement bar and the concrete.

The bond between concrete and FRP rebars has attracted many researchers to investigate with reference to several kinds of bars characterised by different quality and quantity of

fibres and resin matrix and by different treatments of the outer surface to provide the better combination of both the fibre and the matrix. From the experimental results it was found that the bond between FRP rebars and concrete depends on several factors, including resin type rather than fibre type (Al-Zahrani *et al.*, 1999) friction due to surface roughness of FRP (Malvar, 1995, and Faza and GangaRao, 1993), the mechanical interlock of the FRP against the concrete, the chemical adhesion (Benmokrane *et al.*, 1996), and the hydrostatic pressure against the FRP rebars due to shrinkage of concrete (Faza and GangaRao, 1993).

In order to investigate the mechanical properties and bond slip behaviour for GFRP bars, Ehsani (1993) performed tests and concluded that a good bond existed between GFRP and concrete due to the relatively large number of narrow cracks in the test beams. Moreover, Benmokrane *et al.*, (1995) suggested a perfect bond between GFRP rebars and concrete, because the GFRP rebars in a pure tension test behaved in a similar manner as tension reinforcement of a concrete tested in flexure.

In another study, Ehsani *et al.* (1995) examined the bond behaviour of hooked glass fibre reinforced plastic bars to concrete. Key factors were varied, including concrete compressive strength, radius of bend of hooked reinforcement, tail length, straight embedment length, and reinforcement bar diameter. They reported a decrease in the maximum slip at failure, with increase in concrete compressive strength, radius of bend, and straight embedment length. Moreover, they recommended details of the bar as a function of its diameter. In other words, the tail length of 12 times the bar diameter and the development length of 16 times the bar diameter were recommended for use in design for 90-deg hooked GFRP reinforcing bars. The minimum ratio of radius of bend to the bar diameter (r/d) is recommended to be 3. Development length, tail length, and radius of bend are shown in Fig. 2.3. The development length is defined as the minimum embedded length required to develop the ultimate tensile force, P_u.

Ehsani *et al.*, (1997) concluded that the ultimate bond stress, between straight GFRP rebars and concrete, increases with an increase in concrete compressive strength.

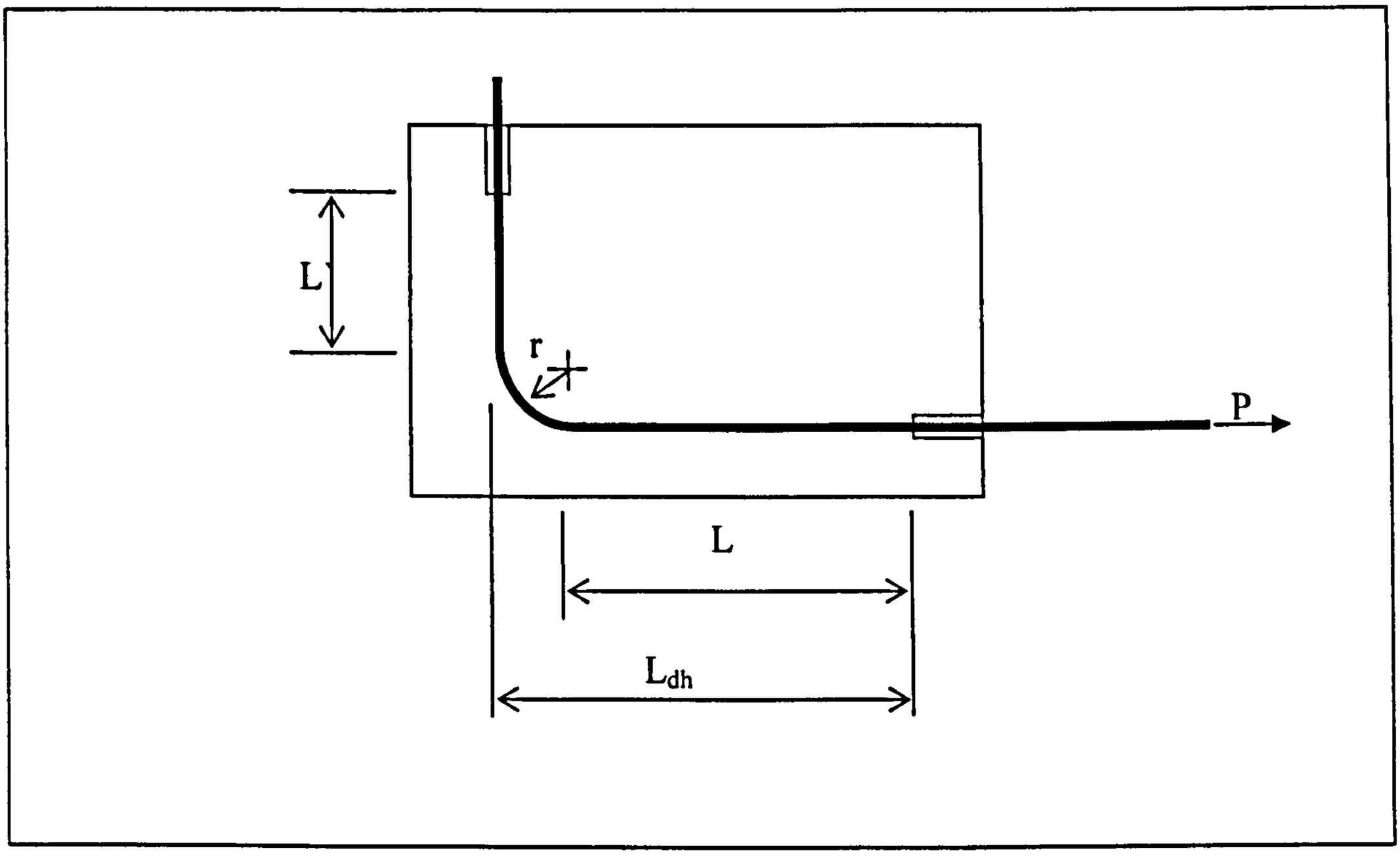

Figure 2.3: Illustration of test specimen

Where, L_{dh} = is the development length

L = is the embedded length

L` = is the tail length

r = is the radius of bend, and

P = is the applied load.

Furthermore, Chaallal *et al.* (1992) suggested that the development length, for GFRP embedded in concrete, is approximately 20 times the bar diameter for both high strength and normal strength concrete. However, Ehsani *et al.*, (1997) concluded a multiply factor increases as the bar diameter increases, namely the embedment length for GFRP rebars No. 3, 6, and 9 placed at the bottom of the beam is approximately 21, 24, and 27 times bar diameters, respectively. For top rebars, the above embedment length should be multiplied by the top bar factor of 1.13.

In fact, surface deformation plays a very important role (Malvar, 1995). After examining four different GFRP bars with different surface deformations but equal bar diameter, he suggested a small surface deformation of about 5.4 percent of the nominal

bar diameter was enough to produce maximum bond stresses up to five times the concrete tensile strength, which is similar to that of steel bars. He did not recommend GFRP rebars with ribs deformation merely glued to the surface as they become un-bonded after loading. He also reported that bond strength for steel bar is greater than that of the studied GFRP bars (i.e., between 1.2 and 1.5 times). Finally, he highlighted the importance of confining pressure (i.e., bond strength can be increased three times by increasing the confining pressure).

Benmokrane *et al.* (1996) studied the distribution of tensile and bond stresses for four different bar diameters of GFRP, as well as the bond strength in comparison to steel bars. They reported, from pull out tests, that the distributions of the embedded GFRP in concrete are non-linear and similar to that of steel rebars. Furthermore, the bond strength of GFRP is approximately 60~90 percent lower than that of steel, depending on the bar diameter and the embedment length. They also concluded that the bond strength values that obtained from beam test are lower than the pullout tests by 55 to 95%. Finally, the diameter of bars has an adverse effect upon the average bond strength of both steel and GFRP reinforcing bars.

In contrast, Pleimann (1991) concluded that, after conducting pullout tests, bond strength increases with the increase of bar diameter.

The bond behaviour of straight GFRP rebars to concrete has been investigated with consideration of concrete cover. Ehsani *et al.*, (1997) compared between beam and pullout tests to investigate the influence of several parameters on bond behaviour of straight GFRP rebars to concrete. They concluded that as concrete compressive strength and concrete cover increase, the ultimate bond stress increases. Pullout tests overestimate both the loaded end slip and ultimate bond stress, which is in agreement with Benmokrane *et al.*, (1996). Therefore, the beam test is recommended because both the rebar and concrete are in tension, whereas in the pullout test the concrete surrounding the rebar is subjected to compression forces from the reaction of the jack.

Tighiouart *et al.*, (1998) examined different types of GFRP rebars in terms of bond capacity by using the pull out test and the joint-beam test in accordance with RILEM

(1978). They observed several points, namely, GFRP rebars normally show a lower bond strength than steel ones, GFRP rebars depend (in their bond strength) on the adhesion and friction, and the bond strength has an adverse relationship with the increase of the embedment length and the bar diameter. The smaller bond strength of big diameters can be explained by the bleeding of water in concrete. The bigger the diameter of the rebar, the higher the quantity of bleeding water trapped beneath the rebar creating a greater void. This void reduces the contact surface between the rebar and the concrete and hence the bond.

Kachlakev (2000) tested hollow GFRP composite rebars, and put very minor emphasis on the influence of concrete compressive strength on bond strength and stress. Other characteristics, namely, rebar surface deformation, embedment length, concrete cover, and microstructure of the composite rebars (i.e., unidirectional or off-axis glass fibre) have great impact. The specimens reinforced with unidirectional glass fibres showed higher bond strength than off-axis fibre reinforced specimens. In that investigation, two different procedures for evaluating the bond strength were performed. One was the conventional pull-out test, and the other was especially developed by the researcher.

Al-Zahrani *et al.*, (1999) tested different types of machined FRP rebars to produce axisymmetric surface deformation in bond with four concrete mixes each one had different concrete compressive strength. In agreement with Kachlakev (2000), they concluded no noticeable effect of concrete strength on bond strength and failure mode.

Bank *et al.*, (1998) addressed the reflection of degradation of different types of FRP rebars (i.e., polyester and vinyl ester resins with smooth and deformed surfaces) on the bond strength and bond stiffness properties (bond stiffness is the slope of the linear portion of the bond stress vs. slip/bar diameter obtained from pullout curve). The results showed different levels of degradation based on the type of resin matrix. Fibres, however, did not show much degradation. They reported a good correlation between material degradation and the decrease in both bond strength and stiffness properties of FRP rebars.

Larralde and Silva-Rodriguez, (1993) studied the bond stress-slip relationship using both pullout and beam tests. They supported the idea of (Ehsani *et al.*, 1997, and Benmokrane *et al.*, 1996) regarding the results obtained from pullout tests. Concrete surrounding the reinforcing bars is under compression, leading to higher bond strength and lower possibility of cracking due to Poisson's effect. Therefore, the result of pullout test does not reflect the reality of flexural reinforced concrete elements, rather, it overestimates the true result. Moreover, they concluded that bond strengths of GFRP rebars varied from 73 to 96% of that of steel, depending on the reinforcing bar diameter and embedment length.

Katz (2000), examined the effect of cyclic loading on the bond mechanism of five different types of FRP bars to concrete. The cyclic load level was within the service stress level. In order to accelerate the deterioration effects, the loading was accompanied by immersion in water at 20 and 60°C. He concluded that the bond capacity was diminished due to cyclic loading. The failure mechanism was one of three things: abrasion of the surface of the bar, delaminating of the outer layer of the resin at the surface of the bar, or abrasion of the cement particles entrapped between the bar and the concrete. He concluded that for some types of bars no significant change in the bond strength was noticed between ageing at 20 and 60°C. Moreover, he emphasised more attention to the mechanical and physical properties of the external layer of FRP bars. For example, on the one hand, he suggested to avoid bars with helical wrapping due to poor behaviour. On the other hand, he recommended embedding sand particles onto the bar's surface, during manufacturing, to improve bond strength.

Despite that some researchers (Faza and GangaRao, 1993; and Ehsani *et al.*, 1995) believe that concrete compressive strength affects the bond strength, the majority (Al-Zahrani et al., 1999; Nanni *et al.* 1995; Kachlakev, and Lundy, 1998; Kachlakev, and Lundy, 1999; and Benmokrane *et al.*, 1996) including ACI 440 believe that unlike reinforcing steel, if concrete splitting is avoided (by providing sufficient concrete cover), the concrete compressive strength does not significantly influence the bond strength of FRP reinforcing bars. Although it is widely accepted in the case of steel reinforcement that bond failure is proportional to tensile strength of concrete, and tensile strength of

concrete is proportional to the square root of its compressive strength, bond expressions also include the square root of concrete's compressive strength term (ACI 318-89).

2.3.6 Durability

Schultheisz (1996) mentioned that the durability of FRP is controlled by the durability of fibres, matrix and the fibre/matrix interface. That is why all of them must be considered when studying durability.

Durability of composites depends mainly on two things: the quality of the manufacturing process and the type of matrix. In regard to quality of the product, the matrix toughness must be high enough to resist the development of matrix micro-cracks and diffusion through the matrix must be minimal. And with respect to type of matrix (Coomarasamy and Ip, 1998, Tannous and Saadatmanesh, 1998, Chin *et al.*, 1997) reported that vinyl ester resin is more durable than polyester resin matrix.

As far as the polymer matrix is concerned, Chin *et al.*, (1998) examined the durability of un-reinforced free films of two different matrices, namely vinyl ester and isophthalic polyester, and revealed that examination with energy dispersive X-ray analysis (EDX) following immersion in salt solution and simulated concrete pore solution at ambient temperature and 60°C for 60 days showed no ionic penetration into the bulk polymers.

Fibre content is very important when diffusivity is concerned because fibre is considered to be negligibly permeable. Therefore, high fibre content coupled with a good protection of resin should provide durable composites. The decision of which polymer resins should be used is of high importance, this decision is made based on the expected working environment to ensure better protection to the reinforcing fibres, enhance mechanical properties and offer longer life span for the whole composite. Moreover, it is worthy to stress on the quality of the manufactured materials, for instance, low viscosity polymers must be provided to guarantee fibre wetting and complete impregnation to achieve low void composites (Li *et al.*, 1998, Clarke, 1996 and Riffle *et al.*, 1998).

As most of the mechanical properties are governed by fibres, resins must provide protection to fibres against any chemical or physical damage. But when resin is attacked and deteriorated, the fibres fall off from the surface and the FRP strength reduces (Uomoto, 2001, Uomoto *et al.*, 2001 and Uomoto, 2003).

Almost all researchers agree that vinyl ester resins offer better protection than polyester ones. That is due to a couple of reasons, one is with respect to alkalinity resistance and the other is with respect to diffusivity. In the vinyl ester resins the weakest ester linkages are partly replaced by the stronger ether linkages that are highly resistant to alkali. Moreover, they (vinyl ester resins) contain less polar groups, and in turn, less diffusivity and absorptibility. In addition, polyester has reactive double bonds distributed throughout the chains while vinyl ester has such bonds only at the ends of the chain. Thus the crosslink density can be better controlled in vinyl ester. In fact, the good crosslink enables the vinyl ester resins to be more stable and better waterproof and the longer distance between crosslink make the vinyl ester tougher than polyester (Riffle *et al.*, 1998, and Li *et al.*, 1998). The epoxy-based composite though, shows a superior behaviour in terms of durability (i.e., humid and water resistance) and mechanical properties even at elevated temperatures when compared with polyester and vinyl ester ones, but at the expense of cost. Regarding the mechanical properties, epoxies offer higher shear strength, better fatigue performance and stronger fibre/matrix interface (Clarke, 1996 and Adimi and Boukhili, 1998).

Studies were performed by Chin *et al.* (1997) including thermosetting of epoxy vinyl ester and isophthalic polyester (isopolyester) resins. The two resins, which were immersed in three different solutions to represent water, alkali and saline solutions, reached an equilibrium state before the first 50 hours had elapsed. Vinyl ester had a better performance because there was no significant mass loss in any of the solutions even at temperature as high as 60°C, while isopolyester exhibited mass loss in both simulated concrete pore (alkali) solution and salt solution at high temperature. The mass loss occurred to isopolyester in salt and alkali solutions at high temperature was due to the possibility of polymer breakdown followed by the leaching of soluble degradation or hydrolysis products. Both pH and cations were involved in the hydrolysis. It is believed that vinyl esters are more stable to hydrolysis than isopolyesters, because ester linkages

in vinyl esters are terminal and are shielded by methyl groups. However, in most other polymers, ester groups are distributed along the main chain, making them more available (and hence more vulnerable) to hydrolysis reactions.

The importance of resins goes beyond the protection of the fibres to govern the bond between the FRP bars and concrete and therefore transfer the stresses, also shear property is governed by the resins. Bank *et al.*, (1998) related the degradation in bond capacity of FRP bar to its surface, which is the type of resin matrix no matter what kind of fibre is used.

The presence of water can greatly influence the properties of thermosetting polymers (Vijay and GangaRao, 1999), in terms of physical, chemical and mechanical properties, due to changes in the composites components, such as, fibre, matrix and fibre/matrix interface.

Among the physical changes of resins due to moisture attack is to plasticize the polymers and lower the glass transition temperature, T_g, (i.e., reduce the temperature at which the polymer shows a transition from glassy to rubbery behaviour) (Nishizaki and Meiarashi, 2002). Consequently, it becomes soft and can enhance creep deformations. The chemical changes caused by moisture ingress include further curing for not fully cured resins, due to lowering in T_g values, and for fully cured ones, water can cause hydrolysis of the polymers. Moisture diffusion in matrix resins is also responsible for introducing internal stresses which result in micro-cracks and debonding between the fibre and the matrix, all that being due to swelling of the material (Schutte, 1994). Kajorncheappunngam *et al.*, (2002) reported at first an increase in ultimate tensile strength for aged (i.e., immersed in salt, alkali, water and acid solutions) epoxy resin samples. Whenever the polymers are not fully cured at room temperature, immersion in liquid media will raise cross-link density and therefore increase the ultimate tensile strength (Gupta *et al.*, 1985). Ingress of liquid in polymers could be responsible for reduction in T_g. The decrease in glass transition temperature allows the polymer chains to become mobile, consequently encourages cross-linking and full curing (Kajorncheappunngam *et al.*, 2002).

It seems that preference should be given to the use of appropriate epoxies or vinyl esters, and the use of polyester resins is not recommended.

Whith regard to fibres, namely glass, carbon, and aramid composition, together with the environment, they play a very important role with respect to degradation of FRP. As far as glass is concerned, Adams (1984) mentioned that there are two mechanisms of this attack known as etching and leaching. The etching mechanism is driven by an alkali attack. Wakabayashi and Tomozawa (1989) reported that this process depends on temperature and activity of the aging solution. The existence of alkali solution will allow the corrosion by-products to build up on the surface of the glass. Unless the by-products are flushed off, the corrosion reaction will slow. The reaction rate will go up as new glass layer is exposed to the aging solution (Wakabayashi and Tomozawa, 1989; and Adams, 1984).

The leaching mechanism promoted by an acid attack removes the alkalies present in the glass by exchanging hydronium ions in the acid with alkalies in the glass. The alkalies removed from the glass will then go into solution outside of the glass and attack the glass once again by etching. Water attack on the glass is similar to the acid attack. Therefore, the latter two attack processes, namely acid and water, produce both leaching and etching to the glass (Adams, 1984; and Wakabayashi and Tomozawa, 1989).

It is believed that there is a strong relationship between glass composition and dissolution rate. The addition of alumina to the glass will increase the resistance of the glass to water attack; however its resistance to alkali attacks will be adversely affected. Since the water attack eventually evolves into an alkali attack, the addition of alumina to the glass (E-glass contains alumina and does not contain zirconium) will, certainly, not help long-term degradation resistance of glass (Doremus *et al.*, 1983 and Perera *et al.*, 1991). By adding Zirconium to the glass, a limited improvement of resistance to the alkali attack can be noticed (Yilmaz, *et al.*, 1991).

Yilmaz and Glasser (1991) mentioned a couple of mechanisms involved in the alkali attack; these are hydroxylation and dissolution, and notching.

Hydroxylation occurs when pH exceeds 10. At the beginning it is rapid, but as the by-product accumulates over the surface of the glass the process slows (Al Cheikh and Murat, 1988).

In conjunction with the hydroxylation, dissolution of Na^+ exists in the glass takes place. As soon as the calcium is leached out of the glass, it will combine with the water to form a calcium hydroxide. In turn, this compound will adhere to the surface of the glass and act to slow the aging reaction (Adams, 1984, Al Cheikh and Murat, 1988 and Yilmaz, *et al.*, 1991).

Following the hydroxylation and dissolution process, notching of the glass fibres will occur due to the build up of calcium hydroxide crystals. The notching of the glass fibre will reduce the cross section and therefore the tensile strength of the fibre. Last but not least, it will expose a new layer of the glass to further degradation process (Al Cheikh and Murat, 1988).

E-glass fibre composites are the most widely used because of their lower cost. Anderson *et al.* (1994) and Katsuki and Uomoto (1995), however, showed serious durability problems in FRP bars and segments made from E-glass in environment with high alkalinity such as in concrete.

Oka *et al.*, (1979) immersed silica glass in an alkaline solution of NaOH and $CaCl_2$, as a result, the formation of calcium silicate hydrogel took place on the surface of the silica glass as a solid surface layer. Interestingly, the higher the alkalinity of the solution, the greater the deposition of calcium on the surface.

Uomoto (2001) highlighted the importance of fibre/resin interface in determining durability of GFRP rebars, as he noticed by studying SEM images of aged specimens that the migration of deleterious ions, such as Na, was through the interface region. Further investigation by Uomoto (2003) confirmed the vulnerability of fibre/resin interface, when SEM images showed that glass fibres deteriorated from the interfaces between fibres and resin after immersion in alkali solution. Moreover, high concentration of Na ions was observed at the boundary between fibres and resin. It was

suggested, therefore, in order to enhance the durability of GFRP materials is to improve the resistance against harmful ions by forming a good interface between fibres and resin. This can be achieved by combining glass with aramid fibres when producing FRP materials (Uomoto, 2003).

Coomarasamy and Ip (1998), noticed a decrease in mass of GFRP grid samples when immersed in alkali solution at 60°C. The reduction in mass was due to dissolution of the fibres and some disintegration of the matrix (vinyl ester resin).

The detrimental effect on GFRP rebars due to long term exposure to a high alkaline environment (i.e., GFRP tendons were submerged in solution of 60°C, and pH of 12.5 and 13 for approximately 2 to 3 months) was proven to be high in terms of tensile strength. That aging technique simulated 50 years in concrete (Porter *et al.*, 1997).

Sheard, *et al.*, (1997) assessed the durability of 8 mm square GFRP bars with respect to its interlaminar shear strength and bond strength. They reported very little evidence of deterioration in the interlaminar shear strength of the bars immersed in simulated pore solution at 38°C, mentioned elsewhere (Clarke and Sheard, 1998). For the bars embedded in concrete and within the first 12 months of exposure to different environments, they reported no deterioration of the bars, and no migration of the mobile alkali ions into the bars or out to the concrete. In the light of the above, they concluded that interlaminar shear strength assessment can be used as a quality control parameter.

Gangarao and Vijay (1997), assessed the long term strength and stiffness degradation trends of GFRP bars using traditional accelerated aging factors in addition to sustained stress. The accelerated tests suggested strength and stiffness loss for both naked and embedded bars, the stiffness reduction was higher than strength reduction for beams reinforced with GFRP bars and vice versa for the bars on their own.

Devalapura *et al.*, (1997) and Nanni *et al.* (1998) undertook two accelerated test schemes to assess the prediction of long-term performance of GFRP bars: environmental, namely alkaline solution and mechanical, namely sustained load (i.e., working stress level and high stress levels). Nanni *et al.* (1998) indicated that the

mechanical conditioning is not an accelerator of FRP/concrete bond degradation, however the environmental conditioning is.

Porter and Barnes (1998) reported that long term exposure to a highly alkaline environment together with or without sustained stress proved to be very detrimental for some GFRPs.

Malvar (1998) pointed out that the resin matrix used in composites must prevent the development of matrix microcracks by having high toughness and prevent diffusivity as much as possible. In order to come across the durability problems he recommended the use of pH-neutral concretes to prevent alkali attack, as well as all FRP reinforcement must be protected against moisture and UV. Because even if the fibres are not affected by water like carbon, the matrices usually are, and in turn, the composite properties will be affected.

Alsayed and Alhozaimy (1998) highlighted reduction of the weight and the tensile strength of the GFRP rebars due to alkalinity of cement paste and alkaline solution. The adverse effects on the rebars due to alkaline solution are higher than that of cement paste.

All silicate glasses seem to corrode in alkaline environment with a threshold of pH greater than 10. In fact, typical Portland cement mixes, normally, give pH values well above that threshold (i.e., pH 12.5 to 13 or even more) depending on the total alkali content (i.e., Na_2O and K_2O) of the cement. However, the use of pozzolanic materials, for instance, silica fume and fly ash is thought to be effective in inhibiting the corrosion of glass fibres because they reduce alkalinity and inhibit the formation of $Ca(OH)_2$.

Not only does alkali threaten the FRP but also moisture can badly affect it in a different manner. Sridharan (1997) determined degradation in FRP after immersion in water for 600 hours at 80°C. It is believed by the author, that the reduction in longitudinal tensile modulus by 10% was due to degradation of both glass fibre and failure of the fibre/matrix interface.

Springer *et al.* (1981) and Pantuso *et al.* (1998) agreed that losses in tensile and flexural strengths in the order of 10% may be expected when glass fibres are exposed to moisture for few months. Although some studies indicated that the losses may be negligible (Rahman et al., 1996).

Shen and Springer (1976) performed a number of tests using different types of orientation of fibre reinforced composites. These tests were performed at different temperature ranges and in different environments (i.e., humidity from 0 to 100%, and fully submerged in water). They concluded that the maximum moisture content depends on the type of material and environment (water or humid air). Moreover, diffusivity and moisture content of samples can be estimated by Fick's Law until the maximum moisture content is reached.

Marshall *et al.* (1982) examined the diffusivity of water in stressed damaged material (E-glass, Vinyl ester), unstressed damaged material, and undamaged stressed material. They found that diffusivity decreased in this order: stressed damaged material, unstressed damaged material, and undamaged stressed material. That pointed out the importance of capillarity in moisture ingress and the consequences of surface and volume damage of composites.

Water can reduce polymer composite durability by adversely affecting the matrix, fibre and fibre/matrix interface, (Nguyen *et al.*, 1998). Furthermore, shear strength and spectroscopic results and visual observation proved that accumulation of water at the polymer/fibre interface contributes significantly to the shear strength loss of epoxy/E-glass fibre composites.

Tannous and Saadatmanesh (1998) studied the moisture absorption and predicted the associated changes in mechanical properties of E-glass GFRP rebars under accelerated exposure to an aggressive environment. Different environments included seven chemical solutions, ultraviolet radiation, and finally, de-icing salts. Results indicated that:

- GFRP-vinyl ester rebars showed better performance than GFRP-polyester ones in all environments in terms of moisture absorption and diffusivity.

- Higher temperature increased the degradation of GFRP expressed in higher results in maximum moisture content and diffusivity.

- Higher diffusivities in the GFRP were recorded in seawater and de-icing salt solutions than alkaline and acidic solutions due to the presence of Cl^-, Na^+, Ca^{+2}, Mg^{+2} ions in higher concentrations and their ability to penetrate (i.e., diffuse) into the rebars.

Dimbleby and Turner (1926), introduced a new type of glass fibres. They showed that the addition of small amount of ZrO_2 to silicate glasses improve their resistance to alkali.

Hence, an alternative glass fibre is used to improve the durability of FRPs in this type of environment, which is the alkali resistant (AR) glass. Majumdar (1974) studied the corrosion of commercial glass fibres by immersing type E glass and type AR (alkali resistant) glass fibres into cement extracted solutions. The key factors were period of exposure and temperature. As a result of that study, it was reported that the alkali attack started on AR glass fibres slowly and slightly increased with time. However, it was rapid on E glass fibres at the beginning but it stopped later. The addition of ZrO_2 reduces corrosion by increasing the corrosion resistance of glasses in alkaline environments by forming a thin stable passive layer on the surface. Also, Larner, *et al.*, (1976) and Simhan, (1983) pointed out that AR glasses do not inhibit corrosion completely; rather they dramatically reduce the corrosion speed.

Simhan (1983) examined two glasses containing 17 % and 9 % ZrO_2 and exposed them to water and alkaline solution. He reported that in both solutions the glass with higher ZrO_2 has the lower loss in sodium and silica.

Yilmaz (1992) examined the corrosion behaviour of AR glass fibres reinforced cement matrix. He reported that the chemical attack led to a hydroxylation process of the glass fibre surfaces. During this process a shell of glass corrosion products was developed with much higher Zr and Ca contents (due to migration of Ca ions from the cement matrix into the glass), and lower Si and Na contents (due to dissolution of Si in the cement matrix) than the bulk glass.

In fact, not only can alkaline destroy glass fibres but also acids have detrimental effect. Chakraborty *et al.* (1979) followed another approach to investigate the corrosion of AR glass fibres. The fibres were exposed to solutions of different pH. The results revealed that in alkaline solution (i.e., saturated $Ca(OH)_2$ solution), SiO_2 dissolved from the glass surface leaving a ZrO_2-rich layer, which was in agreement with Yilmaz (1992). In the other extreme, in an acidic solution (i.e., HCl solution) ZrO_2 dissolved from the glass surface leaving a SiO_2-rich layer.

Yilmaz (1992) also pointed out that the Zr-rich passive layer, which was formed at the initial stage of hydration of cement (within 90 days), was not enough to cease Si depletion and penetration of OH ions.

In another study, Tannous and Saadatmanesh (1999) studied a number of bar samples and concrete beams. They were tested to examine the durability of AR glass bars. The bar specimens were exposed to different chemical solutions, simulating accelerated exposure to field conditions, and then tested in tension to determine the loss of mechanical properties (i.e., changes in their ultimate tensile strength, ultimate strain, and elastic modulus). In addition, a number of shorter bar segments [100mm long] were also exposed to the same environments to determine the diffusivity coefficient. The authors concluded that:

- Both temperature and the type and concentration of the solution govern the diffusion in FRP rebars.

- Confirmed previous study (Tannous and Saaddatmanesh, 1998), the vinyl ester exhibited lower diffusivity and provided a better protection to fibres against chemical attack than polyester.

- Cl^- ions are not as damaging to glass as the OH^- ion, however Cl^- ions can penetrate the matrix, causing macro cracking and fracturing of the matrix and resulting in rapid moisture diffusion as well as debonding of the fibres. Debonding of the fibres, in turn, will result in the loss of the strength of the bar.

Clarke (1999) reported about a programme that was carried out by EUROCRETE on durability. This project covered work on the materials and composites embedded in concretes. Samples were stored in laboratories and on sites in Europe and the Middle East. The results revealed that the composite bars showed a good resistance to alkaline environment.

Clarke and Sheard (1998), suggested that tensile strength test is not the best way of monitoring the quality control, due to its insensitivity to determine the fibre/matrix bonding. Instead other test techniques can be used such as the interlaminar shear strength test. Also they highlighted that good matching and compatibility between the fibres and the matrices should be taken into consideration to achieve a durable and strong composite product.

Prian and Barkatt (1999) performed a series of measurements on E-glass/vinyl ester bars. They concluded that when GFRP is subjected to aqueous environments the pH at the fibre/matrix interface will increase due to leaching out of alkaline components from the silicate glass fibres, and that can enhance attack on the fibres. Moreover, high pH leads to rapid fibre dissolution, followed by interface de-bonding.

Bakis *et al.* (1998) examined the weight and cross sectional area changes due to conditioning (i.e., after immersion in saturated $Ca(OH)_2$ solution at 80°C for 28 days, and after 5 days of drying). The E-glass rod segments were made with three different resins, namely, 100% vinyl ester, 50% vinyl ester and 50% iso-polyester, and 20% vinyl

ester and 80% iso-polyester. They reported that the 100% vinyl ester segments lost the least amount of weight and cross sectional area during drying. In the light of that, they suggested a higher permeability of blended resin rods to moisture diffusion following the conditioning.

Another experimental method is the laser ultrasonic technique. It has been utilised to determine FRP's elastic constants and density non-destructively (Littles *et al.*, 1998a, b). Tracking the degradation (in terms of stiffness changes) of GFRP, after subjecting to environmental aging, with this technique together with another technique, namely 2D-FFT, is also possible (Dokun *et al.*, 2000).

Nguyen *et al.* (1997) tested the effect of water, simulated concrete pore (alkali) solution and salt solution at 60°C in terms of interlaminar shear strength (ILSS) on E-glass reinforcing three different polymers, which are epoxy, vinyl ester and isopolyester. The immersion time was up to 700 hours. At first, they observed reduction in the ILSS for all composites. Later, however, a stable situation of minimum ILSS was reached. The rate and the time of reaching the minimum were a function of the matrix as well as the test solution. Vinyl ester showed a better performance with respect to ILSS reduction after treatment than the other matrices.

According to Barkatt and Bank (1995), temperature is the most critical parameter used to accelerate the degradation of FRP subjected to moisture or chemical attack.

Most researchers believe that accelerated aging studies, such as exposing FRP samples to high pH environment at elevated temperature for relatively short time, can obviously never replace a real time and real surrounding for an aging investigation. Accelerated aging is an experimental tool that can provide indications, but not absolute answers, of the long-term behaviour in regard to FRP. Consequently, the results obtained from accelerated aging investigations must be analysed and interpreted with some caution.

In light of the above, a variety of different constituent materials are commercially available and the appropriate combination of these constituents allows for the

development of a FRP composite system that provides the performance attributes for its intended use.

2.3.7 Test techniques for mechanical properties of FRP

There are ways to test the mechanical properties of the FRP rebars such as shear, tensile and flexure. These techniques used are not necessarily similar to the ones used to test steel rebars. Moreover, there are standard tests proposed by organizations such as ASTM and British Standards.

All FRP rebars cannot be tested in tension using the same conventional gripping systems that are used for steel bars. This is because the traditional wedge-shaped frictional grips would actually apply high compressive stresses at the contact zone between the bar and the grips. As a result of that, premature failure will occur to the grip zone (ACI 440R-96, 1996).

In fact, several attempts to propose gripping systems have already succeeded to enable tensile testing of FRP bars without facing the problem mentioned earlier (Rahman *et al.*, 1993; Holte *et al.*, 1993; Erik and Rizkalla, 1993, and Tannous and Saadatmanesh, 1998). The majority of them involve embedding the ends of the bar into tubes filled with a matrix (e.g., epoxy mortar). Researchers seem to utilise systems they have developed themselves.

ASTM D 3916 developed an approach for tensile tests for pultruded thermosetting FRP bars for diameters ranging between 3.2 and 25.4 mm. Unfortunately, these tab adapters cannot be used with deformed and squared FRP bars.

Faza and GangaRao (1993) developed sand grips similar to those of ASTM D 3916 and suitable for deformed round bars, for providing bond between the bars and the grooves. The grooves were coated with an epoxy-sand mixture, and fine wet sand was used to fill the remaining gap between the bars and the grooves.

Castro and Carion (1998) did not recommend the use of epoxy resin as a gripping material. They attributed that to a messy operation and time consuming clean-up time after the test being done. On the other hand, they developed a successful system, after several trials, for gripping the ends of FRP bars in order to perform tensile tests. This system has several distinctive advantages, such as, the system is suitable for all bar types and sizes, i.e., smooth, deformed, round, square, etc, the system is inexpensive and relatively easy to perform. All it needs are steel tubes and a high-strength gypsum cement mortar to stick tight to both ends of the FRP bar so it can spread the shear stresses coming from the ordinary wedge grips of the testing machine. The researchers noticed that free length-to-bar-diameter ratios (L/d) in the range of 40-70 had no statistically significant effect on the mean strength.

Several tests in uniaxial tension revealed elastically linear behaviour for the GFRP rebars up to failure (Chaallal and Benmokrane, 1996; and Tannous and Saadatmanesh, 1998). The tensile test that was conducted by Faza, and GangaRao, (1993) showed linearity in stress-strain curve up to 95-98% of the ultimate failure load.

Clarke and Sheard (1998) suggested that tensile strength test is not the best way of monitoring the quality control, due to its insensitivity to determine the fibre/matrix bonding. Instead other test techniques can be used such as the interlaminar shear strength test.

Other researchers have used the same technique, namely, the interlaminar shear strength test, to monitor durability of FRP bars (Nguyen *et al.* 1997, Sheard, *et al.*, 1997).

Other studies propose another important way to test the mechanical properties and monitor changes of FRP when exposed to damaging environments, which is the bending test.

Nishizaki and Meiarashi (2002), examined the effect of water and moisture at 40 and 60°C on the durability GFRP by observing changes in bending strength. The bending strength was found to be lower compared to initial bending strength values. The rate of reductions in bending strength were greater in a 60°C water-immersion condition

compared to both a 40°C water-immersion condition and a 60°C moist-atmosphere condition. The difference was attributed to fibre/resin debonding in water at 60°C.

Sonawala and Spontak (1996) examined two types of GFRP laminates in bending after being immersed in brine and NaOH solutions for 270 days at 25°C. The bending strength of GFRP exposed to both solutions fell compared to initial bending strength values.

Both flexural strength and flexural modulus depend on the properties of the fibres while interlaminar shear strength and the shear modulus depend mainly on the properties of the matrix and the fibre/matrix interface (Adimi and Boukhili, 1998).

Most of standards require for each type of mechanical testing (e.g., tensile, compression, or flexural test) a number of at least five specimens. However, some researchers examine three specimens only, for instance, Chaallal and Benmokrane, (1996); and Ehsani *et al.*, (1995).

2.3.8 Flexural behaviour of concrete reinforced with FRP

Benmokrane *et al.*, (1995) observed larger and deeper cracks in concrete beams reinforced with GFRP rebars than in those reinforced with steel, due to low modulus of elasticity of GFRP compared to steel rebars.

Alsayed (1998) published a paper that presented the results of the comparisons made between the numerical and experimental load-deflection relationship of concrete beams reinforced by GFRP bars and by steel bars. The numerical computations were carried out using three models. The key factors considered in the experimental study included the reinforcing material type (steel and GFRP), the deflection limit at service load, and the concrete ultimate compressive strength. The author concluded that the current ACI model for predicting the load-deflection relationship for steel reinforcing beams underestimates the actual deflection of GFRP reinforcing beams. Moreover, the deflection at service load for GFRP-RC beams may control the design of FRP-RC structures. The average ratio of the measured service load deflection of GFRP-RC

beams to that of steel-RC beams of the same ultimate flexural capacity and the same dimensions is about 2, which is with agreement with (Ehsani, 1993; and Brown, and Bartholomew, 1993).

Al-Salloum *et al.* (2000) agreed with the foregoing (Alsayed, 1998) when they investigated the ability of using the ACI model as well as some modified models available in the literature to predict deflection at service load for beams reinforced with GFRP. They proposed a model to predict the deflection at service load for beams reinforced with FRP. Then those models were compared with experimental results and showed that the ACI model underestimates the measured deflections and the proposed model correlated well with the measured deflection.

Grace *et al.* (1998) studied the behaviour of beams reinforced with FRP. It was concluded that the use of GFRP stirrups instead of steel ones increased the shear deformation, and in turn, the deformation increased.

The non-ductile behaviour of FRP reinforcement necessitates a reconsideration of the flexural design philosophy of steel reinforced concrete elements, namely under reinforcement to ensure yielding of steel before crushing of concrete.

Theriault, and Benmokrane (1998); Burgoyne (1997); and Nanni (1993) believed that the concrete crushing failure mode (i.e., over reinforcement) is more desirable for flexural members reinforced with FRP rebars, because the member in this case exhibit some plastic behaviour before failure. While for FRP reinforcement rupture mode, the failure was sudden and catastrophic.

Sanhdars and Oehlers (2000) managed to overcome the problem of brittle behaviour of beams reinforced with FRP. When placing FRP bars in the compression zone of the beams, they behave in ductile fashion. That is because FRP bars in the compression zone takeover from the crushed concrete. Nonetheless, ACI 440.1R-01 (2001) does not recommend using FRP as longitudinal reinforcement in columns or as compression reinforcement in flexural members.

Moreover, Benmokrane *et al.* (1995) highlighted the importance of span-to-height ratio in controlling the deflection and crack width of beams reinforced with GFRP rebars, namely, as the span-to-height ratio decreases, the ratio of GFRP-reinforce-beams deflection to steel-reinforce-beams deflection also decreases. Therefore, the span-to-height ratio will play a very important role in design procedure.

Burgoyne (1993) concluded that beams reinforced with FRP will be unable to use the full strain capacity of the rebars to avoid unacceptable curvature. Therefore, it is unlikely there will be a problem caused by rebars snapping due to the lack of ductility.

To compensate for the lack of ductility then, the member should possess a higher reserve of strength (ACI 440.1R-01, 2001), that can be achieved by using higher margin of safety against failure than that used in steel reinforced concrete design.

2.3.9 Compression characteristics of FRP rebars and concrete reinforced by FRP

FRP rebars including GFRP are weaker in compression than in tension and is subject to variation depending on whether the rebar is smooth or with surface treatment. In general, FRP rebars compression behaviour shows a linear stress-strain relation for smooth rebars, while a slight deviation from linearity is observed for ribbed rebars (Faza and GangaRao, 1993; Kobayashi and Fujisaki, 1995; and Wu, 1990). Moreover, higher compressive strengths are expected for rebars with higher tensile strengths (Ehsani, 1993).

Wu (1990) reported a compressive strength ranging from 320 to 470 MPa for rebars having a tensile strength in the range of 550-900 MPa with failure mode includes transverse tensile failure, fibre micro-buckling, or even shear failure. The mode of failure depends on the type of fibres, the fibre volume fraction, and the type of resin. Some studies suggested that the compressive strengths of GFRP, CFRP, and AFRP are 55, 78, and 20% of the tensile strengths, respectively (Wu, 1990; and Mallick, 1988).

It is typical for composites including FRP to have different stiffness values in tension and compression (Faza and GangaRao, 1993). The compressive stiffness for FRP rebars appears to be smaller than its tensile modulus of elasticity (Wu, 1990). According to literature the compressive modulus of elasticity is between 77 and 80% of the tensile modulus of elasticity for GFRP (Bedard, 1992; and Mallick, 1988). The lower values of modulus of elasticity could be related to the premature failure in the test resulting from internal fibre micro-buckling under compressive loading (ACI 440.1R-01, 2001). Nevertheless, Chaallal and Benmokrane (1996) concluded a modulus of elasticity of 42GPa in tension and 43GPa in compression for GFRP rebars.

As mentioned earlier, ACI 440.1R-01 (2001) does not recommend using FRP as longitudinal reinforcement in columns or as compression reinforcement in flexural members. Furthermore, Almusallam *et al.*, (1997) stated that the strength of any FRP rebars in compression should be ignored in design calculation.

In some cases, nevertheless, avoiding placing FRP bars in the compression zone of flexural members is not possible, such as the supports of continuous beams or where bars secure the stirrups in place. In these cases, ACI 440.1R-01 (2001) suggests that confinement should be considered for the FRP rebars in compression regions to prevent their instability and to minimise the effect of the relatively high transverse expansion of some types of FRP rebars.

The author is not entirely sure why they have come to this conclusion. Because presumably although the bars, some times, could have inferior figures in compression, one would have a characteristic value and design the required compression loadings around it. Besides, most of the literature that is against utilising FRP in compression zones accepts the opinion mentioned in one source, namely Almusallam *et al.*, (1997).

In addition, Sanhdars and Oehlers (2000) have another thought, they recommended placing FRP bars in the compression zone of the beams to enhance the beams' ductile behaviour.

ASTM D695-96 is a standard test method to characterise the compressive behaviour of FRP bars.

2.3.10 Admixture

Neville and Brooks (1998) stated that a very high strength concrete (i.e., as high as 100MPa or even more) can be obtained when superplasticising is added to concrete. Regarding workability, however, the influence of superplasticisers on concrete disappears after some 30 to 90 minutes.

Brooks (1989) highlighted the difficulty of assessment the influence of admixtures on creep and shrinkage. That is referable to a very small amount of data, and the use of admixtures allows changes in mix proportions, which might affect the deformations. To overcome this problem, an approximate method was proposed for estimating changes in creep and shrinkage of plain concrete when mix proportions change and when the admixtures are used as water and cement reducers. Therefore, the influence on deformations is isolated from the influence of w/c ratio and cement paste content.

Rixom and Mailvaganam, (1999) reported based on previous studies that shrinkage and creep results of both plain concrete and concrete contains superplasticisers are similar.

Kristiawan (2002) concluded that the use of shrinkage reducing admixture (SRA) in concrete reduces the drying shrinkage.

2.4 Aging mechanism

2.4.1 Moisture/solution effects

Since FRP composites are used in the civil infrastructure, the composite components are likely to experience, to some extent, exposure to rain, moisture, or even diffused solutions passing through other infrastructure elements (for example concrete). The determination of the consequences of such contact, especially when prolonged time periods are considered, is of critical importance.

In fact, attacking glass by water or any other near neutral solutions is less damaging than for alkali, and similar to acid attack. It usually involves two processes, namely, ion exchange and silica network destruction (Adams, 1984 and Doremus *et al.*, 1983).

Ion exchange takes place when alkali ions in the glass exchange with hydrogen bearing from the water:

Na^+ (glass) + $2H_2O = H_3O^+$ (glass) + $Na^+ + OH^-$,

where H_3O^+ is the hydronium.

Silica network destruction occurs when surface of the glass dissolves in water:

H_2O + Si-O-Si = SiOH + HOSi

It maybe worth mentioning that some silicate glasses, when reacting with water, develop layers on their surfaces which have greater ionic mobility than dry glass, leading to more rapid reaction of water with glasses that develop the layer. Moreover, aqueous attack can easily lead to alkaline attack (when pH reaches between 8 and 11) but not as high as alkalinity of concrete (Doremus *et al.*, 1983).

As far as FRP is concerned, things are more complicated when FRP composites are immersed in water. Prian and Barkatt (1999) tested FRP composites in de-ionised water and concluded the following:

1. The composite will release *acrylic acid* into the leachate solution. This phenomenon increases as the temperature increase. As a result, the pH of the aqueous medium in contact with the composite (matrix) will decrease, due to hydrolysis of the matrix.

2. The pH at the internal fibre/matrix interface will go up due to leaching out of alkaline components from the silicate glass fibres, leading to enhanced attack on the fibres in the interface region.

3. Interfacial de-bonding resulting from water clustering and the dissolution of silica network from the fibres, this phenomenon increasing with elevated pH.

2.4.2 pH Effects

FRP composites are likely to be used in the civil infrastructure with concrete in a variety of forms, such as embedded in concrete, bonded to concrete or encapsulating concrete. The problem is that concrete has pore water with pH up to 13.5 which is not good news for durability concerns of FRP composites.

It was reported (Adams, 1984) that the corrosion of glass can be either etching process, leaching process or a combination of both. Etching is usually characterised as alkaline attack, which involves the silica network destruction. On the other hand, leaching is usually characterised as acid attack, which includes ion exchange (i.e., hydrogen or hydronium ions exchange for alkali and other positively charged mobile ions in the glass: Na^+ (glass) + HCl = H^+ + NaCl

With regard to FRP composites, an elevated pH can cause a rapid attack to both the fibres and the matrix, in the form of:

1. Rapid fibre dissolution, followed by interface de-bonding.
2. Enhanced matrix hydrolysis and extraction of acrylic acid.

From the above, the susceptibility of the acrylic acid of the matrix to hydrolysis can be expected to be enhanced by the alkali extracted from the fibres in the interface region.

As mentioned earlier regarding the loss acrylic acid from the matrix when exposed to water, it is actually more severe in alkali media than in water.

2.4.3 Brine Effects

The derogatory effect of NaCl salt on GFRP bar properties is due principally to the presence of water (moist), which ingresses and permeates into the composite, carrying

with it Na^+ and Cl^- ions. Although the Cl^- ions are not as damaging to glass fibres as OH^- ions, they could adversely affect the matrix and the fibre/matrix bond.

The solubility of brine in composites varies depending on the structure of the composites. The temperature difference and the existence of salt in water have little effect on the equilibrium mass uptake of water in composites (Sonawala, and Spontak, 1996, and Tannous, and Saadatmanesh, 1998).

2.5 Summary

In this chapter some physical and mechanical properties of FRP have been reviewed and compared with steel rebars. In addition, a general review was carried out in relation to this study to gain more knowledge about FRP and to identify areas that have not been completely investigated, for instance, movement characteristics and durability.

The main findings of this review are:

1. Fibres, normally, do not exhibit much creep, while that is not true for most resins. Hence, due to the different constituent materials (fibre and resin) significantly different creep behaviour can be observed for different FRP materials. Furthermore, each type of FRP rebars exhibited a unique behaviour of creep failure depending on the degree of loading and the characteristic of the fibres, namely aramid, glass or carbon.

2. FRP composites exhibit creep at relatively high degree of loading, i.e., 60 % or more of its strength. In addition, the influence of creep is greater when the stresses are significantly large with off-axis of fibre orientation.

3. Long-term testing of shallow concrete beams reinforced with GFRP showed greater deflection, namely, 1.7 times of those of beams reinforced by steel due to creep and shrinkage.

4. Bond between FRP rebars and concrete is developed through a mechanism similar to that of steel reinforcement and is a function of: concrete cover, FRP type, elastic modulus, development length (together with tail length and radius of

bend for hooked rebars), surface deformation, diameter, and microstructure of the rebars. Furthermore, bond capacity can be measured by using both pull-out and beam tests. However, the latter is preferable because the result of pull-out test overestimates the true result.

5. In order to achieve the largest bond strength for 90° hooked GFRP rebars, the development length should be 16 times the bar diameter, and the tail length of 12 times the diameter. For straight bars the development should be at least 20 times the bar diameter, and this factor increases with the increase of the bar diameter.

6. The surface of the FRP plays a major role in bond with concrete, and any degradation of the composite reinforcement will result in decrease in bond strength. Moreover, several ways of creating surface deformation patterns for the rebars are used such as: helical wrapping, sand-coated, ribbed (could be glued ribs), or treating the surface to produce small deformation. Some researchers prefer the last pattern option. Presently, there is no standardised classification of surface deformation patterns.

7. Many researchers have developed equations to provide a conservative estimate of the development length of FRP rebars including ACI 440. It is recommended, however, that manufacturers develop alternative values of the required development length that suite their products most.

8. Most researchers who believe that compressive strength of concrete does not play a major role in bond capacity with FRP rebars had either conducted pull-out tests only, for instance Kachlakev and Lundy (1999); and Al-Zahrani *et al.*, (1999), or had not tested very strong concrete specimens. In most studies, the concrete strength was below 60MPa, also the difference between the concrete compressive strengths was not very big (Ehsani *et al.*, (1995); Ehsani *et al.*, (1997); Benmokrane *et al.*, (1995); Kachlakev and Lundy (1999); and Malvar, (1995)). In general, the influence of concrete compressive strength on bond strength has been underestimated and many authors do not include it in their investigation when examining the variables that could influence the bond

strength between concrete and FRP rebars. Moreover, ACI 440.1R-01 does not consider it in its proposed equation for determining the developing length of FRP in concrete.

9. In order to ensure long-lasting composites, an appropriate combination of these constituents, namely fibres and matrix resins should be used. Durable resins are those with high toughness that prevent microcracks and are able to keep diffusivity to minimal, for instance, most researchers are of the opinion that vinyl ester resins have superior protection to fibres due to alkalinity resistance and higher resistance to moisture ingress in comparison with other commodity resins. In general, high fibre content together with a good protection of resin should provide durable composites.

10. The adverse effects on the rebars due to alkaline solution are higher than that of cement paste because ions are free to travel. Furthermore, high temperature increases the degradation of GFRP because chemical reactions are enhanced at elevated temperatures. Consequently, the results obtained from accelerated aging investigations must be analysed and interpreted with some caution.

11. The addition of pozzolanic materials is thought to be effective in inhibiting the corrosion of GFRP rebars because they reduce alkalinity and inhibit the formation of $Ca(OH)_2$. Moreover, FRP reinforcement must be protected against moisture and UV.

12. There are several techniques to examine the mechanical properties of FRP rebars, each of which has strong and weak points.

13. Due to variation in the mechanical properties between steel and FRP rebars (such as, the stiffness of GFRP reinforcement is less than that of steel, GFRP is rather brittle and exhibits linear stress-strain relationship up to failure in tension, compression and flexure, while steel is ductile and yields before failure, and unlike steel, GFRP is weaker in compression than in tension in terms of strength and stiffness), the design philosophy of each one is not the same.

14. There are some technical suggestions to improve the mechanical properties of concrete elements reinforced with FRP rebars, for instance placing FRP bars in the compression zone of beams to make them behave in ductile fashion, also reducing the span-to-height ratio of beams reinforced with FRP would reduce the ratio of FRP-reinforced-beams deflection to steel-reinforced-beams deflection. Moreover, the use of high strength concrete (as high as 52MPa) should reduce the crack widths, eliminate the sudden propagation of the cracks towards the compression zone, and increase the ultimate moment capacity of beams element.

The areas identified of requiring investigation were:

1. Introductory examinations at the beginning to develop better understanding of the material's characteristics. These examinations include bond strength with concrete at different concrete strength having a relatively high concrete compressive strength (i.e., about 80MPa), flexural and compression characteristics of the GFRP rebars, and viewing the micro-structure of the material under the scanning electron microscopy (SEM). Finally, checking the possibility of studying the characteristics related to the pore size of the composite reinforcement including the pore size distribution, porosity and so on.

2. Monitoring potential changes in flexural properties including flexural strength and elastic modulus in flexure, and micro-structural properties through mercury intrusion porosimetry (MIP) test of GFRP specimen due to exposure to hostile solutions namely alkali and brine at different temperatures and for different ageing times. Finally, try to establish a correlation between changes in flexural properties and porosity.

3. Shrinkage and creep behaviours of control (non-reinforced) and reinforced concrete specimens by GFRP and steel rebars. In addition, testing similar specimens containing shrinkage reducing admixture (SRA). Finally, draw a comparison between the movements that were determined experimentally and theoretically.

Chapter Three Experimental: Materials, Mix Design, and Hardened Concrete Testing

3.1 Introduction

In this chapter, information of the instrumentation and materials used in this study is presented including details of their sources and properties. The method used for the concrete mix design and the environmental condition under which the experiments are undertaken are also given.

3.2 Materials

3.2.1 Cement

The cement used throughout this research was Ordinary Portland Cement Type-I (OPC) conforming of the requirements of British Standards (BS 12:1996).

OPC is the main material used to combine the other components of concrete. It is manufactured from calcareous materials such as limestone, and from alumina and silica. In addition, marl is used which is a mixture of calcareous and clay minerals materials. During the manufacturing process these raw materials are ground up and then mixed before burning in large rotary kilns at high temperatures of about 1400°C. The material sinters and partially fuses to form clinker. This is then cooled and ground up into a fine powder. Gypsum is added during manufacturing and the end product is the cement (Neville and Brooks, 1998).

Cement in its anhydrous form is constituted of several different compounds including tricalcium silicate or alite (C_3S), dicalcium silicate or belite (C_2S), tricalcium aluminate (C_3A) and tetracalcium aluminoferrite (C_4AF). These hydrate at varying rates giving rise to different hydration products such as calcium-silicate-hydrate (C-S-H) and calcium hydroxide (CH).

In this investigation, the cement was supplied by Castle Cement Ltd in the United Kingdom in water-proof air-tight bags, to provide a better protection and minimise its deterioration with time. The main chemical composition and physical properties of the cement, as supplied by the manufacturer, are given in Table 3.1.

Table 3.1: Chemical composition and physical properties of OPC

Oxide composition	% by weight
CaO	63.63
SiO_2	21.03
Al_2O_3	4.73
Fe_2O_3	2.93
MgO	2.67
K_2O	0.65
Na_2O	0.3
SO_3	3
Compound composition	**% by weight**
C_3S	51.33
C_2S	21.14
C_3A	7.49
C_4AF	8.86
Physical properties	
Specific surface area	0.341 m^2/g
Specific gravity	3.15 g/cm^2

3.2.2 Fine aggregate (sand)

The fine aggregate used was natural quartzitic sand obtained from Tarmac Roadstone Ltd. A sieve analysis was carried out. The grading complied with zone M (medium) in BS 882: 1992. The general properties of the fine aggregates are shown in Table 3.2 based on sieve analysis test.

Table 3.2: Sieve analysis of fine aggregate

Sieve size	Percentage by mass passing BS sieves	
	BS 882 grading zone M for fine aggregate	Grading used in this research
2.36 mm	65 – 100	83.8
1.18 mm	45 – 100	77.9
600 μm	25 – 80	71.3
300 μm	5 – 48	19

3.2.3 Coarse aggregate

The coarse aggregate used was uncrushed quartzitic gravel with maximum size of 10 mm which had irregular shape and smooth surface texture. The gravel also came from Tarmac Roadstone Ltd. They were in surface-dry condition. The grading of the aggregates is given in Table 3.3 as obtained from sieve analysis test.

Table 3.3: Sieve analysis of coarse aggregate

Sieve size	Percentage by mass passing BS sieves	
	BS 882 range for graded coarse aggregate	Grading used in this research
14 mm	100	100
10 mm	85 – 100	96.7
5 mm	0 – 25	0.7
2.36 mm	0 – 5	0.14

3.2.4 Water

Local tap drinking water of the county of West Yorkshire was used in all the mixes.

3.2.5 Superplasticisers

Superplasticisers are classified as high range water-reducing agents, because they are produced from materials that allow higher workability of concrete mix, or lower water content along side with lower possibility of side effects (superplasticisers significantly reduce the amount of entrained air) (Neville and Brooks, 1998).

Superplasticising admixtures are an advancement and more effective type of the normal water-reducing admixtures (plasticizers) in that they disperse cement agglomerates more efficiently.

The three major types of raw materials used in superplasticisers are sulfonated naphthalene formaldehye (SNF), sulfonated melamine formaldehye (SMF), and polyacrylates, (Rixom and Mailvaganam, 1999). The first two are commonly used in practice, (Neville, 1998).

Within limits, the higher the molecular mass, the better the efficiency of the superplasticisers, (Neville, 1998).

In this study, one type of superplasticiser was used, it was added to the mix with w/c of 0.32 to increase workability. It complied with the requirements given in BS 5075: 1985. Glenium 51 possesses a unique chemical structure that allows higher levels of cement particle separation. The molecules consist of a carboxylic ether polymer with long side chains. At the beginning of mixing, the molecules allow the same electrostatic dispersion mechanism as used in traditional superplasticisers, however the side chains generate the so-called *steric hinderance* which, in turn, aids separation and dispersal of the cement particles. This provides a physical barrier between the cement grains, in addition to the electrostatic one.

The recommended dosage by the supplier is between 0.2 and 0.8 litre per 100kg of cement. Glenium 51 is free of chloride and low alkali, and according to the manufacturer it decreases the risk of shrinkage and creep (information taken from manufacturer's data sheet).

3.2.6 Shrinkage reducing admixture (SRA)

Shrinkage reducing admixture for concrete or virtually any portland cement based material which reduces the materials shrinkage due to drying.

The admixture used in this investigation is called Eclipse®, and it is in the form of liquid admixture. Eclipse contains no expansive material, but instead acts chemically to attack the primary mechanism causing shrinkage. One litre of Eclipse shrinkage reducing admixture weighs approximately 0.93kg.

Drying shrinkage of concrete is a function of several mechanisms. The primary driver in the predominant mechanism causing shrinkage for internal relative humidities in excess of 40% is the surface tension of water. As water-filled pores in the size range between 2.5 and 50nm (or one billionth of a metre) lose moisture, curved menisci are formed and the surface tension of water pulls the walls of the pores. In the case of pores greater than 50nm, the magnitude of the tensile force becomes negligible compared to the size of the pore; and in the other case, namely pores smaller than 2.5nm, the tiny size will not support the formation meniscus. Eclipse reduces the surface tension of water. With reduced surface tension, the force pulling in on the walls of the pores is therefore reduced, and the resultant shrinkage strain is reduced too. With Eclipse at a dosage of 2% by weight of cement (which is the recommended addition rate), this effect results in ultimate shrinkage reductions on the order of 25 to 50%.

When it is added to a mix it will contribute to the overall porosity of the concrete in the same fashion that same amount of water will do. In addition, the effect on concrete slump will be virtually the same as the equivalent volume of water. It is therefore recommended that Eclipse should replace an equal volume of water in any mix.

In addition its drying shrinkage, this admixture can have another impact on hardened concrete properties. It may cause a reduction in concrete compressive strengths. These reductions vary from 0 to 15% depending on the mixture and materials used. Typical reduction is about 10% or even less.

Eclipse may be introduced at any time in the batching cycle, but delayed addition is recommended (information taken from manufacturer's data sheet).

3.2.7 Reinforcement

3.2.7.1 Steel reinforcing bar

The steel rebar used in this study was 8 mm deformed diameter. Due to the difficulty of fixing strain gauges on the ribs of the deformed bars some positions on the bar's surface were machined and treated with chemical solutions in order to smoothen the surface and remove greases from the area where the strain gauges where to be fitted.

3.2.7.2 GFRP reinforcing bar

A pultruded profile consists of a high volume fraction of reinforcing fibre (i.e. fibre volume fraction of around 65%) encapsulated in an organic resin matrix. The major components are glass fibre reinforcement in a Bisphenol A based vinyl ester urethane resin matrix with a glass transition temperature (Tg) of 130°C. The resin mix also contains an internal release agent and may contain pigment and inert filler. The final product is a rod of 8mm square with a uniform surface texture with 0.5mm deep. The surface deformation can be obtained by wrapping an additional resin-impregnated strand around the rebar prior to entering or after coming out of the heated die to enhance the mechanical bond to concrete. The rebars were produced and provided by Fibre-Force in the UK.

The pultruded profile is not flammable or easily ignited but will burn in a fire. It is stiff and strong, does not conduct heat or electricity, and is chemically inert. Moreover it is considered very stable and not biodegradable (information taken from manufacturer's data sheet). Plate 3.1 shows the GFRP bar used in this investigation. For the pultrusion process, refer to Fig. 1.1, Section 1.3.

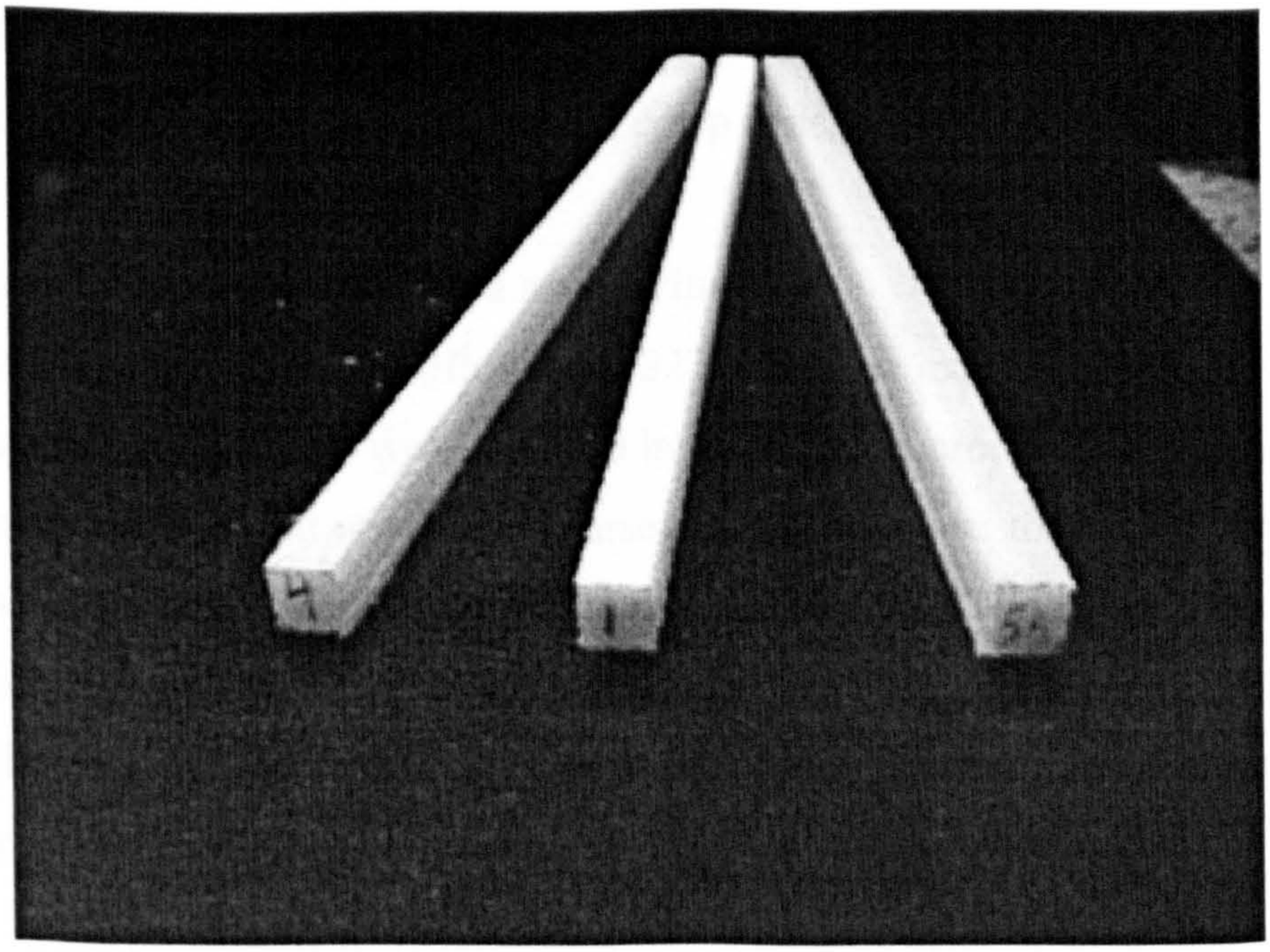

Plate 3.1: GFRP rebar specimens

Vinyl ester resin is the common name of a series of unsaturated resins. Its corrosion resistance and mechanical properties are much improved over standard polyester resin composites (Pepper, 2001).

In addition, vinyl ester is chemically similar to unsaturated polyesters and epoxy resins, and was developed as a compromise between the two materials, providing the simplicity and low cost of polyesters and the thermal and mechanical properties of epoxies.

3.3 Mix design of concrete

In order to perform this study different concrete mixes were prepared. The proportions of fine aggregate, coarse aggregate, and cement content for all the concrete mixes were kept constant, namely 1 part cement, 2 parts fine aggregate, and 3 parts coarse aggregate by mass, the only variable being the water cement ratio in order to get different compressive strengths.

For the bond capacity test, two mixes were used. One mix was with w/c ratio of 0.6 (to give normal concrete strength) and the other was 0.32 (to give a high performance

concrete). To achieve a reasonable workability Glenium 51 superplasticiser was added to the latter mix. Finally, for shrinkage and creep tests, the w/c ratio was 0.5.

3.4 Concrete specimen preparation and curing

Concrete was mixed in a "Cumflow – 5122" mixer of capacity of 0.1m^3. For each concrete mix the constituents were weighed in the required proportions and placed in the mixer in the order: cement, sand, and coarse aggregate. Then they were mixed dry for the first minute to homogenise the batched materials, then water was added and wet mixing took place for three minutes. The superplasticiser was added if needed to the mix (i.e., the one with a w/c ratio = 0.32) in two steps, the first half being added to the water prior to pour and the other half being added during the wet mixing.

The moulds were filled in layers to produce 100mm cubes and 100×100×500mm prisms. The concrete was compacted by means of vibrating table machine at a frequency of 50Hz, and then the top surfaces of the specimens were trowelled off after the occurrence of the initial set and covered with wet mats, polythene sheets being used to prevent evaporation of water.

The following day, the specimens were stripped (de-moulded) and cured in a controlled fog room at a temperature and relative humidity conditions of 20°C ± 2°C and 95-99% respectively. The concrete specimens were left to cure in the fog room until the date of testing.

Prior to casting the concrete specimens, two workability tests (i.e., slump test, and flowtable test) on fresh concrete were carried out. Workability is defined according to Neville and Brooks (1998) "the amount of useful internal work necessary to produce full compaction". The slump test was performed in accordance with BS 1881: Part 102: 1983, while flowtable test was performed in accordance with BS 1881: Part 105: 1984. A flowing concrete usually possesses a flowtable spread value between 500 and 600 mm. The 100mm cubes were used to obtain compressive strength, and the 100×100×500mm prisms to obtain tensile strength (modulus of rupture).

For each mix of joint-beam, cracked beam, and shrinkage specimens, three cubes and two prisms were made and cured under the same conditions of those test beams and specimens.

3.5 Properties of concrete

For the investigation of the mechanical properties of hardened concrete, two tests were carried out, namely compressive strength and flexural strength (4 point bending test). A summary of the main procedures adopted for each test is presented, with reference made to the appropriate British Standards procedures where necessary. Workability tests were performed on the concrete before setting, namely flow table or slump tests. Results are presented later in Table 3.4.

3.5.1 Compressive strength

This is one of the tests which are designed to establish the mechanical properties of concrete. In this test, a 100mm cube is subjected to a gradually applied load, until compressive mechanical failure of the cube occurs. At the failure point, the force was recorded. Three cubes from each mix type were tested and the average of the three was taken as the compressive strength value. The machine used for testing is a Tonipact 3000 (complies with BS1881: Part 117, 1983). The cubes were manufactured and the tests were completed in accordance to BS1881: Part 108 (1983) and BS1881: Part 116 (1983), respectively.

3.5.2 Flexural strength

This test is a four point bending test. Two specimens (prisms) were tested for each concrete type and an average of the results was calculated. The prisms were subjected to a gradually applied load, until flexural failure occurred. At the failure point, the force was recorded. The machine used for testing is a Tonipact 3000 as well, but this time a different module of the apparatus was used.

Specimen set-up for the test is illustrated in Fig. 3.2. In this setting, which complies with BS1881: Part 118, 1983, fracture should occur between the top loading rollers indicated in Fig. 3.2.

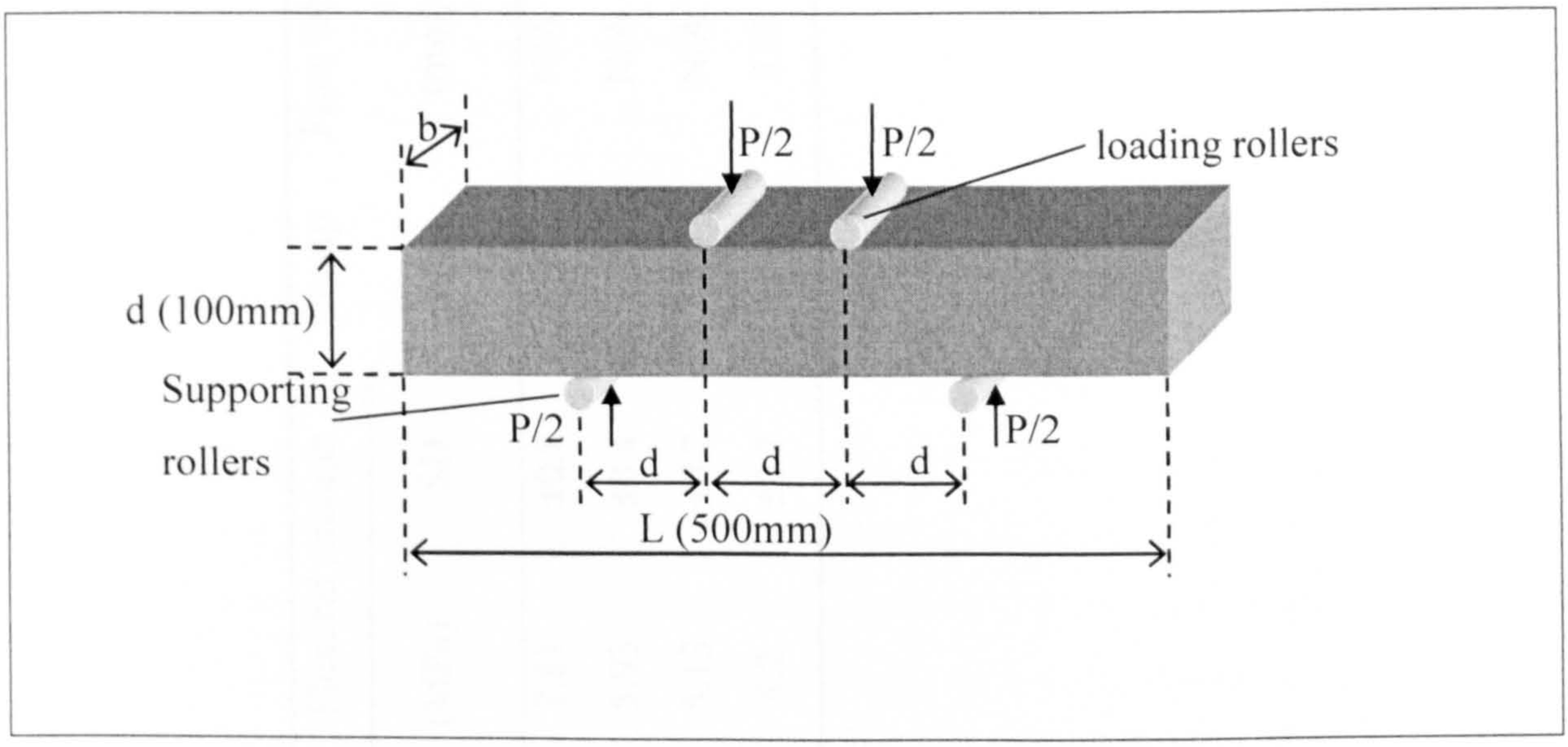

Figure 3.1: Flexural strength test arrangement

To calculate the modulus of rupture or flexural strength the following formula is applied:

$$fb = \frac{P \times (3 \times d)}{b \times d^2} \times 10^3 \qquad (3.1)$$

Where

fb = modulus of rupture or flexural strength (N/mm^2).

P = failure load (kN).

d = depth (100 mm).

b = width (100 mm).

Table 3.4: Properties of concrete

Mix №	Concrete Type			Age	Compressive strength		Flexural strength		Slump	Flow table
	w/c ratio	Superplasticizer	SRA	(days)	(MPa)	SD	(MPa)	SD	(mm)	(mm)
1	0.32	1 %	0 %	28	80	±0.9	7.81	±0.8	15	N/A
2	0.5	0 %	0 %	28	62	±0.9	5.93	±0.4	75	N/A
3	0.5	0 %	2 %	28	49	±1.3	5.13	±0.2	75	N/A
4	0.6	0 %	0 %	28	45	±0.5	4.2	±0.7	N/A	532

Where

SD = standard deviation

SRA = shrinkage reducing admixture

3.6 Instrumentation

The strain and deflection measurements on the joint-beam and shrinkage/creep specimens tests are described below.

3.6.1 Strain measurement

The strains, which generate in the reinforcement during loading, were measured in some experiments by using either extensometer or electrical resistance strain gauges installed on the rebars. The extensometer was connected to the Instron machine. While the electrical strain gauges were connected to an Intercole Compulog data logging system. The electrical strain gauges are produced by Kyowa with length of 2mm, gauge resistance of $120.2 \pm 0.2\Omega$ and gauge factor of $2.11 \pm 1.0\%$.

For the steel rebars, ribs were machined to be removed from small area (10mm length) to install the strain gauges and terminators. Similar step was accomplished in the case of GFRP, but because the surface is relatively smooth, the profile on the rebar's surface was flattened by using different sets of sand paper. After fixing the strain gauges, they were connected to electrical wires then were painted with a waterproof layer. Finally, the treated area was enclosed with a heat shrinking tube to provide protection against any physical damage. In general, using the electrical resistance strain gauge is not preferred for creep measurement due to the possible creep of the bonding material (Neville, 1970).

Concrete strain for shrinkage and creep specimens was measured by using a 150mm demountable Demec gauge mechanical extensometer. The gauge points were stainless steel inserts glued with epoxy cement to the concrete.

3.6.2 Deflection and end-slip measurements

Deflection at the mid-span position of the joint-beams was measured by two LVDTs with a resolution of 0.01mm. Additionally, one LVDT was installed on the rebar either side of the joint-beam to measure the slips at the free ends of the reinforcing bar.

Chapter Four Experimental: Engineering Properties and Pore Structure Studies

4.1 Introduction

In this chapter the introductory examinations are described, which were done at the beginning to develop familiarity with the material's characteristics and gain experience into the possible ways of further testing for this material. The tests were bond strength with concrete, flexural and compressive strengths, and micro-structural aspects together with observations of the micro-structure of the material under the scanning electron microscopy (SEM).

In addition, a detailed coverage was undertaken of the ability of glass fibres reinforced polymers bars to cope in what should be considered unpleasant surroundings during its service life in a structure. This was achieved by monitoring changes in flexural characteristics, representing a mechanical property, and the manner in which pores are distributed with respect to pore size and structure. Moreover, the total porosity was determined using mercury intrusion porosimetry (MIP). Pore size distribution and porosity measurements for GFRP segments were carried out on both aged and not-aged (as received) samples. Finally, descriptions of the experimental procedures are also included.

4.2 Introductory testing

Several tests related to GFRP rebars are presented in this chapter for the introductory testing programme designed to increase the level of understanding of this material and to examine the possibility of setting new test techniques to monitor its reaction to hostile solutions later on in this investigation program. These introductory tests included bond strength with concrete, flexural strength of GFRP rebars, micro-structural aspects and scanning electron microscopy (SEM). All these tests took place on not-aged specimens of GFRP composites.

4.2.1 Bond strength test

A preliminary test that measures bond capacity between concrete and reinforcement is vital. This test should help in understanding one of the most important behaviours of concrete and its reinforcement.

4.2.1.1 Apparatus

An Instron 8500 testing machine was used because it could be properly calibrated and operated at constant rates of crosshead motion, and also it allowed relative displacement of the loading nose with respect to the supports at a constant speed.

4.2.1.2 Description of test specimen

After reviewing the previous literature regarding bond tests, a special arrangement for the so called joint-beam was made. The joint-beam consists of two rectangular reinforced concrete blocks jointed at the top by a steel roller joint and at the bottom by a reinforcement bar to be tested for bond with concrete, as performed in the RILEM specifications for testing beams (RILEM, 1978) and illustrated in Fig.4.1. One part of the reinforcement was anchored in each block while the remaining part was isolated from the concrete using a plastic tube around the reinforcement, which eliminated the effect of the support reactions on the bond behaviour of the reinforcing bar. Auxiliary and shear reinforcement were provided by 8 mm hot-rolled mild steel bar. The shear reinforcement was bent into closed links (stirrups), the details are shown in Fig. 4.2. These reinforcements were used in flexural test for joint-beams as described in the RILEM specifications for testing beams (RILEM, 1978). The strain in the reinforcement was measured using electrical resistance strain gauge that was glued on the surface of the bar in the middle part of the reinforcement. Slippage at the free ends of the reinforcing bar was measured using two LVDTs. Finally, two LVDTs were installed as close as possible (75 mm either side from the middle span) to the middle span of the beam to detect deflection. Two rollers were placed to support the beam at the ends of the effective span, and another two rollers were placed in the top of the beam

at a distance of 75 mm from the middle span to support the load spreader steel beam. The joint-beams were simply supported and loaded in bending by two equal forces applied symmetrically on either side of the roller joint. The strain in the reinforcement at mid-span as well as the slip at both free ends were measured after each increment of applied load.

4.2.1.3 Test Procedure

As it was mentioned earlier the bond strength test was performed according to the RILEM specifications for testing beams (RILEM, 1978).

After setting up the beams and just before application of load, the beams were checked carefully for any cracks either due to shrinkage or miss-handling during transportation. Also, the strain gauge and the alignment of the rebar that links both blocks of the beam were checked. The jack was centred over the beam and then the steel load spreader beam was placed in its position. The strain and deflection readings were taken.

The load was applied as a function of tensile stress in the bar as it is specified in RILEM 1978. The incremental stress (f_f) in the bar were: 0, 78.5, 157, 235.5, ... MPa. For each increment the total load (P) applied to the specimen is given by:

$$P = \frac{A_b \times f_f}{1.25} \tag{4.1}$$

Where, A_b = cross-sectional area of bar (A_b = 50.3 mm^2, for steel rebar and = 64 mm^2, for GFRP rebar).

The load increment was achieved in half a minute. At each increment the load was kept constant for two minutes to ensure stabilisation of the slip. The readings of strain, deflection, and relative end-slip were taken at each increment.

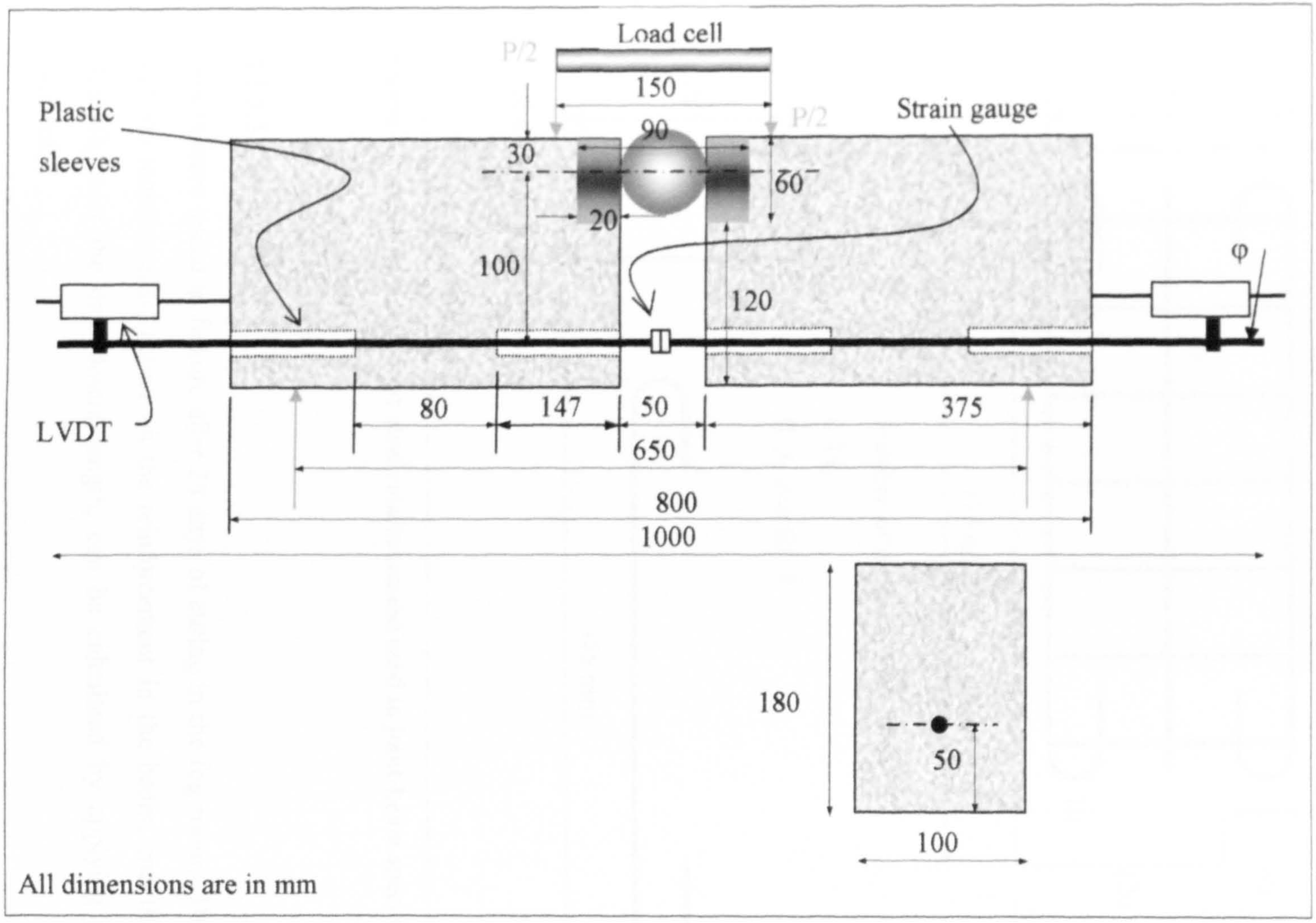

Figure 4.1: Details of joint-beam specimen for the bond strength test

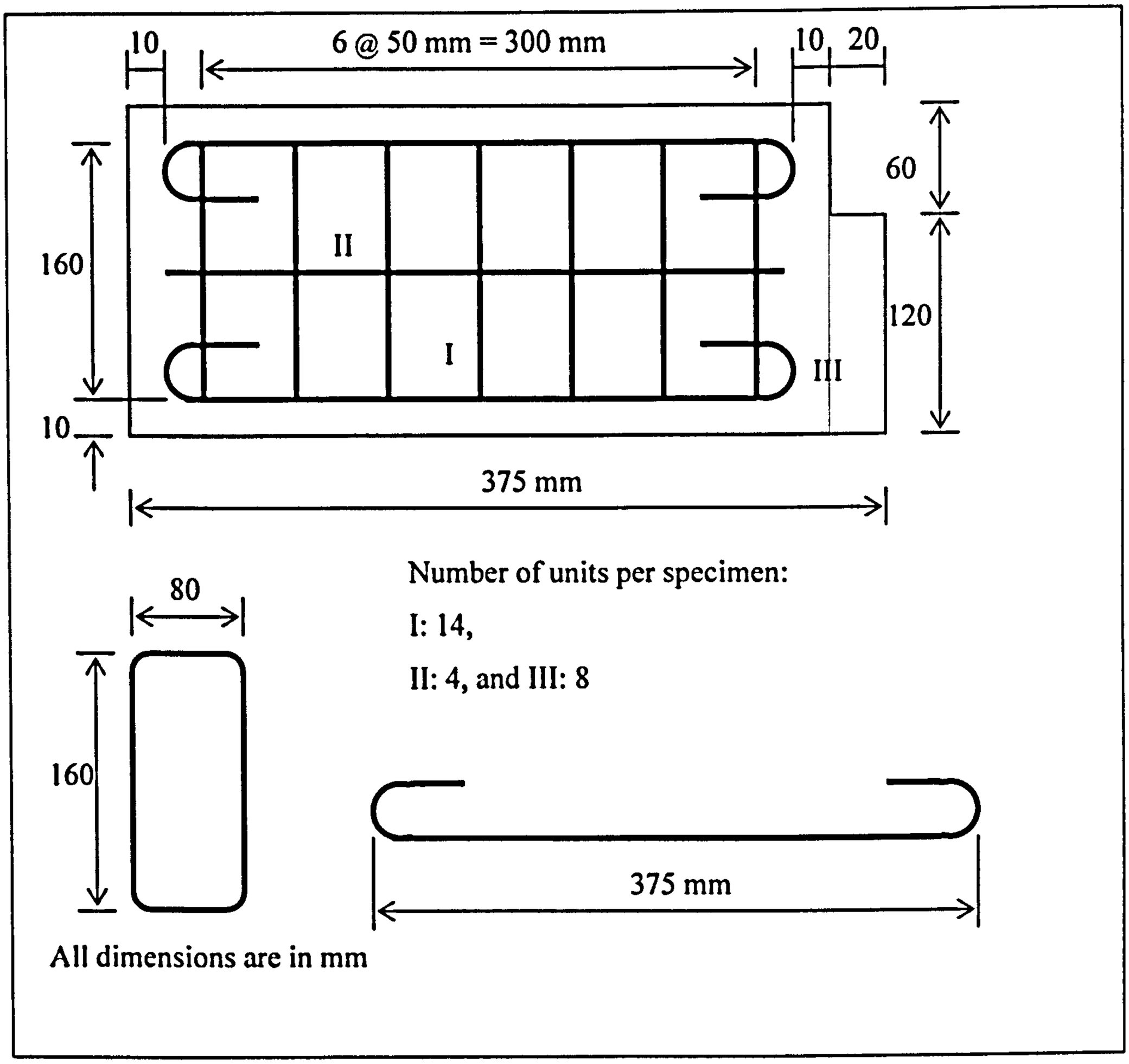

Figure 4.2: Auxiliary and shear steel reinforcement used in joint-beam specimens

4.2.1.3 Calculations

Beams were tested in flexure after 28 days of curing in the fog room. The tensile load and the tensile stress, acting on the reinforcement in the beam, and the mean bond strength, over the embedment length, can be calculated by applying pure bending moment:

$$T = \frac{M}{z} \tag{4.2}$$

$$f_f = \frac{T}{A_b} \tag{4.3}$$

$$T = (P/2) \times (a/z) = 1.25 \times P, \text{ where } a = 250 \text{ mm and } z = 100 \text{ mm} \tag{4.4}$$

$$\mu = \frac{T}{\pi \times d_b \times l} \text{ (for a square bar the term } (\pi \times d_b) \text{ is replaced by } (4 \times b)) \tag{4.5}$$

Where, T = is the resultant tensile force in the reinforcement (N); M = is the moment resulting from the applied load (N mm); a = is the distance between the applied load on one block and the support; z = is the lever arm between the resultant forces T and C; C = is the resultant compressive force in the concrete (N); f_f = is the tensile stress in the reinforcement (MPa); A_b = is the cross section area of the reinforcing bar (mm^2); μ = is the average bond strength (MPa); d_b = is the bar diameter (mm); and l = is the embedment length (mm), as shown in Fig. 4.3.

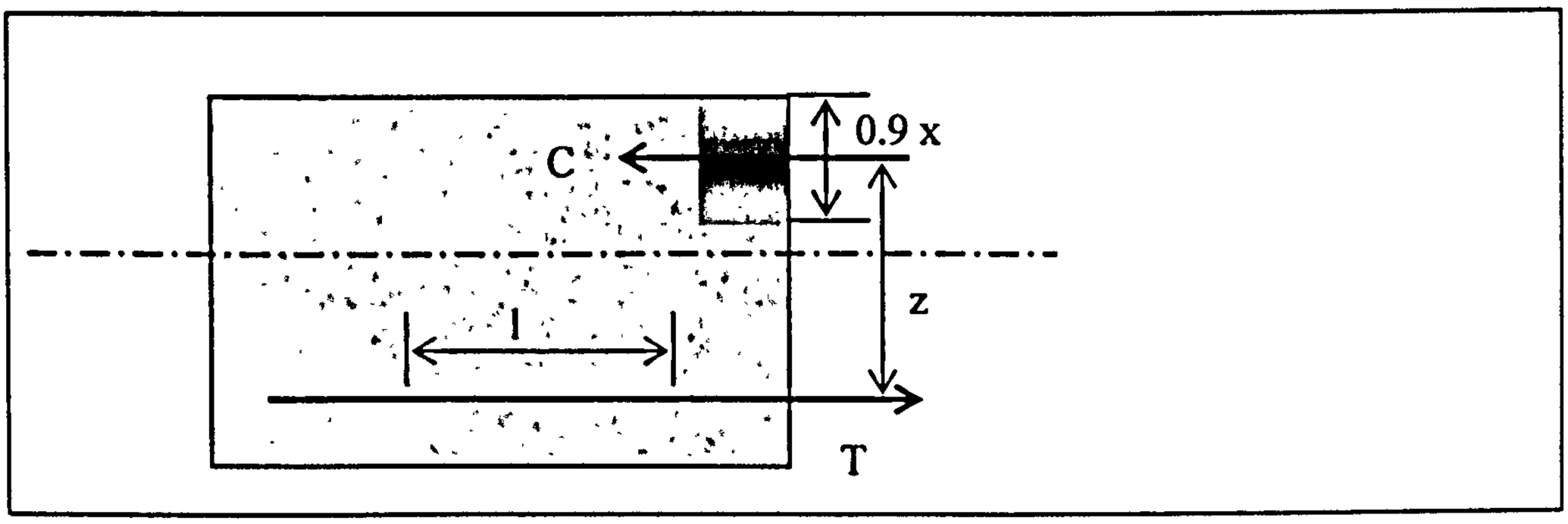

Figure 4.3: Singly reinforced section with rectangular stress block

4.2.2 Flexural characteristics of GFRP bars

4.2.2.1 Introduction to flexural test

The test method used for the determination of the flexural properties of GFRP bars was to a combination of the tests of ASTM D 4476-97 and BS EN 2746:1998 with some modifications. Testing are carried out with three point bending fixtures designed to allow testing of the composite rebars with variable support span length in order to get the suitable one that guarantees flexural failure instead of interlaminar shear failure. The test details are shown in Fig. 4.4. The test was performed by using the Instron machine shown in Plate 4.1. A tested sample is shown in Plate 4.2.From a previous study (Adimi and Boukhili, 1998) suggested that, in flexure, the failure mode was

influenced by the length to depth ratio (i.e., at low ratios, the interlaminar shear failure was predominant while at high ratios the flexural failure was more frequent, and between these extremes the failure was a mixture of both). Different span lengths were tested until a flexural failure occurred. According to BS EN 2746:1998, the span length was insufficient to avoid a shear failure.

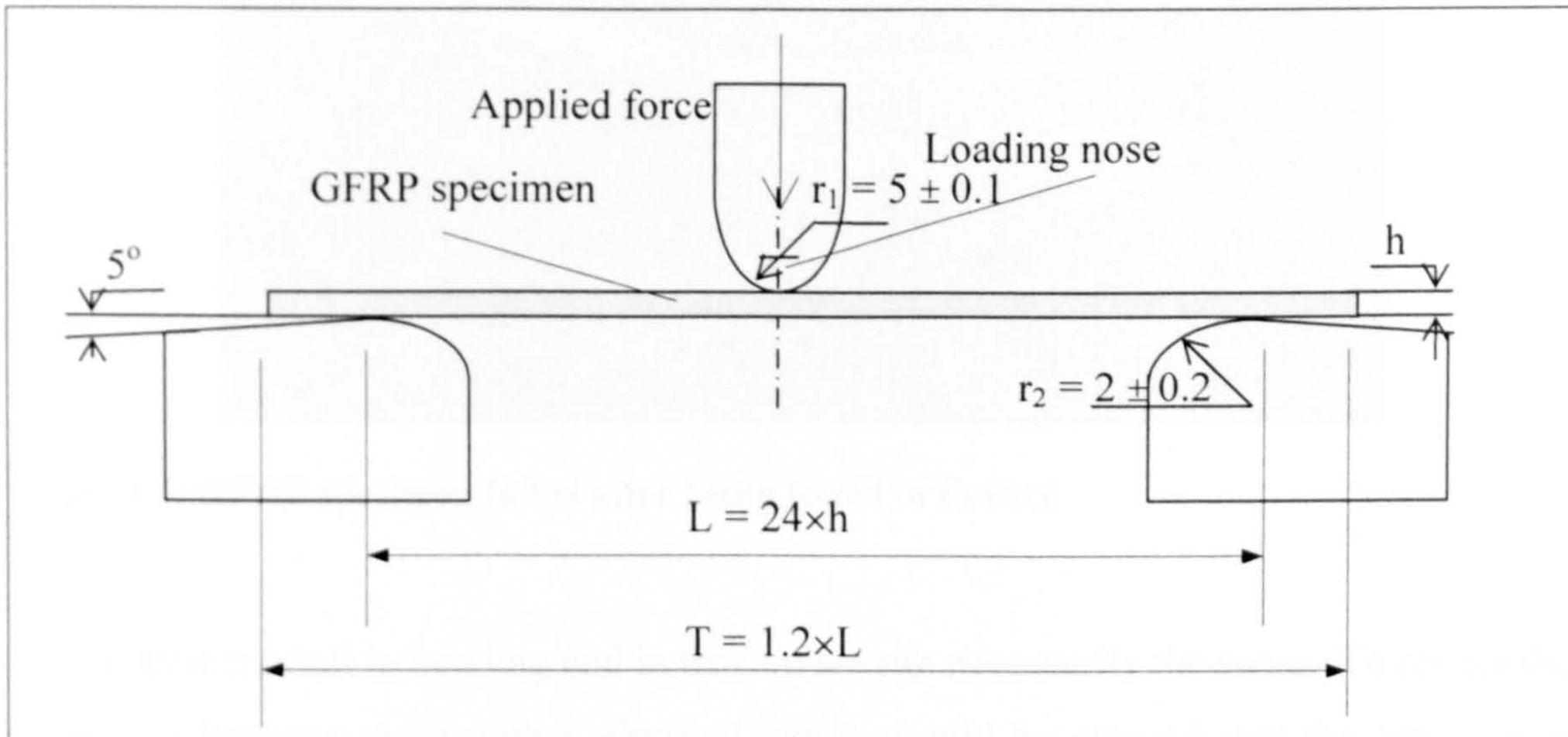

Figure 4.4: Details of flexural test for GFRP specimen

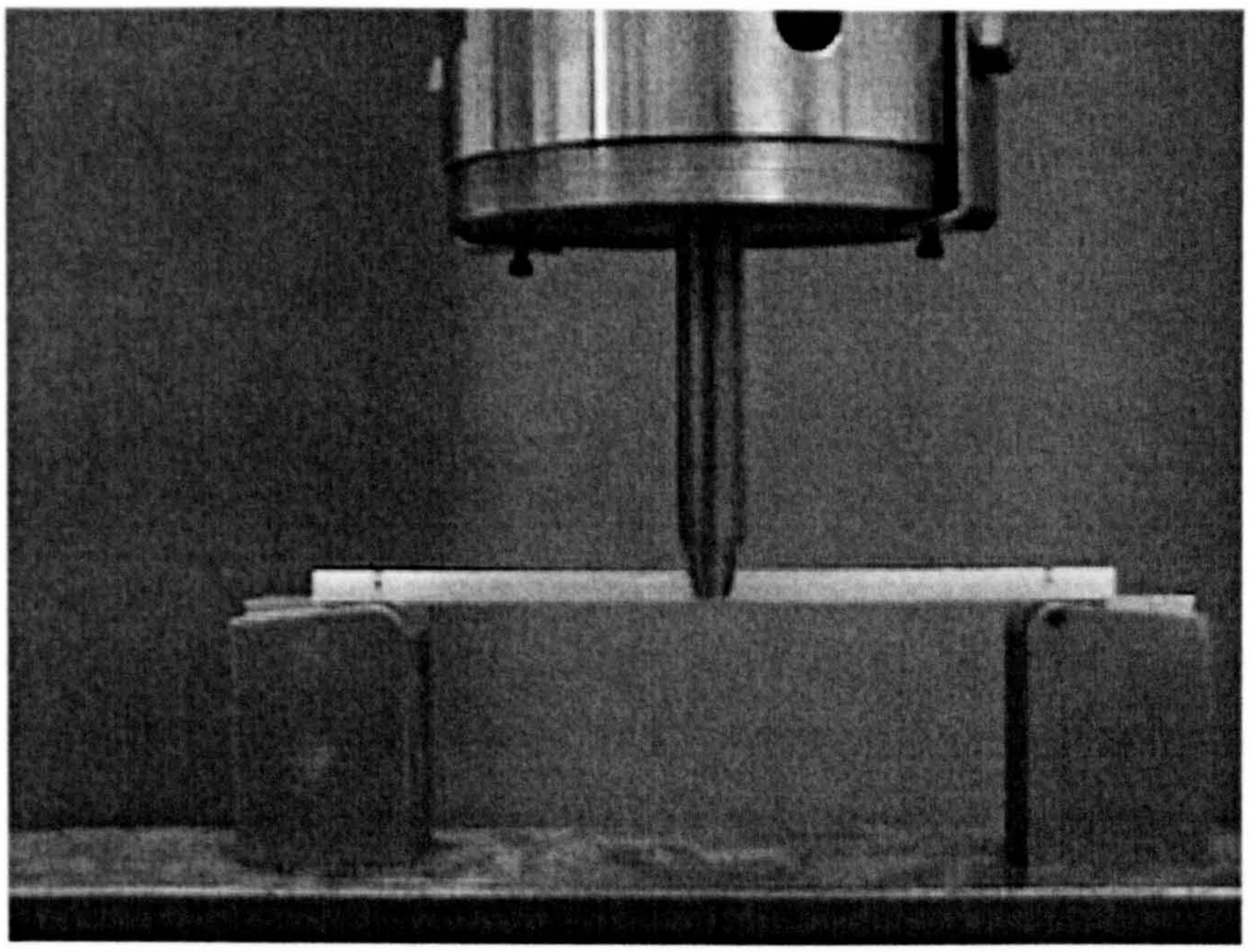

Plate 4.1: GFRP specimen mounted on the Instron machine to be tested in flexure

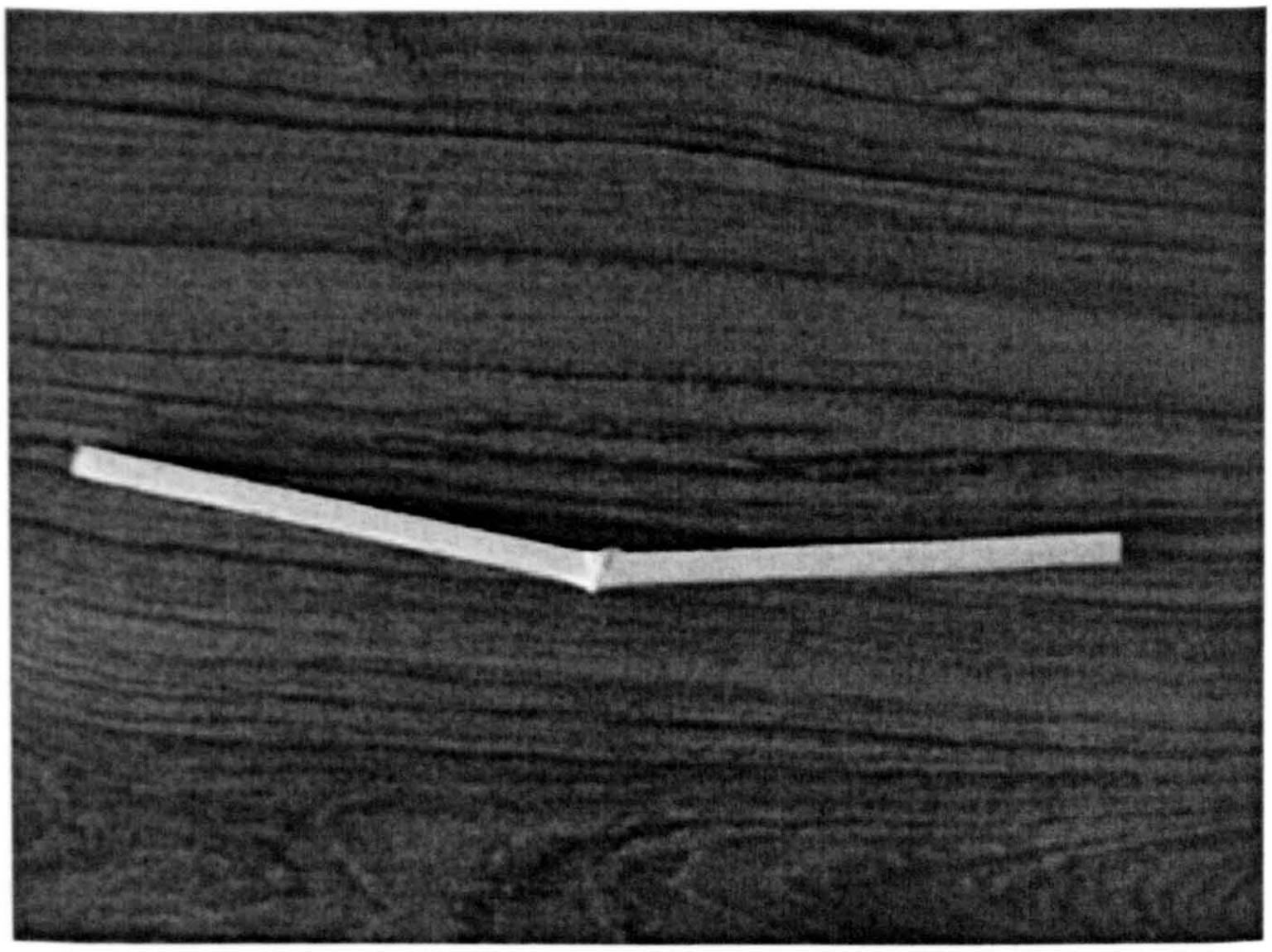

Plate 4.2: GFRP specimen failed after being tested in flexure

The elastic moduli in bending and in tension are not necessarily the same. To reduce the variation between them with a physical test it should be ensured that the test span is large enough that extra deflection due to shear is negligible. Clarke (1996) suggested that for GFRP beams a span to depth ratio should be greater than 25, therefore negligible shear deflection in comparison to bending is ensured. Nevertheless, both BS EN 2746:1998 and ASTM D 4476-97 standards recommended lower values. For the test specimen in this investigation a ratio of 24 was enough.

4.2.2.2 Significance

The results obtained from this test will, hopefully, help in fields of research and development, quality control and structural design and analysis.

In addition, this relatively easy and cheap test will provide, later in this investigation, a mean for monitoring the degradation of GFRP composites when exposed to different environments.

4.2.2.3 Apparatus

Instron 8500 testing machine was used. The supports and the loading nose were mounted on the machine. They were parallel to one another and at least as wide as the specimen (i.e., ≥ specimen's width).

4.2.2.4 Specimen preparation

The specimen length shall be 24 times its depth, plus at least 20 % of the support span to allow a minimum of 10 % overhang at the supports.

4.2.2.5 Test conditioning

Test was carried out at an average laboratory atmosphere of 20±2°C and 50±5% relative humidity.

4.2.2.6 Test procedure

1. Use an untested specimen for each measurement.

2. When mounting the test specimen on the apparatus, care shall be taken to ensure that the load is applied at mid-span of the test specimen.

3. Machine crosshead rate is to be taken as 3.3 mm/min, which is within the range of the standard tests.

The test method is detailed in Table 4.1.

Table 4.1: Conditions for bending test

Number of specimens for each condition	5
Span length	24 * thickness of specimens
Method of loading	three-point bending test
Rate of loading mm/min	3.3

4.2.2.7 Calculations

The bending stress at any point depends on the strain at that point in a manner given by the stress-strain diagram of any material. Since the stress-strain diagram of GFRP is proportional up to the point of failure, then the compression and tension stresses are proportional with strains for both compression and tension sides of the specimen subject to flexure, or in other words the specimen behaves elastically up to failure. Those bending stresses are normal to the section of specimen simply supported and loaded at the middle, also can be related to as the bending moment, as shown in Fig. 4.5, to yield the following equation:

$$\sigma_f = \frac{M \times C}{I} \qquad \text{bending stress at midspan, (MPa)} \qquad (4.6)$$

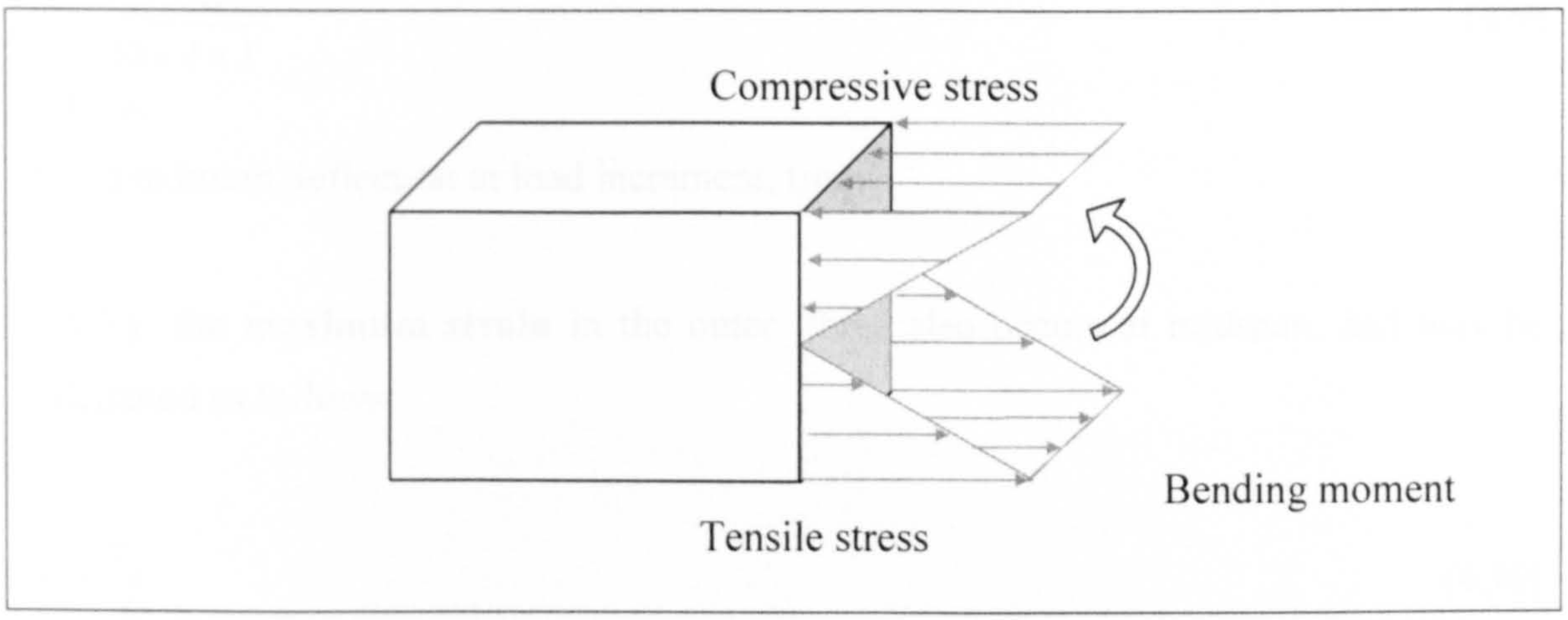

Figure 4.5: Bending stresses of specimen simply supported and loaded at the middle

This equation shows that the stresses are proportional to the bending moment and inversely proportional to the moment of inertia of the cross section. Equation (4.6) is known as **flexure formula**, and stresses calculated from this formula are called **bending stresses**.

$$M = \frac{P \times L}{4} \qquad \text{bending moment, (N mm)} \qquad (4.7)$$

$$I = \frac{b \times h^3}{12} \qquad \text{Moment of inertia, (mm}^4\text{)} \qquad (4.8)$$

Where,

C = distance from centroid to extremities (the outer fibres), (mm).

L = support span, (mm).

h = height of specimen, (mm).

b = width of specimen, (mm).

In addition, the **modulus of elasticity in bending** can be obtained by drawing a tangent to the steepest initial straight line portion of the load-deflection curve using at least five points and implementing Equation (4.9). If the initial part of the curve is not linear, then a straight line shall be drawn between 10% and 25% of the maximum force (ASTM D 4476-97, 1997).

$$E = \frac{P \times L^3}{48 \times I \times Y} \tag{4.9}$$

Where,

Y = maximum deflection at load increment, (mm)

Finally, the **maximum strain** in the outer fibres also occurs at midspan, and may be calculated as follows:

$$\varepsilon = \frac{\sigma_f}{E} \tag{4.10}$$

Therefore,

$$\varepsilon = \frac{12 \times C \times Y}{L^2} \qquad \text{strain at midspan, (mm/mm)} \tag{4.11}$$

The standard's equations for determining flexural properties of FRP composites appear to be simplified. Using these equations is acceptable, however, providing that they are not used for design purposes.

Otherwise, it is typical for composite materials to have different characteristics in tension and compression. Therefore, many issues have to be accounted for in the derivation of these equations, such as, Young's modulus in tension is different from that in compression, for instance, Faza and GangaRao (1993) reported an average value for

flexural stiffness in tension as 46.9GPa, whereas the average value for flexural stiffness in compression is 41.4GPa, also the tensile strength is higher than the compressive strength for the same composite material (Mallick, 1988; and Ehsani, 1993).

In addition, the role of the resin matrix in tension is different from that in compression, local buckling of fibres is more serious in compression zone than in tension even at low stresses, shear-lag is more severe in tension than in compression, etc, and hence during bending test, the response varies in tension and compression zones. Therefore, the simple-classical equations for bending stress may not be 100% accurate.

4.2.3 Compression characteristics of GFRP rebars

4.2.3.1 Introduction to compression test

This test method is used for the determination of the compression properties of GFRP bars, such as modulus of elasticity and compressive strength, in accordance with ASTM D695-96. The test was performed by using the Instron 5800 machine shown in Plate 4.3.

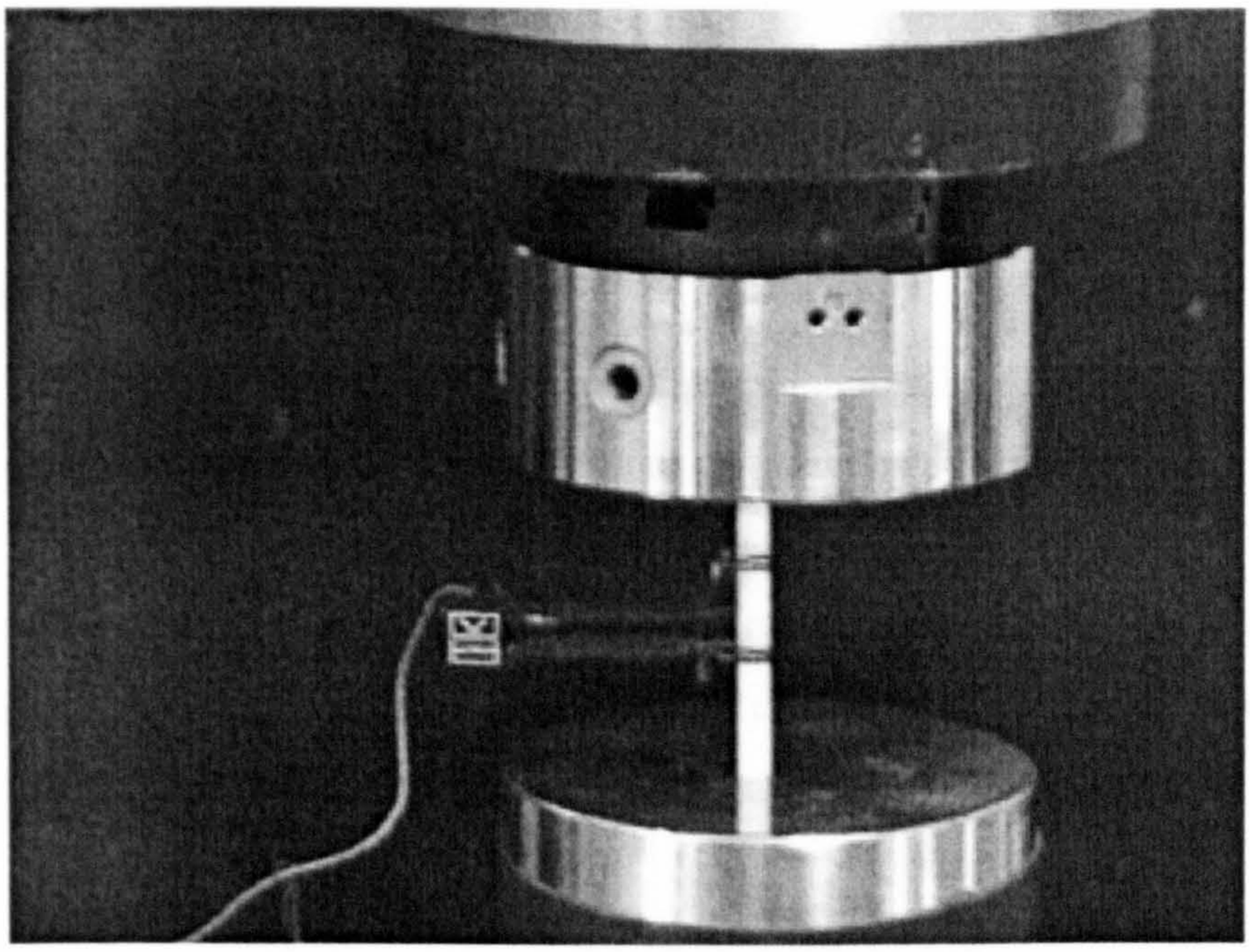

Plate 4.3: Compression test specimen mounted on Instron 5800

4.2.3.2 Significance

The results obtained from this test will help in fields of research and development, quality control and structural design and analysis. However, the test cannot be considered for engineering design in applications differing widely from the load-time scale of the standard test. Such applications require additional tests, for instance, impact, creep and fatigue.

In addition, this test will provide, later in this investigation, vital information for creep and shrinkage for specimens reinforced with GFRP rebars.

4.2.3.3 Apparatus

Instron 8500 testing machine was used in preference to testing machine that was suggested by the ASTM D 695-96 standard test, because it was more convenient as it can be properly calibrated and operated at constant rates of crosshead motion, also an accurate compressometer (i.e., extensometer) can be easily mounted on the specimens to measure strain. Compressometer is an instrument for determining the distance between two fixed points on the test specimen at any time during the test.

The upper and lower supports were mounted on the machine.

4.2.3.4 Specimen preparation

According to ASTM D 695-96, the specimen length shall allow a specimen slenderness ratio in the range from 11 to 16:1. For this test it was taken 16:1.

Specimens were cut by a diamond saw into the required length making sure the ends were perfectly flat and perpendicular to the longitudinal axis to avoid premature failure and to achieve the right failure mode.

4.2.3.5 Test conditioning

Test was carried out at an average laboratory atmosphere of 20±2°C and 50±5% relative humidity.

4.2.3.6 Test procedure

1. Use an untested specimen for each measurement.
2. Place the test specimen between the upper and lower surfaces of supports, ensuring the ends of the specimen are parallel with the surfaces of the Instron. Adjust the crosshead of the Instron until it just contacts the top end of the specimen.
3. Attach compressometer to the specimen to determine strain, and set the speed control (machine crosshead rate) to 1.3 mm/min.

The test method is detailed in Table 4.2.

Table 4.2: Conditions for compression test

Number of specimens for each condition	5
Span length	Slenderness ratio of 16:1 (37mm)
Method of loading	Compression
Rate of loading mm/min	1.3±0.3

4.2.3.7 Calculations

- **Compressive strength**

Compressive strength (σ_c) was measured by dividing the maximum compressive load (P) carried by the specimen during the test by the original cross-sectional area (A_b) of the specimen. Results were expressed in megapascals.

$$\sigma_c = P / A_b \qquad (4.12)$$

- **Modulus of elasticity**

Modulus of elasticity was determined by drawing a tangent to the load deformation curve and determining its slope. Results were expressed in gigapascals. Finally, the arithmetic mean of all values obtained was calculated and reported in this investigation as the average value, standard deviation was reported too.

4.2.4 Study of pore structure using mercury intrusion porosimetry (MIP)

4.2.4.1 Introduction

Considering the durability of FRP bars (i.e., fibres in a resin matrix) embedded in concrete, it is likely that the main aggressors would be the free chloride and hydroxyl anions. Most of the resins utilised are meant to be resistant to this kind of attack, but of course some fibres are not. In general resins will always contain pores, although very compact, of different size and shape. This pore system will determine the degree of contact between composites and the outside environment. The amount of pores and the pore size distribution are thus crucial in determining how far and how fast fluids/moisture or ions penetrate into composites. If the ions manage to penetrate through the resins, then the fibres are attacked. But not only pores on their own are responsible for the moisture ingress, it is believed that there are a number of variables, including fibre and resin characteristics, processing conditions, stress state, damage state and moisture exposure history, are responsible too.

The **total porosity** of a material is a fraction of the bulk volume of the material occupied by the voids. These voids may be filled with air and/or water depending upon the degree of pore saturation.

The total porosity and its pore sizes and distribution can influence ions and fluid ingress within the GFRP and therefore, affect the durability.

There is a variety of experimental techniques to determine the porosity and pore size distribution of materials that contain pores. The main techniques in use are: low temperature gas sorption, mercury intrusion porosimetry, and optical/scanning electron

microscopy. The MIP, however, is sometimes preferred due to its capability in detecting a wide range of pore size diameters, typically in the range of 200μm-0.003μm (Hassan, 1993; and Bajracharya, 2001) and easer to perform.

In fact, different fibres respond (with respect to the environments) in different ways, glass fibres are, for example, vulnerable to OH^- and Cl^- ions attack. However, aramid fibres are only very slightly attacked by OH^- and carbon fibres are almost inert to most environments. Therefore, the following remarks are relevant to GFRP composites.

OH^- ions are present in the pore solution of concrete and usually present in large quantities. It should be noticed that the concentration of hydroxyl ions differ depending on higher or lower alkalinity of the cement type used.

Cl^- ions present in salt water, so if GFRP reinforced concrete is used in seawater, this attack will be more pronounced.

4.2.4.2 Background of MIP

The MIP is based on forcing the mercury to intrude the open pores of a solid sample by applying pressure. This technique involves, first evacuating the voids in the sample, and then introducing the mercury into the pores of the sample under gradual increase in pressure. As the test proceeds, the pressure will increase automatically in steps and therefore enable the mercury to penetrate in the pores. Obviously, as the pressure increases the mercury will occupy smaller pores. By controlling the pressure and measuring the volume of mercury intruding the sample, by the apparatus, a relationship between the intruded volume of pores and the applied pressure can be established. This relation can be converted into a pore volume/pore size relationship by using the Washburn equation (Washburn, 1921) that assumes all pores are straight right angle cylindrical, the Washburn equation is given as:

$$p = \frac{-(SF) \times \gamma \times \cos\theta}{d} \tag{4.13}$$

Where:

p = the pressure required to intrude a pore of diameter (d), in MPa

SF = pore shape factor, for cylindrical pore SF = 4,

γ = the surface tension of mercury (Hg), in N/m

and θ = the contact angle of Hg with the pore wall.

Equation (4.13) is derived from equating the work (W_1) needed to force a non-wetting liquid (mercury) in a pore of a diameter (d) and length (l) with the work (W_2) needed to force a mercury of a volume (v) into the pore under external pressure (p) as follows:

$$W_1 = \pi \times d \times l \times \gamma \times \cos\theta \tag{4.14}$$

$$W_2 = p \times v = p \times l \times \frac{\pi \times d^2}{4} \tag{4.15}$$

If, $W_1 = W_2$ (4.16)

Then Equation (4.13) can be achieved.

In addition to pore size distribution and total intrusion volume, other information can also be gained, which includes total porosity, and average and median pore diameters. These average and median pore diameters give an approximation of shape of the distribution and whether large or small pores are predominant, since large pores contribute more to volume and small pores to the surface area.

Liquids that form contact angle greater than 90° are termed "non-wetting". Liquids that form a contact angle less than 90° are called "wetting". If the liquid does not form any shape of droplet, that is, the contact angle is 0°, it is regarded as "spreading liquid". Therefore, the value of mercury contact angle (θ) is widely assumed to be between 117° and 140°, and the frequently assumed value is 130°. Similarly, the value of surface tension (γ) is equal to 0.48 N/m is commonly assumed (Drzal, 2001; Hassan, 1993; and Cook and Hover, 1993). The cross section of a mercury meniscus across the diameter of a circular pore is shown in Fig. 4.6.

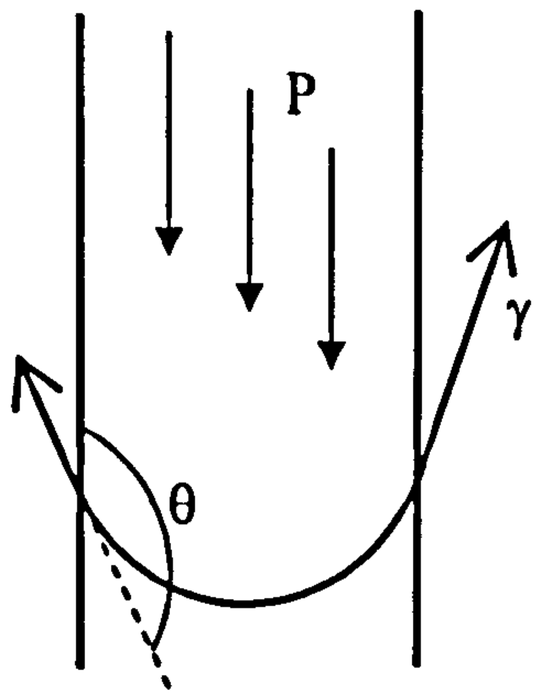

Figure 4.6: Cross-section of a mercury meniscus across the diameter of a circular pore

The pore volume is normally presented as a cumulative distribution curve. This curve is the cumulative intrusion volume of mercury plotted against the log of diameter. This curve can show the limiting pore size beyond which no further mercury intrusion occurs. It also reveals the total porosity and median pore diameter.

4.2.4.3 Definitions of porosity and pore size distribution

Total porosity is defined as the fraction of the bulk volume of the material occupied by voids.

Total porosity is a parameter which is independent of the shape and size of the pores. While pore size distribution is the manner in which pores are distributed with respect to pore size, shape and structure. Despite the fact that FRP is a very compact material, it might have a wide range of pore sizes. This technique, namely mercury intrusion porosimetry, is implemented in order to gain better understanding and full picture of the pores detected by this technique.

4.2.4.4 Parameters representing the pore size distribution

The parameters that are frequently used to represent the pore size distribution of the tested samples can be summarised as follows:

- **Total intrusion volume (TIV):**

Is the maximum volume of mercury intruded into the sample at the highest pressure attained during the test.

- **Total pore (surface) area (TPA):**

Is the surface area within all the pores, which is directly related to the number of pores. At a specific porosity, greater pore area indicates higher number of smaller pores.

- **Median pore diameter by pore volume (MPD):**

Is the diameter (pore size) at 50% intrusion obtained from the cumulative intrusion curve. The median pore diameter by volume relates to the relative volume of smaller pores. For two specimens have similar cumulative pore volume, the one with greater MPD value is the one that has greater volume of larger pores.

- **Average pore diameter (APD):**

Is the ratio of total intrusion volume and the total pore (surface) area, assuming that all pores are of right cylinders shape.

4.2.4.5 Limitation of MIP technique

Together with the previously mentioned possible source of error, namely the undetected true shape of pores, due to an incorrect assumption of straight right angle cylindrical pores in Washburn equation (Equation (4.13)). The assumption of a particular contact angle may be incorrect which is affected by the type of material tested, the drying method and mercury purity.

Another problem can be included which is the pore diameters recorded by mercury porosimetry. They do not have to be the real pore diameters, but are the pore entry diameters that could some times be smaller than the pore diameters themselves (Winslow and Diamond, 1970). In this case, higher pressure is required and, therefore, the volume of the small pores is over estimated. On the other extreme, if the pore entrance is too small, the maximum applied pressure will not be enough to intrude mercury in the pore entrance. Both of these un-intruded and completely isolated pores,

which have no communication with the outer surface of the sample, if exist, will of course result in under estimation of the pore volume called "the lost porosity" (Hassan, 1993).

Despite the limitations mentioned above, MIP is widely used in studying a lot of materials, and generally the results obtained are regarded reliable and consistent.

4.2.4.6 Apparatus

The instrument used in this experiment was a Micromeritics Autopore Model 9200, in the School of Civil Engineering, Leeds University. The apparatus is capable of generating a maximum pressure of 414 MPa. The method of measurement for this test was chosen to be the maximum intrusion volume rather than setting a pressure table, which has the advantage of providing a greater number of readings in the region of major volume of voids (Micromeritics, 1990).

The apparatus is shown in Plate 4.4, and it consists of the following parts:

Penetrometers,
Four built-in low-pressure ports,
Two built-in high-pressure chambers,
Low and high pressure generators,
Pressure transducer for monitoring mercury penetration and applied pressure.

The processing of low- and high-pressure runs, data collection and display were all automatically performed by the control module.

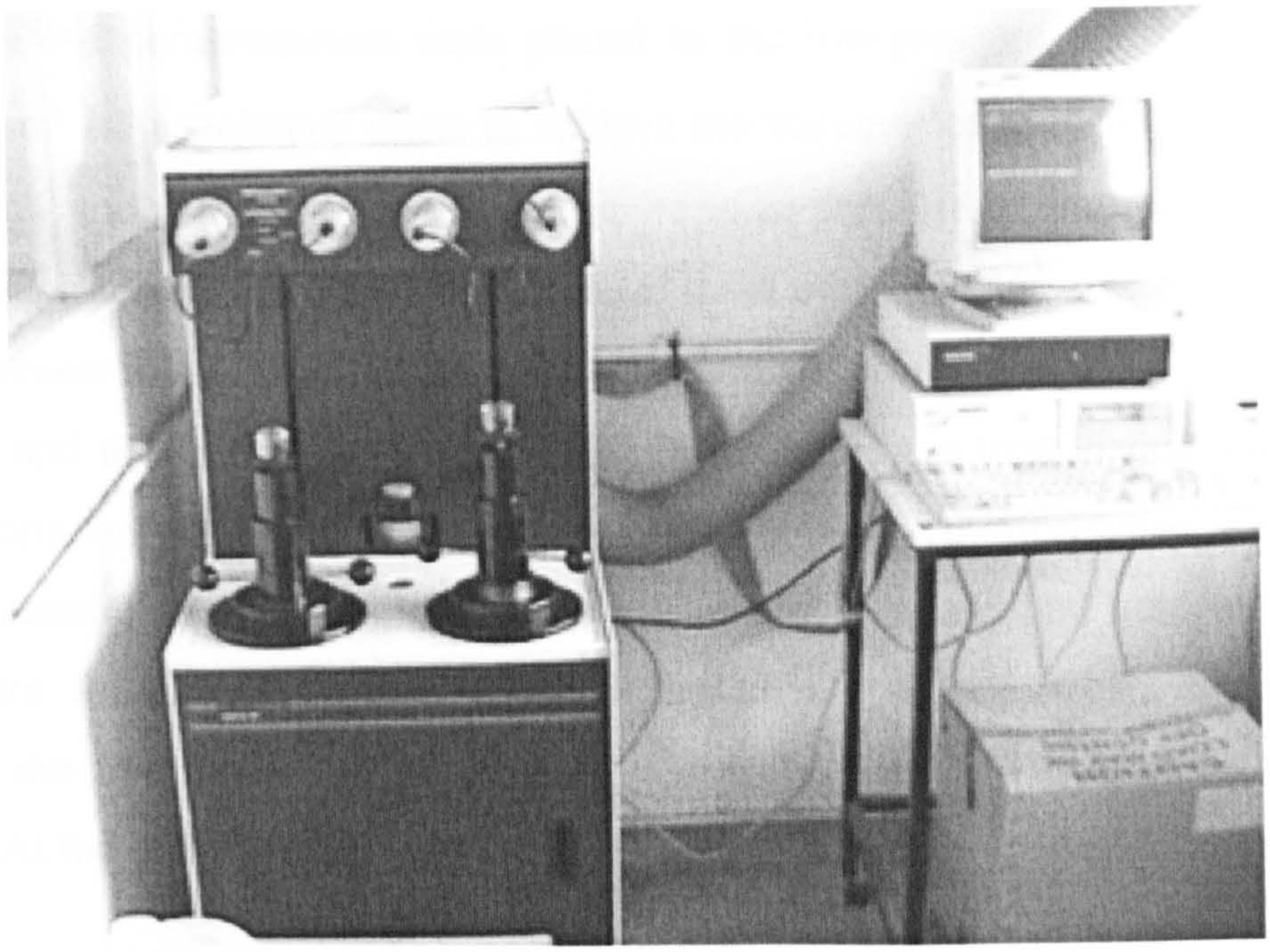

Plate 4.4 Mercury porosimeter model Micromeritics Autopore 9200

4.2.4.7 Specimen preparation

After cutting the GFRP by a diamond saw into segments of 18 mm long, the specimens were then washed thoroughly but gently to remove any dust on the surface of the segments.

Subsequently, the segments were dried in an oven at a temperature of 105°C for 24 hours to remove volatile particles in order to minimise the time required to get the desired vacuum reading prior to mercury intrusion.

4.2.4.8 Test procedure

The dry samples were weighed and placed into pre-weighed penetrometers (five segments, each 18 mm long, fitted in one penetrometer and represented one specimen). Then the penetrometers were sealed. A maximum of four penetrometers could be tested for low-pressure run at a time. The required information regarding weights and run conditions were entered via keyboards for each of the penetrometers.

As soon as the penetrometers were placed in the low-pressure ports and locked in, evacuation of the specimens starts to achieve the vacuum level of 50 μm Hg and fills with mercury and pressurizes them with appropriate pressure in the low-pressure ports. The low-pressure run takes about 45 minutes to be accomplished. After completion of the low-pressure run, the penetrometers are reweighed (the weight includes the specimens and the mercury). Two of the penetrometers are then loaded into the high-pressure ports, only two can be tested at a time. The required information is entered and the high-pressure analysis begins. The machine automatically and gradually increases the pressure following a pre-set schedule up to 414 MPa. When this analysis is complete, the specimens are automatically depressurised and goes back to ambient pressure. At the end, the data from the low-pressure and high-pressure files are printed.

4.2.5 Micro-structural imaging

4.2.5.1 Introduction

In this research, scanning electron microscopy (SEM) was used due to its advantages as well as its multipurpose characteristics. It is versatile equipment with very high magnification images of up to 20000 times for both surface and subsurface of a specimen. Moreover, it can develop three-dimensional images with higher resolution than optical micrographs. Normally, it can be utilised when micro-structural examination and elemental or compositional analysis are required. A number of forms of imaging have been developed that include Secondary Electron Imaging (SEI) and Backscattered Electron Imaging (BSE). Finally, latest SEM can provide several images, and quantitative results with respect to porosity and composition (Ananta, 1999 and Richardson, 2001).

4.2.5.2 Background about scanning electron microscopy

The idea of SEM is to form a fine probe of electrons to examine a specimen. In order to achieve that, electrons are emitted by a cathode and allowed to pass through a voltage between the cathode and anode to be accelerated and then, by the help of a group of lenses, the probe is formed on the surface of the specimen. When a beam of Primary

Electrons (PE) hits the specimen, they are scattered after a number of collisions with specimen atoms. As a result of that, the electrons bounce leaving the specimen surface and get back with two different categories of electrons distinguished by their energies. Electrons with energy between the PE energy and 50eV are called the Backscattered Electrons (BSE), they can provide information about internal structure of the specimen and give average atomic number and crystallographic information on surface. They also can be used for elemental and chemical analysis. The others with energies less than 50eV are called Secondary Electrons, and they leave the specimen from a thin surface layer (Richardson, 2001). A brief definitions of secondary and backscattered electrons is given below:

- **Secondary Electrons**

As mentioned before secondary electrons can be defined as the electrons that escape from the material surface with low energies. These are electrons ejected from atoms after a series of collisions with primary and backscattered electrons. Because of their relatively low energy and very abundant, they are most commonly used for SEM specimen surface imaging (Head, 2001).

- **Backscattered Electrons**

Backscattered electrons are considered primary electrons that leave the specimen surface with energies between that of primary and secondary electrons.

In this investigation, only secondary electrons were used.

4.2.5.3 Apparatus

The microscopy study was carried out in the Electron Microscopy Laboratory of the School of Civil Engineering, University of Leeds with a Cambridge Series 4 Scanning Electron Microscope (Plate 4.5) and analytical software Link Isis V.3.2. This test was performed on the cross-sectional of GFRP and cross-sectional interface between concrete and GFRP reinforcing bars.

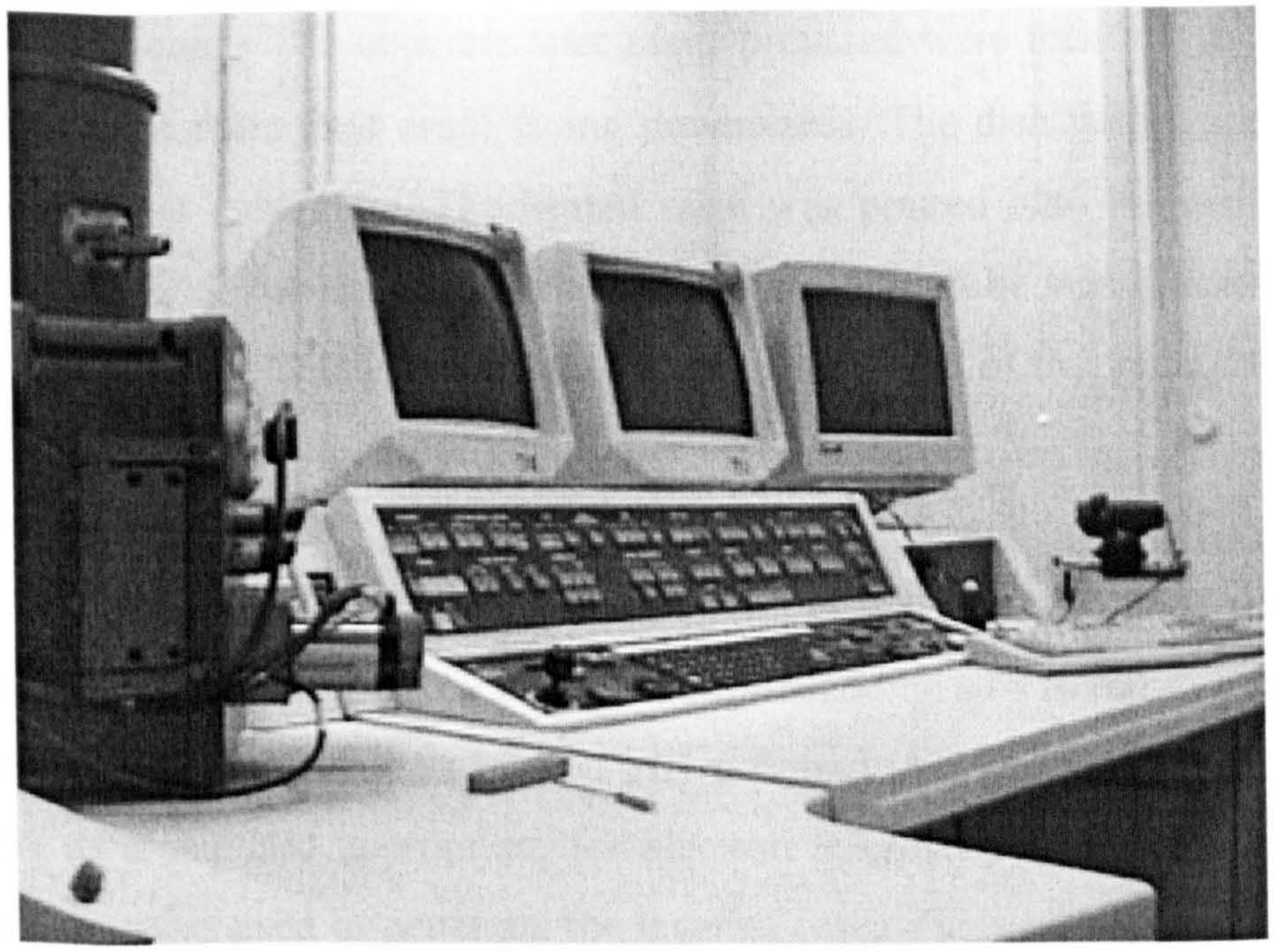

Plate 4.5: Scanning electron microscopy (SEM)

4.2.5.4 Preparation of specimen

A procedure for preparing polished sections of steel/concrete interface that can be studied under an SEM was developed and performed in the University of Leeds by A T Horne. Similar procedure was used for GFRP/concrete specimens, the technique is described below.

Two concrete cores were cut to size using a diamond saw (Disco Plan – TS model). Once a GFRP/concrete section was obtained, moisture was removed to halt the hydration process. A freeze-drying method was utilised as will be described in Section 4.3.4. The samples were then removed and placed in a vacuum for a period of two days, to ensure removal of all water.

Once the specimens were free of water, they were resin-impregnated to ensure the preservation of the specimen's structure. A resin and hardener (Struers' Epo-fix epoxy resin) were mixed in a ratio of 15 parts resin to 2 parts hardener. The resin mixture was placed in a vacuum for ten minutes to remove all air bubbles incorporated during mixing. Prior to impregnation, the resin was heated (using a blow dryer) to decrease the

viscosity of the liquid. The concrete specimens prepared were then placed in a plastic dish with the cut surface (test area) facing downwards. The dish with a specimen was placed in a vacuum container. The heated resin was poured onto the dish via a tube attached to the top of the container. The other end of the tube was placed in the cup containing the resin, and sucked out as a result of the force of the vacuum. The flow was controlled with a clamp on the tube.

The resin was left to set for 24 hours before removing the mould from the hardened specimens. The specimens were then cut using the diamond saw to remove excess resin. The surface of the specimen was ground and polished in a grinding machine (Struers Rotopol-35) to a standard appropriate for electron microscopy. Initially a grade 500 coarse grit paper was used to penetrate the layer of resin. This was applied for a period of 2-5 minutes at a speed of 80rpm. Finer grade 1200 and 2400 grit papers were then used for periods of 5-10 minutes (at 80rpm). After grinding, the specimens were polished using cloth impregnated with diamond abrasive starting with size 6μm, followed by 3 and 1μm using a hydrocarbon lubricant. Polishing was performed for a period of 1-2 minutes with each abrasive paper at a speed of 80rpm. The polished sections were then placed in pierced plastic bags and stored in a desiccator. Before being examined under the electron microscope, the specimens were coated with either gold or carbon. This prevented the build up of charge on the concrete surface causing interference when looking at the sample under the SEM. A gold or carbon ribbon was heated in a vacuum above the specimen by passing a large current through it as seen in Plate 4.6. This resulted in a thin layer of gold or carbon coating the whole of the specimen surface. Similar procedure was used for GFRP sections also.

4.3 Durability

4.3.1 General

With the continuous deterioration of the world's infrastructures and the consequence high cost of maintenance, fibre reinforced plastics composites have become increasingly important to be considered in some structural applications. However, the risk of durability degradation of the composites in some environments is one of the primary issues limiting the acceptance of these materials. It is important to recognise the hostile

environments and understand the mechanisms that govern composite components degradation to optimise material properties and gain information for use in accelerating aging tests.

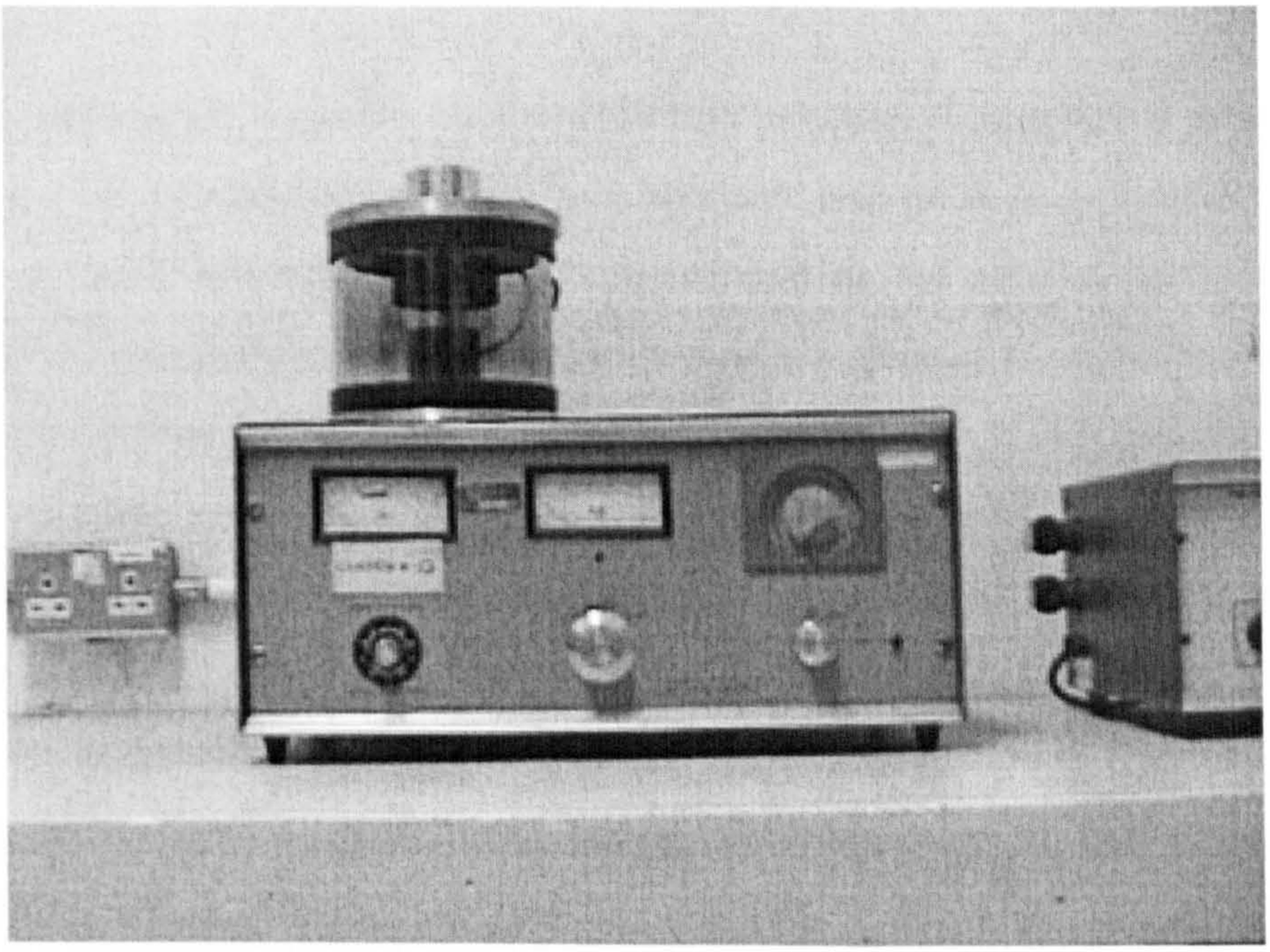

Plate 4.6: Gold spotter coater apparatus

4.3.2 Definitions and scope

Durability is defined "as the ability of a material or structure to resist cracking, oxidation, chemical degradation, delamination, wear and/or the effects of foreign object damage for a specified period of time, within the appropriate load conditions, under specified environmental conditions" (Karbhari *et al.*, 2000).

Based on previous research, the response of GFRP materials to specific hostile media that are expected to exist during life service of GFRP in reinforcing concrete is considered.

4.3.3 Aging aqueous

It is the recommendation of several researchers (Benmokrane *et al.*, 1998) to test FRP bars in its real environment, namely embedded in concrete, rather than in simulated environments, namely chemical solutions, for the realistic evaluation of durability.

However, it is believed by other researchers (Alsayed and Alhozaimy, 1998, and Takewaka and Khin, 1996) that providing a real environment is time consuming. Moreover, good correlation between the two environments has been reported (Porter *et al.*, 1997).

The rate of aggression depends on the available amount of aggressive ions (e.g., OH^- ions), also on the possibilities of these ions to move and on their velocity. This means testing of the composite materials in a bath (simulating the alkaline environment) will show higher effects than its natural environment, i.e., when it is embedded in concrete, where free ions movement is very restricted.

It is generally known that chemical reactions can be enhanced by temperature increase (ions move faster) as long as no other chemical influences are interfering. This means prediction on future behaviour might, within a reasonable period of time, be derived by an accelerated aging procedure, using increased temperature as well as bath solution (Micelli *et al.*, 2001; and Vijay, and Gangarao, 1999).

In this investigation, the specimens were immersed in the following solutions:

- **Alkali solution**

Alkali aqueous to simulate pore solution that exists in concrete (i.e., Na^+ of 0.16 mol/l, K^+ of 0.55 mol/l, and OH^- of 0.71 mol/l of distilled water). These are ions concentration typically exist in pore solution after 180 days for pastes with a water/cement ratio of 0.5 (Taylor, 1997).

- **Brine solution**

Brine solution of 3.5 % of NaCl, simulating exposure to sea water.

Two sets of temperature were applied for each solution, namely 20 and 60°C. The high temperature was implemented to increase the rate of deterioration.

4.3.4 Drying of specimens

There are several ways of drying specimens, each of which is preferably used for the preparation of certain tests. The methods used are mentioned in the following sections:

- **Oven drying at 105°C**

In this technique the specimens were dried at high temperature as high as 105°C±5°C. It was used to dry GFRP specimens during testing for mercury intrusion porosity (MIP).

- **Vacuum oven drying at 50°C**

In this technique the specimens were dried at temperature of 50°C±5°C in a vacuum oven (-1 bar). It was used to dry GFRP specimens during testing for flexural test. This technique does not remove quite as much moisture as the oven drying at 105°C technique. The two techniques were tested using GFRP control specimens, and the results are given in Table 4.3.

Table 4.3: Comparison of oven drying techniques

	Vacuum Oven at 50°C				Oven at 105°C	
Pre-oven weight	After 24 hours	% weight loss	After 72 hours	% weight loss	After 24 hours	% weight loss
10.7707	10.7372	0.311	10.7365	0.317		
11.0108					10.9712	0.359

- **Vacuum freeze drying at -40°C**

This technique was used for the preparation of reinforced concrete specimens for the image processing study. The procedure was as follows:

Specimens (reinforced concrete of 20mm cores) were immersed in liquid nitrogen until thermal equilibrium was achieved. The specimens were then placed in a vacuum freeze drying apparatus and left under vacuum for a period of three days at a pressure of 1.5×10^{-1} Mbar, and at temperature of -40°C±5°C to attain constant weight (Head, 2001).

The removal of moisture from frozen specimens works through the process of sublimation. In spite that the specimens are placed into the freeze dryer machine in a frozen state, the temperature in the machine's bell jar is approximately ambient. This means that a slow thawing of the specimens will occur. As the specimens are also subjected to a vacuum, H_2O molecules are driven away in the vacuum as soon as the molecules change their state from a frozen to a liquid. Therefore, molecules of H_2O actually pass from a frozen state to a gaseous state without stopping at a liquid state.

By avoiding the high temperature usually associated with oven drying techniques, damage to the microstructure of the specimen (micro-cracking), and hydrated phases of the concrete can be avoided due to thermal expansion and contraction is reduced to minimum.

4.3.5 Change in flexural strength of GFRP rebars

In this part of the investigation, a similar test of flexural examination was implemented for GFRP rebars after being immersed in the aging solutions (i.e., alkali and brine solutions at different temperatures) for different periods of time. That was done to monitor the detrimental effects of different aging conditions on the flexural properties of the composite reinforcement.

A similar test procedure was followed and same apparatus was used apart from the specimen preparation, where there was a slight different approach. Flexural testing was carried out on the specimens immediately after being removed from the aging solutions, but prior to that they were washed and dried in oven/vacuum at about 55°C.

All other details of this test programme were mentioned previously in Section 4.2.2, and the different aging conditions were also mentioned in Section 4.3.3.

Five specimens were tested for each aging condition after different periods of aging, namely, 30 days, 90 days, 180 days, and 270 days.

4.3.6 Why flexural test?

Due to the high tensile strength and low shear resistance of FRP bars, they cannot be tested in tension using the same conventional gripping systems that are used for steel bars. The reason is because the traditional wedge-shaped frictional grips would actually apply high compressive stresses at a particular area, which is the contact zone between the bar and the grips. As a result of that, premature failure will occur to the grip zone (ACI 440R-96, 1996).

Instead, a technique is required to test the bars in tension, in which a gripping system distributes the shearing stresses on the bar at the contact zone between the bar and the jaws during the tensile test. There have been several attempts by researchers, such as Lees *et al.*, (1995); and Castro and Carino, (1998), through utilising metal tubes coated by a matrix to enhance bonding between the bar and the tube.

Although ASTM D 3916 developed an approach for tensile tests for pultruded thermosetting FRP bars for diameters ranging between 3.2 and 25.4 mm, researchers (Rahman *et al.*, 1993; Holte *et al.*, 1993; Erik and Rizkalla, 1993, Tannous and Saadatmanesh, 1998; Faza, and GangaRao, 1993; and Castro and Carino, 1998) seem to utilise systems they have developed themselves.

In each adopted technique there has been limitations. For examples, the tab adapters that have been developed by ASTM D 3916, cannot be used with deformed and square FRP bars, in addition should the bars not be aligned with the tubes; the tensile test's results will not be accurate. Furthermore, although some have used epoxy resin, to provide bond between the bar and the tube, Castro, and Carion (1998) did not recommend that due to messy operation and time consuming to cleanup after the test.

Last but not least, when adopting a mechanical test to monitor the degradation of FRP composites, such a test should consider changes in any part of the composites, and this cannot be achieved by tensile test, because the resin matrix should contribute only little to the composite tensile strength. However, when taking into consideration the flexural test, the resin matrix plays a noteworthy role in determining the strength of the

composites. Therefore, any reduction in ultimate strength in flexure, after aging, has to be the result of degradation of the glass fibres, the fibre/matrix interface, and/or resin matrix. This point is of a great importance because when one is studying the deterioration mechanisms in composites, the most important parameter is bond between concrete and FRP reinforcement, which is determined by the surface of the composites, since if the bar just loses its surface, the bond can be damaged without significant degradation of the tensile strength.

To sum up, obviously there is no specific system has been widely used, in addition to some technical difficulties in performing tensile test for FRP bars, such as the assurance of the alignment of the specimen and the guarantee of tensile failure achievement within the span length. Therefore, the result of tensile strength of bars is not an absolute value, but is relative to the test. Hence, another way of testing the mechanical properties of FRP bars, namely flexural test (three point bend method), was used in this research. Despite that this method has some limitations, it is easer and cheaper to be prepared and accomplished, also it is considered a time saver method in comparison with the direct tensile test, although it should not be used alone for design purposes. This test method determines ultimate stress and maximum strain in the outer fibres and bending modulus of elasticity.

4.3.7 Change in pore structure of GFRP (MIP testing)

In this part of the investigation, mercury intrusion porosimetry (MIP) was used for detecting possible changes in the pore structure of GFRP composite after being immersed in the aging solutions (i.e., alkali and brine solutions at different temperatures) for different periods of time.

After removing the GFRP samples from the aging solutions, they were cut by diamond saw into segments of 18 mm long. The specimens were then washed thoroughly but gently, and submerged in deionised water and kept in a temperature of around 60°C. The containers (including the deionised water and the segments) were shaken from time to time and the deionised water was renewed occasionally, and finally removed after three days. The segments were put in a chamber of (-1 bar) pressure, until they surface-

dry naturally, to facilitate the removal of most crystals accumulating within the segments due to previous submergence in the aging solutions.

Subsequently, the specimens were dried in an oven at a temperature of 105°C for 24 hours to remove volatile particles in order to minimise the time required to get the desired vacuum reading prior to mercury intrusion.

All other details of this test programme were mentioned previously in Section 4.2.4, and the different aging conditions were also mentioned in Section 4.3.3.

Five segments were tested for each aging condition after different periods of aging, namely, 90 days, 180 days, and 270 days.

Chapter Five Experimental and Theoretical Studies of Drying Shrinkage and Creep

5.1 Introduction

Shrinkage and creep affect deformation and stresses in concrete. The effect depends on many factors such as the inherent shrinkage and creep of the concrete, the size of the members, and the amount and distribution of reinforcement. Reinforcement of concrete greatly reduces the magnitude of shrinkage and creep.

For many reasons it is desirable to discuss both the drying shrinkage and creep together. For instance, both of them originate from the same source (both are assumed to be related mainly to the removal or movement of adsorbed water from or within the hydrated cement paste), the strain-time curves are similar, they share similar factors that influence them, the micro-strain of each, typically 400 and 1000×10^{-6}, is large and cannot be ignored in structural design, and both are partially reversible.

In this chapter, experiments to determine the influence of reinforcement on creep in compression and drying shrinkage of concrete are described. Different reinforcement types, namely GFRP and steel, and reinforcement percentage were used. In addition, companion specimens with no reinforcement were also tested in creep and shrinkage and regarded as datum specimens. For creep specimens, the compressive creep was determined by applying a compressive stress at 25% of the ultimate compression strength of concrete. From the creep tests, the modulus of elasticity of concrete was also determined.

This chapter also presents the methods for estimating elasticity, shrinkage and creep and considers techniques for allowing for the presence of reinforcement. A new composite model is developed.

5.2 Shrinkage behaviour

5.2.1 Background of shrinkage

In general, shrinkage takes place when water is lost from the concrete by evaporation (drying shrinkage), by hydration of cement (autogenous shrinkage) and by carbonation (various cement hydration products are carbonated in the present of CO_2). Shrinkage is normally measured as a linear strain. Its unit is thus in mm per mm, usually expressed in micro ($\times 10^{-6}$) strain.

Therefore, a hardened concrete will not remain dimensionally stable when exposed to ambient humidities that are below saturation conditions. This is because the withdrawal of physically adsorbed water from **C-S-H** and, to a smaller extent, the removal of capillary water that is held by capillary tension in small capillaries (i.e., 5 to 50nm) result in a shrinkage strain. It should be noted that part of this moisture movement is irreversible.

The shrinkage of concrete can be explained as follows: first, when concrete dries, there is the loss of free water which is not physically bound, i.e. capillaries > 50nm. This process introduces internal relative humidity gradients within the structure of the cement paste, so that water molecules are transferred gradually to the exposed surface of the concrete. Consequently, the cement paste contracts. However, the reduction in volume is not equal to the volume of water removed because the initial loss of free water does not cause a significant volumetric contraction of the paste due to the internal resistance to consolidation by the **C-S-H** structure (Mehta and Monteiro, 1993).

The magnitude of shrinkage is affected by the size and shape of specimen, being a function of the surface/volume ratio (Ross, 1944). Therefore, shrinkage cannot be regarded as an inherent property of concrete without reference to the size of the concrete member. This is illustrated in various equations for shrinkage prediction.

Embedding reinforcement in concrete affects shrinkage behaviour and introduces extra stresses. Reinforcement in concrete does not shrink, whereas concrete does. The action of concrete shrinking and being resisted by the reinforcement causes some phenomena, such as deflection of slabs and beams if asymmetrically reinforced. In addition of developing internal tensile stresses within the concrete, and this gives rise to micro-cracks (i.e. the concrete is shrinking and the reinforcement is trying to hold it back). For example, when the shrinkage takes place in a reinforced concrete element, the concrete tries to compress the reinforcement and simultaneously the reinforcement tries to apply tension to the concrete.

5.2.2 Shrinkage test specimens and procedure

Non-reinforced (control) and reinforced prisms (200×75×75mm) were used to investigate the influence of reinforcement on concrete shrinkage. Specimens, reinforced with either bars of GFRP or steel were cast and cured in the fog room at a temperature and relative humidity of 20°C ± 2°C and 95-99%, respectively. The specimens were cured for 28 days. Shrinkage was measured by a Demec gauge on a daily basis in the early stages. As the shrinkage rate decreased with time, the intervals of taking the reading were adjusted accordingly.

Before testing the specimens, they were prepared as follows:

At the age of about 14 days the specimens were taken from the fog room. The surface of the specimens where the Demec points would be placed was wiped off using a dry cloth and then marked accurately. For a single specimen, four pairs of Demec points were attached, one pair on each side of the specimens at a gauge length of 150mm.

The specimens were then kept in a control room with temperature and relative humidity of 20 ± 3°C and 67 ± 3%, respectively (see Plate 5.1).

Two concrete mix designs were used. One with mix proportions of by mass 1/2/3/0.5 for cement/sand/aggregate/water, respectively. The other was similar to the former but also included 2% of shrinkage reducing admixture, called Eclipse®, by weight of cement. (As recommended in the data sheet of Eclipse®, the volume of water was reduced equal to the amount of admixture added). For more details about the properties of the two concrete mixes, refer to Table 3.4 in Section 3.5.2.

In addition, three sets of reinforcement ratios were used for each reinforcement type (shown in Table 5.1) and details of distribution of reinforcement are illustrated in Fig. 5.1.

Table 5.1: Reinforcement types and ratios

Reinforcement type	Steel			GFRP		
Number of bars	4	6	8	4	6	8
Reinforcement ratio (ρ)	0.036	0.054	0.071	0.045	0.068	0.091

It can be seen that there is a difference in reinforcement ratios between the GFRP and steel bars despite the similarity in bars number. This was because of the dissimilarity in cross-sectional areas, GFRP bars were 8mm square bars, however steel bars were rounded with 8mm diameter.

5.3 Creep behaviour

5.3.1 Background of creep

The gradual increase in strain with time of a specimen subjected to a constant stress is due to creep. Creep can thus be defined as the increase in strain under a sustained constant stress after taking into account other time-dependent deformations not associated with stress, such as shrinkage, and swelling (Neville and Brooks, 1998). Creep is of considerable importance in structures, because this increase in strain can be several times as large as the strain on loading.

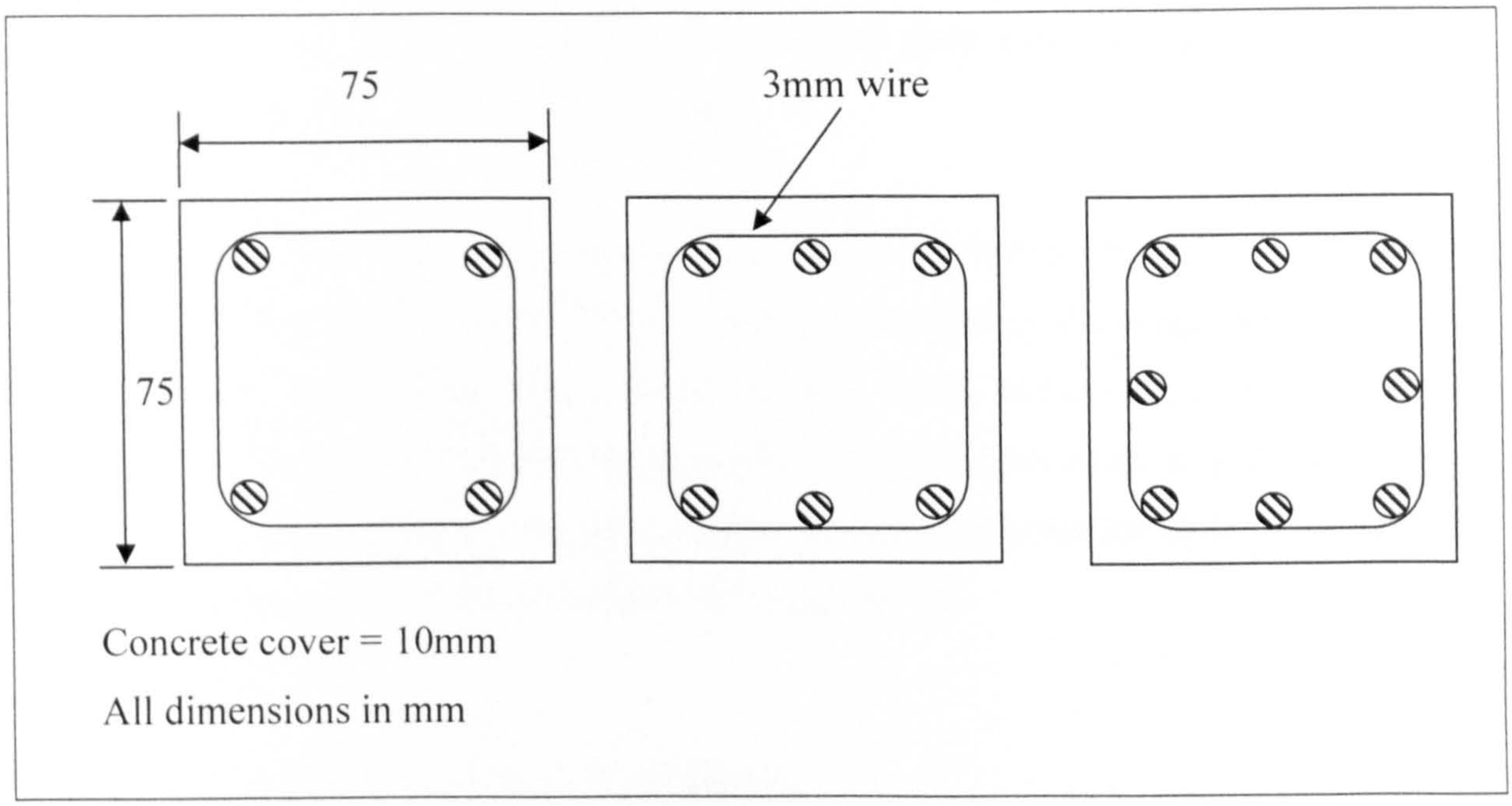

Figure 5.1: Cross section of shrinkage prisms

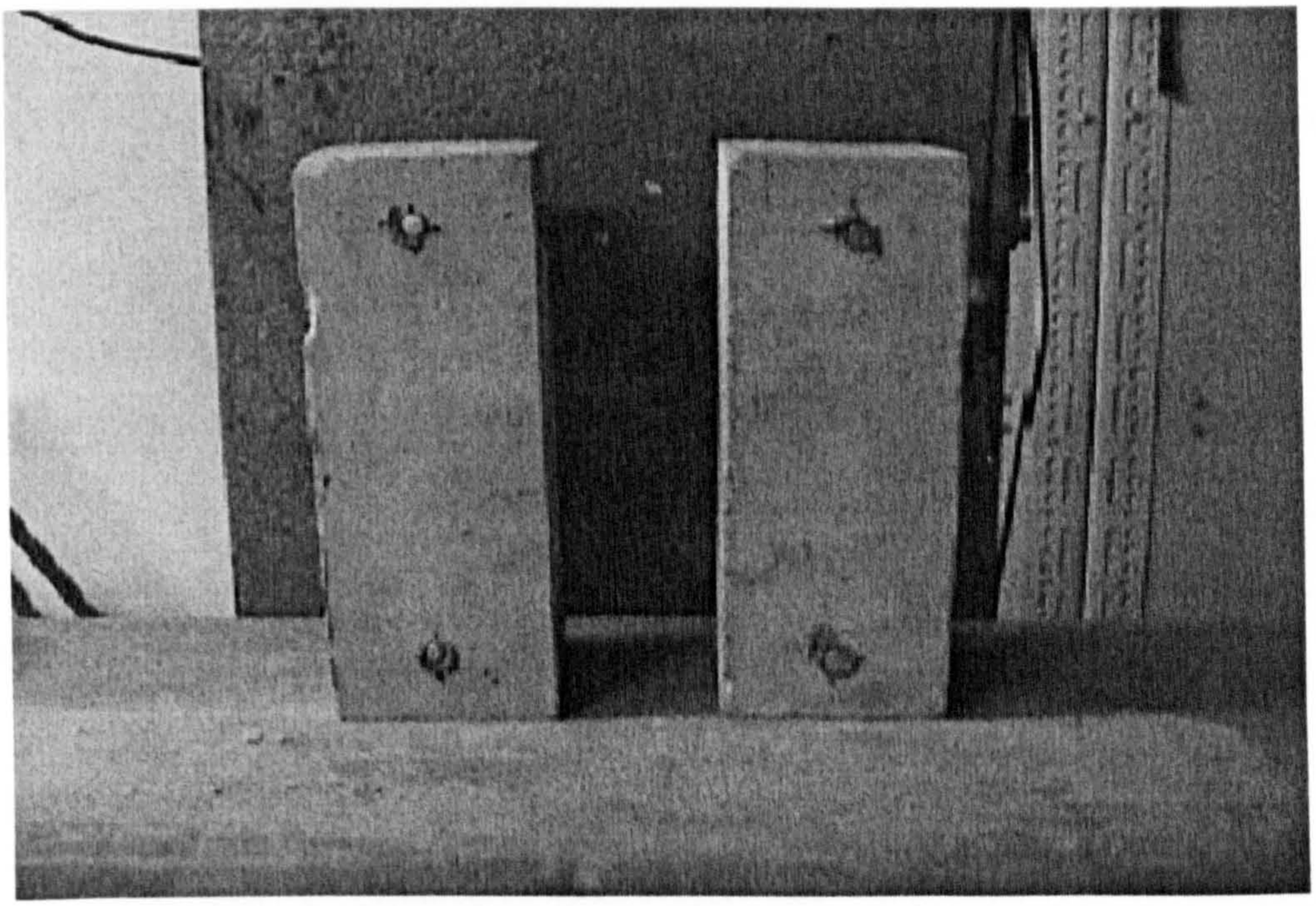

Plate 5.1: Shrinkage specimens stored in control environment room

When concrete is subjected to a sustained stress, the **C-S-H** loses an amount of physically adsorbed water and exhibits creep. Movement of water both internally, within the concrete, and externally to the environment causes creep.

Application of a constant stress to a concrete where there is no moisture movement to or from the surroundings, leads to basic creep.

When concrete is under load and simultaneously exposed to drying at a low relative humidity, the total strain is the sum of: elastic strain, drying shrinkage, basic creep, and drying creep. Total creep is the sum of the basic creep, and drying creep under drying condition. However, normally the distinction between the basic and drying creep is ignored. Creep is, therefore, simply considered as the deformation under load in excess of the sum of the elastic strain and free shrinkage strain.

5.3.2 Creep test specimens and procedure

As for shrinkage, creep tests were undertaken on concrete prisms sized 200×75×75mm. All specimens were cast and cured in accordance with Section 5.2.2.

The same three sets of reinforcement ratios were used for each reinforcement type, shown in Table 5.1 and Fig. 5.1.

Creep tests were performed using a loading frame and a method of measurement of strain developed at the Department of Civil Engineering, the University of Leeds (Liszka, 1972). This loading creep frame is designed to hold two 200×75×75mm concrete prisms and a calibrated steel-tube load dynamometer in series by four tie rods. Prior to loading, the Demec gauge readings of the dynamometer and the concrete specimens were recorded. The latter were recorded as zero strains.

The dynamometer and the specimens were installed in the frame and separated by steel spacers recessed to accommodate their ends and to ensure the alignment of the dynamometer and the concrete specimens. The load was transferred between the dynamometer and the specimens via a 25mm diameter metallic ball located between them. The loss of load due to creep of concrete, was checked through reading the change in strain of the dynamometer by a 200mm Demec gauge and then applying any

compensation manually by tightening the four nuts. Details of the creep loading frame are shown in Plate 5.2 and Fig. 5.2.

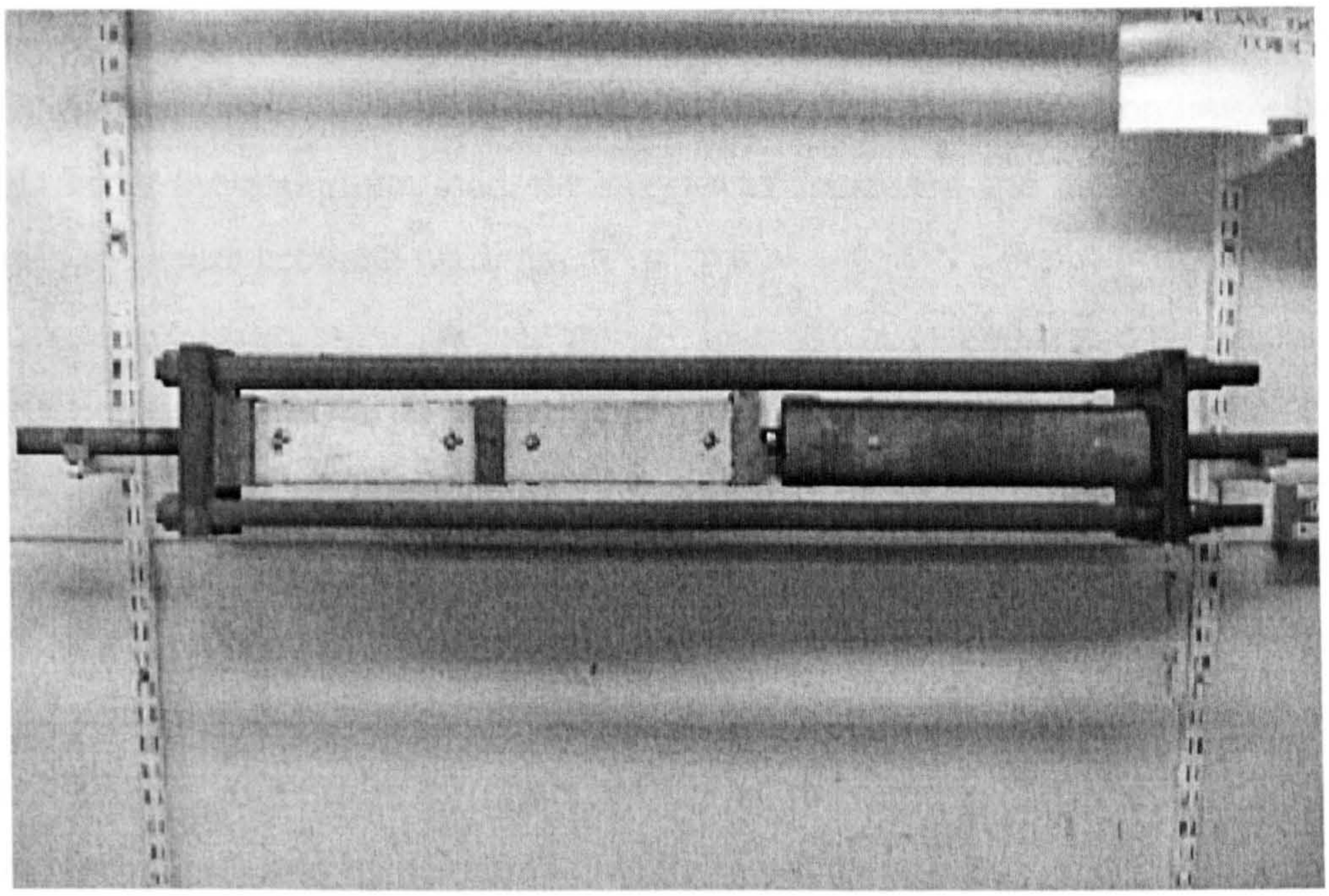

Plate 5.2: Simplified creep frame and specimens stored in the control environment room

The steel dynamometer was used to check the required applied load. The stress imposed on the concrete specimens was maintained to within 4% of working load for the duration of the test by tightening the four nuts, as mentioned earlier. The tightening process was done little by little and evenly to minimise eccentricity. The concrete specimens were loaded to a stress of 25% of the average compressive strength. The creep was measured by the 150mm Demec gauge, as for shrinkage specimens.

5.3.3 Calibration of the dynamometer

The stress applied to the specimens was measured using a steel tube dynamometer 296mm long, 76mm internal diameter, and 3mm wall thickness. The surface of the dynamometer contained Demec points with a gauge length of 200mm and at intervals of 90° around the circumference. The dynamometer was calibrated by cyclic loading up to

the required load (i.e. 25% of concrete compressive strength) in an Avery Denison Universal testing machine.

After taking a zero reading (i.e. when the dynamometer was not loaded), the load was applied until the required load was reached and then the corresponding strain was recorded. From the maximum load, the stress was decreased and the cycle was repeated three times to ensure accurate reading.

5.4 Prediction of elasticity, shrinkage and creep of concrete

In the remaining part of this chapter, the methods of estimating movements of non-reinforced (plain) and reinforced concrete are presented. Firstly, the existing methods for creep of plain concrete subjected to a constant stress are given. Secondly, analytical means of allowing for a variable stress or strain are presented for creep of plain concrete. Thirdly, the effect of reinforcement on movements is considered by existing analytical techniques and by development of composite model.

5.4.1 Existing methods for plain concrete subjected to a constant stress

Mostly, these methods are given in codes of practice and require no experimental input data. However, they are not very accurate and for better results experimentally determined parameters such as modulus of elasticity or a short-term value of shrinkage and creep improves the accuracy of prediction considerably.

The current methods available are: ACI Committee 209 recommendations (1992), CEB-FIP Model Code (1990), RILEM Model B3 (1996), Gardener and Zhao (1993), British Standards (BS 5400-4 (1990), and BS 8110-2 (2001)).

In the British Standard (BS), namely, **Appendix C of BS 5400-4:1990**, and **Section 7 of BS 8110-2:1985**. The free (i.e. unrestrained) shrinkage strain ε_{cs} at any instant may be determined by the product of four partial coefficients:

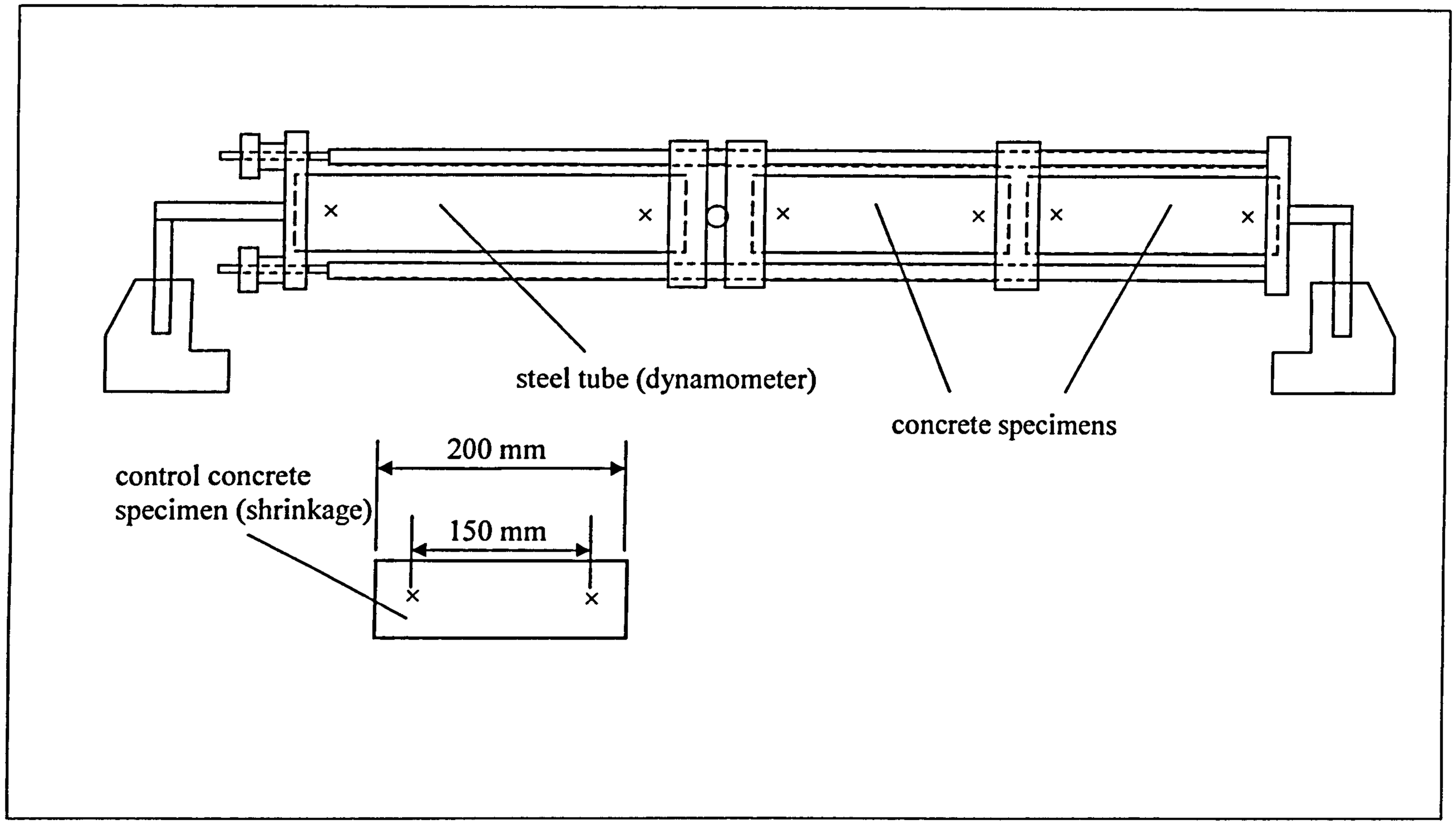

Figure 5.2: A simple test rig for the determination of creep of concrete under an approximately constant stress (After Neville and Liszka, 1973)

$$\varepsilon_{cs} = k_L \times k_c \times k_e \times k_j \quad (5.1)$$

Where

k_L = depends on the environment.

k_c = depends on the composition of the concrete.

k_e = depends on the effective thickness of the member.

k_j = defines the development of shrinkage as a function of time.

The k values for shrinkage are presented as graphs in BS 5400-4:1990, and BS 8110-2:1985. However, these factors were converted into formulae to give similar values by **Gilbert** (1988) and **Alexander** (2002) respectively. These are shown in Table 5.2.

Table 5.2: Values of coefficients for shrinkage in accordance with BS 5400-4 and BS 8110-2

	BS 5400-4	BS 8110-2
k_L	$400+300r-690r^2$	$625-1320r+3050r^2-2570r^3$
k_c	$(1.3+0.007c)(w/c)-0.85$	$0.0065c\ (w/c)=0.0065\ w$
k_e	$1.3-3.1h_e+3h_e^2$	$0.94-0.95h_e+0.6h_e^2$
k_j	$1/(1+250h_e t^{-0.8})$	$1/(1+550h_e t^{-0.8})$

Where

Units are in micro-strain, με.

r = relative humidity as a decimal.

c = cement content in kg/m^3.

w/c = water/cement ratio.

w = water content in $litres/m^3$.

h_e = 2×area/perimeter(m), maximum 0.6m.

t = duration of loading in days.

k_j = 1 at 30 years.

5.4.2 Concrete subjected to varying stress or strain

In reality, concrete members are often subjected to a varying load or some form of restraint which can vary with time. To allow for those factors, the creep estimated by any of the methods given in Section 5.4.1 can be modified by the following methods:

- Effective Modulus (EM) method.
- Trost-Bazant (AAEM) method.

The method for the prediction of creep based on the **Effective Modulus (EM) method** is well known. In this method, creep of concrete is accounted for by reducing the modulus of elasticity of concrete by a factor of $[1 + \phi(t,t_0)]$, where $\phi(t,t_o)$ is the creep coefficient at time t for concrete loaded at age t_0; thus the effective modulus is expressed as follows:

$$E_e = E(t_0) / [1 + \phi(t,t_0)] \qquad (5.2)$$

Where

$E(t_0)$ = modulus of elasticity at the age at first application of load (t = 28 days)

The ratio of creep deformation to initial elastic deformation is known as *creep coefficient* or *characteristic creep* ϕ.

The purpose of these tests is to measure the reduced modulus of concrete specimens to be used in the equations that calculate shrinkage and creep, instead of the 28-day modulus of elasticity of concrete. The latter does not take account of time and is therefore less accurate.

In light of the above, the EM method gives good results if two conditions are satisfied: first, where the concrete stress does not vary significantly during the period under investigation, and second, when aging of the concrete is negligible, as in old concrete (Neville *et. al*, 1983).

The total deformation, $\varepsilon(t)$, under conditions of drying at any age, t, is expressed as follows:

$$\varepsilon(t) = \sigma(t) / E(t_0) \times [1 + \phi(t,t_0)] + \varepsilon_{sh}(t) \quad (5.3)$$

There is another method which can be regarded as a modified version of the EM method to allow for the influence of aging on creep. This method was developed by Trost and improved by Bazant, it was therefore called **Trost-Bazant (AAEM) method.** The age-adjusted effective modulus (E_{ea}) is expressed as follows:

$$E_{ea} = E(t_0) / [1 + \chi(t,t_0)\, \phi(t,t_0)] \quad (5.4)$$

Where

$\chi(t,t_0)$ = the aging coefficient.

The total deformation, $\varepsilon(t)$, under conditions of drying at any time, t, is given by:

$$\varepsilon(t) = \sigma(t) / E(t_0) \times [1 + \chi(t,t_0)\, \phi(t,t_0)] + \varepsilon_{sh}(t) \quad (5.5)$$

The aging coefficient, χ, depends on the age at application of load t_0, the time under load $(t-t_0)$, and the form of the creep-time function. However, the load duration $(t-t_0)$ was found to have only a minor effect on the magnitude of χ and was, therefore, neglected. Values of $\chi(t,t_0)$ range from 1 to 0.5 with an appropriate of 0.82.

5.4.3 Effect of reinforcement

5.4.3.1 Existing methods

When symmetrically reinforced specimens are left to dry, the reinforcement will be under compression as it is trying to restrain the shrinking concrete. If the strain in the compressed reinforcement is ε_s, the total force in the reinforcement is $\varepsilon_s E_s A_s$, where E_s is the modulus of elasticity and A_s is the cross sectional area of the reinforcement. The

tensile strain in the concrete is $\varepsilon_{cs}-\varepsilon_s$ and the tensile force in the concrete is $(\varepsilon_{cs}-\varepsilon_s)E_cA_c$, where E_c is the modulus of elasticity and A_c is the cross sectional area of the concrete.

Since these two forces are opposite, the resulting equation that calculates the **restrained shrinkage** is as follows:

$$\varepsilon_{cr} = \varepsilon_{cs}/(1+m\times\rho_n) \quad \text{Alexander (2002)} \tag{5.6}$$

$$\varepsilon_{cr} = \varepsilon_{cs}/(1+m\times\rho) \quad \text{BS 8110-2} \tag{5.7}$$

Where

m = the modular ratio between the reinforcement and the concrete (E_r/E_c).

ρ_n = the net ratio of reinforcement area to concrete area.

ρ = the ratio of reinforcement area to total section area.

$$\rho_n = \rho/(1-\rho) \tag{5.8}$$

The difference between ρ_n and ρ is only significant at large reinforcement densities.

The restraint of the reinforcement means that **tensile stress** is induced in the concrete with value (Alexander, 2002):

$$\sigma_{ct} = \varepsilon_{cs} \times E_s \times \rho_n / (1+m\times\rho_n) \tag{5.9}$$

Reducing shrinkage by restraint of reinforcement is referred to in BS 5400-4 without mentioning a method for calculation.

Creep coefficient is estimated in a similar way as shrinkage, namely as the product of five k-factors as shown below:

$$\phi = k_L\times k_m\times k_c\times k_e\times k_j \tag{5.10}$$

The k-factors for creep from **BS 5400-4** and **BS 8110-2** were also converted into formulae by **Gilbert (1988)** and **Alexander (2002)** respectively. These are shown in Table 5.3.

Table 5.3: Values of coefficients for creep in accordance with BS 5400-4 and BS 8110-2

	BS 5400-4	BS 8110-2
k_L		$3.2+0.8r-3r^2$
k_m	$0.45+1.76e^{\wedge}(-0.267j^{0.44})$	$1.45-0.107(\ln j)-0.031(\ln j)^2+0.0039(\ln j)^3$ But $k_m = 0.55$ for $j > 365$
k_c		As in Table 5.1
k_e	$0.7+0.77e^{-9he}$	$5.88-1.62(\ln h_e)+0.125(\ln h_e)^2$
k_j		As in Table 5.1

Where

Units are in micro-strain, με

r = relative humidity as a decimal

j = age at loading in days

If temperature (T) varies from 20°C, $\delta_m=\Sigma j_m(T+10)$, and $j=\delta_m/30$

j_m = hardening time in days

c = cement content in kg/m^3

w/c = water/cement ratio

w = water content in $litres/m^3$

h_e = 2×area/perimeter(m), maximum 0.6m

t = duration of loading in days

k_j = 1 at 30 years

5.4.3.2 Composite models

Composite models can be used to predict the modulus of elasticity of reinforced concrete if both elastic moduli of concrete and reinforcement are known. For example,

Neville and Brooks (1998) and Domone (2001) mentioned a model for testing of concrete in terms of aggregate and matrix (cement paste). Assumptions used are:

1. Strain is proportional to stress.
2. Poisson's ratio is neglected.
3. The bond between the matrix (cement paste) and the particle (aggregate) remains intact.
4. The composite is a unit cube (side = 1).
5. ρ = volumetric fraction of the particle phase.
6. The stresses acting on the phases are different but for any cross-section the strain is assumed to be constant.

$$E_c = E_m \times (1 - \rho) + E_p \times \rho \qquad (5.11)$$

Where

E_c = modulus of elasticity of composite.

E_m = modulus of elasticity of matrix (cement paste).

E_p = modulus of elasticity of particle (aggregate).

In this investigation, the matrix is considered the concrete and the particle is considered the reinforcement.

For modelling creep, the reduced modulus for composite (E_{ec}) can be used to consider the effect of time, and Equations (5.2) and (5.4), can be used in conjunction with Equation (5.12).

$$E_{ec} = E_{em} \times (1 - \rho) + E_{ep} \times \rho \qquad (5.12)$$

Where

E_{em} = effective modulus of matrix (concrete) which can be substituted in Equations (5.2) and (5.4).

E_{ep} = effective modulus of particle (reinforcement). It remains the same (i.e. $E_{ep} = E_p$) as reinforcement is not affected with time.

A similar approach to that used by Hassan *et al.* (2001) for concrete repair can be used to predict shrinkage, modulus of elasticity and creep in reinforced concrete, if these assumptions are considered:

1. Strain is constant over any cross section.
2. Stress is proportional to strain.
3. Unit volume (volume = 1) of combined material.
4. Effect of autogenous shrinkage is neglected.
5. Thermal effects on volume change are neglected.

For equilibrium of forces:

$$\sigma_o \times A_o = \sigma_c \times A_c + \sigma_r \times A_r \qquad (5.13)$$

Where

σ_o = total stress of the composite (reinforced concrete) specimen (MPa)

A_o = total area of the composite (reinforced concrete) specimen (mm^2)

σ_c = stress of concrete (MPa)

σ_r = stress of reinforcement (MPa)

A_c = area of concrete (mm^2)

A_r = area of reinforcement (mm^2)

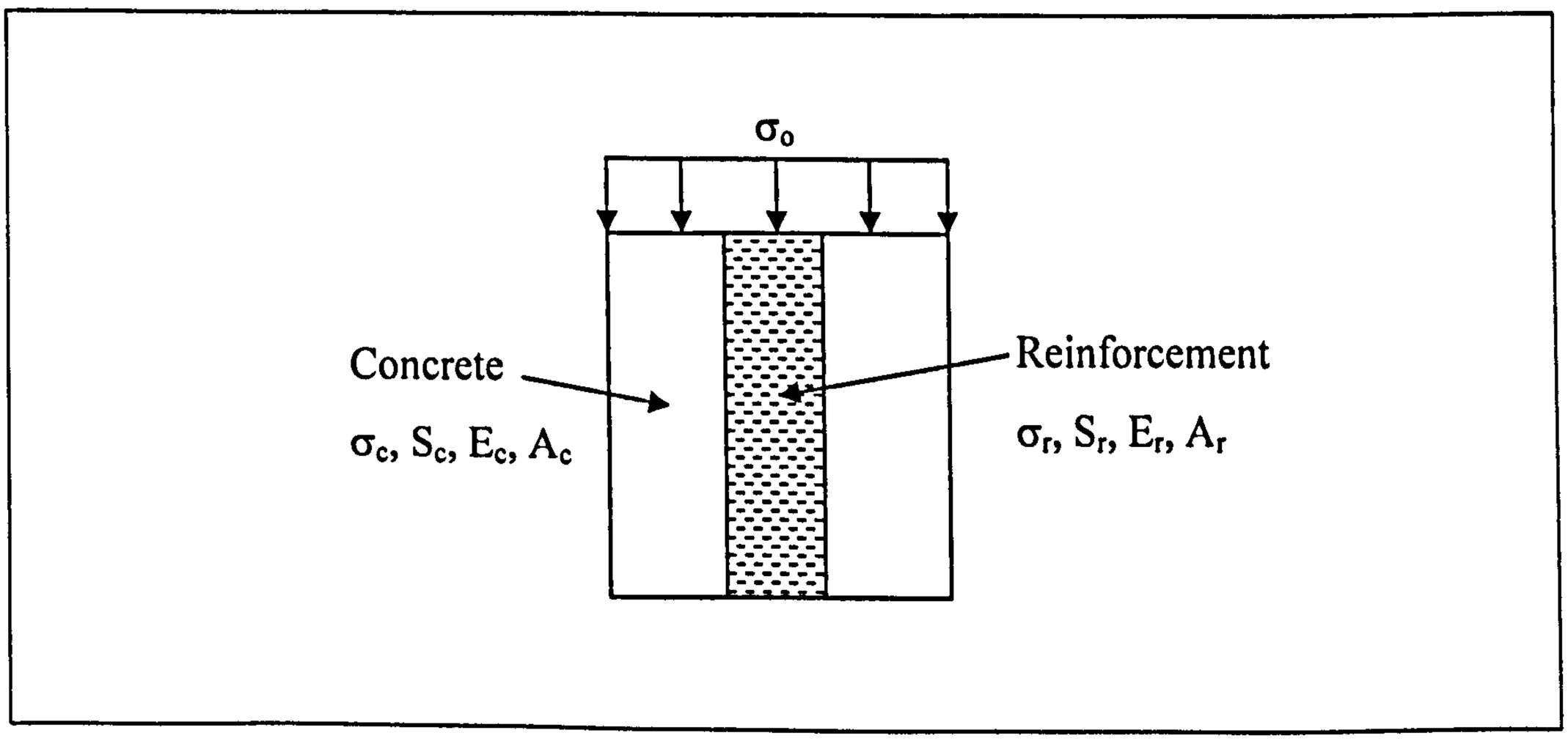

Figure 5.3: Stresses and strains of the composite system

For equality of strain:

$$\sigma_o/E_o\,(1-2\,\mu_o)+3\,S_o=\sigma_c/E_c\,(1-2\,\mu_c)+3\,S_c=\sigma_r/E_r\,(1-2\,\mu_r)+3\,S_r \qquad (5.14)$$

From which:

$$\sigma_c=[\sigma_o/E_o\times(1-2\,\mu_o)+3\,(S_o-S_c)]\,E_c/(1-2\,\mu_c) \qquad (5.15)$$

and

$$\sigma_r=[\sigma_o/E_o\times(1-2\,\mu_o)+3\,(S_o-S_r)]\,E_r/(1-2\,\mu_r) \qquad (5.16)$$

Where

μ_o , μ_c and μ_r = Poisson's ratio for reinforced concrete, non-reinforced concrete and reinforcement, respectively.

S_o , S_c and S_r = shrinkage for reinforced concrete , non-reinforced concrete and reinforcement, respectively.

E_o , E_c and E_r = elastic moduli for reinforced concrete , non-reinforced concrete and reinforcement, respectively.

Equations (5.15) and (5.16) give stresses in concrete and reinforcement, respectively.

Substitute Equations (5.15) and (5.16) in Equation (5.14):

$$\sigma_o=A_c/A_o\,[\sigma_o/E_o\times(1-2\,\mu_o)+3\,(S_o-S_c)]\,E_c/(1-2\,\mu_c)+A_r/A_o\,[\sigma_o/E_o\times(1-2\,\mu_o)+3\,(S_o-S_r)]\,E_r/(1-2\,\mu_r) \qquad (5.17)$$

Consider **modulus of elasticity** only, $S_o=S_c=S_r=0$

Then from Equation (5.17):

$$\sigma_o=\sigma_o/E_o\times(1-2\,\mu_o)\,[E_c\,A_c/(A_o(1-2\,\mu_c))+E_r\,A_r/(A_o(1-2\,\mu_r))] \qquad (5.18)$$

Therefore:

$$E_o=(1-2\,\mu_o)/(1-2\,\mu_c)\times(A_c/A_o)\times E_c+(1-2\,\mu_o)/(1-2\,\mu_r)\times(A_r/A_o)\times E_r \qquad (5.19)$$

If Poisson's ratios are neglected, then:

$$E_o=E_c\times\left(A_c/A_o\right)+E_r\times\left(A_r/A_o\right) \qquad (5.20)$$

Note that Equation (5.20) is similar to Equation (5.11).

Consider **creep** and replace E by E_{ea}:

$$E_{ea} = 1/(1/E + C_s) = E/(1 + E\,C_s) \tag{5.21}$$

Where

C_s = specific creep

E_{ea} = effective modulus

Substitute effective modulus in Equation (5.20)

$$E_o/(1 + E_o\,C_{so}) = E_c/(1 + E_c\,C_{sc}) \times (A_c/A_o) + E_r \times (A_r/A_o) \tag{5.22}$$

Assuming reinforcement does not creep:

$$C_{so} = \frac{1}{E_o} \times \left(\frac{E_o}{\frac{E_c}{1 + E_c \times C_{sc}} \times \left(A_c / A_o \right) + E_r \times \left(A_r / A_o \right)} - 1 \right) \tag{5.23}$$

or

$$C_{so} = \frac{1}{\frac{E_c}{1 + E_c \times C_{sc}} \times \left(A_c / A_o \right) + E_r \times \left(A_r / A_o \right)} - \frac{1}{E_o} \tag{5.24}$$

Consider **shrinkage** (S), $\sigma_o = S_r = 0$, then from Equation (5.17)

$$(S_o + S_c)\,E_c\,(A_c/A_o) / (1 - 2\,\mu_c) + S_o\,E_r\,(A_r/A_o) / (1 - 2\,\mu_r) = 0 \tag{5.25}$$

$$S_c\,E_c\,(A_c/A_o) / (1 - 2\,\mu_c) = S_o\,[E_c\,(A_c/A_o) / (1 - 2\,\mu_c) + E_r\,(A_r/A_o) / (1 - 2\,\mu_r)] \tag{5.26}$$

$$S_o = \frac{S_c \times E_c \times \left(A_c / A_o \right)}{E_c \times \left(A_c / A_o \right) + E_r \times \left(A_r / A_o \right)} \tag{5.27}$$

Chapter Six: Presentation and Discussion of Engineering and Pore Structure Results

6.1 Introduction

This chapter brings together the analysis of results, discussions and summary of findings from the test investigations accomplished in Chapter Four. The first section presents the results of engineering tests for concrete (flexural, compressive, and slump tests), in addition to introductory examinations, including bond between the reinforcement and concrete, flexural strength of GFRP rebars, and micro-structural aspects. The second section presents some methods of monitoring the detrimental effects of both alkali and brine solutions on the composite rebars. The means of observing these effects include engineering tests for GFRP bars (flexural strength), and pore structure of GFRP segments from mercury intrusion porosimetry (MIP).

6.2 Discussion and test results of engineering properties and introductory investigation

6.2.1 Properties of concrete

The engineering tests were performed on the concrete before setting and on the hardened concrete. Bulk specimens illustrated in Section 3.5. Average results were taken for each test, and are summarised in Table 3.4.

From Table 3.4, mix 1 has an average compressive strength of 80MPa after 28 days. However the degree of workability was very low; the slump test was in the order of 15mm. Mixes 1 and 4 were used to draw a comparison between the concretes in terms of strength and bond capacity. Mix 2, namely the one with w/c ratio of 0.5, was used for SEM specimens.

6.2.2 Bond strength

It is generally believed that the joint-beam test in accordance with RILEM (1978) can realistically simulate the stress conditions of reinforced concrete elements under bending conditions. All details related to this test including test procedure, specimen preparation, and calculations are referred to in Section 4.2.1.

6.2.2.1 Beams reinforced with steel

This section discuses the direct flexural test on joint-beams reinforced with steel. The beams were loaded until bond failure occurred or the bar itself failed. By the end of this test the results reported were mid-span deflection, relative end-slip and strain of the reinforcement during loading.

In this test, the failure was when the steel yielded. Therefore, the bar failed before bond failure in both concrete types, namely, concrete compressive strengths of 80 and 45MPa.

Figure 6.1 shows the deflection of joint-beam using concrete with an average compressive strength of 45MPa. The load was applied automatically to ensure a stress increment of 78.5MPa. As it can be seen from the figure, the deflection took two trends. The first part of the curve was almost linear. The second part was more non-linear with deflection began to decrease due to stiffening effect for each increment in load. The deflection was taken at 75mm each side from the centre of the beam and the average of these readings is displayed in the figure.

Figure 6.2 shows the deflection of joint-beam with the average concrete compressive strength of 80MPa. In this curve rather similar behaviour was detected. At first, the relationship was almost linear, then the curve indicated a stiffening effect as the applied load increased, and finally deflection started to increase indicating yield and failure of the steel bar.

Figure 6.3 illustrates the linear part of the stress-strain diagram of a steel rebar in an un-imbedded zone of a joint-beam with concrete compressive strength of 45MPa. The slope of this line was about 200GPa which is the modulus of elasticity of the steel bar.

It was only possible to detect strain of the reinforcement within the first part of the stress strain curve (i.e., when it was linear). That is because as the bar elongated, the strain gauge in it expanded until it was damaged and could no longer sense the strain development.

Figures 6.4 and 6.5 demonstrate the bond stress against end slip for steel rebars embedded in concrete with compressive strengths of 45 and 80MPa respectively. These graphs show strong bond capacity and relatively no movement of the free ends of the reinforcement up to yielding point.

6.2.2.2 Beams reinforced with GFRP

This section discuses the direct flexural test joint-beams reinforced by GFRP. The beams were loaded until bond failure occurred or, if the bond was strong, until the bar itself failed. As in the case of steel reinforced beams, the mid-span deflection, relative end-slip and strain of the reinforcement during loading were measured.

In the case of the joint beams reinforced with GFRP, failure occurred due to the GFRP lost bond with the concrete for both concrete strengths (80 and 45MPa). Therefore the failure mode was in bond.

Figure 6.6 gives the deflection of the joint–beam with the average concrete compressive strength of 45MPa reinforced by GFRP rebar. The load was applied automatically to ensure stress increment of 78.5MPa. As the figure shows, the first part of the curve was straight line up to a proportional limit, and the second part showed rapidly increasing deflection. Initially, the deflection reached up to 4mm when the applied load was about 16kN. The deflection then increased by around 8mm with no substantial increase in the applied load, when bond between the GFRP rebar and the concrete was finally lost.

Figure 6.7 illustrates the deflection of the joint–beam with the average concrete compressive strength of 80MPa reinforced by GFRP rebar. The figure confirms similar behaviour to that in Fig. 6.6. However, the deflection was 6mm when the applied load

on the specimen was just about 24kN. The deflection, then, increased dramatically until the bond between the GFRP bar and the concrete failed.

Figure 6.8 shows stress-strain relationship of the un-embedded part of the GFRP reinforcing the joint-beam. From this figure the modulus of elasticity of the reinforcement was found to be 40GPa which is consistent with this type of material.

Figure 6.9 reveals that with concrete of average compressive strength of 45MPa, the specimen suffered a bond failure. The specimen failed when the tensile stress on the GFRP rebar was slightly above 310MPa and slippage increased significantly after that. From this figure the bond strength was 7.7MPa.

Figure 6.10 shows the corresponding result for the joint-beam with the concrete of average compressive strength of 80MPa. In this case, the bond failure occurred when the tensile stress on the GFRP rebar was about 466MPa after which a dramatic slippage occurred. The bond strength was 11.6MPa.

Despite that bond capacity of GFRP rebars is relatively low; having some intermediate level of bond strength may be desirable due to the lack of ductility of the rebars. If the strain is increased too much in a beam reinforced with FRP rebars, then the reinforcement can reach the top of its stress-strain curve, leading to rupture of the reinforcement which can be sudden and catastrophic, also FRP unlike steel do not need corrosion protection provided by concrete (Burgoyne, 1993 and Burgoyne, 1997).

It is important to mention that in Figs. 6.9 and 6.10, only concrete compressive strength was varied. Therefore, when comparing the results of these two figures, the influence of concrete compressive strength on the bond capacity between the reinforcement and concrete is clear, despite some studies by (Ehsani *et al.*, 1995, and Kachlakev, and Lundy, 1999, Benmokrane *et al.*, 1996) undermining the importance of concrete compressive strength if there is adequate concrete cover. It is worthy to state that, most researchers who believe that compressive strength of concrete does not play a major role in bond capacity with FRP rebars had either conducted pull-out tests only, for instance Kachlakev and Lundy (1999); and Al-Zahrani *et al.*, (1999), or had not tested very

strong concrete specimens. In most studies the concrete strength was below 60MPa, besides the difference between the concrete compressive strengths was not very big (Ehsani *et al.*, (1995); Ehsani *et al.*, (1997); Benmokrane *et al.*, (1995); Kachlakev and Lundy (1999); and Malvar, (1995)).

In this investigation, the increase of compressive strength from 45 to 80MPa resulted in an increase of bond strength with GFRP rebar. In Fig. 6.9, the concrete compressive strength was 56% of that in Fig. 6.10. This was reflected in the bond strengths with the GFRP. The average bond strength in the concrete with 45MPa compressive strength was around 66% of that of the 80MPa concrete. In other words, the bond strength went up from 7.7 to 11.6MPa.

From the results in Figs. 6.9 and 6.10, it was concluded that concrete strength does influence the bond capacity. As concrete compressive strength increases, the modulus of rupture increases too. Therefore, when loading a reinforced beam for example, the tension zone in the beam will tolerate higher loads before cracking, i.e. when tensile load reaches the modulus of rupture of concrete. In turn, concrete will resist higher amounts of tensile stresses; and this will reduce the tensile force in the reinforcement. As soon as concrete cracks in the tensile zone, it will fail to take any tensile stresses where a crack is located. Consequently, the reinforcing bars will have to carry further stresses at the concrete cracked zones. Later on, if bond stresses become excessive, bond failure ensues.

The average bond strengths at three levels of slippage including the maximum bond strength are given in Table 6.1, for each concrete compressive strength. Results show that at around 0.01 and 0.1mm slippage, the bond strength of GFRP rebars in concrete compressive strengths of 45 and 80MPa was approximately 17-82% and 50-84% of the maximum bond strength, respectively.

The bond strength at different slippage stages and the bond strength at maximum slip were calculated by Equation (4.5), and the maximum slip was regarded as 0.5mm.

Table 6.1: Bond strength of concrete samples reinforced with GFRP rebar

Average bond strength (MPa) at different slippage level (mm)			
Concrete strength (MPa)	0.01 mm	0.1 mm	Maximum slip
45	1.3 ± 0.02	6.3 ± 0.04	7.7 ± 0.2
80	5.8 ± 0.0	9.8 ± 0.1	11.6 ± 0.5

6.2.3 Flexural characteristics of GFRP bars

Figures 6.11 and 6.12 show a series of stress-strain diagrams obtained from flexural tests on fibre reinforced plastic rebars. Details of the test procedure and specimen preparation were given earlier in Section 4.2.2.

The figures are for control specimens, meaning the specimens were tested as received from the manufacturer without aging in different environments and different temperatures. Therefore, they are referred to as not-aged specimens.

All specimens were tested up to failure and several results in relation to flexural properties were obtained. The failure mode was supposed to be one of three types; namely, failure initiated at the surface by the tensile stresses, failure initiated at the surface by the compressive stresses, or internal failure due to the shear stresses. In this investigation, however, the dominant failure mode was appeared to be by matrix cracking with no buckling of fibres in the compressive zone. These types of failure were mentioned in the literature and British standard test (BS EN 2746:1998). The dominant failure mode in this investigation, namely, tension failure has been identified also by Faza and GangaRao (1993) as the main mode of failure.

It is understandable why shear failure did not take place in this test. In flexure, the failure mode is influenced by length to depth ratios, i.e. at low ratios, the interlaminar shear failure is predominant while at high ratios the flexural failure is more frequent, and between these extremes the failure is a mixture of both. In this investigation, different

span lengths were tested until the right one was chosen to ensure no shear failure would occur.

Tensile-initiated failure can be either tensile fracture of fibres or tensile fracture of the outermost layer. Similarly, in a compression-initiated case it could be compressive fracture or compressive fracture including interlaminar shear. Table 6.2, summarises the results from this test.

Table 6.2: Flexural characteristics of five GFRP specimens

Specimen Number	Strength (MPa)	Max. strain (mm/mm)	Max. deflection (mm)	Elastic modulus (GPa)
1	1371.94	0.036	27.5	41.2
2	1286.76	0.032	24.5	41.8
3	1317.3	0.034	26.2	40.9
4	1293.2	0.035	27	39.8
5	1308.24	0.034	26.3	40.8
Average	1315.5 ± 33.8	0.034 ± 0.001	26.3 ± 1.14	40.9 ± 0.73

As mentioned above, it is worthy to stress the importance of the length to depth ratio of specimens and its influence on the failure mode. According to BS EN 2746:1998, the span length was not enough, namely, 16 times the depth. However, in ASTM D 4476-97 the span length was a range between 16 and 24 times the depth. In this investigation, the span length was checked until the most suitable span to depth ratio was implemented, namely 24. As the FRP material is of a composite nature, and any changes in the components, namely fibres and resins, should affect the properties of the final product, the span to depth ratio should not be assumed from the standard tests. Instead several tests should be carried out to determine the suitable span to depth ratio.

6.2.4 Compression characteristics of GFRP bars

The test method used for the determination of the compression properties of GFRP rebars, namely, modulus of elasticity and compressive strength, was in accordance with ASTM D695-96.

Figure 6.13 shows a series of five stress-strain diagrams obtained from the compression tests of fibre reinforced plastic rebars. In general, the stress-strain curves are seen to be almost linear elastic up to failure. Details of test procedures and specimen preparation was discussed earlier in Section 4.2.3.

Figure 6.13 is for control specimens, meaning the specimens were tested as received from the manufacturer without aging. All specimens were tested up to failure and several results in relation to compression properties were obtained. Table 6.3, summarises the results extracted from this test. Plate 6.1 shows two GFRP specimens tested in compression.

Table 6.3: Compression characteristics of five GFRP specimens

Specimen Number	Strength (MPa)	Max. strain (mm/mm)	Elastic modulus (GPa)
1	545	0.01009	51
2	606	0.01491	48
3	715	0.01684	45
4	622	0.01436	49
5	522	0.01169	48
Average	602 ± 75	0.01358 ± 0.003	48 ± 2

It can be seen that the average compressive strength, namely 602MPa, is less than the average flexural strength, namely 1315MPa. On the other hand, the average stiffness in compression is greater than in flexure, namely 48GPa and 41GPa, respectively. The variation in compression and flexural stiffness results was due to different methods of testing, this was also the case with other researchers. Chaallal and Benmokrane (1996) obtained compressive strength and stiffness for GFRP rebars in accordance with ASTM

D695-96, as 532MPa and 43GPa, respectively, and flexural strength and stiffness for the same rebars in accordance with ASTM D4476, as 1260MPa and 64GPa, respectively. In this investigation, the result of t-test for significance was 7.27 for stiffness in flexure and in compression, and the critical value of t for ($\alpha = 0.05$) and degree of freedom of 8 was 1.86. Since the t-test result was grater than the critical value, therefore the difference was significant.

6.2.5 Mercury intrusion porosimetry (MIP) for GFRP

The test procedure is detailed in Section 4.2.4. When considering the graph of cumulative pore volume against pore diameter illustrated in Fig. 6.14, it can be seen that the intrusion and extrusion curves do not coincide. This could be attributed to the existence of the so-called *ink-bottle pores* whose entry diameter is smaller than that of the pore itself. The existence of the ink-bottle pores is not accounted for in the Washburn equation. Therefore, smaller diameter pores tend to be overestimated, at the expense of larger ones.

Figure 6.14 shows the cumulative intrusion pore volume vs. pore hole diameter for not-aged segments. Moreover, the total porosity is found to be 2.641%, and the cumulative intrusion is 0.0132ml/g. Both the total percentage porosity and Fig.6.14 show the degree of compactness of the GFRP material, which is required to make it durable, since the principal role of the resin matrix is to provide protection to the glass fibres which determine the strength of this composite material. However, having compact surrounding to the fibres is not enough. It is also of high importance to have durable resins in order to provide continuous protection to the fibres whatever the harsh conditions this material could face in service. Similar test, namely MIP, to aged GFRP segments was carried out in this investigation, to determine the vulnerability of this material to different aging conditions.

The rest of the results relating to the not-aged (control) segments are summarised with the aged ones later in Table 6.4, for convenience.

The results of this test seem to be promising, besides highlighting very important characteristics regarding FRP materials, especially how the pores are distributed and connected to each other. This is very important in governing the ingress and permeation of ions in the composites.

6.2.6 Micro-structural imaging

Figures 6.15 and 6.16 show two SEM images at different magnifications. During preparation of these specimens different coatings, namely gold and carbon respectively, were used for comparison. The figures reveal a high fibre content of GFRP (approximately 65% by volume, according to the data sheet) which is evenly distributed across the section. Also, these images show the resin binding the fibres together and separating them to provide protection from abrasion due to fibre surface friction during service life. In Fig. 6.16 there are some dark areas on the fibres due to overdosing of the carbon coated specimen.

Another two SEM images are shown in Fig. 6.17 (A and B) using a higher magnification factor. They show glass fibres of white colour and rounded shape surrounded by the resin matrix (dark areas between fibres). It can also be seen that the fibres used for the rebar have an average diameter of about 25 μm.

Figure 6.18 shows an enlarged SEM image of a single cross section of glass fibre surrounded by resin and other fibres. Cracks appearing in Figs. 6.17 and 6.18 are due to surface polishing of the specimens during preparation.

Figures 6.19 through 6.21 illustrate a series of SEM images for GFRP/concrete interface. The specimens consist of concrete with water/cement ratio of 0.5 and mix proportions of 1/2/3 for cement/sand/aggregate respectively reinforced by GFRP rebar and cured in the fog room for 28 days. The irregular and rough surface of the composite rebars, which was provided by the outer layer of the resin matrix, allows for interlock between the reinforcement and concrete and therefore enhances bond strength. In addition, there is a section within the interface with either a thin resin surface layer or with no resin at all (Fig. 6.21, A and B). This is due to either poor fabrication or surface

damage to the composite reinforcement during handling and it is of high importance because durability of composites depends mainly on two things: the quality of the manufacturing process and the type of matrix that provides protection to the fibres.

It seems likely that there should be micro-cracks within the interface zone, similar to the ones exist between concrete and steel reinforcement. However, it is possible that any micro-cracks existing between concrete and reinforcement could have been filled with resin impregnation during preparation of the specimen. Therefore, detecting these micro-cracks, if existed, was not possible in these images. Figure 6.22 shows a longitudinal interface between steel rebar and concrete.

6.3 Discussion of test results on durability

In this section, resistance to degradation of GFRP composites in severe environments is examined. Changes in flexural strength and pore structure of GFRP segments from mercury intrusion porosimetry (MIP) were monitored.

6.3.1 Flexural strength

In this section, all specimens were submerged in aging solutions and tested periodically as a function of immersion time between 30 and 270 days of exposure.

The importance of this test is to reflect the changes that can take place in glass, resin, or the glass/resin interface.

All specimens were tested, as mentioned in Section 4.2.2, up to failure. In such test the failure mode is supposed to be one of three, namely, failure initiated at the surface by the tensile stresses, failure initiated at the surface by the compression stresses or internal failure due to the shear stresses. However, it was concluded that the dominant failure mode was illustrated by the matrix cracking with no buckling of fibres in the compressive zone. The dominant failure mode in this investigation, namely, tension failure was observed, by Faza and GangaRao (1993) also as the main mode of failure.

Tensile-initiated failure can be either tensile fracture of fibre or tensile fracture outermost layer. Similarly, in compression-initiated failure, it could be compressive fracture or compressive fracture including interlaminar shear. Possible failure modes are detailed in BS EN ISO 14125:1998.

6.3.1.1 Degradation in brine solution

Figures 6.23-6.30 show stress-strain diagrams obtained from flexural tests of the fibre reinforced plastic rebars. The figures are for aged specimens subjected to a sea-like environment in terms of salinity, including different temperatures, and varying period of exposure. Each figure displays the test results of five specimens under the same condition.

With regards to the stress-strain relationship of aged rebars in brine solutions, this was linear until the point of failure. The variation in temperature and period of ageing had no effect on the elasticity of the material. However, an examination of most of the flexural results revealed a reduction in both strength and failure strain upon aging. An exception to this was the case of aging in the presence of NaCl salt at ambient temperature when the samples were aged for one month. This may suggest that an induction period exists initially after submerging during which time water absorption was relatively slow, probably due to the absence of excessive cracking and fracturing of the matrix and non-existence of fibre damage, which can cause further curing to the resins. This phenomenon was reported by Sonawala, and Spontak (1996) and Kajorncheappunngam *et al.* (2002).

Strength loss of composites in solutions normally occurs when the aging solution diffuses through the surface resin layer and reaches the underlying glass fibres, or penetrates into the composite core through micro-cracks or other surface faults and damage due to poor manufacturing processes or handling (Vieth, 1991).

However, the aging solution will attack the resin matrix first, causing hydrolysis of the polymer. In turn, acid is released and pH of the aging solution is lowered. In addition, solution diffusion and clustering in the resins is also responsible for swelling and

introducing internal stresses which result in micro-cracks and debonding between individual fibres and the matrix.

Furthermore, if the resins are not fully cured, immersion in liquid media will raise cross-link density and therefore increase the ultimate strength (in this investigation flexural strength). Furthermore, ingress of the solution in the polymers could be responsible for reducing glass transition temperature (T_g), which allows the polymer chains to become mobile, and consequently encourages cross-linking and full curing.

Depending on how durable the resin matrix is and how long it will take to hinder the progress of permeation, the aging solution will eventually reach glass fibres. The attack begins and Na is leached from the glass. Consequently pH of the interface zones will go up:

$$Na^+ (glass) + 2H_2O = H_3O^+ (glass) + Na^+ + OH^- \quad (6.1)$$

$$H_2O + Si\text{-}O\text{-}Si = SiOH \quad HOSi \quad (6.2)$$

From the above reactions, it is obvious that an aqueous solution will cause alkaline attack as the OH^- ions start to attack the Si-O-Si structure with rising pH as seen in Equation (6.3) (pH can reach between 8 and 11). As a result, the surface of the glass will dissolve. Moreover, the susceptibility of the acid of the matrix to hydrolysis can be expected to be enhanced by the alkali extracted from the fibres in the interface region:

$$Si\text{-}O\text{-}Si + NaOH = Si\text{-}OH + Si\text{-}O\text{-}Na \quad (6.3)$$

This results in glass fibre corrosion, a reduction in the cross-sectional area of the fibres, further fibre/matrix debonding and loss of strength of the composite.

Figure 6.39 summarises the variation of flexural strength (σ_f) retention with immersion time for GFRP rebars at different temperatures in brine solutions. The flexural strength retention (σ_f) after 270 days for the composite aged in brine at 60°C and 20°C was about

64% and 85%, respectively. Therefore, the influence of higher temperature on degradation is clear.

Gupta *et al.*, (1985), and Kajorncheappunngam *et al.*, (2002) reported that, initially an increase in ultimate tensile strength takes place upon aging in liquid media (i.e., brine, acid, alkali solutions or even water) due to an increase in cross-link density of the epoxy resins. In this investigation, similar finding were obtained (for another type of resin matrix) as there was an increase in the flexural strength of 4% after immersion in saline liquid for 30 days at 20°C.

In order to understand why this happened, manufacturing process needs to be considered. The resins contain reactive sites in their molecular chains. During production processes, cross-linking monomers are added, and in the presence of a catalyst, the monomer cross links the polymer chains at each of the reactive sites to form a highly complex three-dimensional network. The resin is then said to be cured. It is now a chemically resistant and usually hard solid. The cross-linking or curing process is also called polymerisation. However, if the polymers are not fully cured, and later are aged in solutions, it can cause further curing as seen in this investigation.

It is worth pointing out that this percentage of increase occurred after 30 days of submergence, and was not necessarily the maximum increase. In fact, more increase in ultimate flexural strength upon ageing could have taken place either before or after the 30-day immerse but it was not recorded. In addition, similar phenomenon could have occurred for specimens in the other aging conditions namely, brine at 60°C and alkali at 60 and 20°C.

This behavioural variation of GFRP composites in responding to exposure to brine solution could suggest that exposure to such solutions for long period of time classified into two phases, i.e. **early** and **late** phases of exposure.

The **early phase** goes in more than one direction, namely can be a strength gain and a strength loss. On one hand, there is the so called induction period. It exists initially after submerging during which time water absorption is relatively slow. This is

probably due to the absence of excessive cracking and fracturing of the matrix and non-existence of fibre damage, in conjunction with further curing to the resins and increase in cross-link density and strength. This phenomenon was recorded somewhere else (Sonawala, and Spontak, 1996; and Kajorncheappunngam *et al.*, 2002). On the other hand, Cl^- ions can penetrate into the resin matrix (causing macro-cracking and fracturing of the matrix). Furthermore, the derogatory effect of NaCl salt on the composite rebar properties is due principally to the presence of water (moist), which ingresses and permeates into the composite causing hydrolysis to the matrix and facilitating the ingress of Na^+ and Cl^- ions. This phenomenon can result in a loss of strength.

The **late phase** takes place as macro-cracks and fracturing are enlarged and developed rapidly by Cl^- ions and in severe cases (depending on the aging solution, percentage of harmful ions exist in the solution, time and temperature of exposure, and composite material) fibre/matrix debonding can happen too.

As mentioned previously, water on its own and even highly humid air can cause degradation of FRP composites. In fact, Jones (1989) suggested that the NaCl salt does not seem to considerably change the solubility of water in the resin matrix (i.e., isophthalic polyester), and Sonawala and Spontak (1996) indicated that equilibrium mass uptake of composites in brine was just slightly lower than that of distilled water.

It was also noticed that higher temperatures increase the degradation of GFRP rebar specimens expressed in greater reduction in the flexural strength, due to an increase in chemical reaction and therefore the rate of deterioration.

Changes in the mechanical properties, namely flexural strength, reflect the physical and chemical alterations that occur to the composite material, including material softening, which could lead to enhanced deformation, hydrolysis of the polymers and introduction of internal stresses due to water clustering and hence swelling of the composites which results in micro-cracks and debonding between the fibre and the matrix. Water clustering causes fibre/matrix debonding and induces matrix plasticization, which would allow for further debonding.

In this investigation, the continuous and relatively large decline in strength of composite indicates that the harmful ions present in the aging solutions are not restricted to the surface layer of the composite, but actually find their way to the inside. This suggestion is supported by other researchers (Sonawala, and Spontak, 1996) when energy-dispersive X-ray maps obtained from the fracture surfaces of composites confirmed that Cl^- is present throughout the specimens after submerging in brine solution.

6.3.1.2 Degradation in alkaline solution

Figures 6.31 through 6.38 show a series of stress-strain diagrams obtained from flexural tests on fibre reinforced plastic rebars. The figures are for aged specimens subjected to a highly alkaline environment, including different temperatures, and varying period of exposure.

As in aging of specimens in brine solution test, the stress versus strain curves of the not-aged and aged rebar samples were linear until the point of failure regardless the variation in temperature, and period of ageing. However, an examination of all of the flexural results reveals a decline in both strength and failure strain upon aging.

The alkali attack mechanism is similar to that of brine solution, yet it is more severe as can be seen from the results. Moreover, in this particular investigation, the concentrations of hostile ions in the alkali solution are higher than those in brine solution. In addition, when the aging solution gets to the glass fibres, hydroxide ions (OH^-) attack the primary component of glass (silica or SiO_2) and cause a breakdown in the Si-O-Si single bond that forms the glass molecular structure as represented in Equation (6.3). This results in glass fibre corrosion, a reduction in the cross-sectional area of the fibres, fibre/matrix debonding and therefore loss of strength.

In short, elevated pH environments can cause:

1. Rapid fibre dissolution, followed by interface de-bonding.
2. Enhanced matrix hydrolysis and extraction of acid that exists in it (e.g., acrylic acid).

Figures 6.40 summarises the variation of flexural strength (σ_f) retention with immersion time for GFRP bars at different temperatures in alkali solutions. It can be seen that the variation in temperature has a great effect on the rate of degradation. This is due to the influence of temperature on the degradation mechanism. The mechanism at elevated temperatures may not be the same as at ambient temperature. Evidence of other research results (Sonawala, and Spontak, 1996) suggested that, for very high temperatures (as high as 80°C), the diffusion of alkali solution into a resin matrix initially induces a weight increase. However, it is soon followed by a reduction in weight due to dissolution and hydrolysis of the resin. As the temperature of alkali aging solution decreases, the reduction of weight (that follows the mass uptake) decreases too, until in some cases, it shows no evidence of erosion-induced reduction in specimen weight at moderate temperature of about 25°C.

The flexural strength retention (σ_f) after 270 days for the composite aged at 60°C was about 47%, while that at 20°C was around 73%. Despite this big difference between the strength retentions, the initial degree of degradation (i.e., first 30 days) was in close agreement, the strength reductions of 18% and 11% for aging at 60°C and 20°C in alkali solutions, respectively, were recorded. Later on, the influence of higher temperature on degradation was more pronounced. This behavioural variation in responding to exposure to alkali solution could be attributed to the same reason of exposure to brine solutions and could go through the same phases, namely, **early** and **late** phases of exposure.

The strength reduction continued to take place as the dissolution mechanism of glass fibres did not cease. This is because alkali ions, including OH^-, at the interface continued to build up from the aging solution as well as the released alkaline modifiers from the glass. The OH^- ions break up the silica network without being consumed.

Having mentioned that, there was a significant reduction in rate of strength decline when aging between 30 and 90 days at 20°C. This could be due to the shift from the first phase to the second. It also could indicate that the initial period of submergence, namely up to 30 days, caused deterioration to the resin matrix only. The period between 30 and

90 days could allow further destruction of the resin and induction period to the glass fibres, where the latter showed good resistance. After 90 days of immersion, it was clear that the glass fibres were attacked and therefore strength reduction was more distinct. Nishizaki and Meiarashi (2002) related a 20 % reduction in bending strength for glass fibre reinforced vinyl ester resin (bisphenol-A type) specimens in water at 40°C, and in an atmosphere at 60°C and 85% RH to a decline in the strength of the resin only.

However, similar behaviour was not recorded in the 60°C solution. It seems to be that as high temperature increases the rate of degradation, it can cause advert effect on monitoring the details of degradation progress. Sonawala and Spontak (1996) also came to the same conclusion regarding an induction period where the rate of dissolution of glass fibres increases after that period. They also concluded that as the temperature increases the induction period decreases.

In comparing Figs. 6.39 and 6.40 at short and long times of aging, alkali solutions showed more hostility to GFRP than brine ones. In general, the trends in these figures show some similarity. This may suggest that the composites degrade in the same way at normal and high temperatures, which is in agreement with Prian and Barkatt (1999). Also in alkaline and brine solutions, noticed elsewhere by Sonawala and Spontak (1996), i.e. degradation occurs by combination of resin hydrolysis and fibres dissolution leading to fibre/resin debonding.

In addition, when considering these two figures, one can notice that the rates of degradation began very rapidly and then slowed down. The first rapid decline was more likely due to degradation of the resin which was directly exposed to the aging solutions and the fact that it possesses higher porosity, as opposed to the glass fibres which were embedded in the resin and almost non-porous.

The flexural modulus of elasticity of all the samples fluctuated between 38 and 42 GPa. In other words it almost remained the same and there is nothing to suggest that aging of GFRP composites has an effect on the elastic modulus over the period of testing (see

Fig. 6.41). By and large, reduction in strength was reflected on the reduction in the failure strain as shown in Fig. 6.42 as they are related to one another.

In general this material has shown a good durability for the reasons mentioned in the following:

1. Both the fibre and the matrix were chosen carefully by the manufacturer, and there has been extensive work to fabricate the best product to serve in civil infrastructure. For instance, in vinyl ester resins the weakest ester linkages are partly replaced by the stronger ether linkages that are highly resistant to alkalinity. Moreover, they (vinyl ester resins) contain less polar groups, and in turn, less diffusivity and absorptibility. In addition, it is believed that vinyl esters are more stable to hydrolysis than isopolyesters, because ester linkages in vinyl esters are terminal and are shielded by methyl groups, also these ester groups, which are susceptible to water degradation by hydrolysis, are fewer. However, in most other polymers, ester groups are distributed along the main chain, making them more available (and hence more vulnerable) to hydrolysis reactions and any other chemical attack.

2. The locations of the vinyl ester resin's reactive sites are positioned only at the ends of the molecular chains. As the whole length of the molecular chain is available to absorb shock loadings, this makes vinyl ester resins tougher and more resilient than polyesters.

3. Microscopic images show a very good cohesion between the glass fibre and the resin matrix, besides a big percentage number of fibres in the composite and the way fibres are distributed evenly (see Figs. 6.15 to 6.17). The existence of a high percentage of glass fibres in the composite is of great importance because they determine the strength of the composite, and they are negligibly permeable.

4. The adverse effects on the rebars due to alkaline and brine solutions are higher than that of cement paste because in the present case ions are free to travel. In addition, high temperatures increase the degradation of GFRP, because chemical

reactions are enhanced at elevated temperatures. Consequently, the results obtained from accelerated aging investigations must be analysed and interpreted with some caution. For example, according to previous research by Porter *et al.*, (1997), results showed that submerging GFRP tendons in an alkali solution with a pH of 12.5 at 60°C for 2 to 3 months was equivalent to 50 years in concrete.

5. If the same specimens had been aged under the same conditions and tested in tension instead, they would have exhibited a lower decrease in ultimate tensile strength than that in ultimate flexural strength (Sonawala, and Spontak 1996; and Nishizaki and Meiarashi 2002), because in a flexural test the resin matrix plays a remarkable role in determining the strength of the composite. However, same thing cannot be said for direct tensile strength, where the resin matrix should contribute only little to the composite strength. Thus, the reduction in ultimate strength in flexure has to be the result of degradation of the glass fibres, the fibre/matrix interface and/or resin matrix.

The following equation can be used to provide a rough estimate of the influence of temperature on the accelerated aging in alkali solution, although should not be used for prolonged submerging periods (Vijay and GangaRao, 1999; and Micelli, Naani and La Tegola, 2001):

$$t/C' = 0.098 \times \exp(0.0558 \times T') \quad (6.4)$$

Where

t = age in days.

T' = conditioning temperature in °F.

C' = days of accelerated exposure at temperature T'.

$$T'(^{\circ}F) = (9/5) \times T'(^{\circ}C) + 32 \quad (6.5)$$

According to Equation (6.4), 30 days of exposure in an alkali solution at 60°C was equivalent to 20 years in the concrete ambient. That is to say, approximately **20 years** in concrete ambient, the GFRP rebar might lose up to **19%** of its original strength in

flexure. Having mentioned this, the original (not-aged) flexural strength is already very high; i.e. an average of 1315MPa.

There are several points to be highlighted as follows:

1. GFRP rebars retain their elastic behaviour all the way through to failure despite their history of exposure.

2. It is very important to select the correct span to depth ratio to avoid shear deflection. That can be achieved by altering the span length and monitoring the failure mode.

3. Many researchers are interested in studying the durability of FRP after a prolonged exposure in aging solutions, including this investigation, although it overestimates the real life conditioning. It could be more beneficial, however, to shorten the time of exposure and concentrate in changes take place in the initial period (i.e. one month or so), including the further curing of the composite upon early contact with the aging solutions or humidity.

4. When comparing results of the two different aging solutions employed, the alkali solution has a higher degradation effect on composite strength especially with high temperature. This is because, although Cl^- ions can penetrate into the resin matrix causing system damage, they are not as damaging to the glass fibres as the OH^- ions are. Furthermore, the derogatory effect of NaCl salt on the composite rebar properties is due principally to the presence of water (moist), which ingresses and permeates into the composite, carrying with it Na^+ and Cl^- ions. The aging in brine solution with 20°C, on the other hand, has the least negative effect on the composites. These results were in agreement with most researchers.

5. Both immersion solutions, namely alkali and brine had to be replaced from time to time by new ones due to a reduction in pH. The rate of reduction at higher temperature, namely 60°C, was faster than that in lower temperatures, because

submerged composites release acid into the surrounding solution due to hydrolysis of the matrix and this phenomenon increases with a temperature increase.

6. Elevated pH causes rapid fibre dissolution, and enhanced matrix hydrolysis and extraction of acid. This is followed by interface debonding and strength reduction.

7. Examination of the FRP products under electron microscopy should be carried out as one of the quality control tests to ensure sufficient protection to the fibres is provided by the resin.

8. Attacks on fibres (that determine strength of the composite) has been mainly attributed to the highly alkaline nature of the aging solution which simulates ions existing in concrete as hydration products (i.e., $Ca(OH)_2$). To reduce this detrimental effect, pozzolanic materials such as silica fume can be added to concrete. Pozzolanic materials have small particle size and high reactivity especially with $Ca(OH)_2$ components of cement, and therefore can inhibit the formation of such chemical compounds.

6.3.2 Mercury intrusion porosimetry (MIP)

In this section, all specimens were submerged in aging solutions, namely brine and alkaline, and tested periodically at 90, 180 and 270 days of exposure. The importance of this investigation is to highlight changes in the micro-structure of GFRP upon aging and compare it with the original micro-structure. All specimens were tested, as previously mentioned in Section 4.2.4.

The results for MIP, presented in Table 6.4, show a group of results based on the not-aged (control), aging condition and period of immersion. The results can be further observed in Figs. 6.43 through 6.46.

Table 6.4 MIP test results for aged and not-aged GFRP segments

Condition	Age (days)	Total intrusion volume (mL/g)	Median pore diameter (Å)	APD * (Å)	Total porosity (%)	TPA ** (m^2/g)
Control	N/A	0.0132	117	82	2.6414	6.446
Alkali at 60 °C	90	0.0149	164	94	2.9857	6.32
	180	0.0162	164	106	3.2421	6.128
	270	0.0192	252	130	3.8398	5.886
Alkali at 20 °C	90	0.0143	129	90	2.8612	6.372
	180	0.0148	141	94	2.9601	6.312
	270	0.0159	176	101	3.1805	6.277
Brine at 60 °C	90	0.0146	123	93	2.9213	6.311
	180	0.0154	147	99	3.0803	6.253
	270	0.0171	180	111	3.4209	6.189
Brine at 20 °C	90	0.014	118	87	2.7912	6.418
	180	0.0145	120	91	2.9010	6.371

* APD = Average Pore Diameter (Å), (1nm = 10Å)
** TPA = Total Pore (surface) Area (m^2/g)

In addition, a further comparison between other parameters representing this test are illustrated in Figs. 6.47 to 6.51.

6.3.2.1 Degradation in brine

When considering the cumulative intrusion pore volume versus log pore hole diameter for aged segments in brine solutions, i.e. Figs. 6.43 and 6.44, these curves show the limiting pore size beyond which no further mercury intrusion occurs. The effect of both temperature and period of aging upon the micro-structure changes of composite material can be seen. The total intrusion volume and the distances between the adjacent lines increased as the material was left longer in the brine solutions, which means the rate of ion attack increased causing hydrolysis to the resin, dissolution to the fibres and consequently fibre/resin debonding. In fact, the rate of attack increased with time because the hostile ions were given further opportunity to ingress and build up in the composite's different phases and new pore openings and micro-cracks were introduced to the material allowing the ions to get deeper.

In addition, as hydrolysis and dissolution took place other kinds of attack were promoted, namely acid attack to the resin and alkali attack to the fibre/resin interface.

The acid attack, however, was controlled by monitoring the pH of the aging solution regularly and replacing it whenever that was required.

These two figures also reveal that the higher the temperature of aging, the higher the total intrusion pore volume and the distances between the lines. In other words, there was a higher rate of degradation, which is in agreement with the results of flexural strength degradation given in the previous section. For example, the total intrusion volume of specimens immersed for 180 days in the 60°C solution was 0.0154 while in the 20°C solution it was 0.0145mL/g.

6.3.2.2 Degradation in Alkali

In the case of aging in alkali solutions (Figs. 6.45 and 6.46) the degradation was more pronounced than in the brine solutions for each set of temperatures (i.e. aging in alkali caused more micro-cracks and openings than in brine aging at 60°C and 20°C). As a result, more strength degradation took place in alkali aging than in brine solutions. As the micro-cracks increased new micro-channels were opened and hostile ions found better and wider access to the core of the composite material, consequently further degradation occurred.

As mentioned earlier in the case of the brine solutions, the effect of a higher temperature resulted in an increased rate of degradation. In addition, Fig. 6.47 summarises data from Figs. 6.43 to 6.46, which gives the maximum volume of mercury intruded into the sample at the highest pressure attained during the test. It can be seen that the rate increased in the last period as a result of faster attack due to more of the composite surface being exposed to the penetrant ions.

Figures 6.48 to 6.51 provide further illustration of the micro-structural changes in the GFRP due to aging in brine and alkali solutions, in terms of porosity, average pore diameter, pore surface area and median pore diameter.

In all the aging solutions, the porosities for all specimens increased but at different rates as a result of different susceptibility of GFRP to the type of aggressive environments

they were exposed to. In the case of alkali aging at 60°C and 20°C, the porosity increased by 42% and 22% in 270 days, respectively. While, it went up by 30% in the brine solution at 60°C after 270 days.

In Fig. 6.49 which shows the effect of immersion period, temperature, and type of solution on the average pore diameter, which is the ratio of total intrusion volume and the total pore (surface) area, assuming that all pores are of cylindrical shape.

Aging of GFRP in harsh solutions introduces new micro-cracks and widens the existing pores. This is proven by Fig. 6.50 which illustrates changes in the pore surface area upon aging. All curves reveal reductions in this parameter, which could mean a decrease in the number of smaller pores, probably due to smoothen of the rough internal surfaces of the pores. It also shows that the largest decline was in aging in alkali at 60°C and the lowest decline was in aging in brine at 20°C.

Figure 6.51 summarises the median pore diameter which is the diameter (pore size) at 50% intrusion obtained from the cumulative intrusion curve. The median pore diameter (MPD) by volume relates to the relative volume of smaller pores, i.e. for two specimens have similar cumulative pore volumes, the one with greater MPD value is the one that has the greater volume of larger pores.

Figures 6.52-6.55 compare the incremental intrusion pore volume versus pore hole for not-aged and aged specimens in brine and alkali solutions at different temperatures and periods of aging. In general, for most aged specimens there was an increase in larger pores and decrease in smaller pores as can be seen from the trend lines. It can be seen that specimens aged in brine solution at 20°C were least affected. This is in agreement with Figs. 6.50 and 6.51.

The size and continuity of the pores in the polymer network play a very important role in moisture penetration (Diamant *et al.*, 1981). As can be established from the results of this investigation the resin matrix is very compact.

6.3.3 Correlation

A correlation can be made between porosity (P, %) and degradation of flexural strength (σ_f, MPa) of the GFRP specimens tested in this investigation due to aging in different hostile conditions. This is illustrated in Fig. 6.56, and shown below in Equation (6.6):

$$P\ (\%) = -\ 0.0013 \times \sigma_f + 4.358 \qquad (6.6)$$

The correlation coefficient of this relation is = 0.779

The observation in this investigation is that a higher porosity gives rise to a higher effective dissolution rate is in favour with the assumption that as prolonged exposure leads to the formation of micro-cracks and open pores, these in turn increase the surface area exposed to the aqueous solution causing an increase in the effective dissolution rate of the composite.

The rate of porosity increased with aging time, while the rate of ultimate flexural decline decreased. As far as porosity is concerned, the main contribution comes from the resin matrix and its hydrolysis with aging. However, in the case of mechanical strength, it is mainly determined by fibres which are more compact (i.e. with less surface area), embedded in resin (i.e. more protection is provided), and the dissolution process produces a passive layer on the reaction front (i.e. reduces the rate of degradation of glass fibres with time). Therefore, for all the reasons mentioned above, glass fibres are less exposed to hostile ions than the resin matrix.

6.4 Summary

6.4.1 Introductory investigation

1. Bond behaviour was experimentally investigated by using four joint-beams containing straight GFRP and steel rebars in accordance with RILEM (1978). The GFRP bars were 8mm with a square cross section, and steel bars were 8mm diameter. The analysis of the test data led to the following conclusions:

    - GFRP rebars show lower bond strength values than steel rebars despite the greater tensile strength of the composite rebars.

- The average maximum bond strength of the GFRP rebars increases as the concrete compressive strength increases. For an increase in compressive strength of concrete of 1.78, the bond strength increased by 1.5 times.

- The modulus of elasticity of GFRP is approximately 25% of that of steel rebars. This, of course, has an effect on the increase in the deflection of beams reinforced by GFRP rebars.

2. FRP is a composite material and its properties could be sensitive to any changes in its components during manufacturing. Therefore, the span to depth ratio (in flexural test for FRP rebars) should not be taken for granted from the standard tests. Instead the optimum value should be determined from tests.

3. The MIP test showed the GFRP composite to have a low porosity, in which to provide protection to its core, and uniform in pore distribution. The test highlighted some very important characteristics regarding GFRP materials especially how the pores are distributed and connected to each other which determine the ingress and permeation of ions in the composites.

4. Developing SEM images could be added to the set of quality control tests to ensure that the composite materials satisfy the requirements, such as, fibres conditions during manufacturing and whether or not the resin matrix provides protection to the fibres.

6.4.2 Flexural strength

Flexural testing has provided fundamental evidence that GFRP specimens experienced resin hydrolysis, because pH of all the aging solutions decreased. Fibre degradation and fibre/resin debonding occurred with appreciable strength loss with prolonged aging.

Although the alkali attack mechanism was similar to that of brine solution, it can be seen in the results that the former was more severe because alkalinity enhances fibre dissolution and matrix hydrolysis, followed by interface de-bonding.

Higher temperatures increase the rate of degradation in all aging solutions and that can have an adverse effect on monitoring the details of the degradation progress. To avoid this, either aging in a high temperature is avoided or testing the aged specimens more frequent (within shorter intervals) to monitor the changes more clearly is recommended.

It was noticed that aging in different solutions did not affect the failure mode of the GFRP rebars. This means that same span length can be used for aged specimens as well.

6.4.3 Porosity

The size and continuity of the pores in the polymer network play a key role in moisture penetration. Therefore, sufficient protection should be provided to the load bearing component, i.e. glass fibres. Although, the results showed the resin matrix to be compact, examination of aged specimens could indicate an increase in larger pores at the expense of smaller ones.

Distortion of the pore structure of the composite material due to aging in alkali solutions was more pronounced than in the brine solutions for each set of temperatures (i.e., aging in alkali caused more micro-cracks and openings than in brine aging at 60°C, and 20°C). As a result, more strength degradation was proven to take place with alkali aging than with brine solution.

The effect of a higher temperature was reflected upon the increased rate of degradation. Although this effect on degradation was more pronounced at longer ages of exposure.

In all aging solutions, porosities for all specimens increased but at different rates as a result of different susceptibility of GFRP to the aggressive environments.

6.4.4 Correlations

In all aging solutions, the longer the specimens were exposed, the more mechanical degradation, dissolution and hydrolysis occurred. The rate of change depended on temperature and how damaging the ions were to the composite specimens.

An overall correlation between ultimate flexural degradation and porosity for all harsh environments investigated in this research is shown in Equation (6.6).

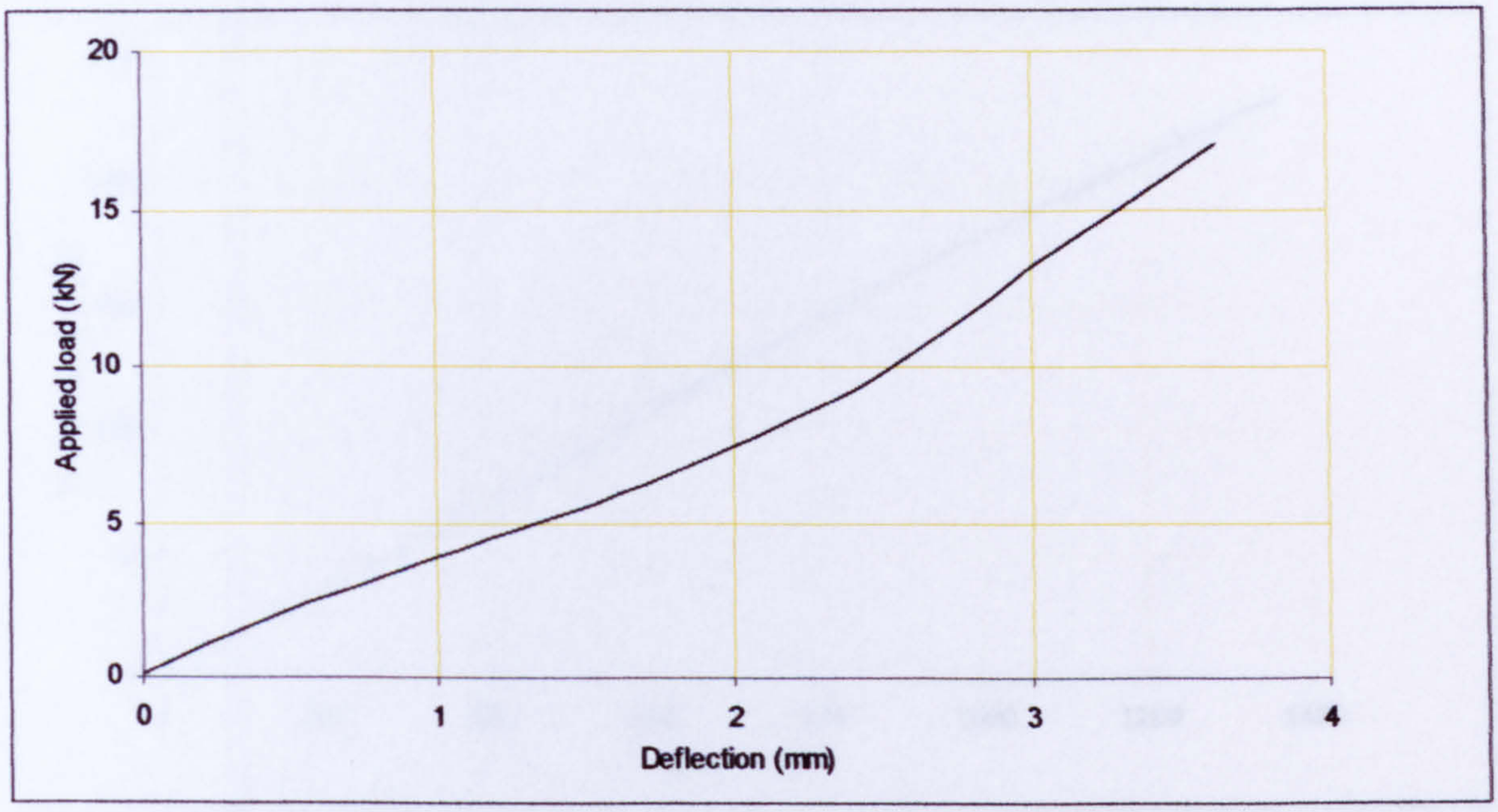

Figure 6.1: Middle span deflection of the joint-beam with concrete strength of 45MPa and steel reinforcement

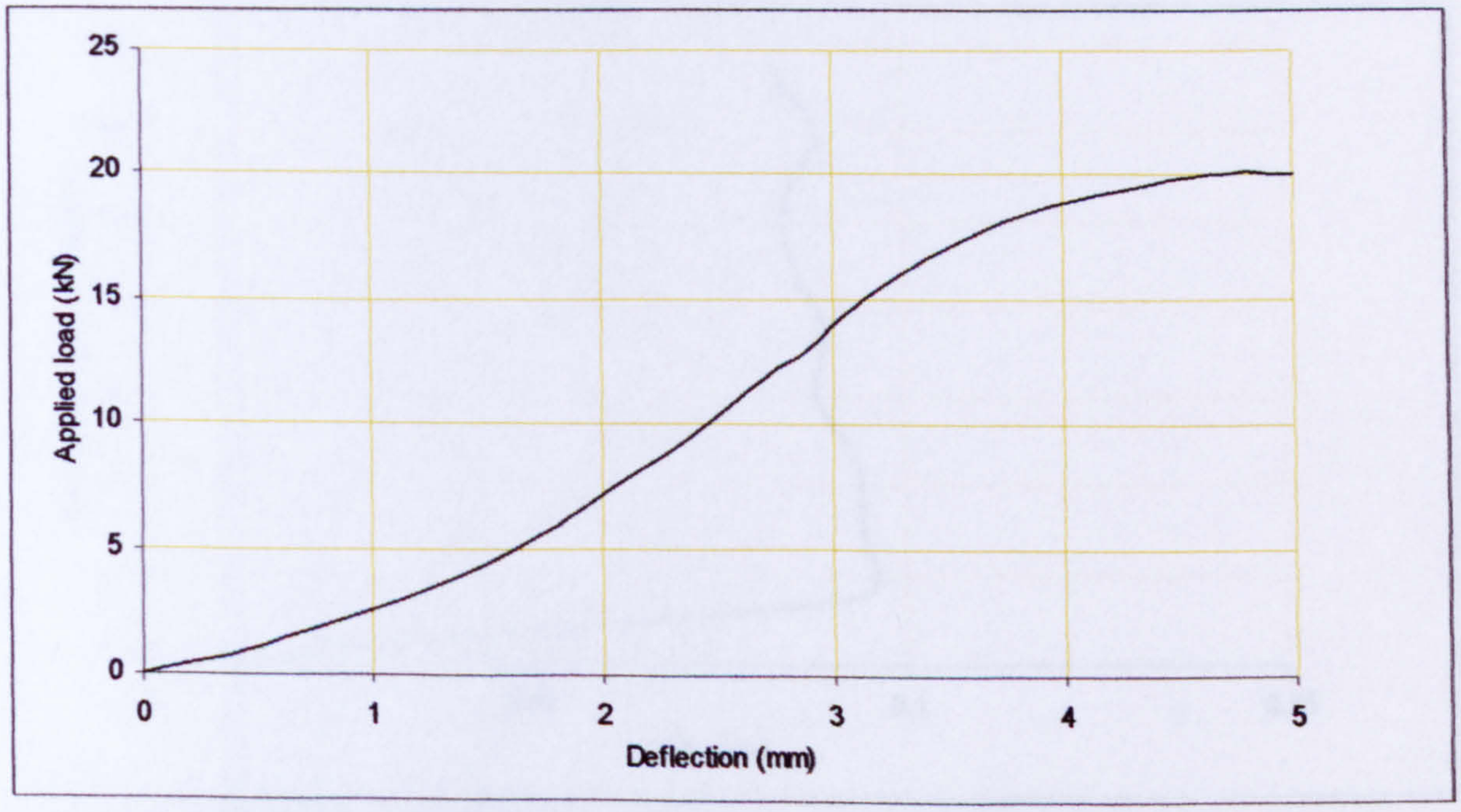

Figure 6.2: Middle span deflection of the joint-beam with concrete strength of 80MPa and steel reinforcement

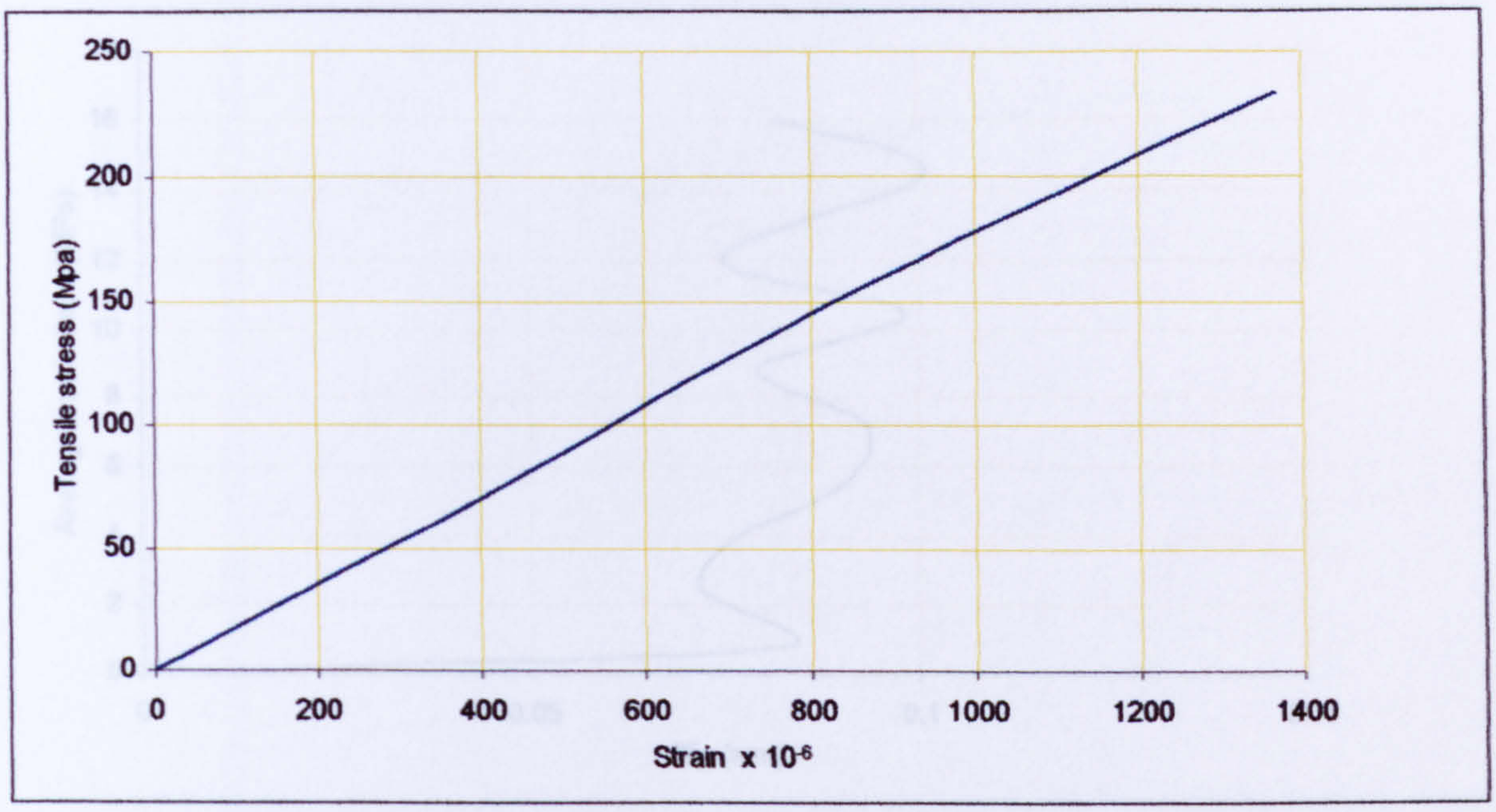

Figure 6.3: Stress-strain relationship of steel rebar in the un-embedded zone of the joint-beam

Figure 6.4: Bond stress vs. slip for steel rebar embedded in the joint-beam with concrete strength of 45MPa

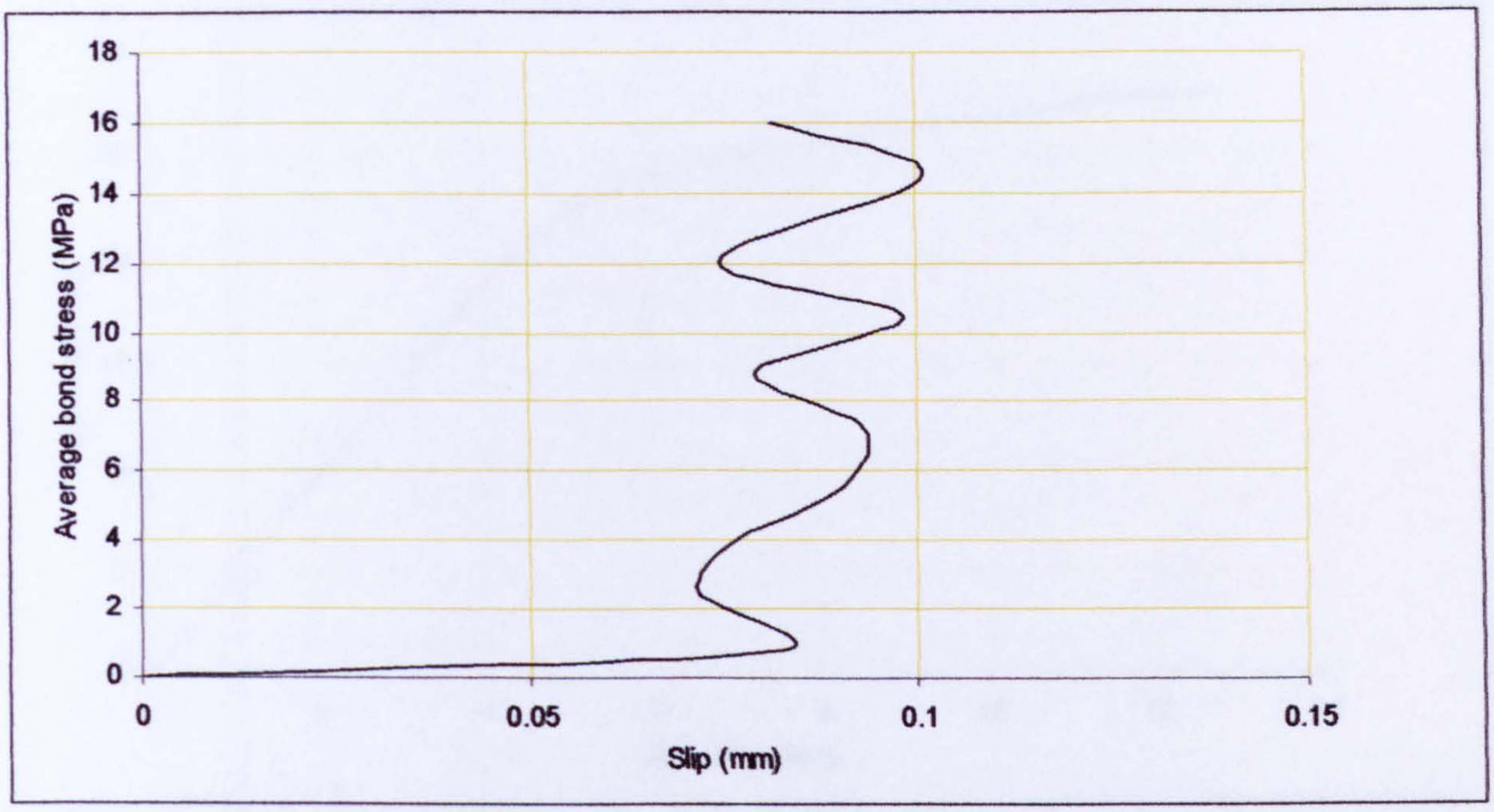

Figure 6.5: Bond stress vs. slip for steel rebar embedded in the joint-beam with concrete strength of 80MPa

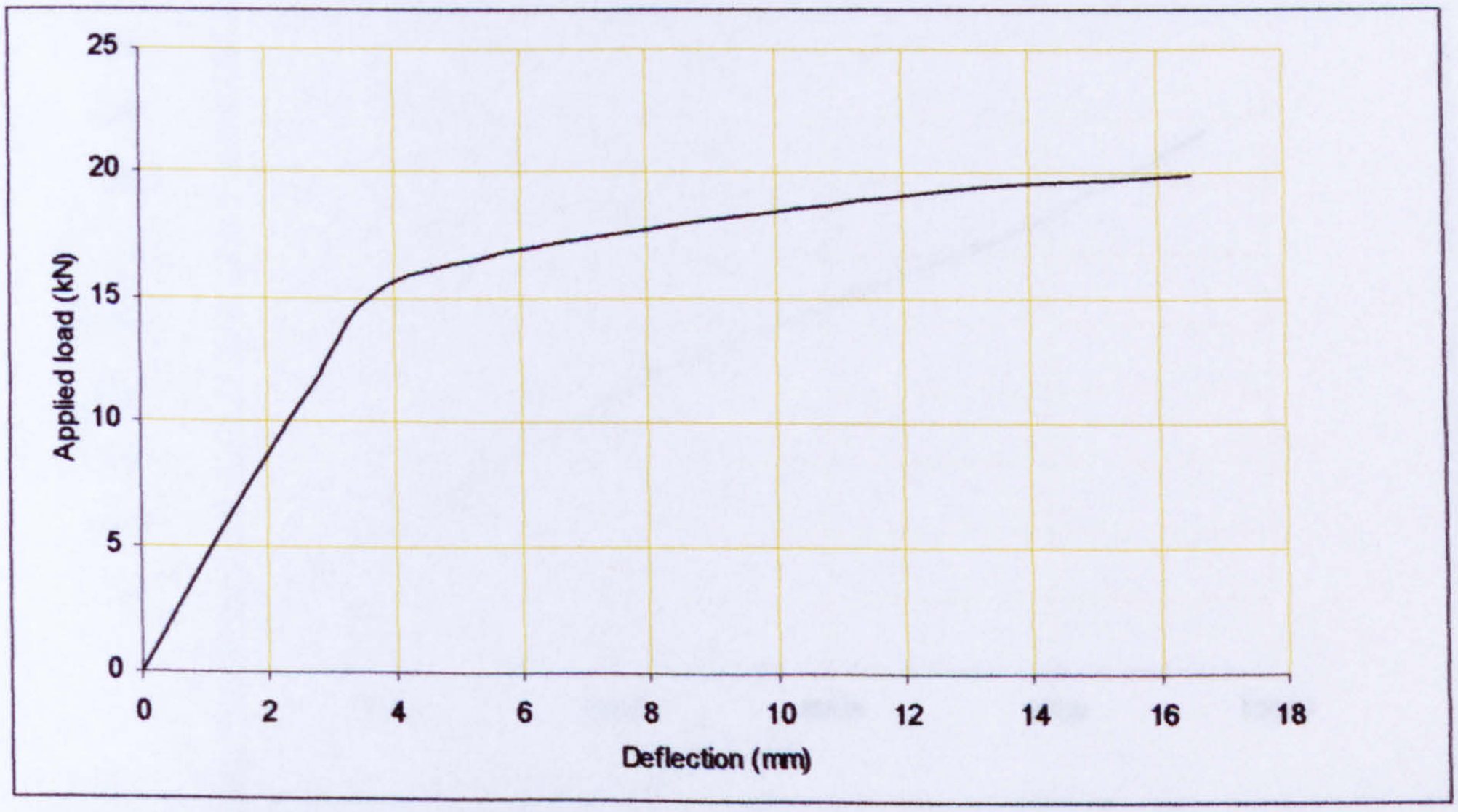

Figure 6.6: Middle span deflection of the joint-beam with concrete strength of 45MPa and GFRP reinforcement

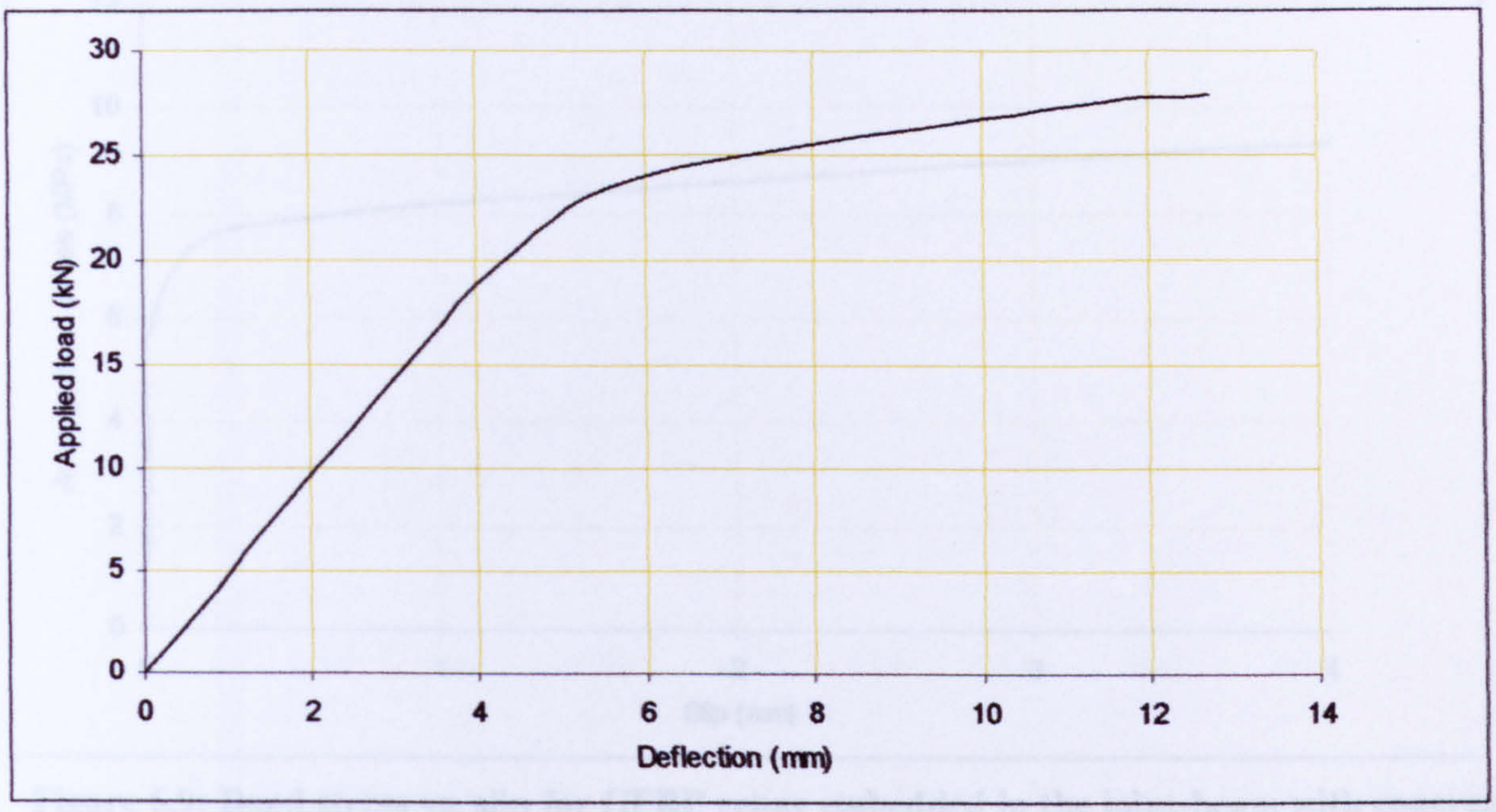

Figure 6.7: Middle span deflection of the joint-beam with concrete strength of 80MPa and GFRP reinforcement

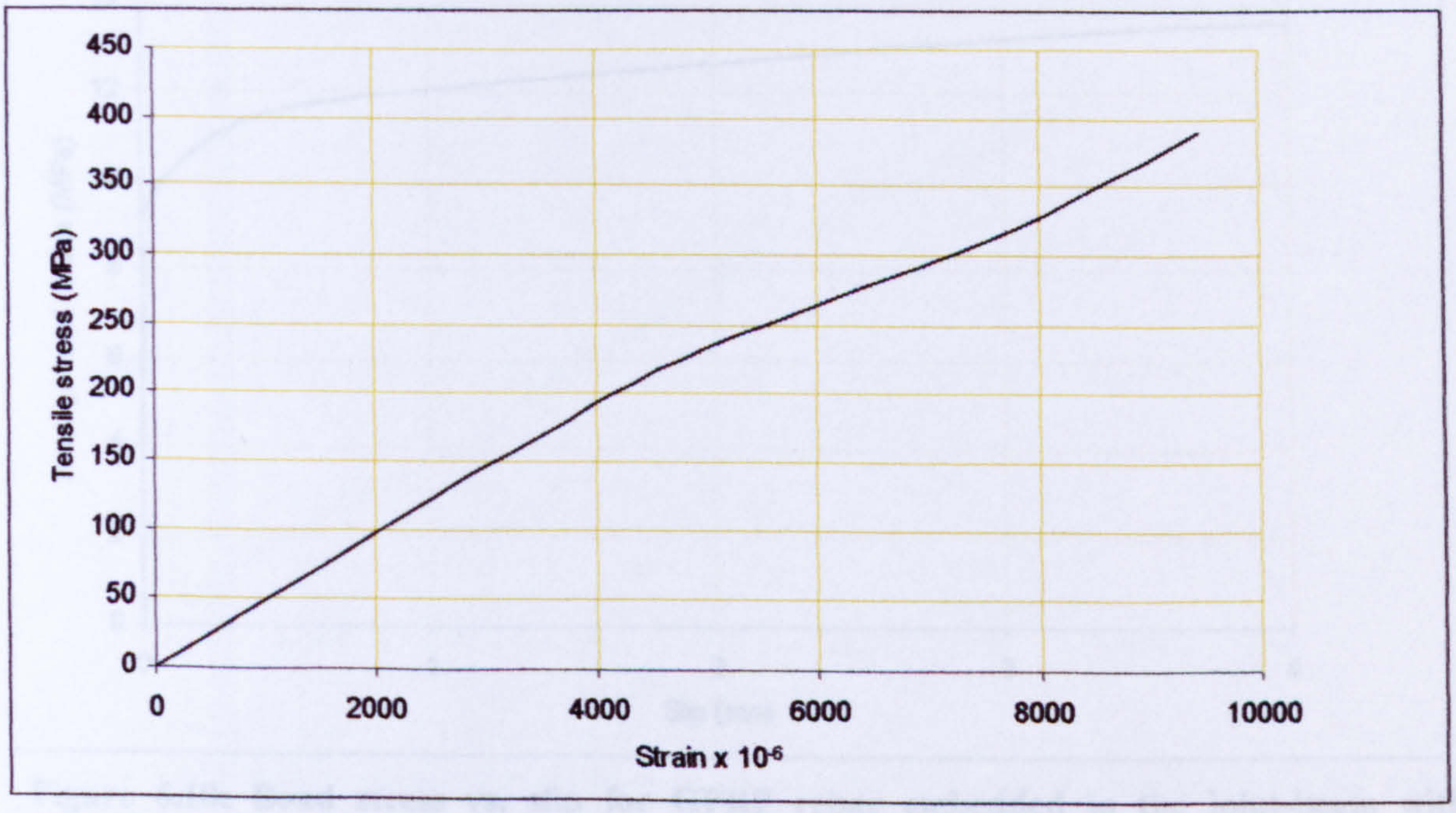

Figure 6.8: Stress-strain relationship of GFRP rebar in the un-embedded zone of the joint-beam

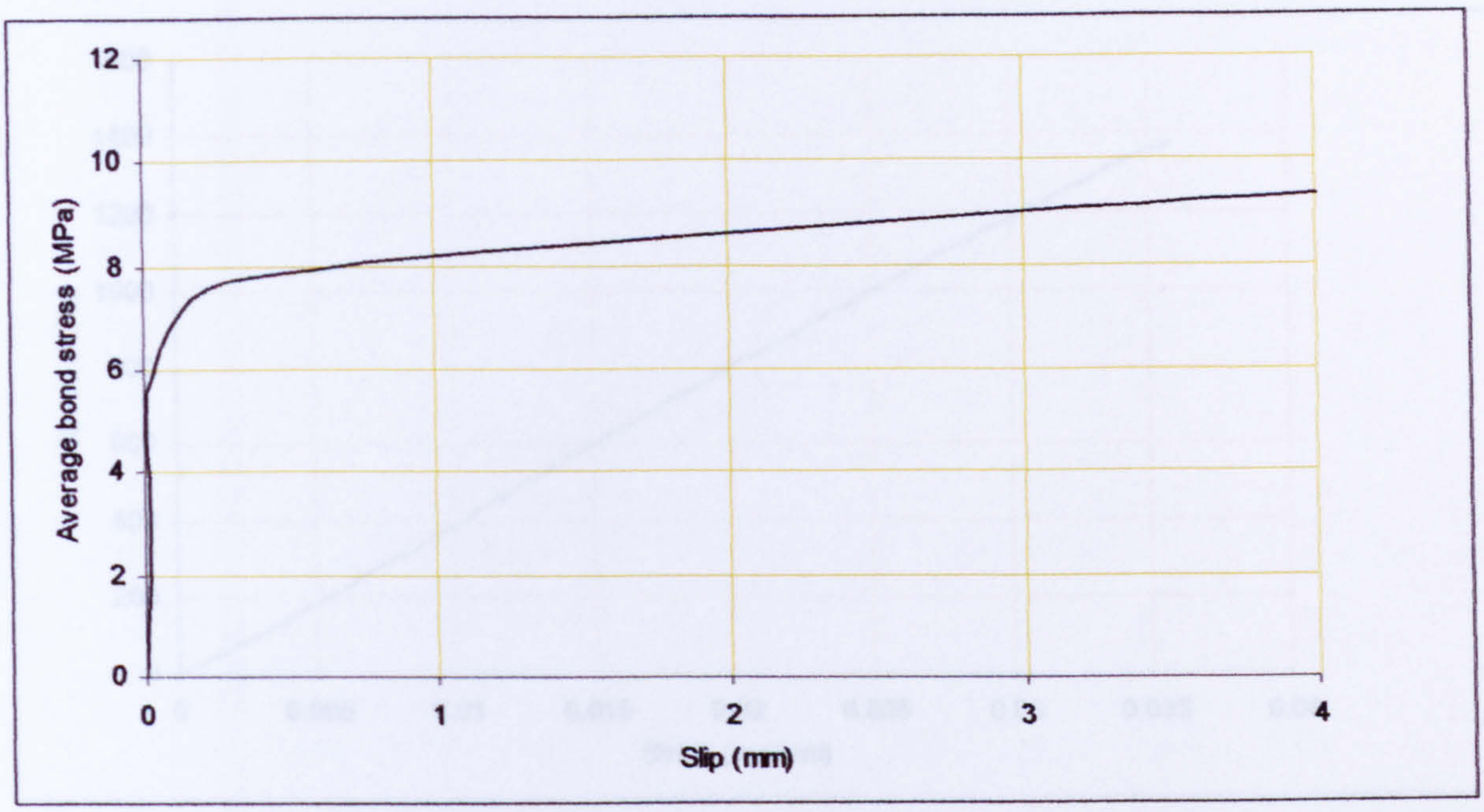

Figure 6.9: Bond stress vs. slip for GFRP rebar embedded in the joint-beam with concrete strength of 45MPa

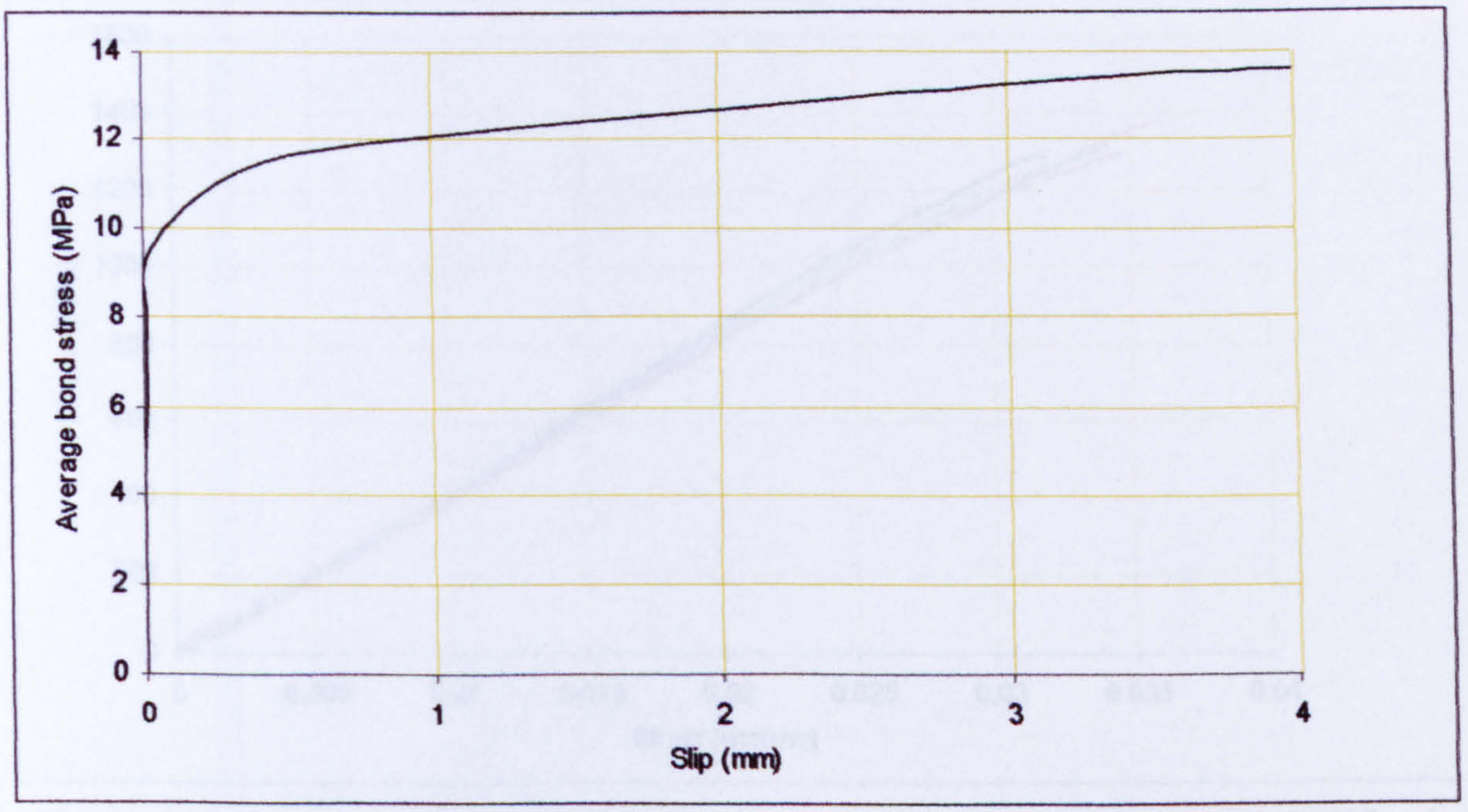

Figure 6.10: Bond stress vs. slip for GFRP rebar embedded in the joint-beam with concrete strength of 80MPa

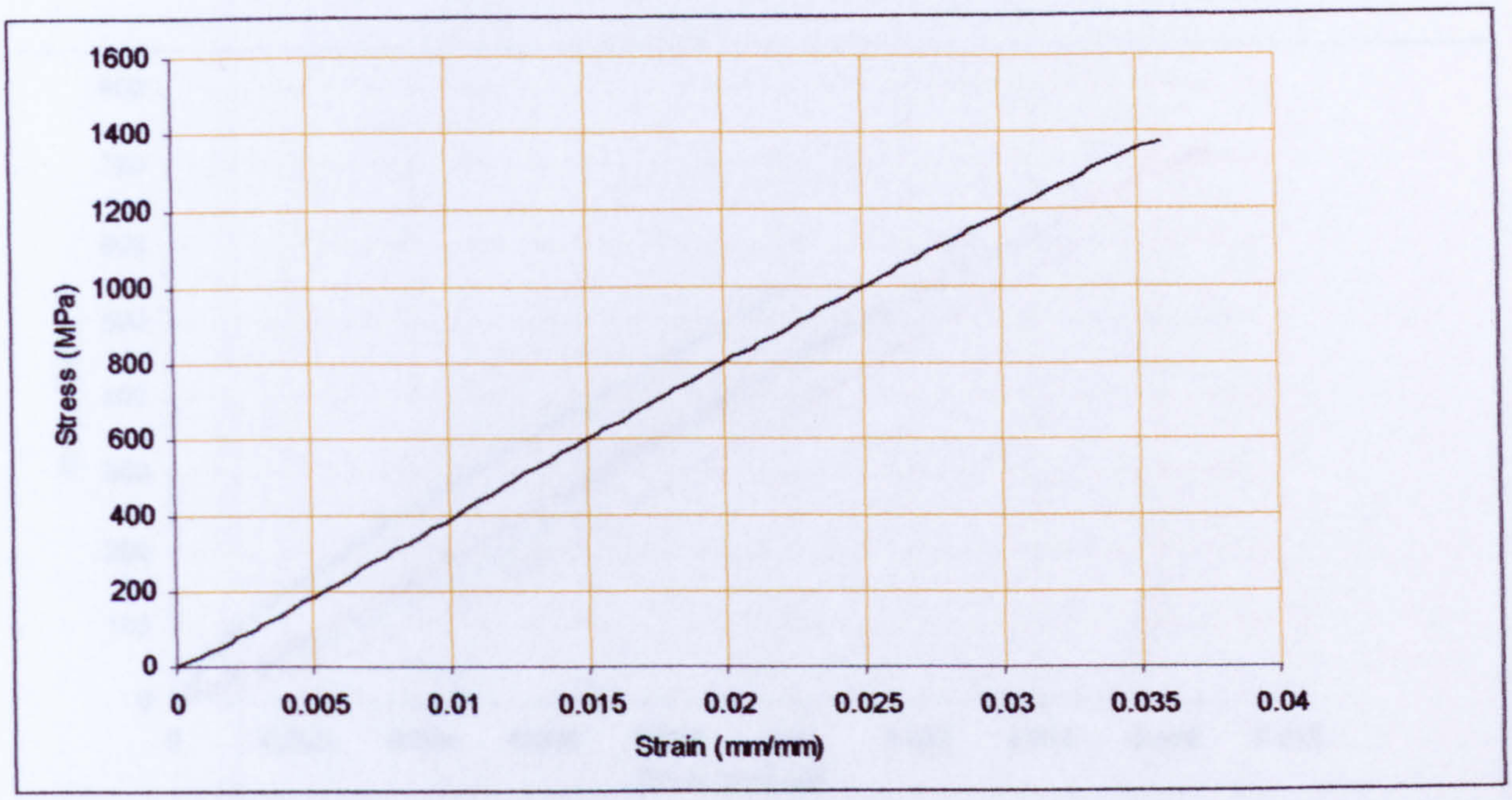

Figure 6.11: Typical stress-strain relationship in flexure for *control* (not-aged) GFRP rebar; specimen failed in tension

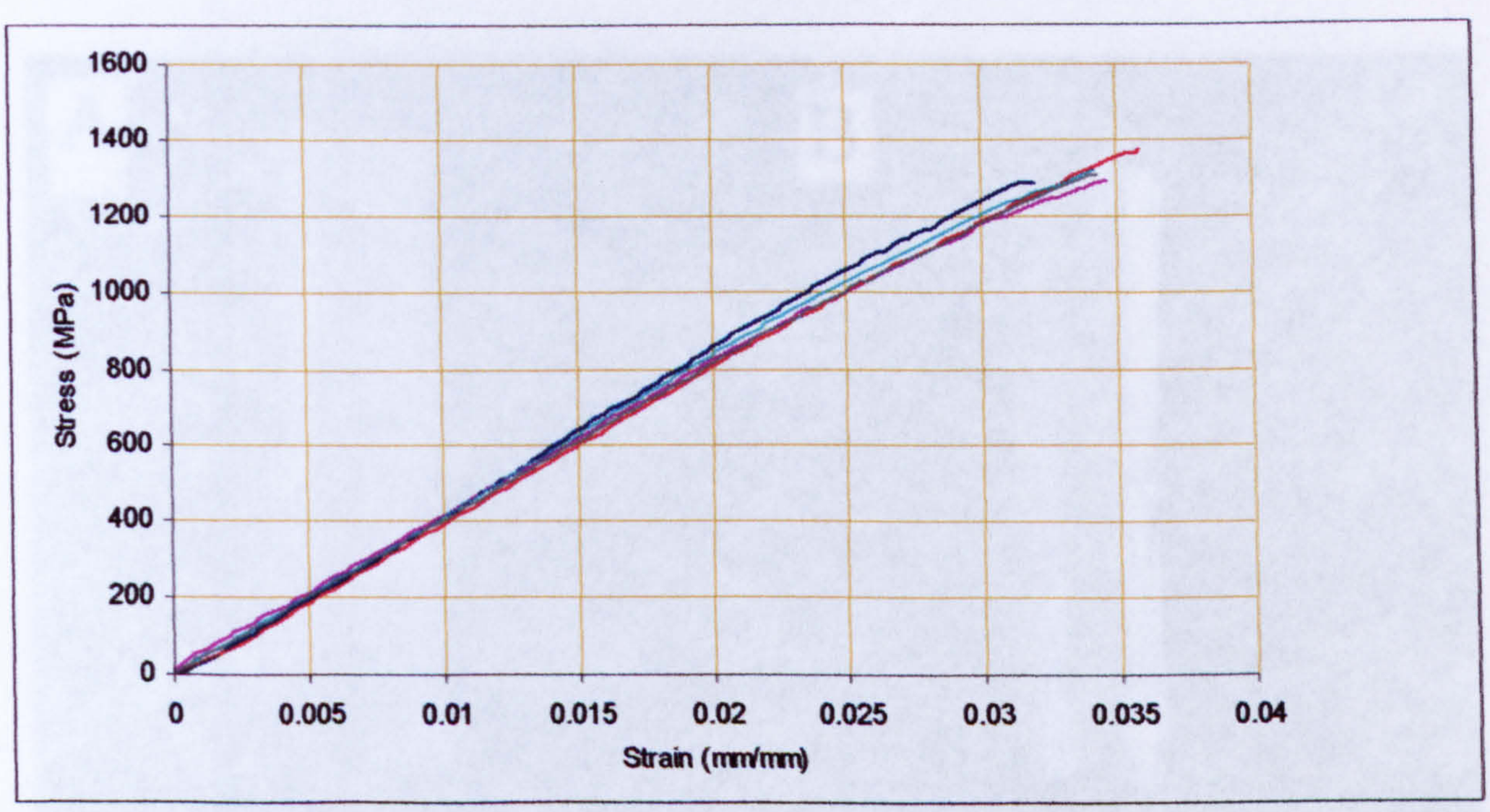

Figure 6.12: Stress-strain relationships in flexure for five *control* (not-aged) GFRP rebar specimens

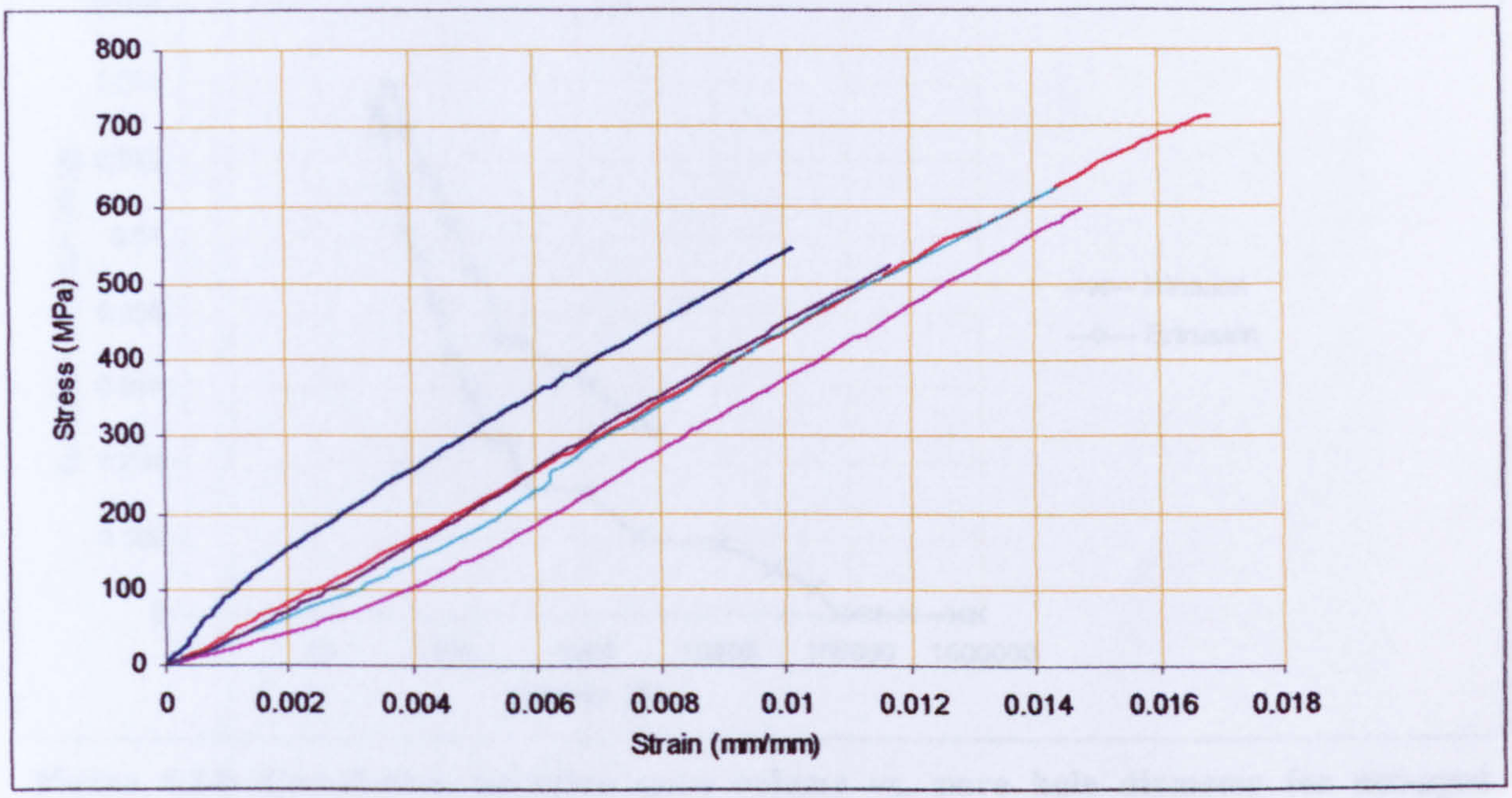

Figure 6.13: Stress-strain relationships in compression for five GFRP rebar specimens

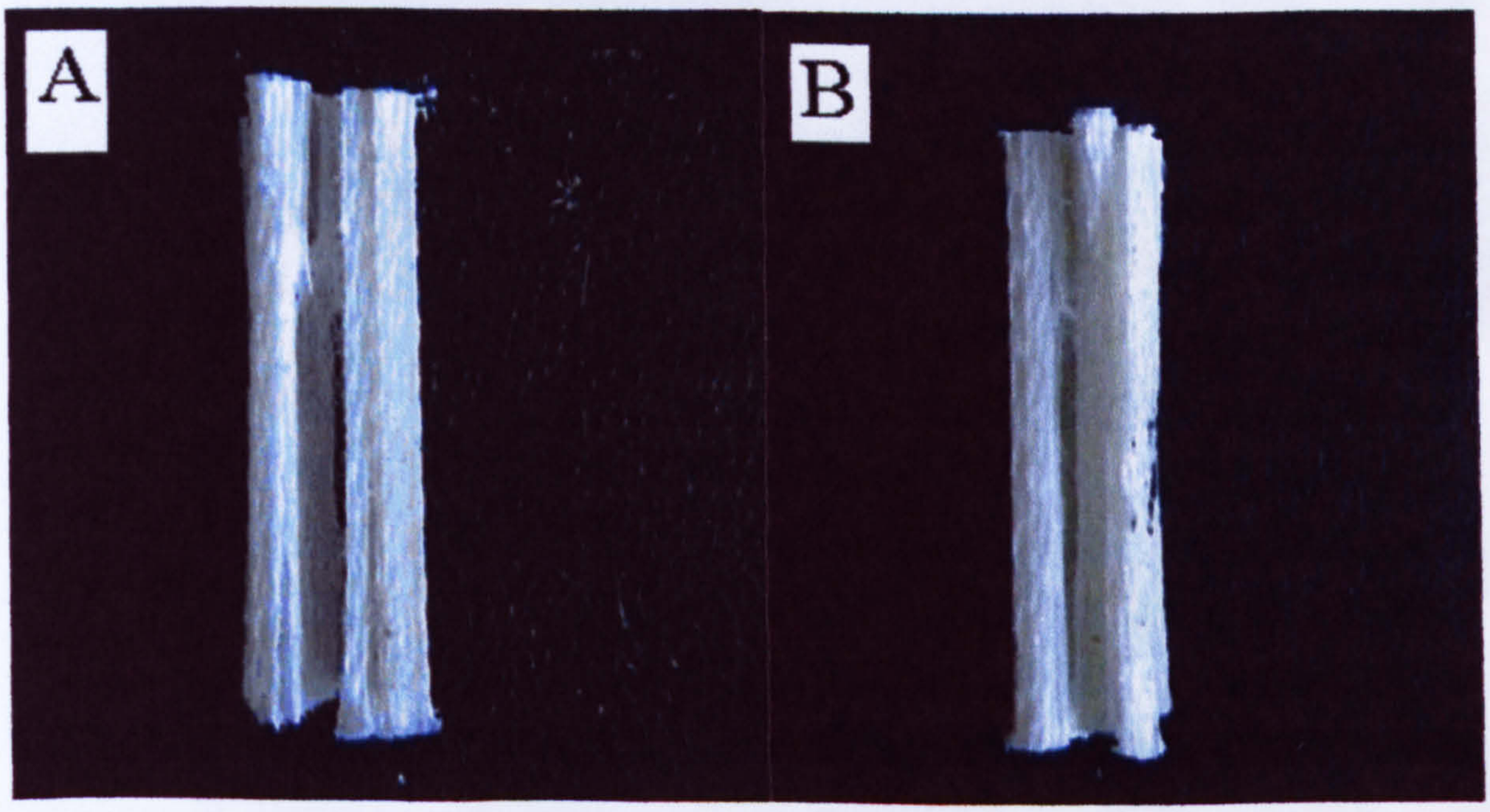

Plate 6.1 (A and B): Two GFRP specimens tested in compression

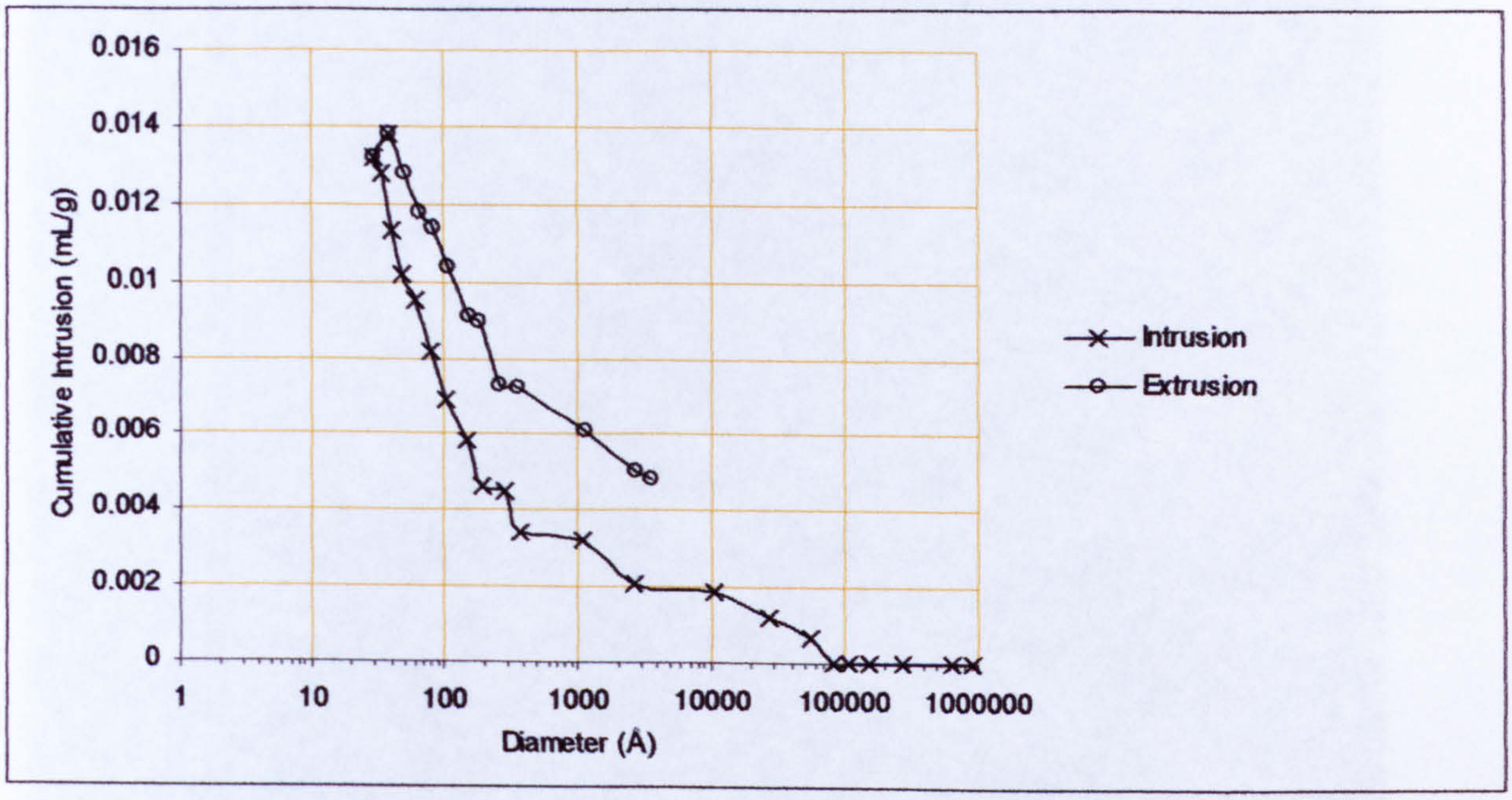

Figure 6.14: Cumulative intrusion pore volume vs. pore hole diameter for not-aged segments

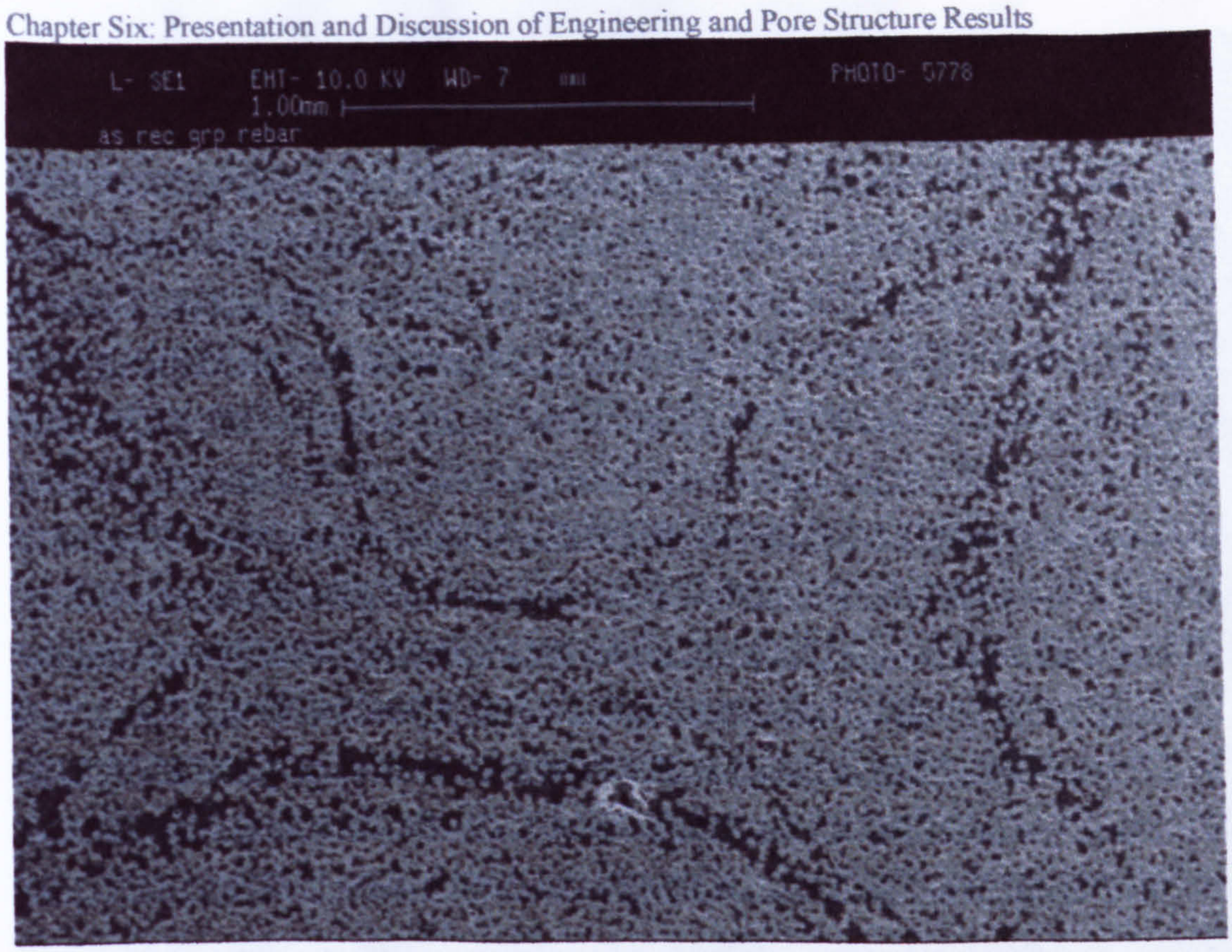

Figure 6.15: Gold-coated SEM image for cross section of the 8mm GFRP square bar

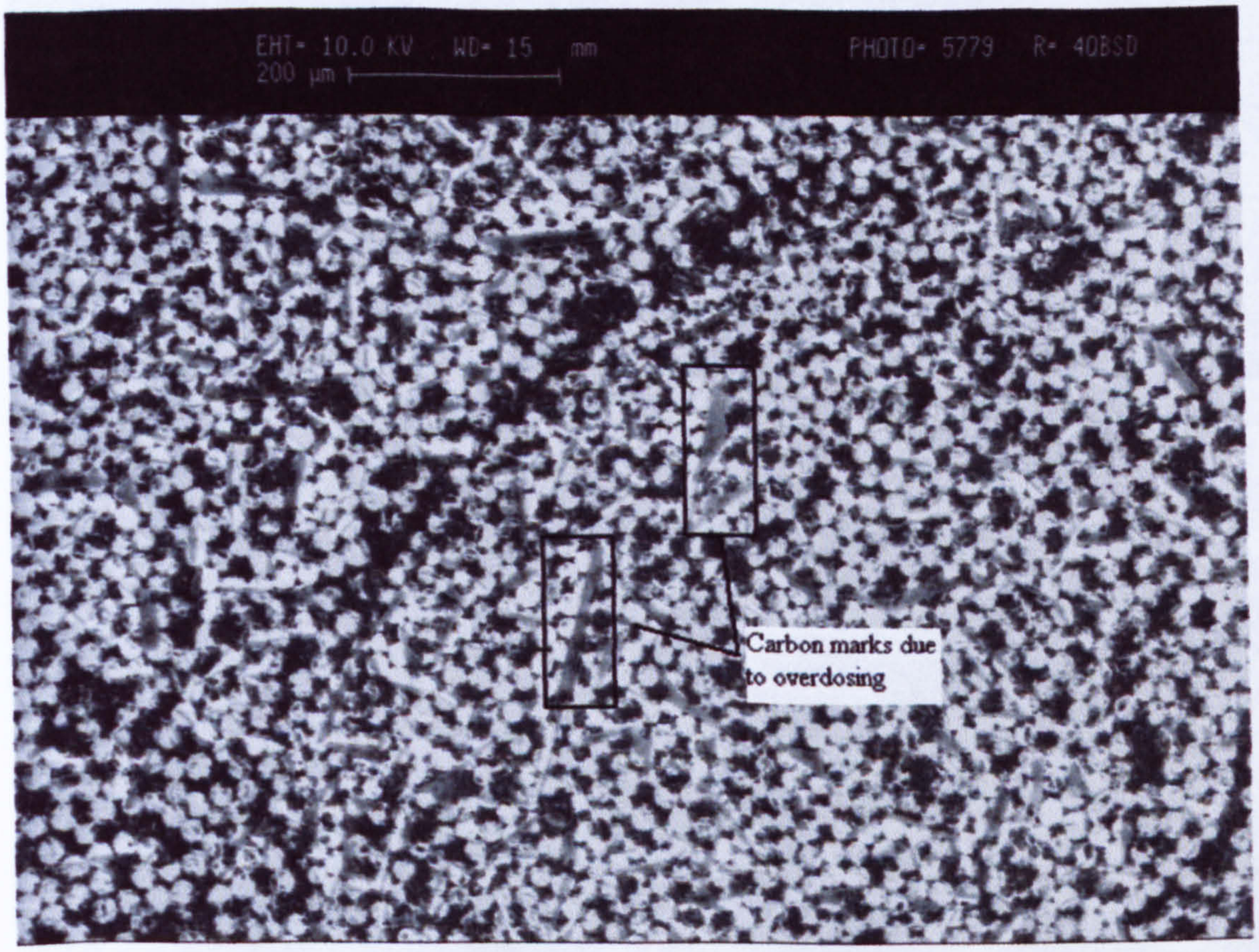

Figure 6.16: Carbon-coated SEM image for cross section of the 8mm GFRP square bar

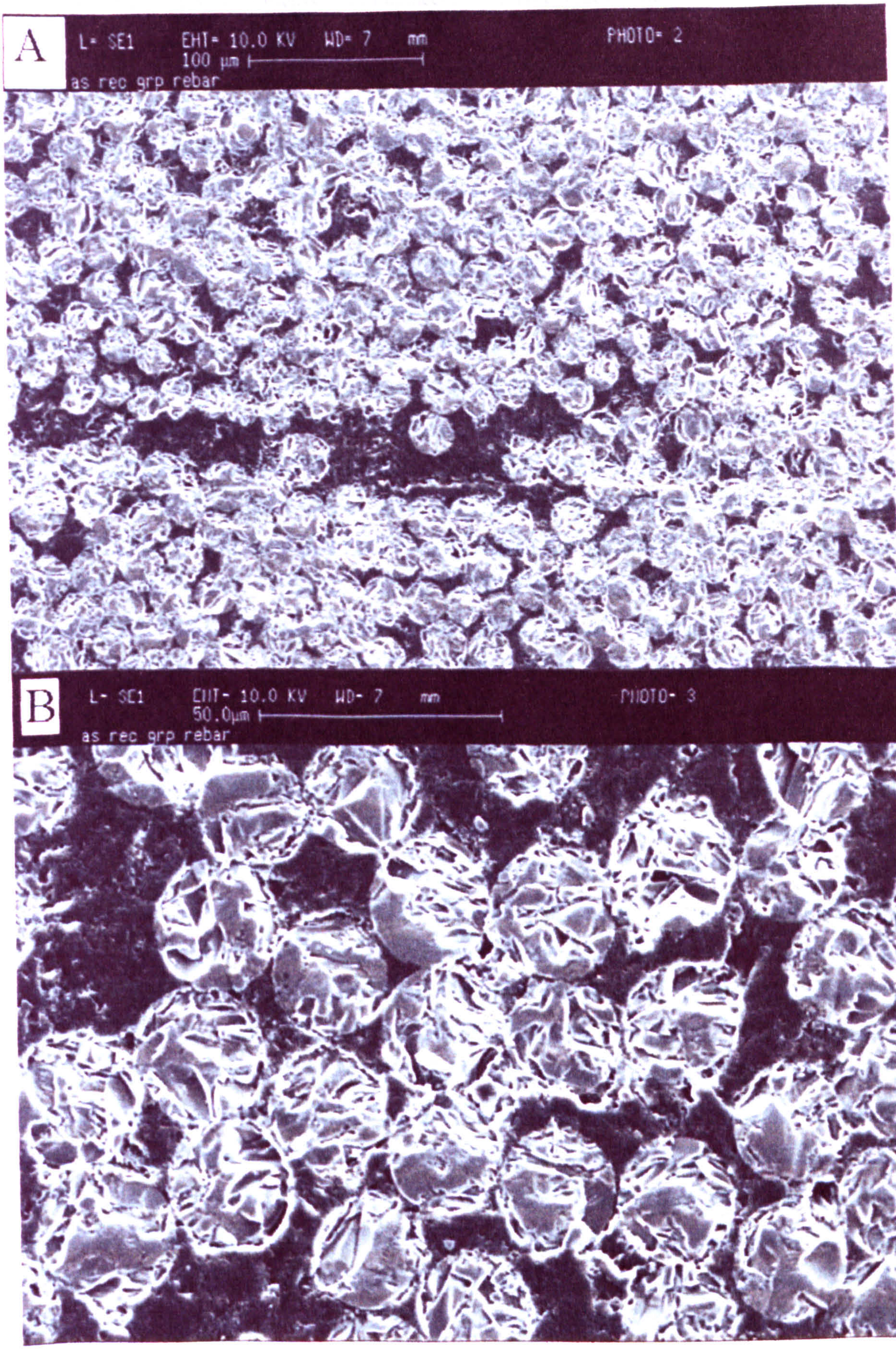

Figure 6.17 (A and B): Gold-coated SEM image at higher magnification factor shows glass fibres (rounded) surrounded by resin (dark areas between fibres). The average diameter of the glass fibres is about 25µm

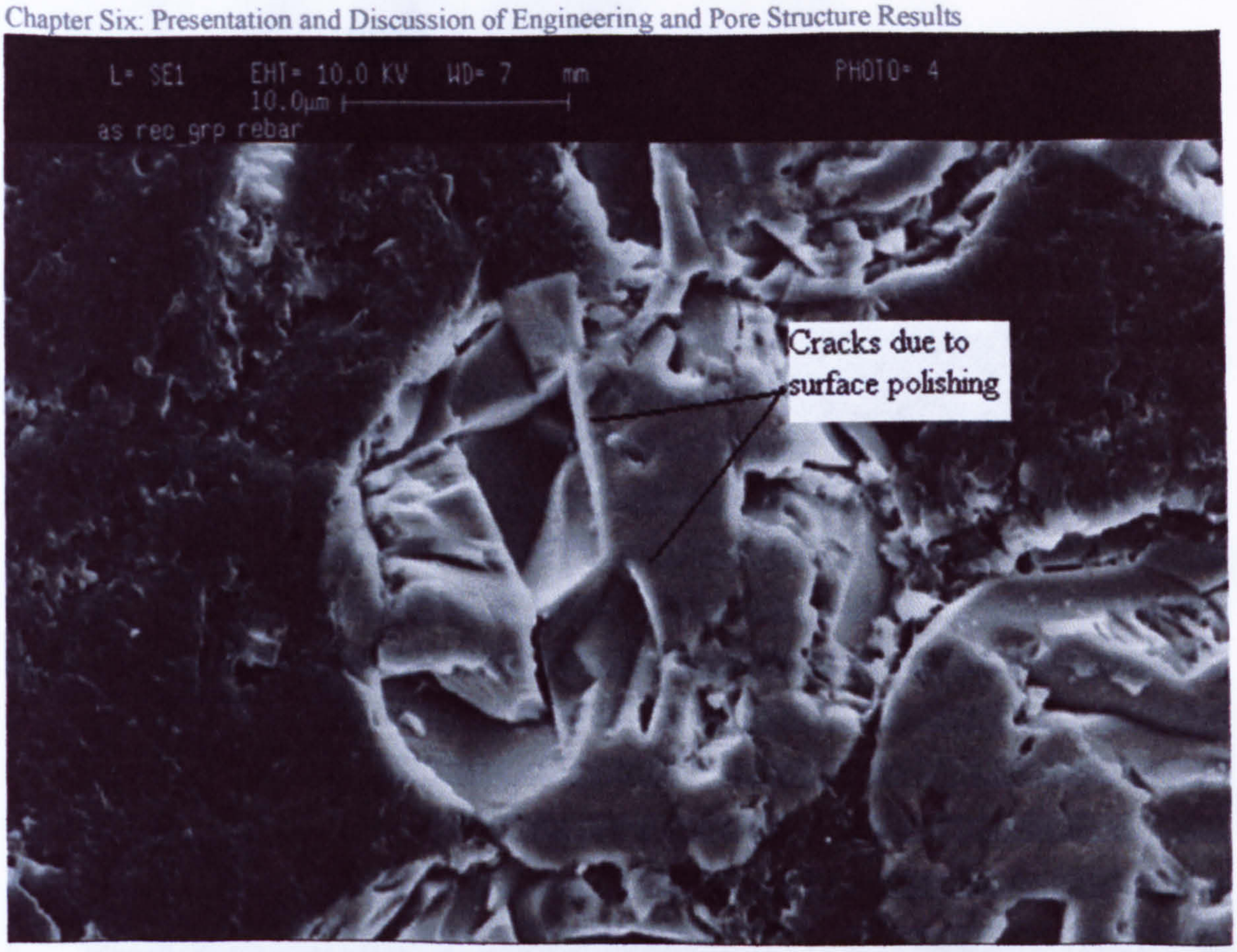

Figure 6.18: Glass fibre/resin matrix interface, also shows fibres contacting each other

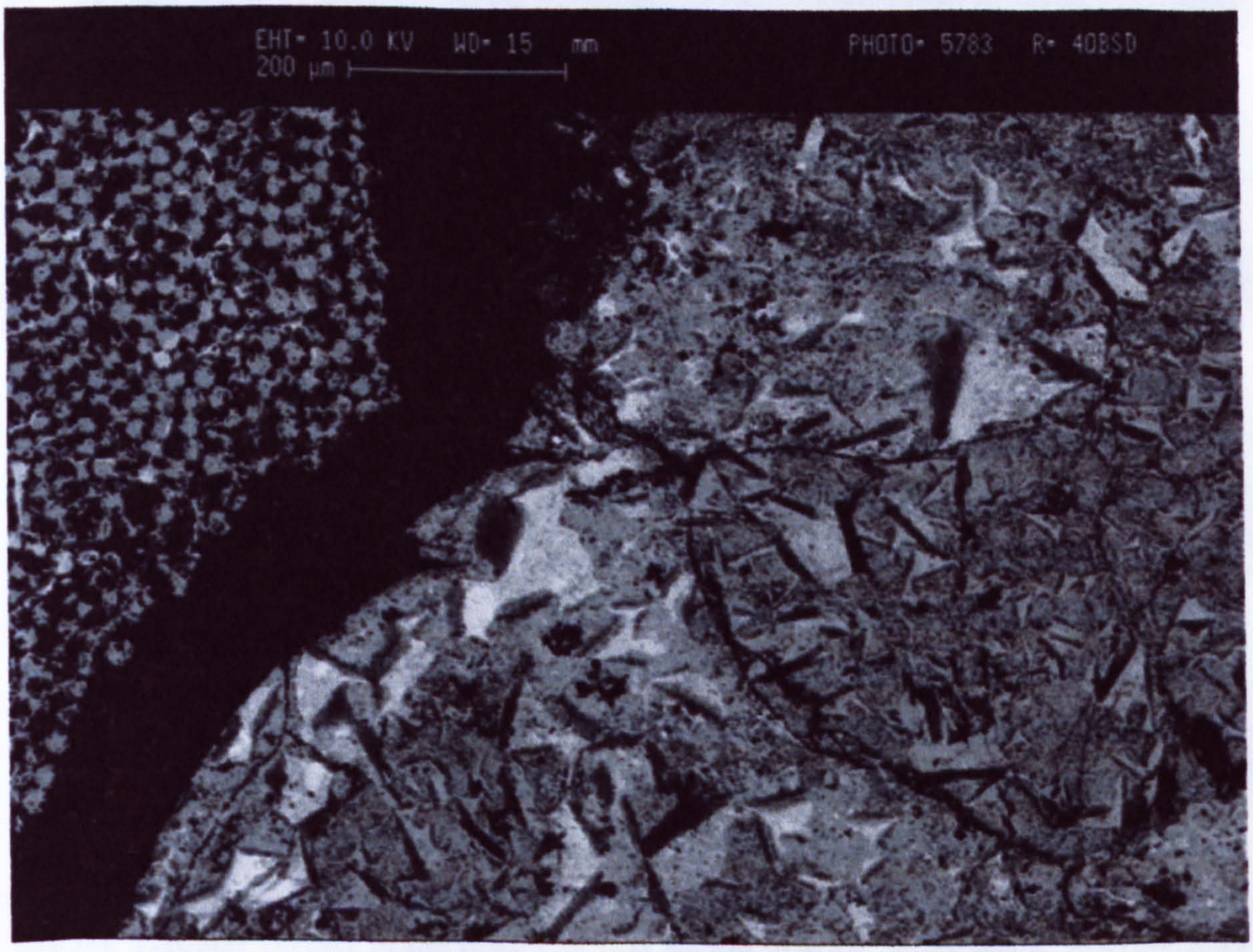

Figure 6.19: Concrete/GFRP interface, notice the irregular surface provided by the resin

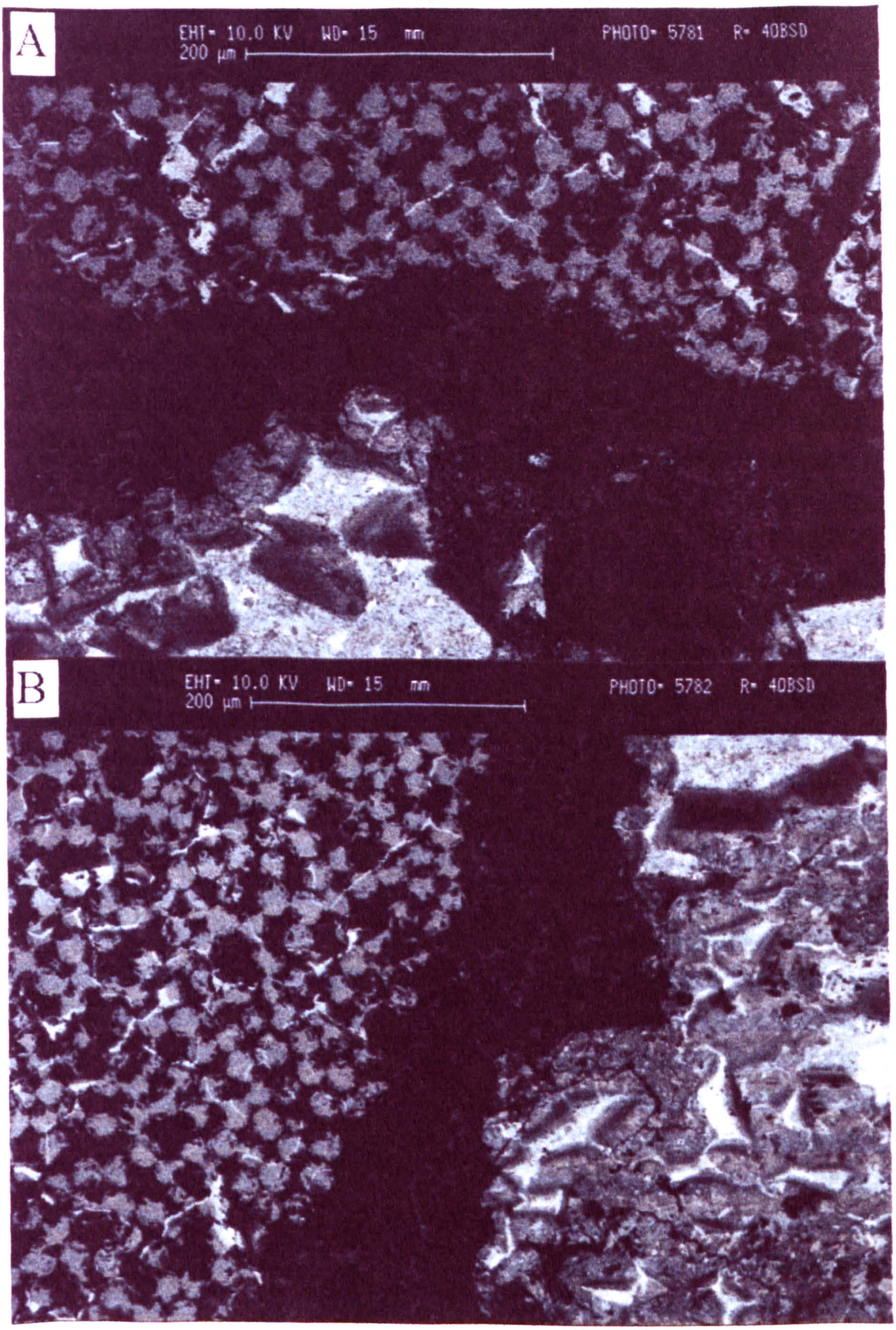

Figure 6.20 (A and B): Concrete/GFRP interface, notice the interlock between concrete and the irregular surface of the resin and that should provide better bond. Micro-cracks in the interface are not clear in the images

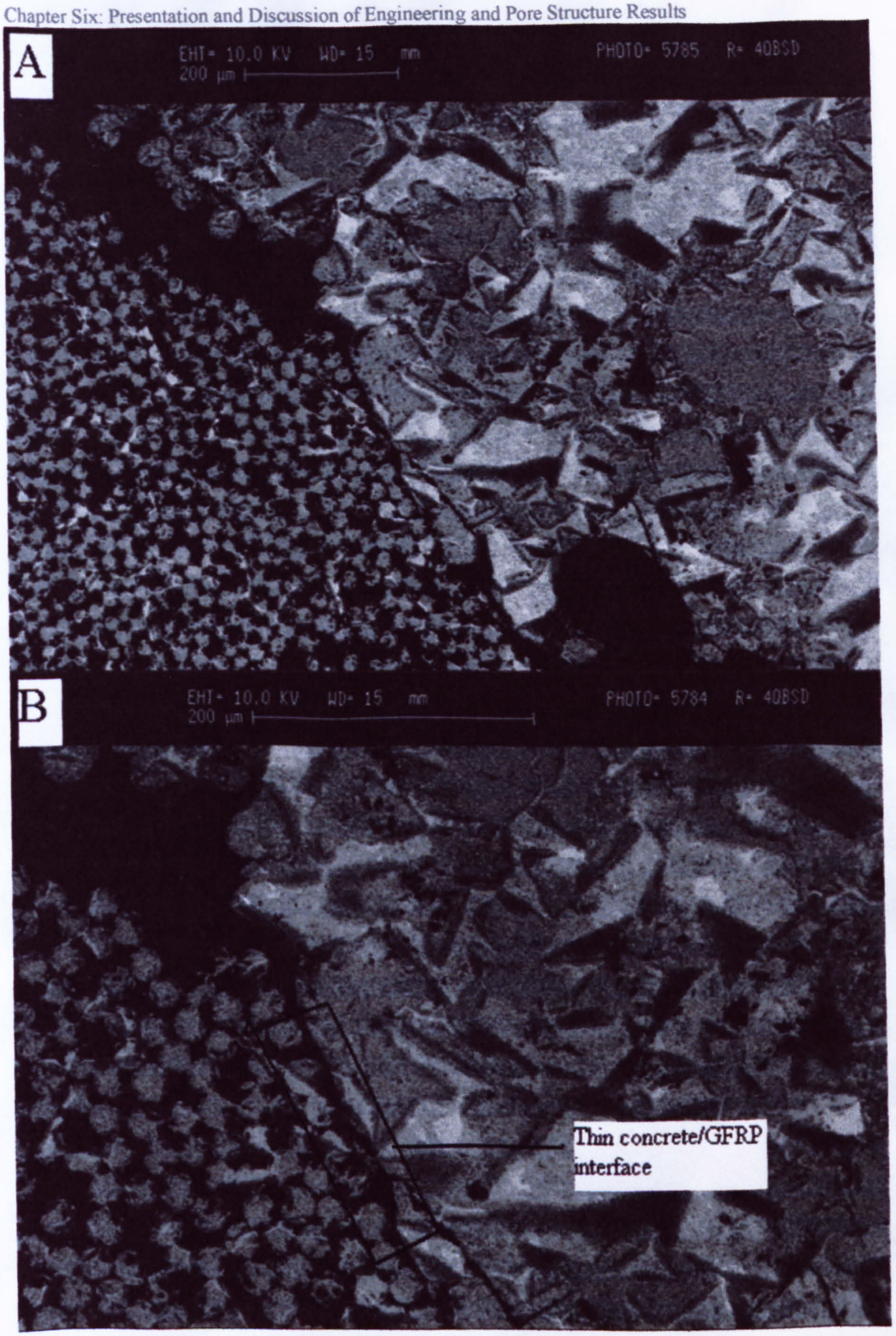

Figure 6.21(A and B): Concrete/GFRP interface, there is an area with either thin resin or with no resin at all and instead, micro-cracks between concrete and glass fibres. This is due to either poor fabrication or surface damage to the composite reinforcement

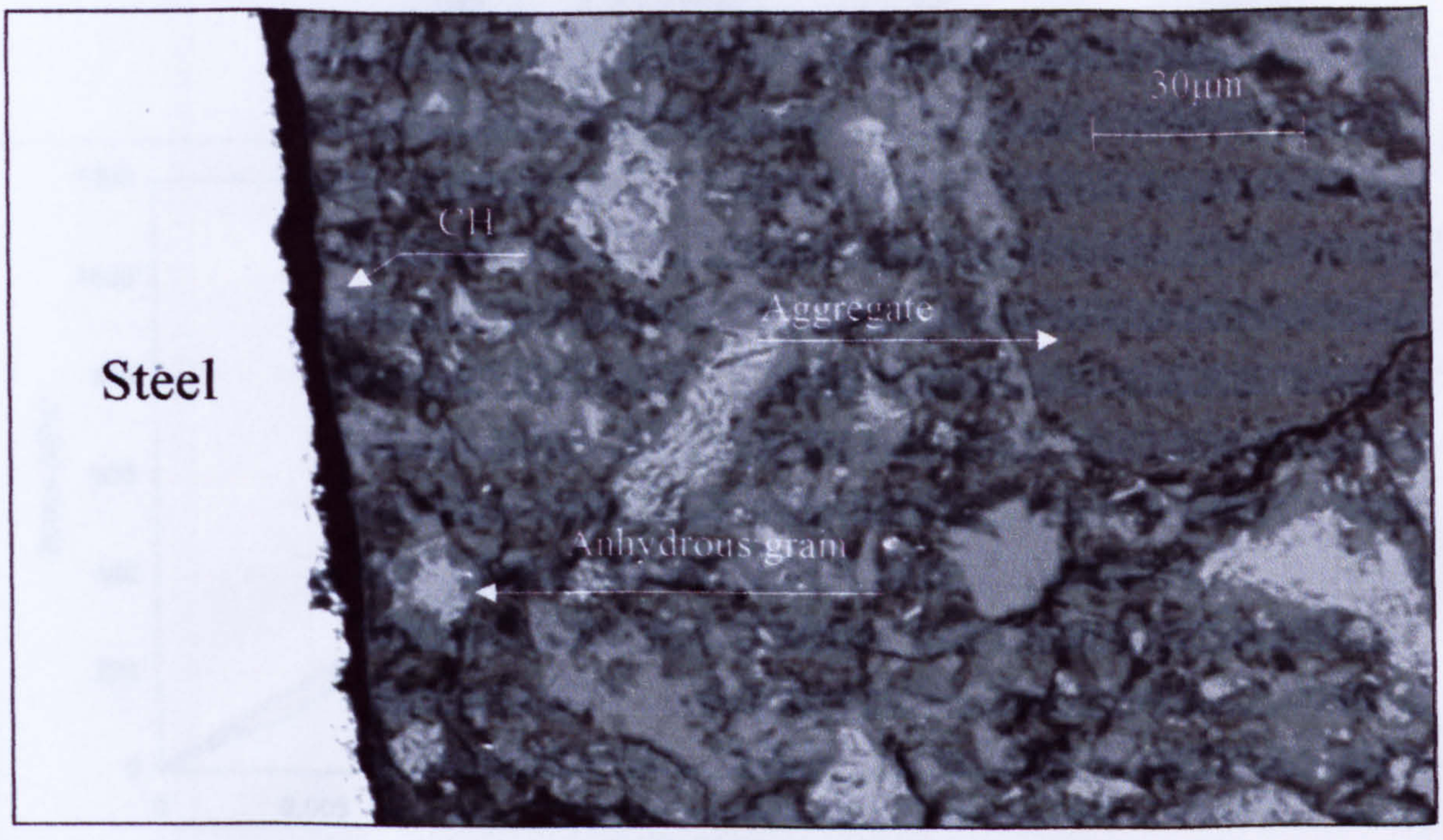

Figure 6.22: Backscattered electron image of the interface between steel and concrete (obtained by A T Horne)

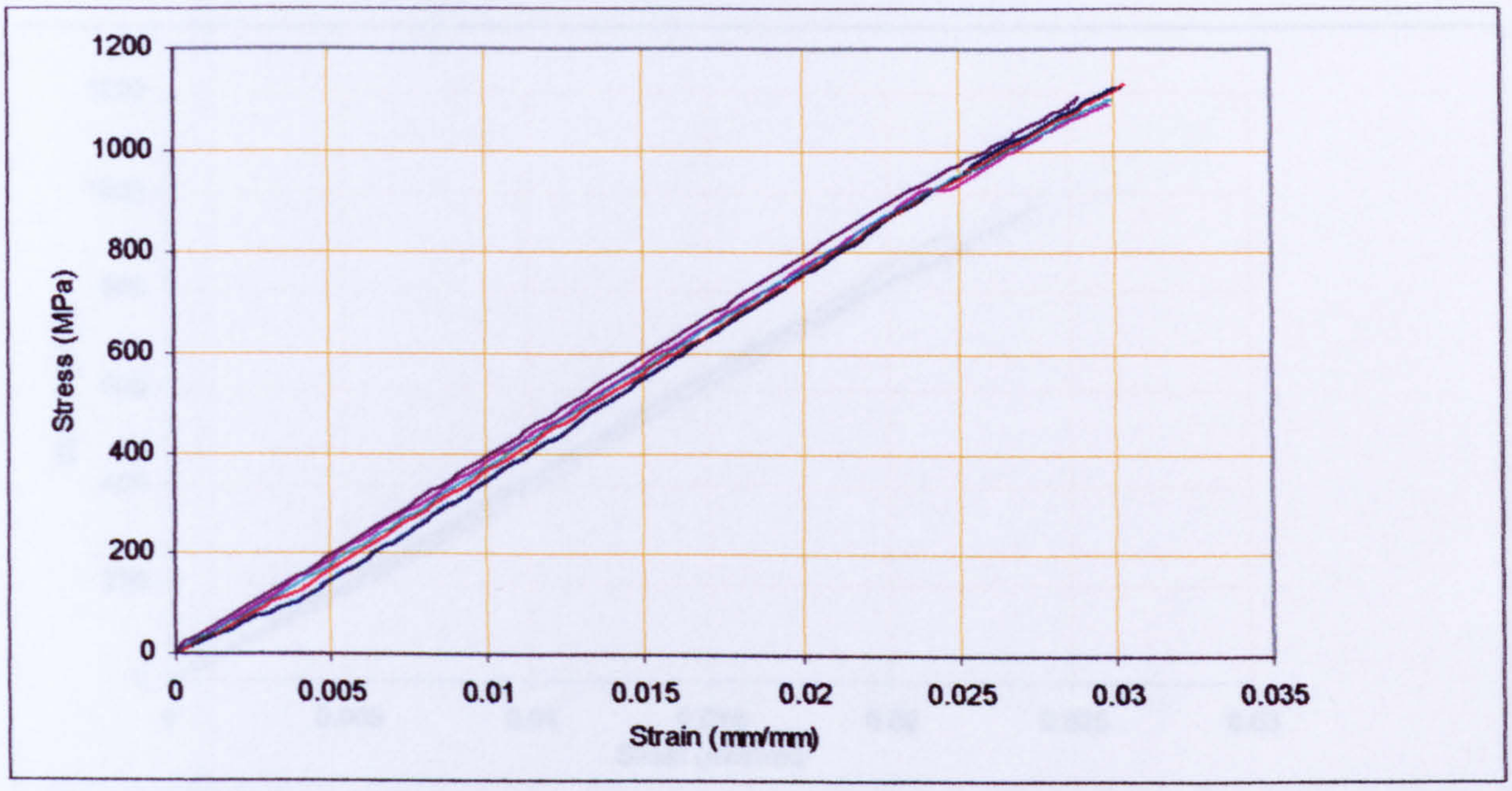

Figure 6.23: Stress-strain relationship in flexure for five GFRP rebar specimens immersed in *brine* solution for *30 days* at *60°C*

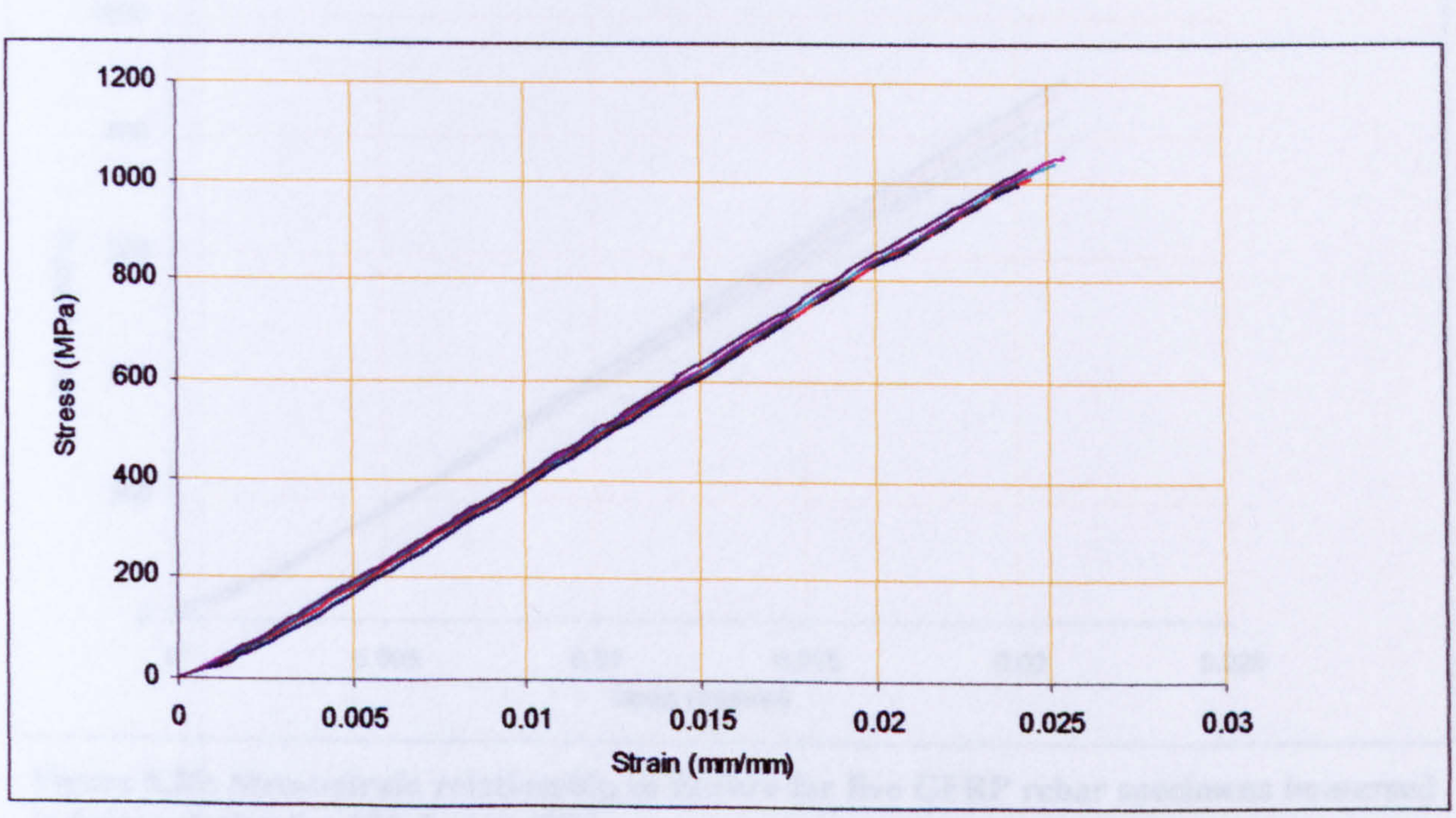

Figure 6.24: Stress-strain relationship in flexure for five GFRP rebar specimens immersed in *brine* solution for *90 days* at *60°C*

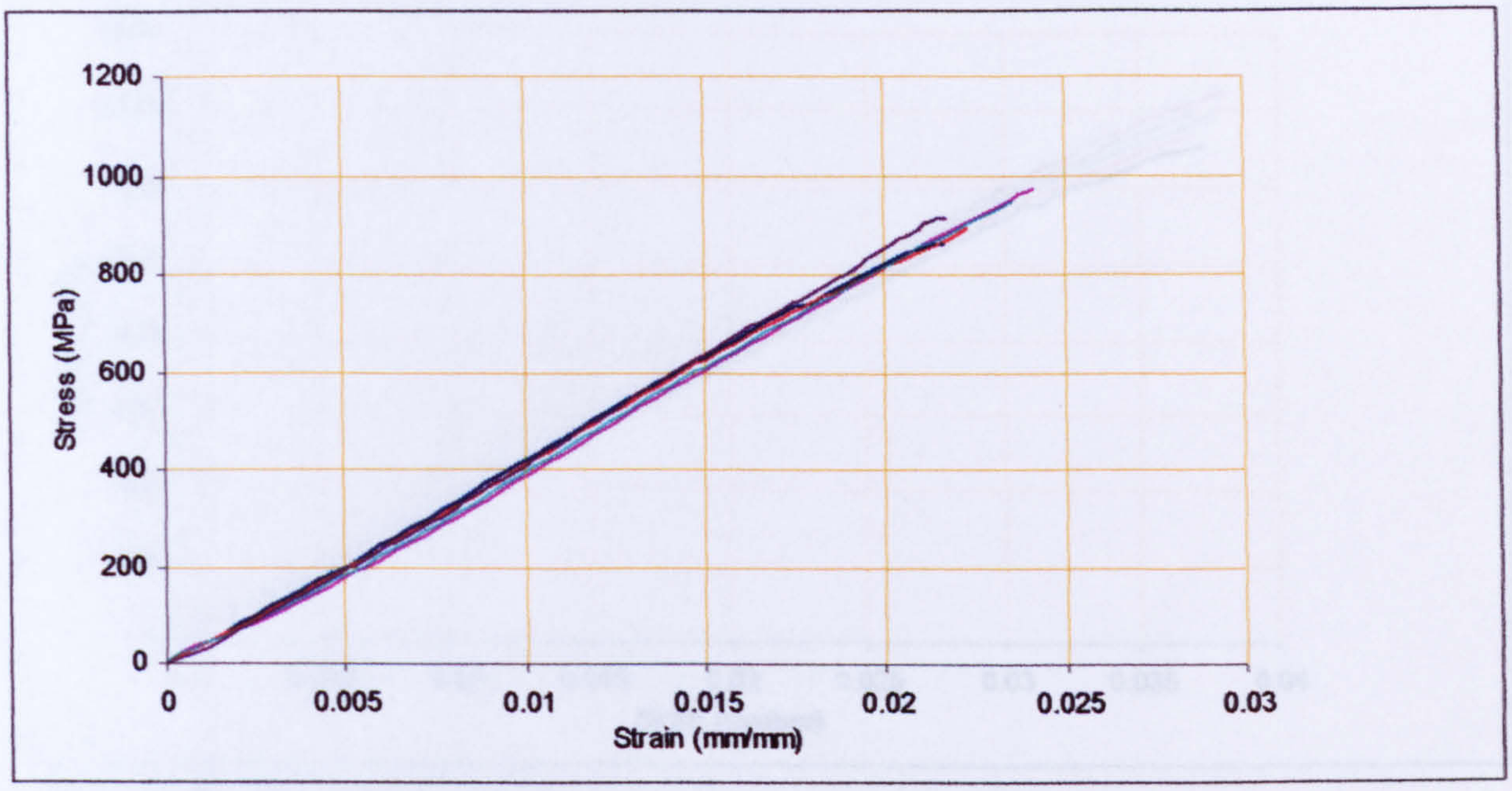

Figure 6.25: Stress-strain relationship in flexure for five GFRP rebar specimens immersed in *brine* solution for *180 days* at *60°C*

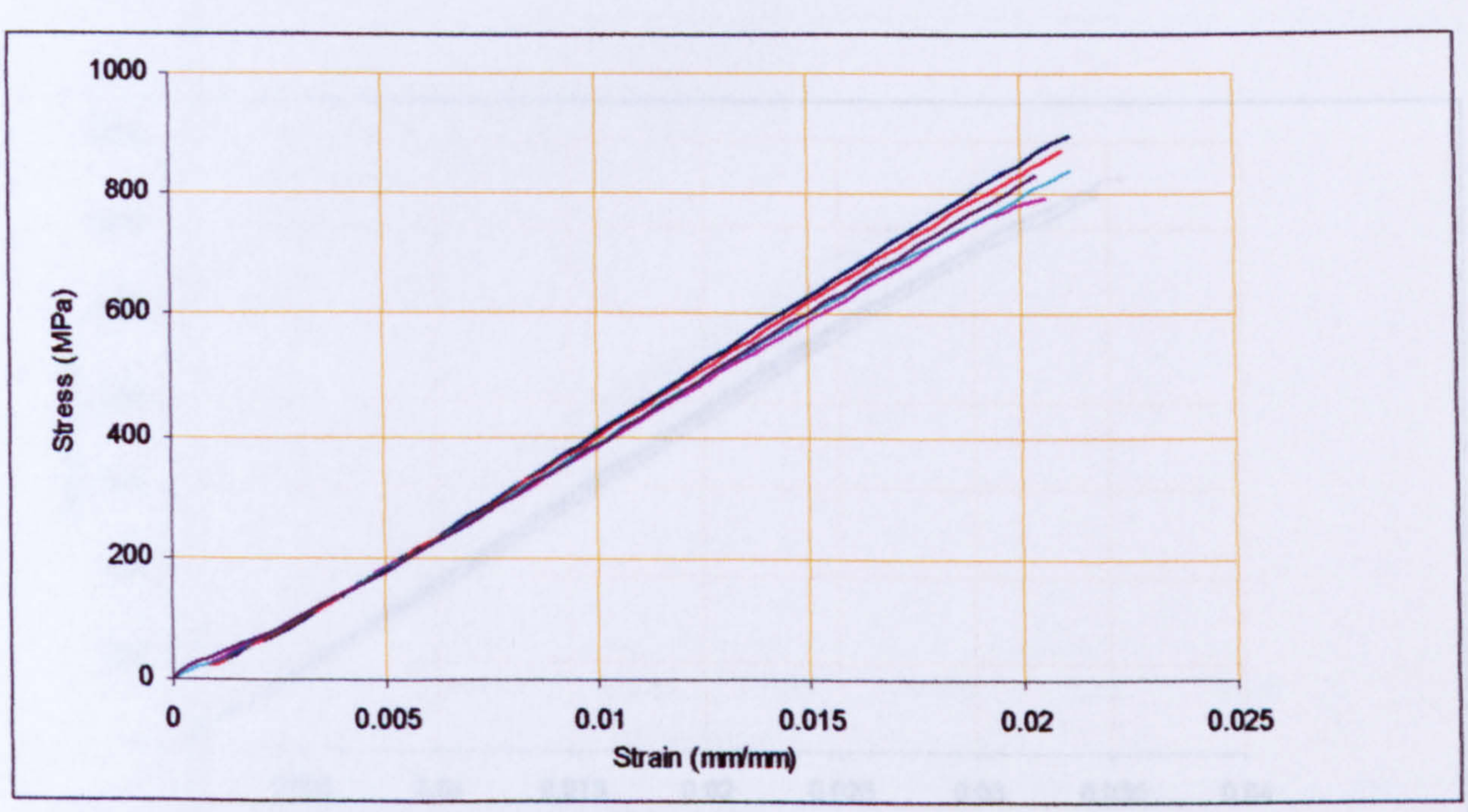

Figure 6.26: Stress-strain relationship in flexure for five GFRP rebar specimens immersed in *brine* solution for *270 days* at *60°C*

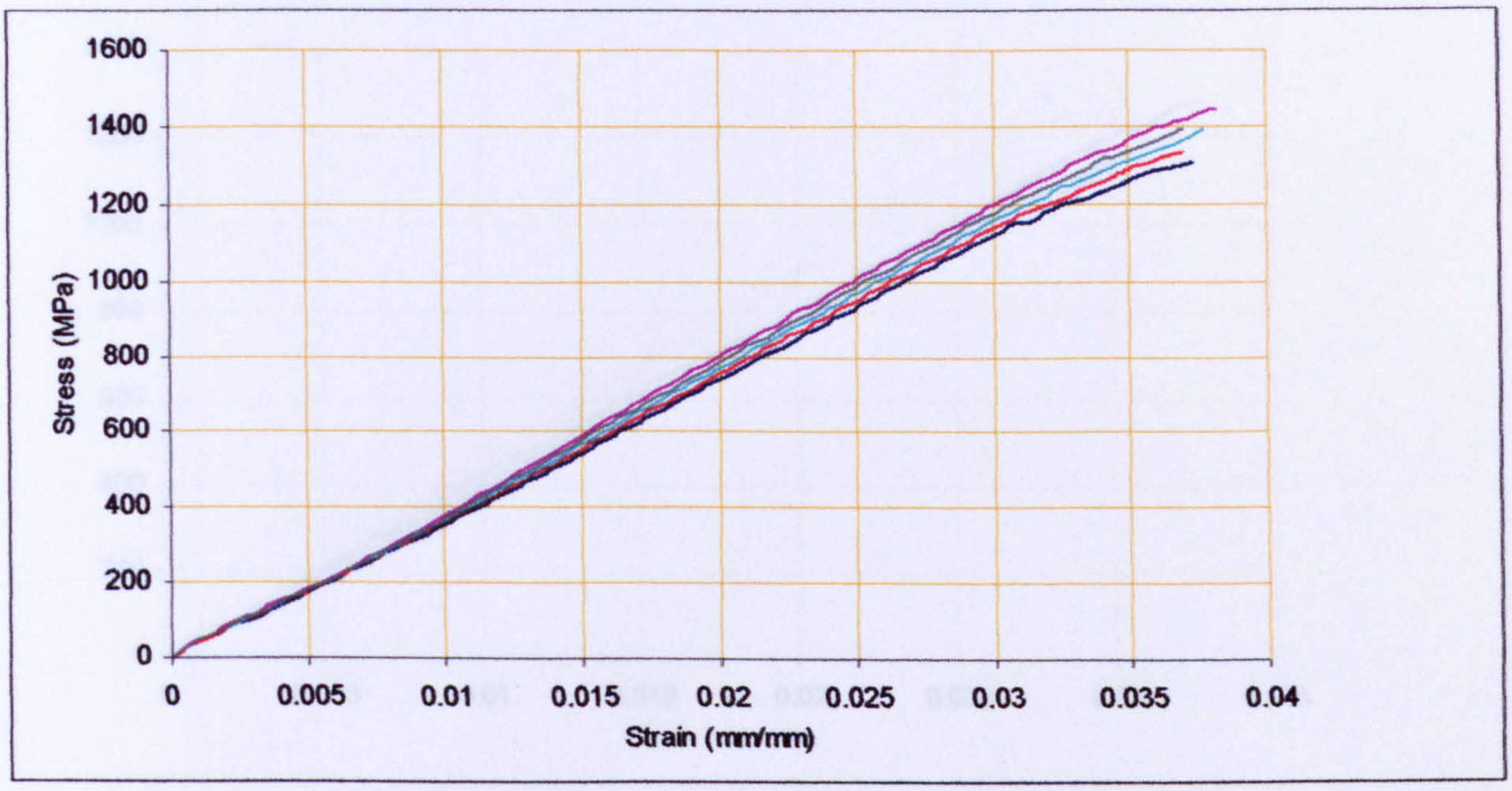

Figure 6.27: Stress-strain relationship in flexure for five GFRP rebar specimens immersed in *brine* solution for *30 days* at *20°C*

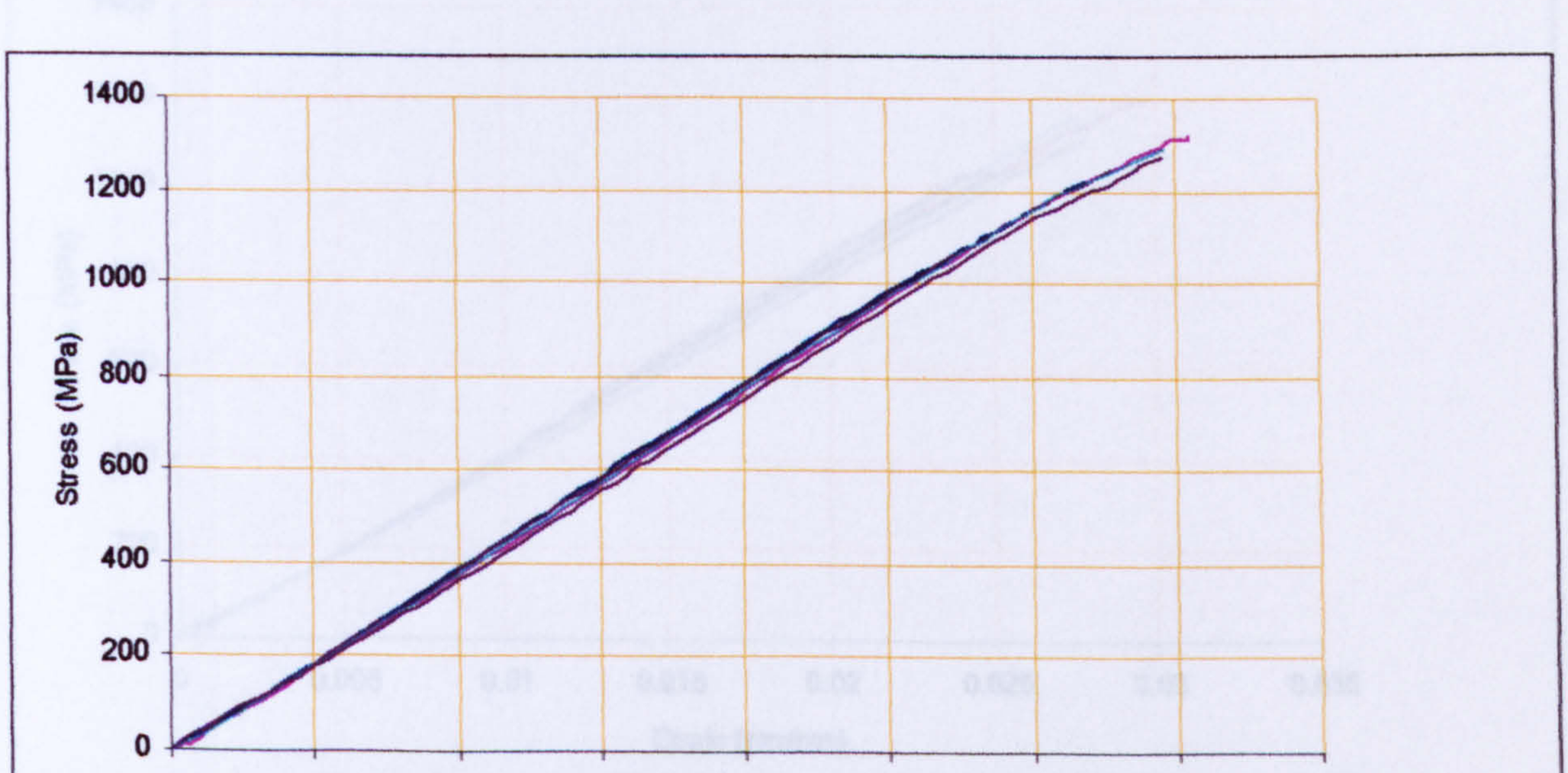

Figure 6.28: Stress-strain relationship in flexure for five GFRP rebar specimens immersed in *brine* solution for *90 days* at *20°C*

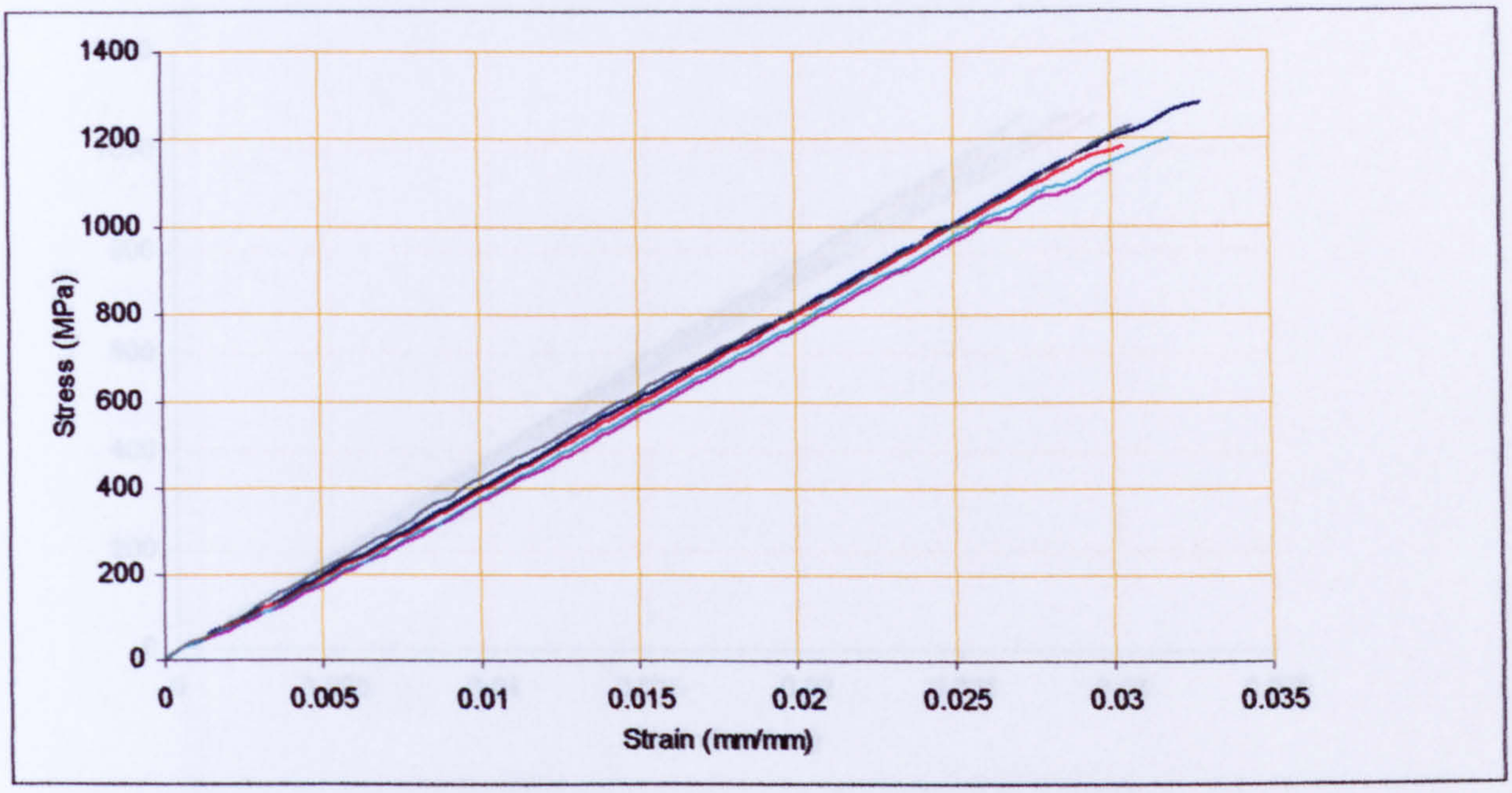

Figure 6.29: Stress-strain relationship in flexure for five GFRP rebar specimens immersed in *brine* solution for *180 days* at *20°C*

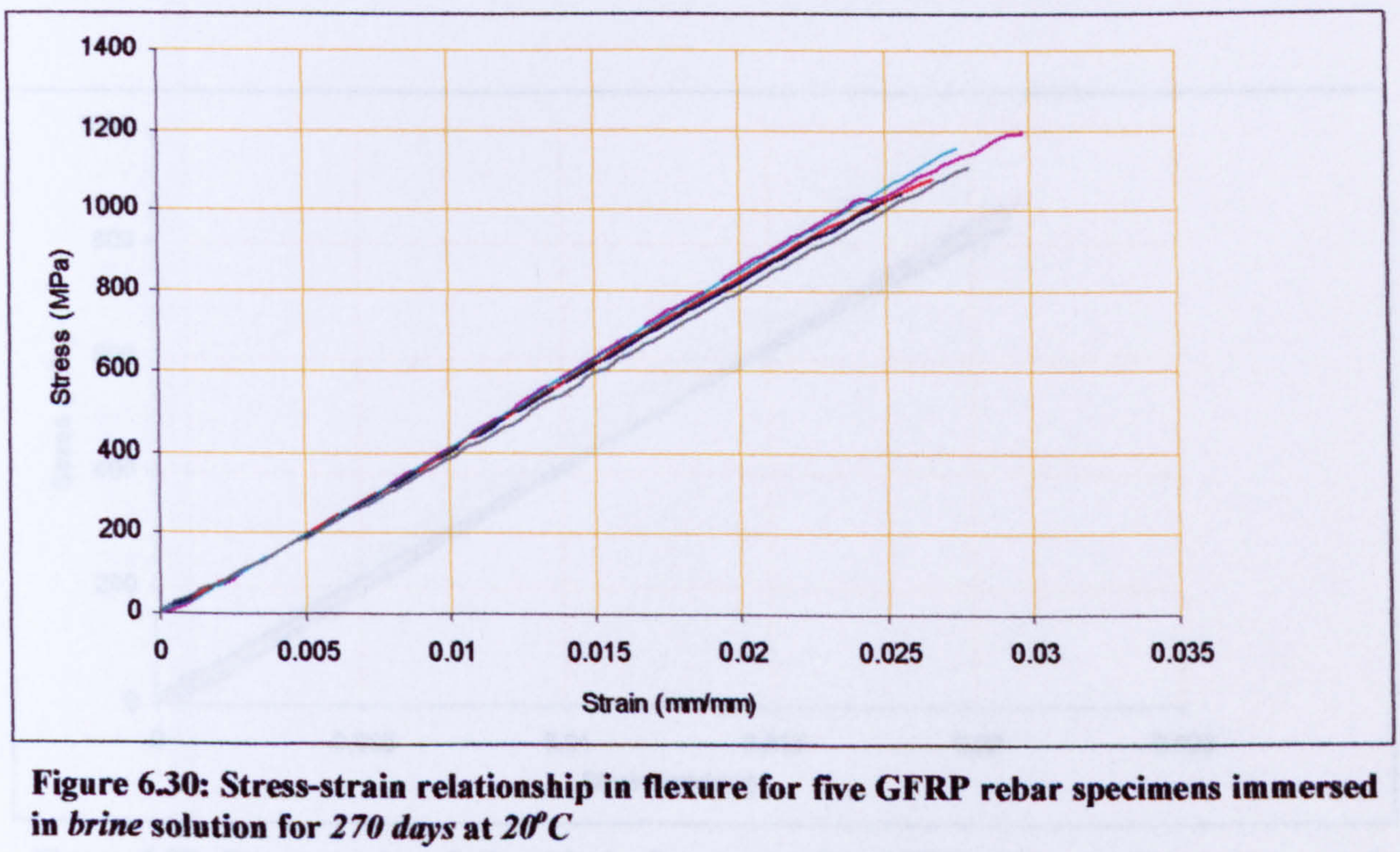

Figure 6.30: Stress-strain relationship in flexure for five GFRP rebar specimens immersed in *brine* solution for *270 days* at *20°C*

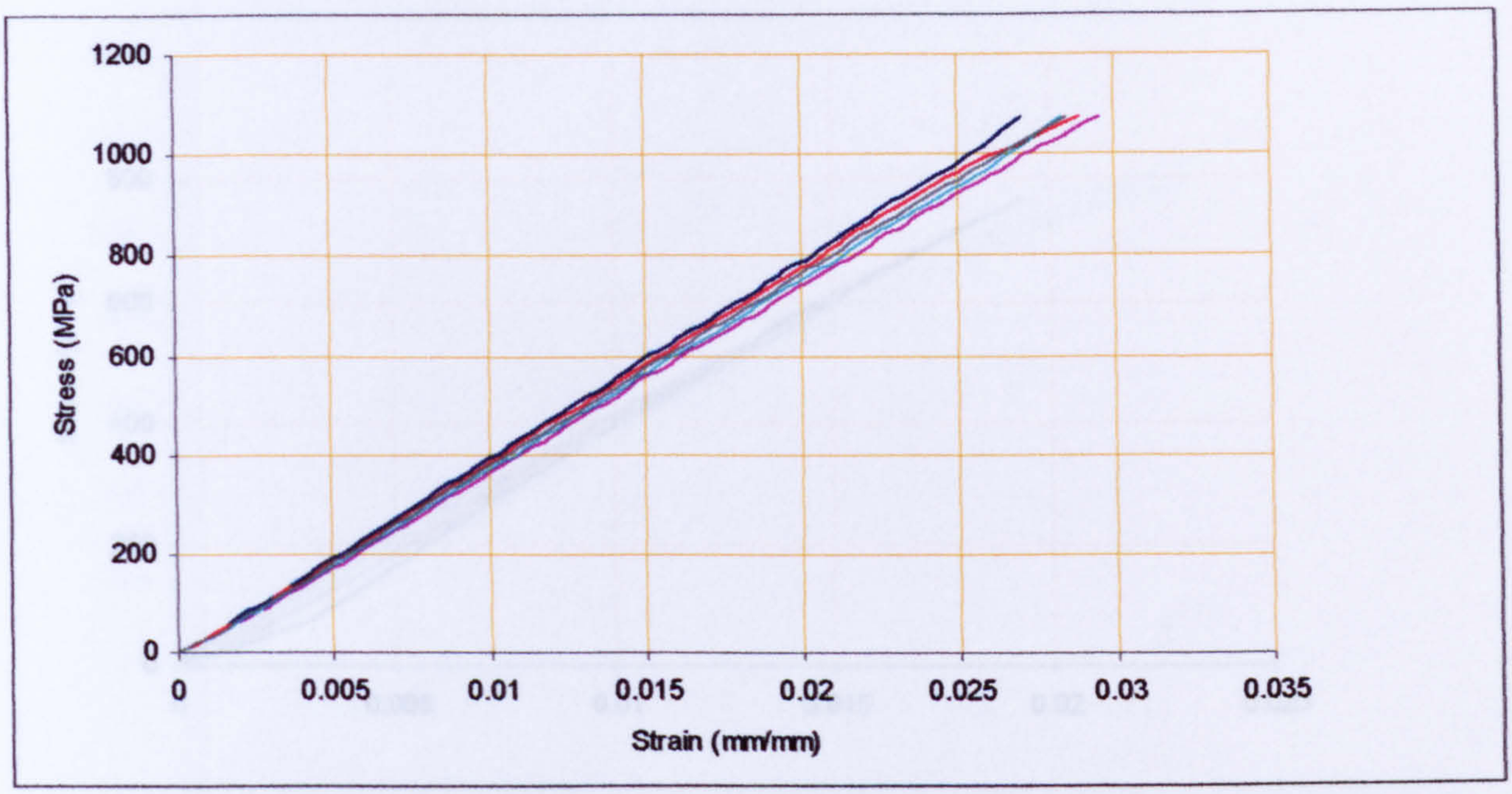

Figure 6.31: Stress-strain relationship in flexure for five GFRP rebar specimens immersed in *alkali* solution for *30 days* at *60°C*

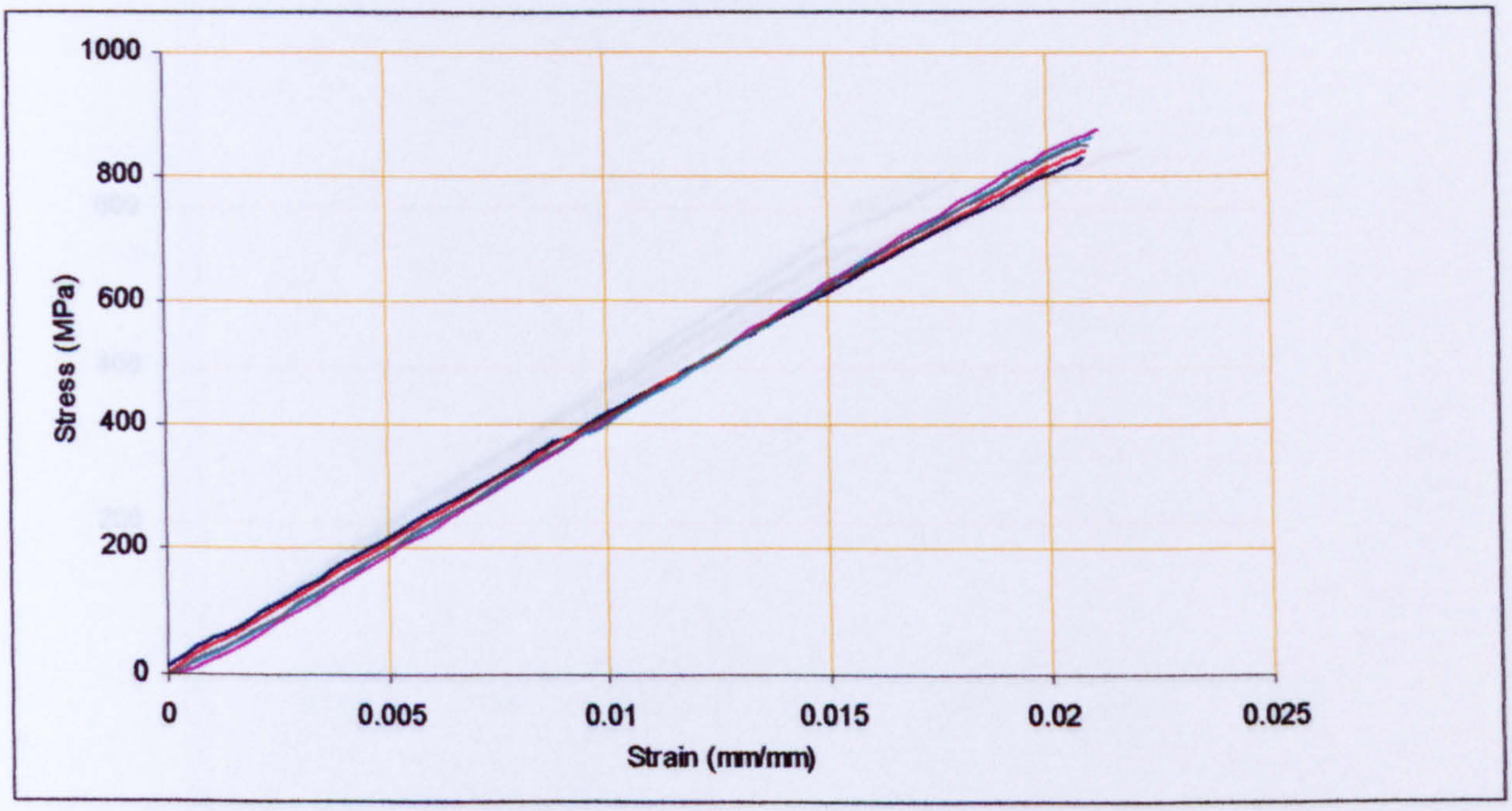

Figure 6.32: Stress-strain relationship in flexure for five GFRP rebar specimens immersed in *alkali* solution for *90 days* at *60°C*

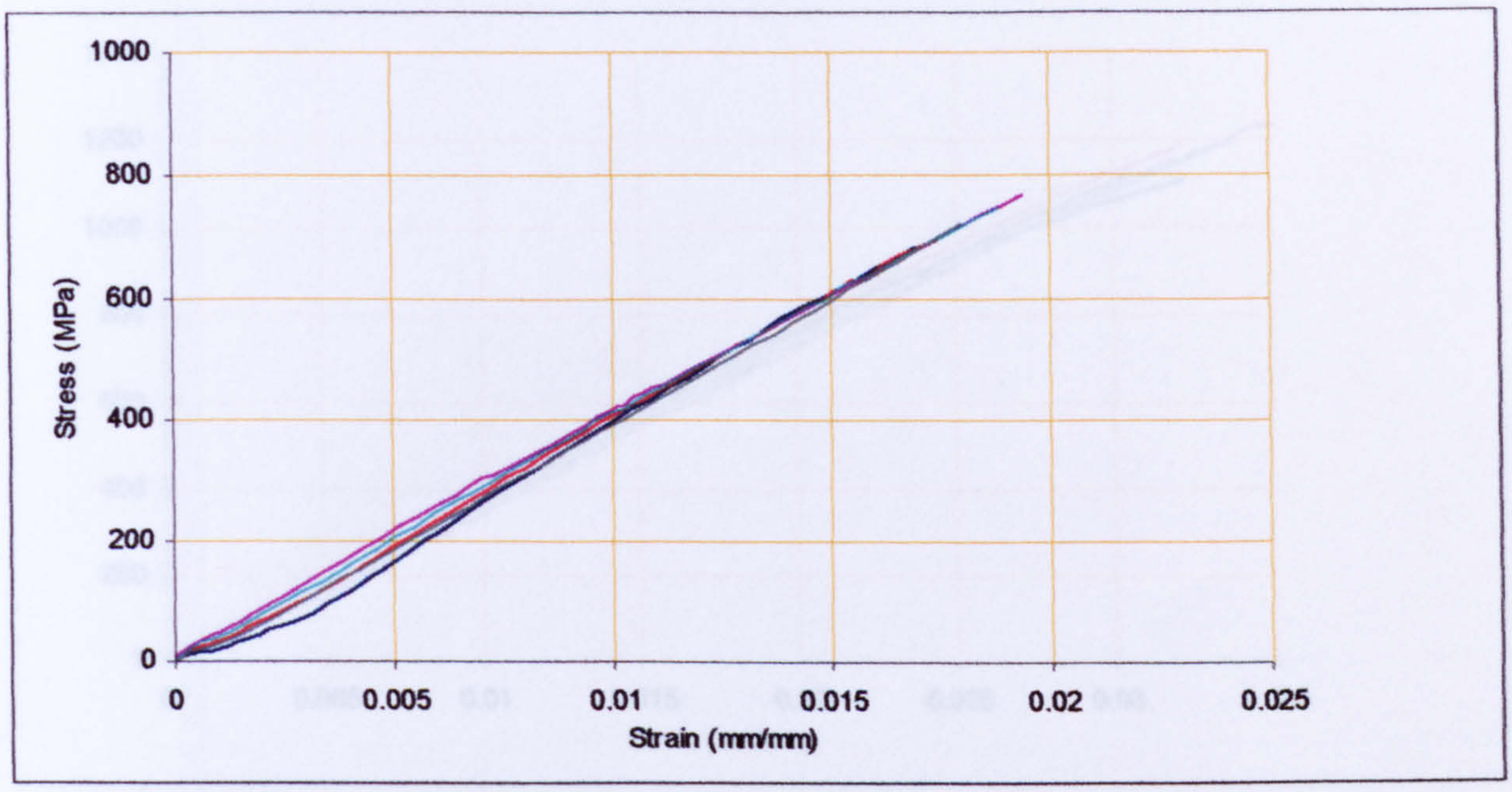

Figure 6.33: Stress-strain relationship in flexure for five GFRP rebar specimens immersed in *alkali* solution for *180 days* at *60°C*

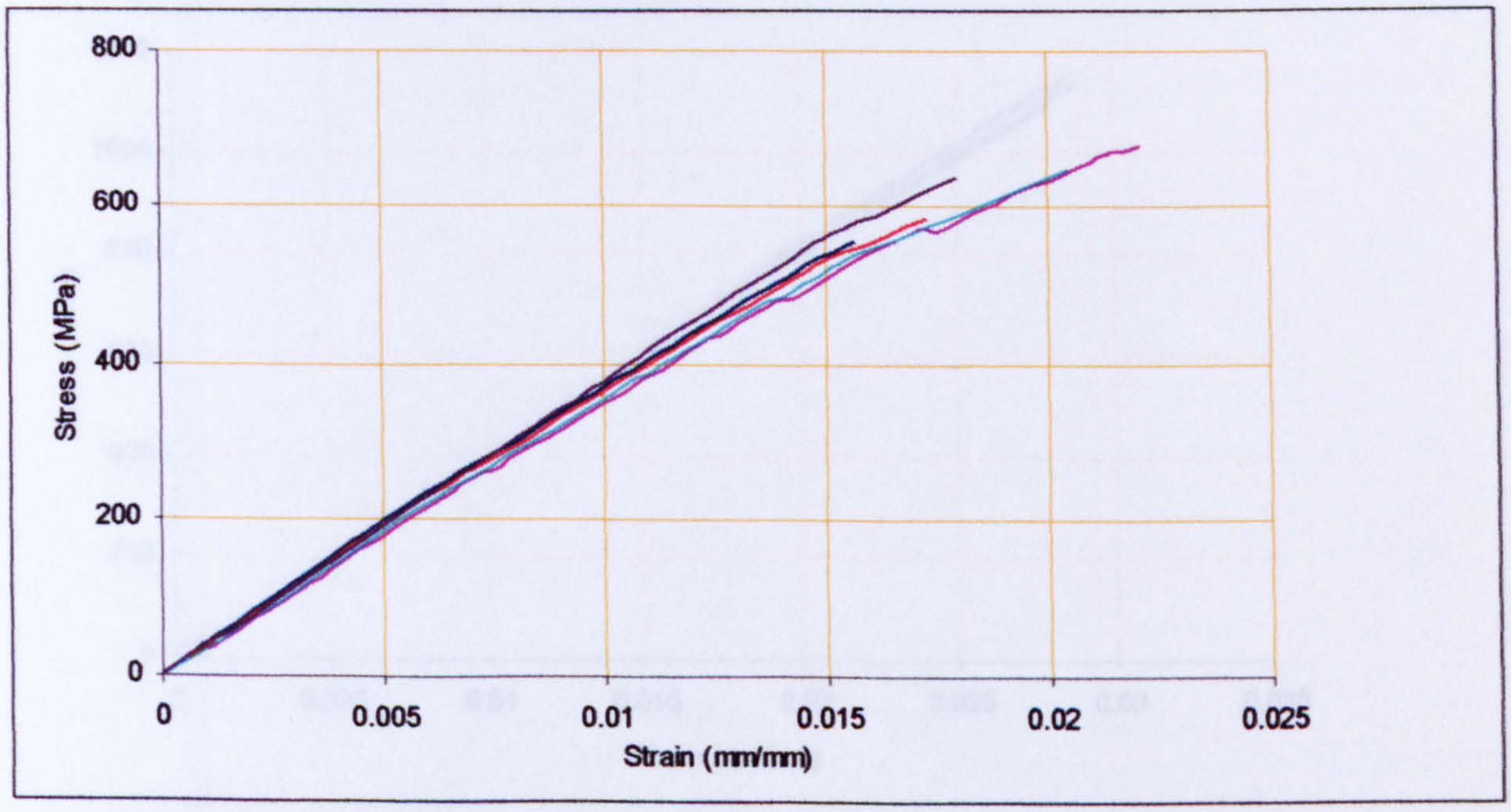

Figure 6.34: Stress-strain relationship in flexure for five GFRP rebar specimens immersed in *alkali* solution for *270 days* at *60°C*

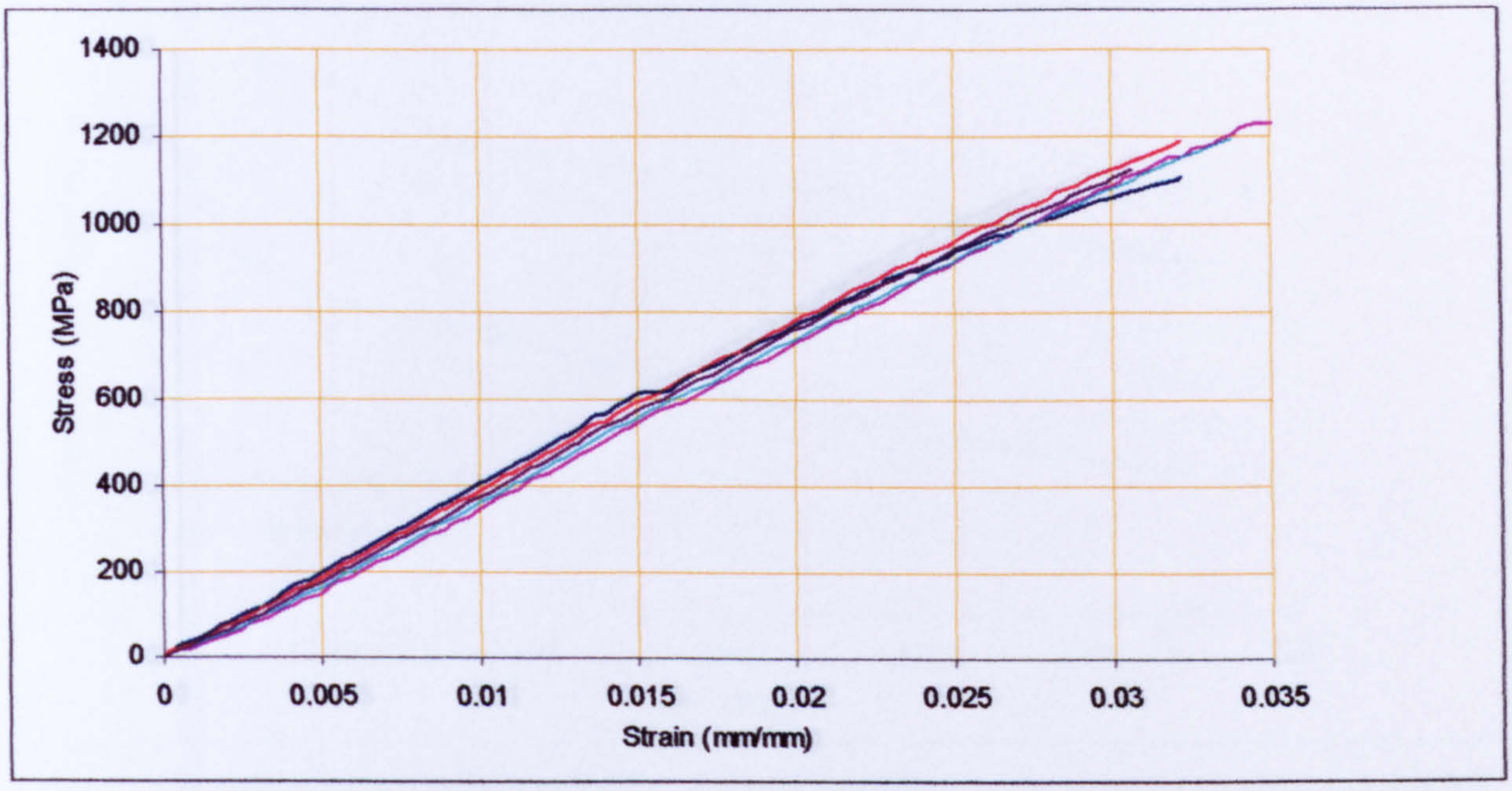

Figure 6.35: Stress-strain relationship in flexure for five GFRP rebar specimens immersed in *alkali* solution for *30 days* at *20°C*

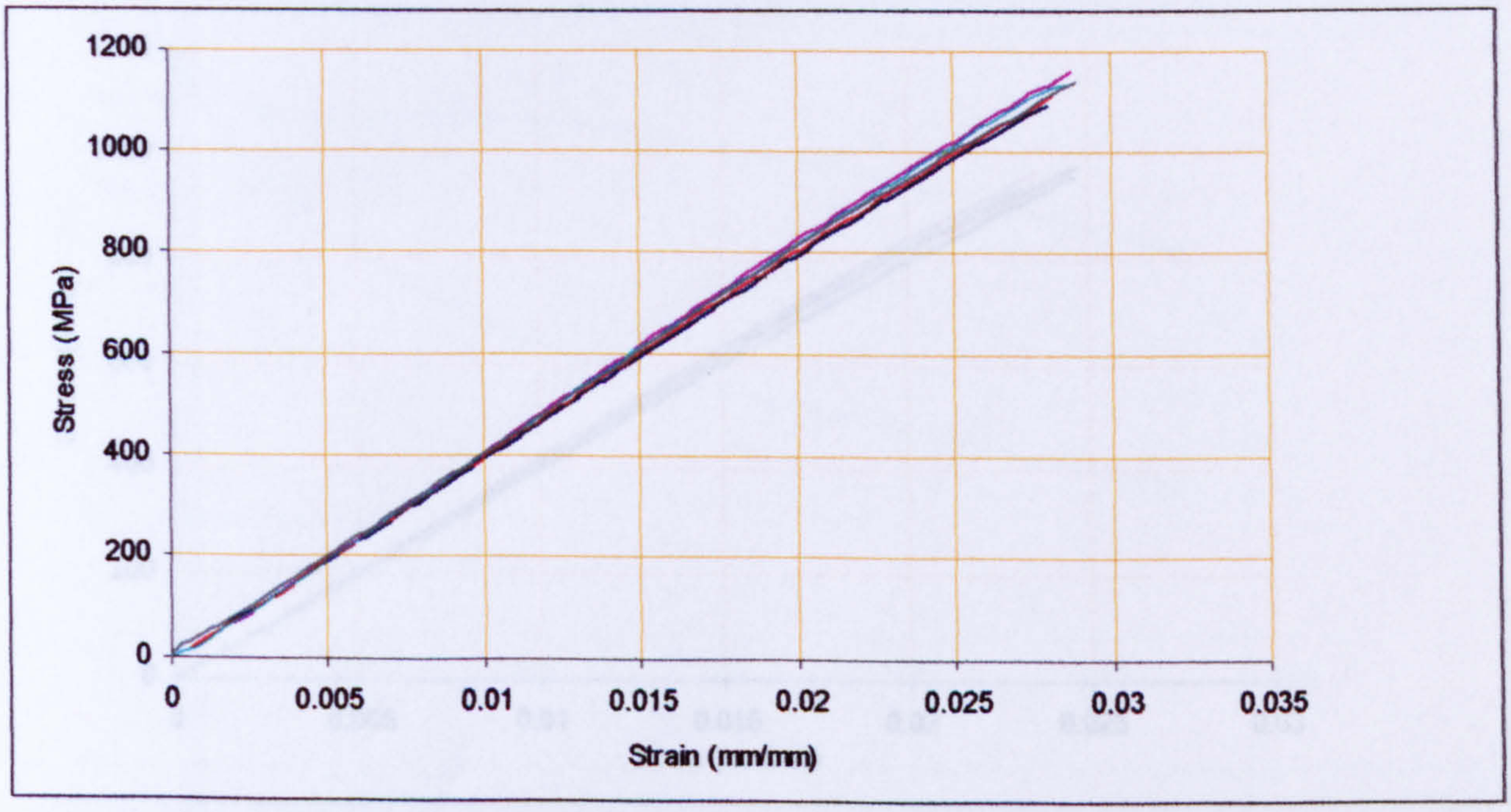

Figure 6.36: Stress-strain relationship in flexure for five GFRP rebar specimens immersed in *alkali* solution for *90 days* at *20°C*

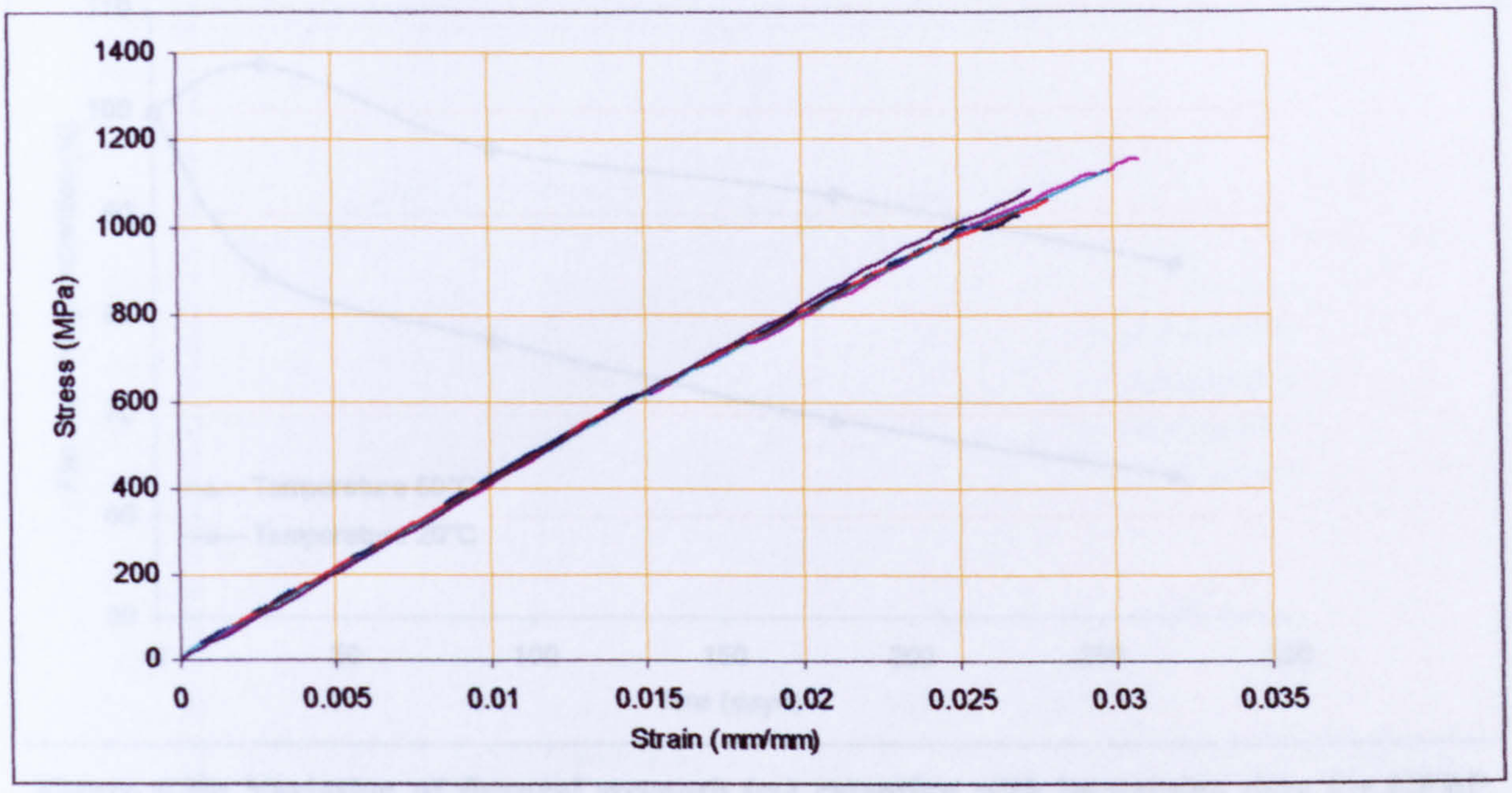

Figure 6.37: Stress-strain relationship in flexure for five GFRP rebar specimens immersed in *alkali* solution for *180 days* at *20°C*

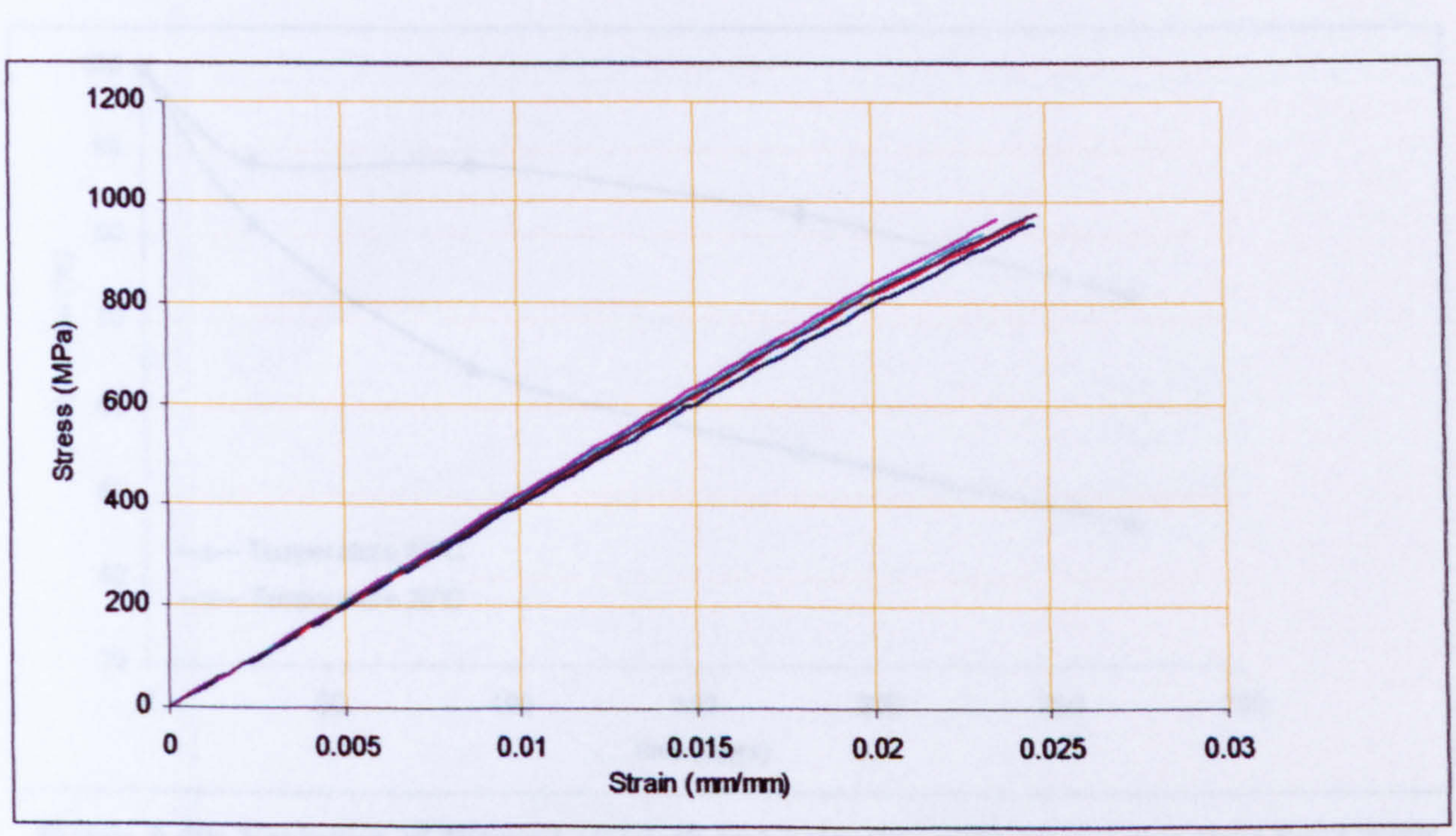

Figure 6.38: Stress-strain relationship in flexure for five GFRP rebar specimens immersed in *alkali* solution for *270 days* at *20°C*

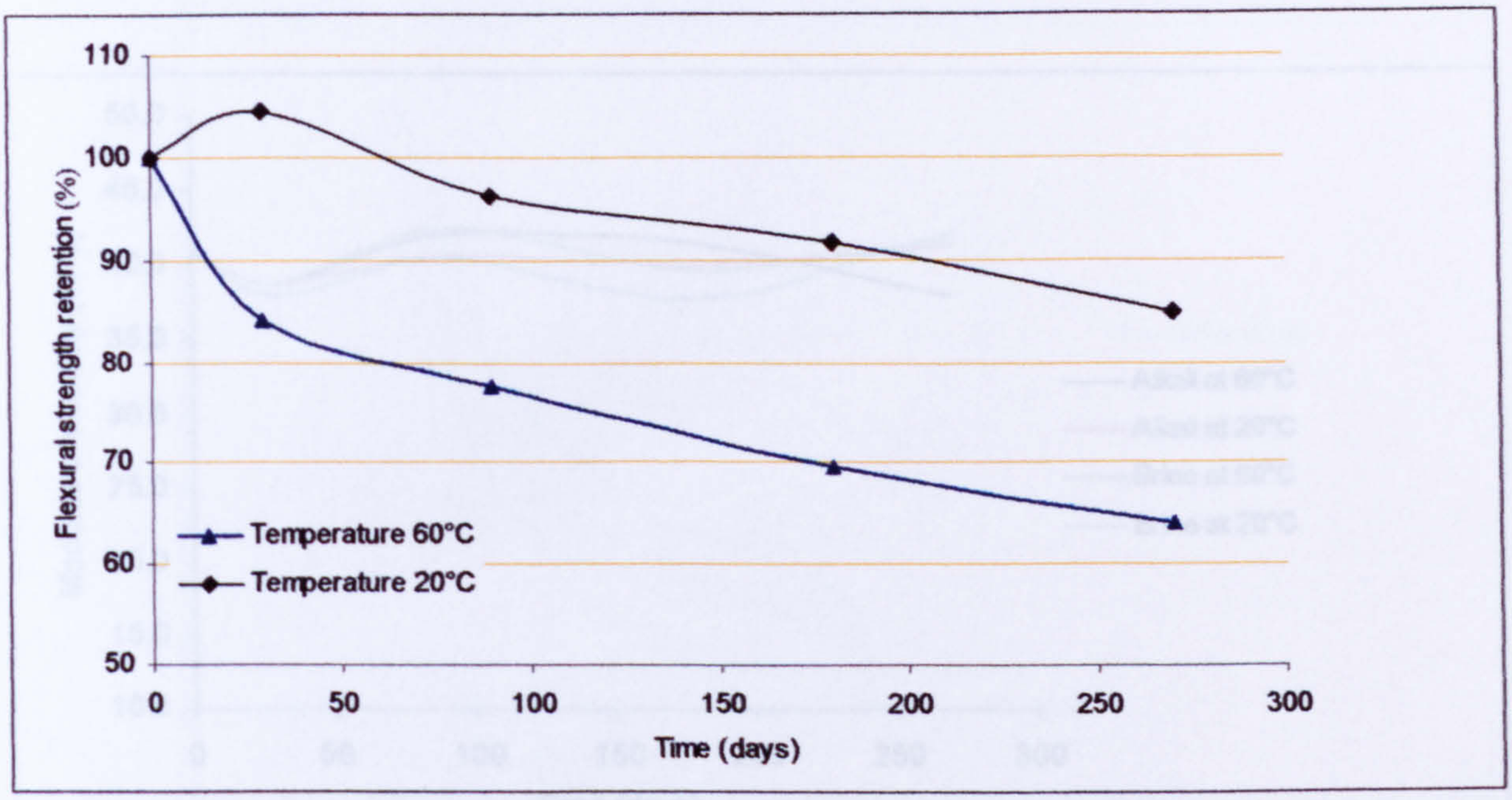

Figure 6.39: Variation of flexural strength (σ_f) retention with immersion time for GFRP bars in brine solutions at different temperatures

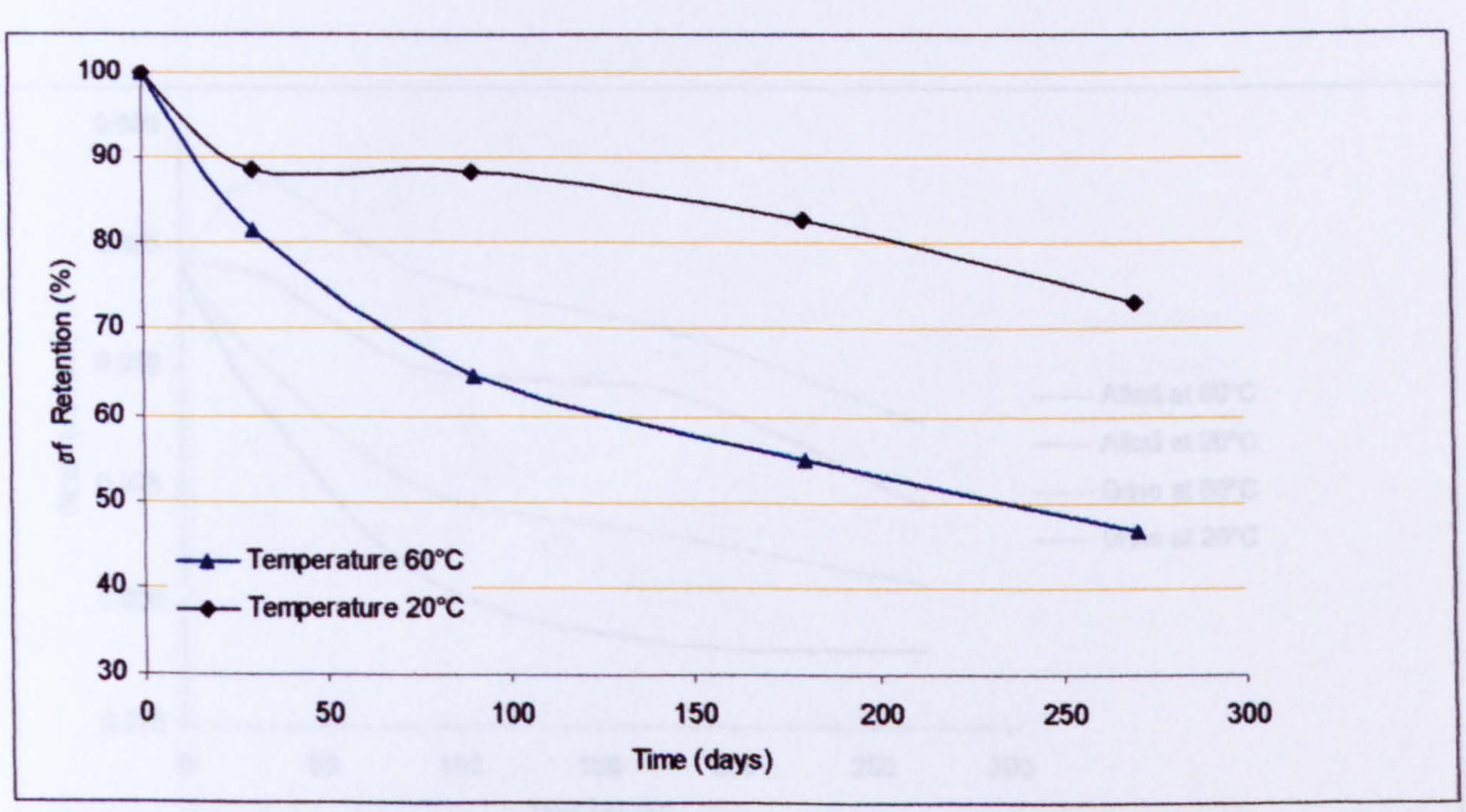

Figure 6.40: Variation of flexural strength (σ_f) retention with immersion time for GFRP bars in alkali solutions at different temperatures

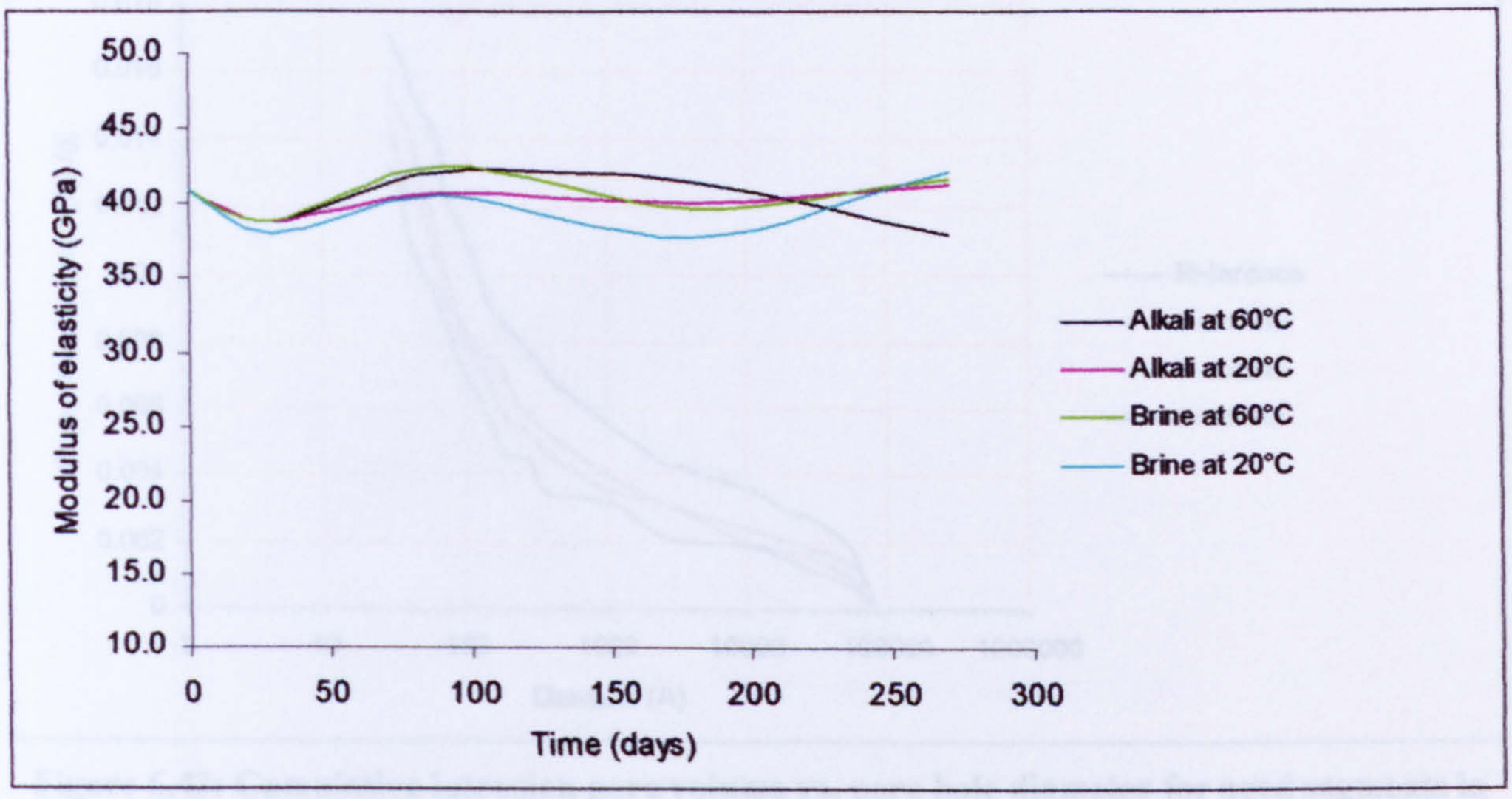

Figure 6.41: Elastic moduli values in flexure for aged and not-aged specimens of GFRP bars at different periods of time and temperatures

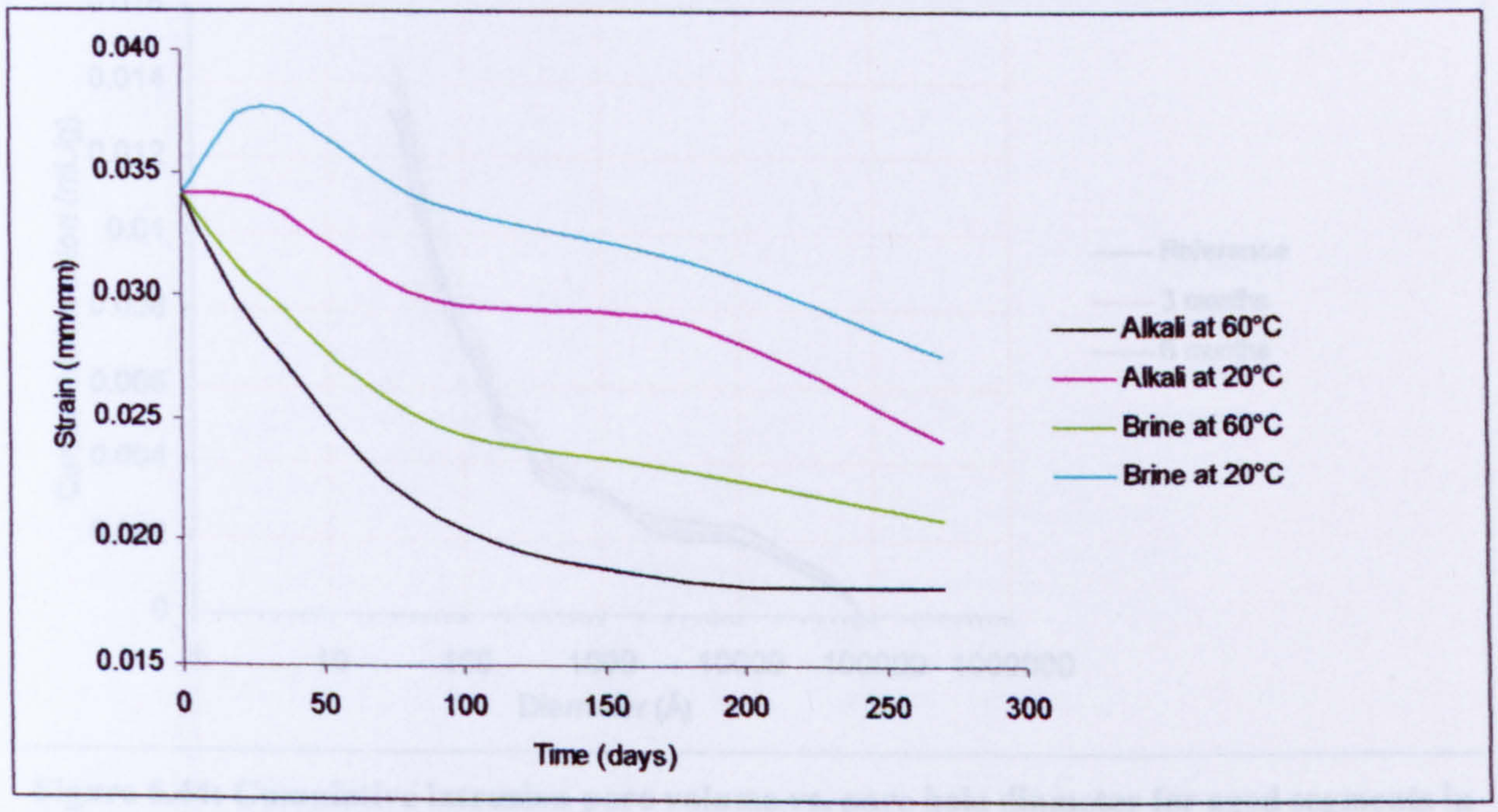

Figure 6.42: Strains at failure in flexure for aged and not-aged specimens of GFRP bars at different periods of time and temperatures

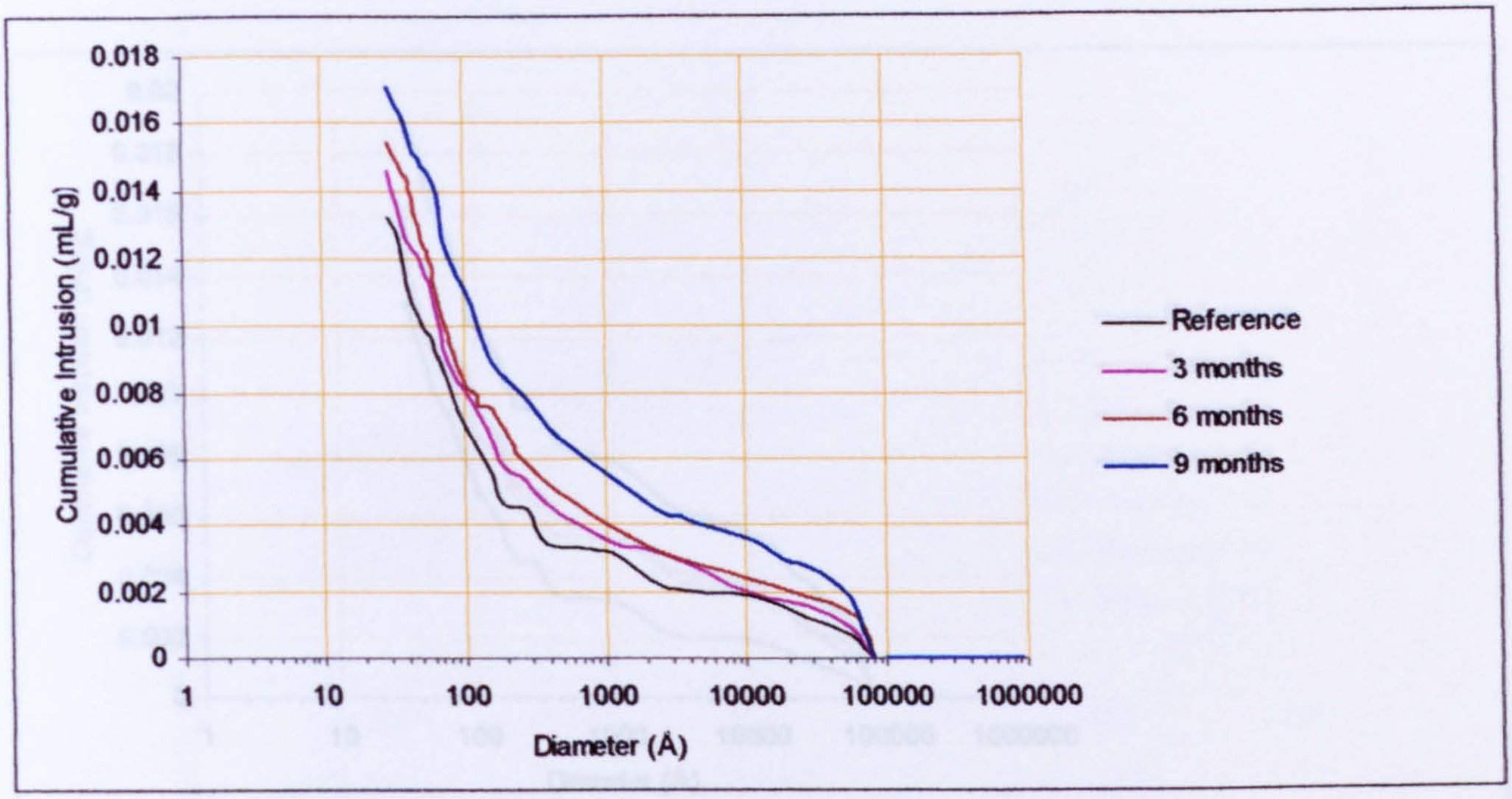

Figure 6.43: Cumulative intrusion pore volume vs. pore hole diameter for aged segments in *brine* solution at *60 ℃* for different periods of time

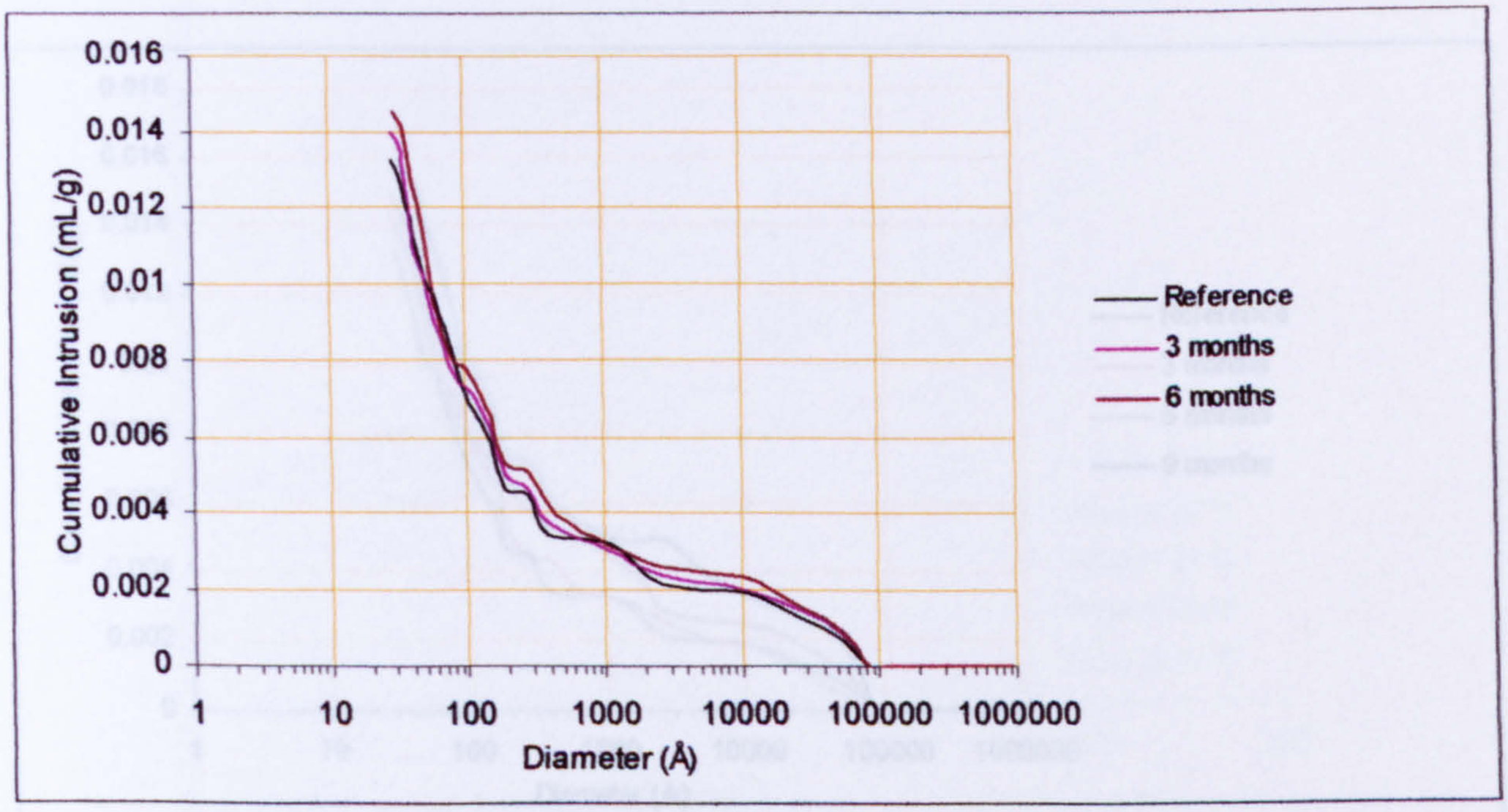

Figure 6.44: Cumulative intrusion pore volume vs. pore hole diameter for aged segments in *brine* solution at *20 ℃* for different periods of time

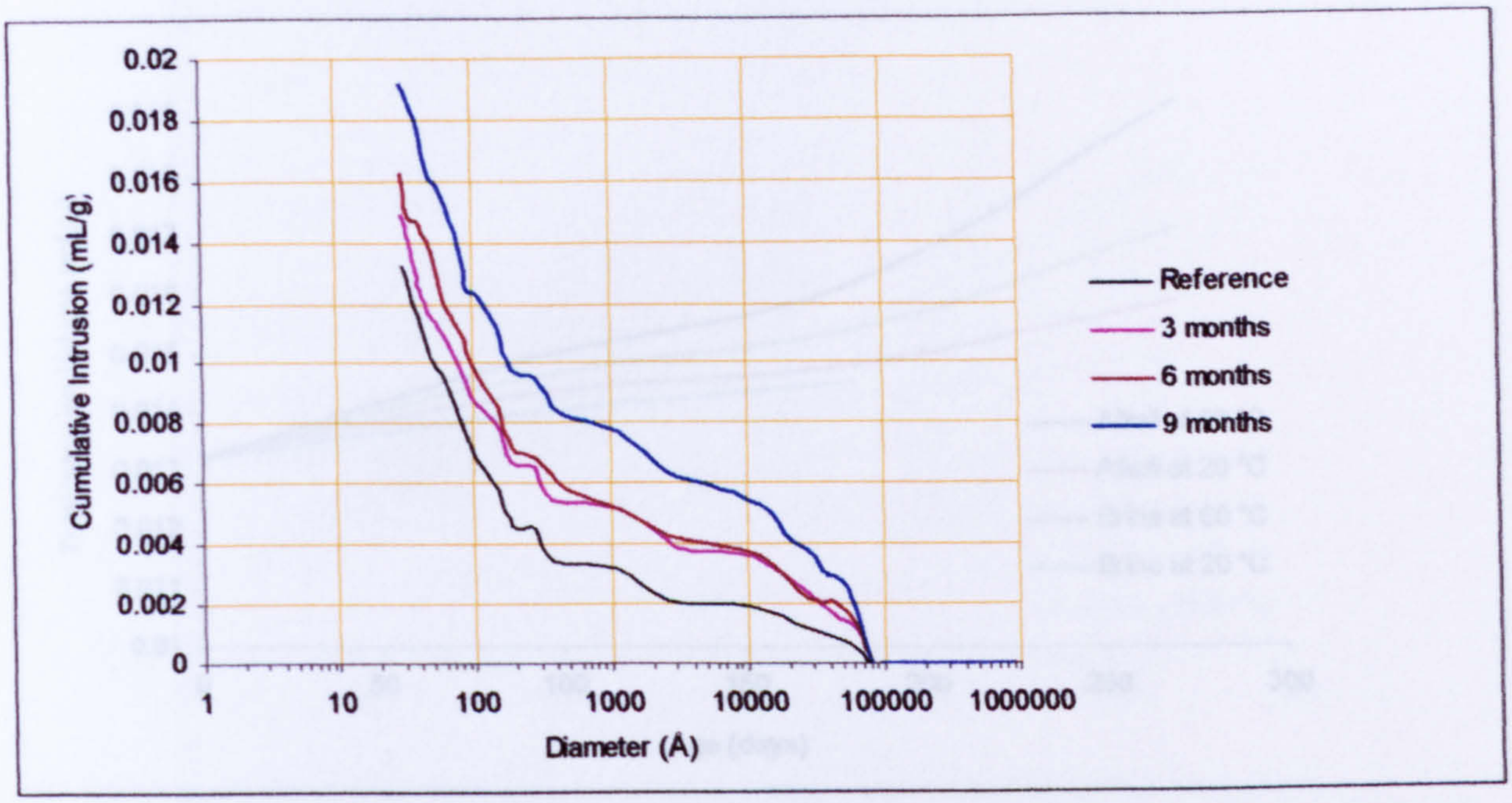

Figure 6.45: Cumulative intrusion pore volume vs. pore hole diameter for aged segments in *alkali* solution at *60 °C* for different periods of time

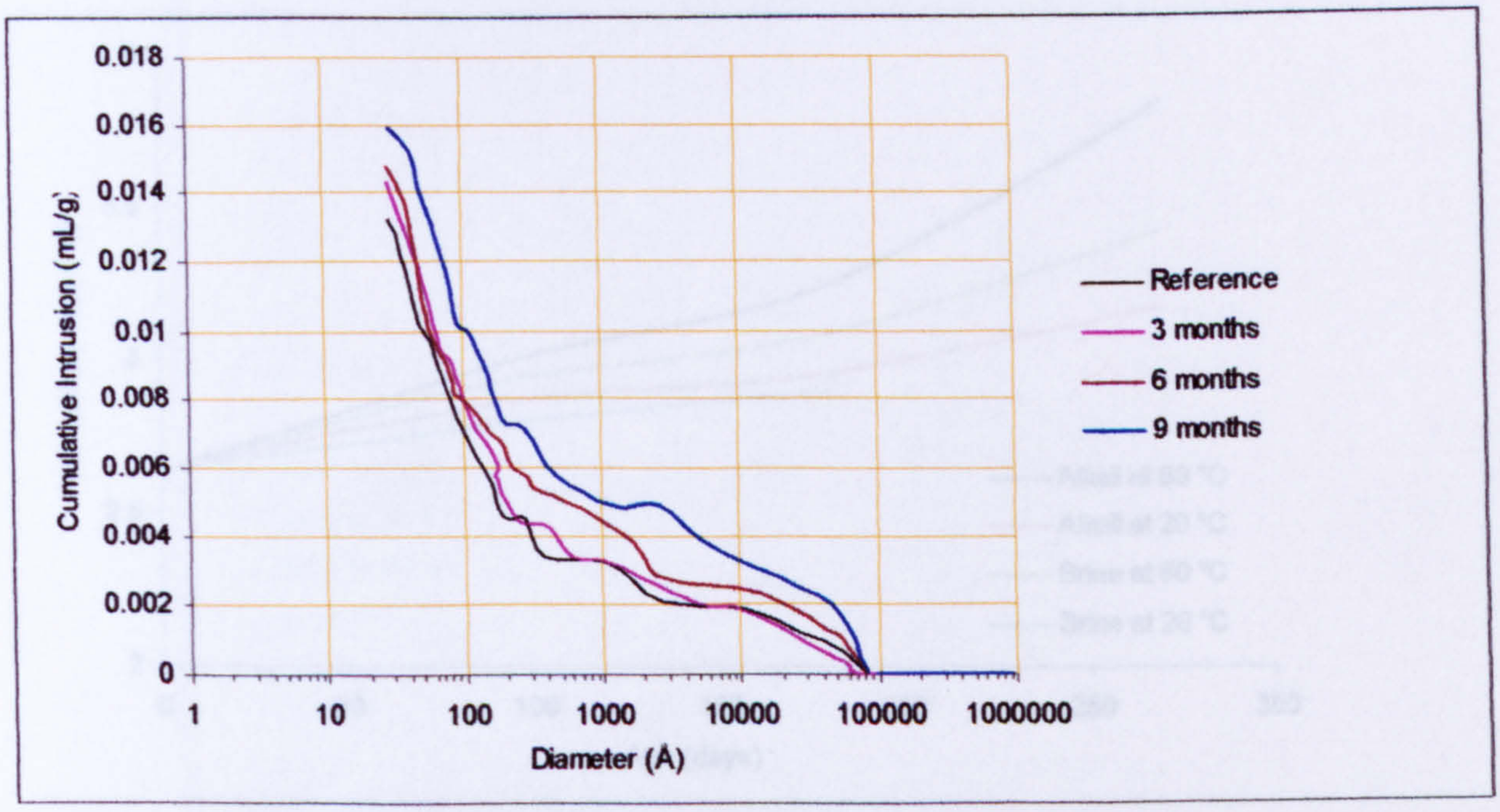

Figure 6.46: Cumulative intrusion pore volume vs. pore hole diameter for aged segments in *alkali* solution at *20 °C* for different periods of time

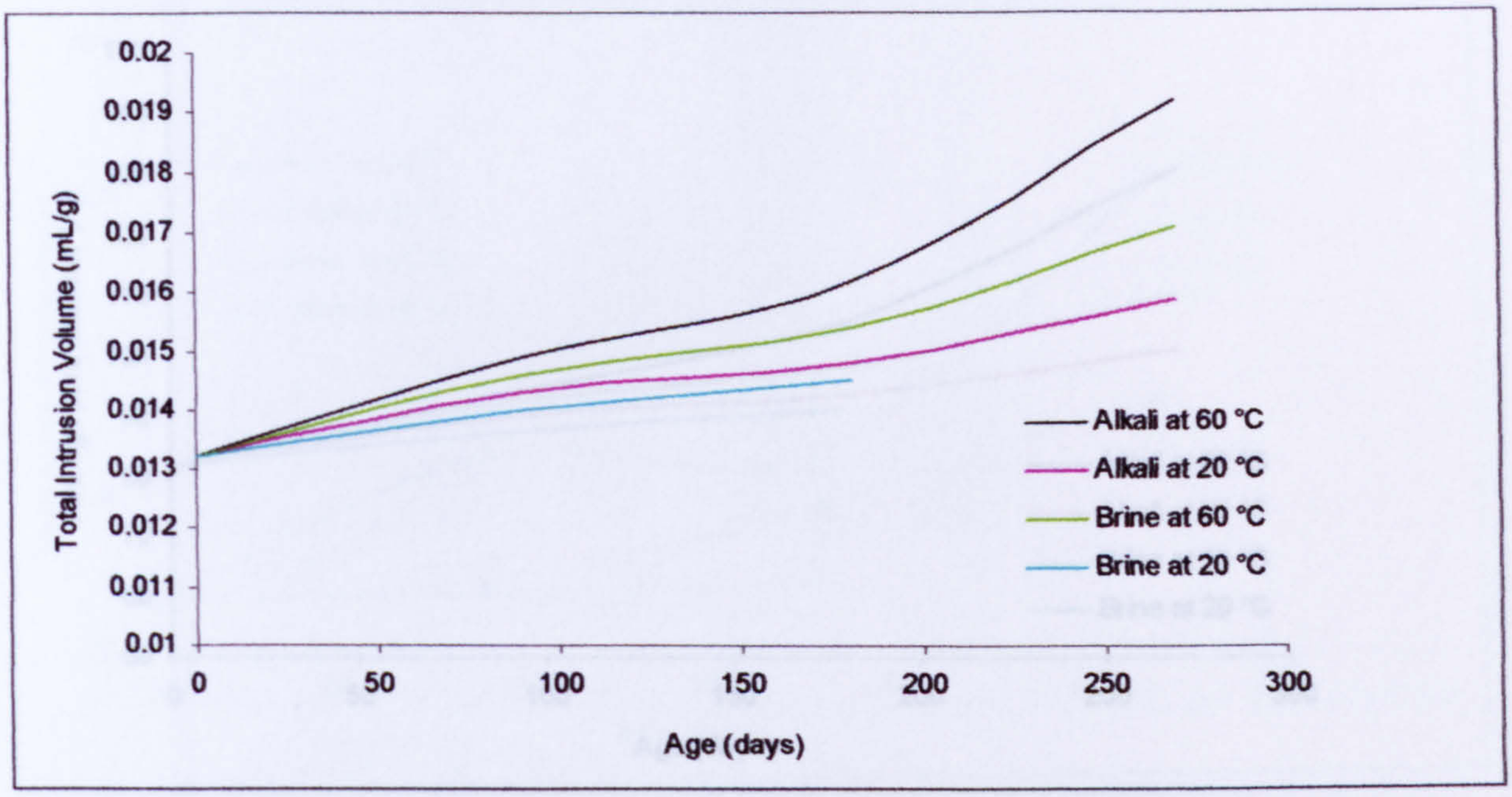

Figure 6.47: The effect of immersion period and temperature on the total intrusion volume in both alkaline and brine solutions

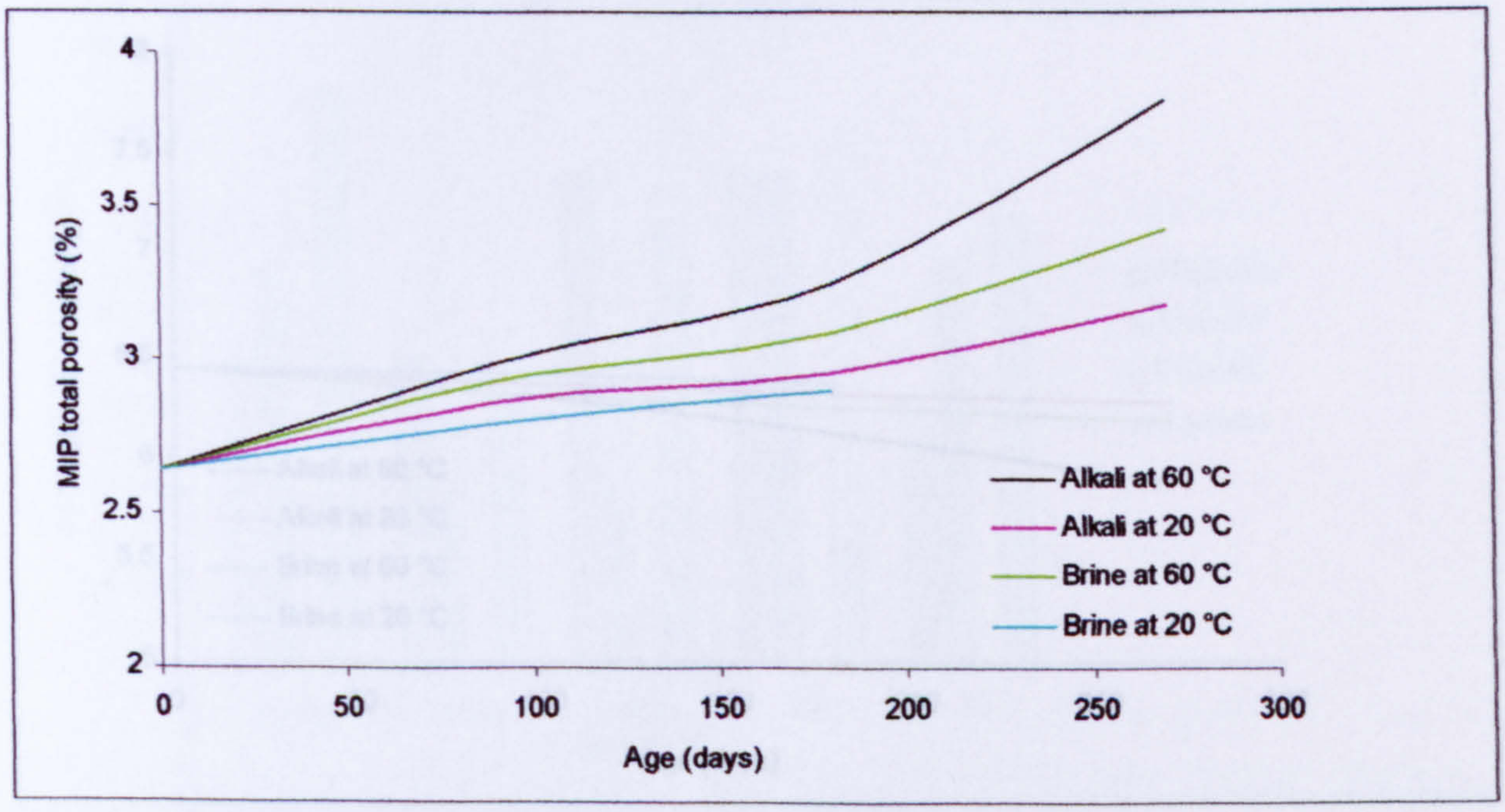

Figure 6.48: The effect of immersion period and temperature on porosity in both alkaline and brine solutions

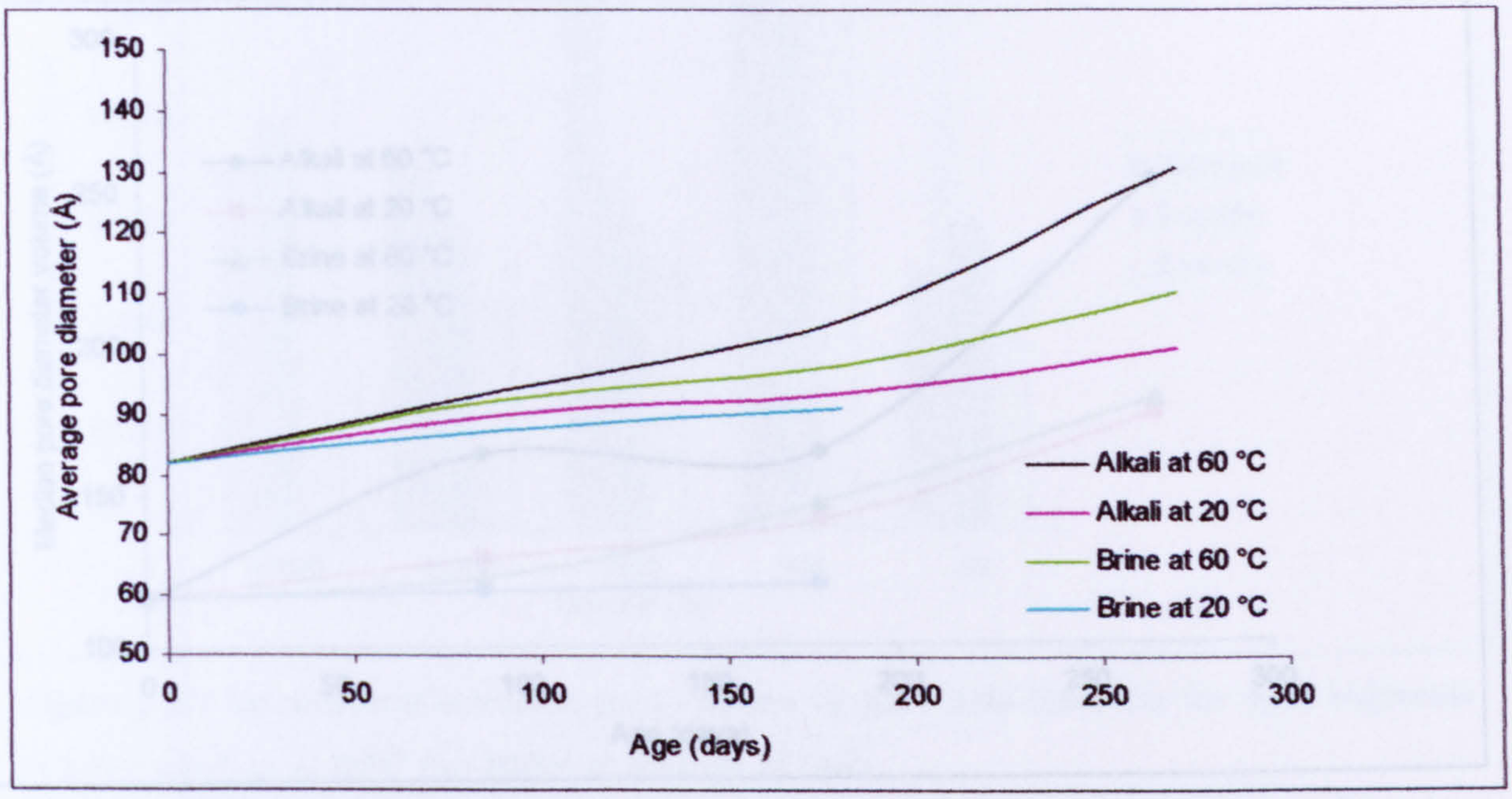

Figure 6.49: The effect of immersion period and temperature on the average pore diameter in both alkaline and brine solutions

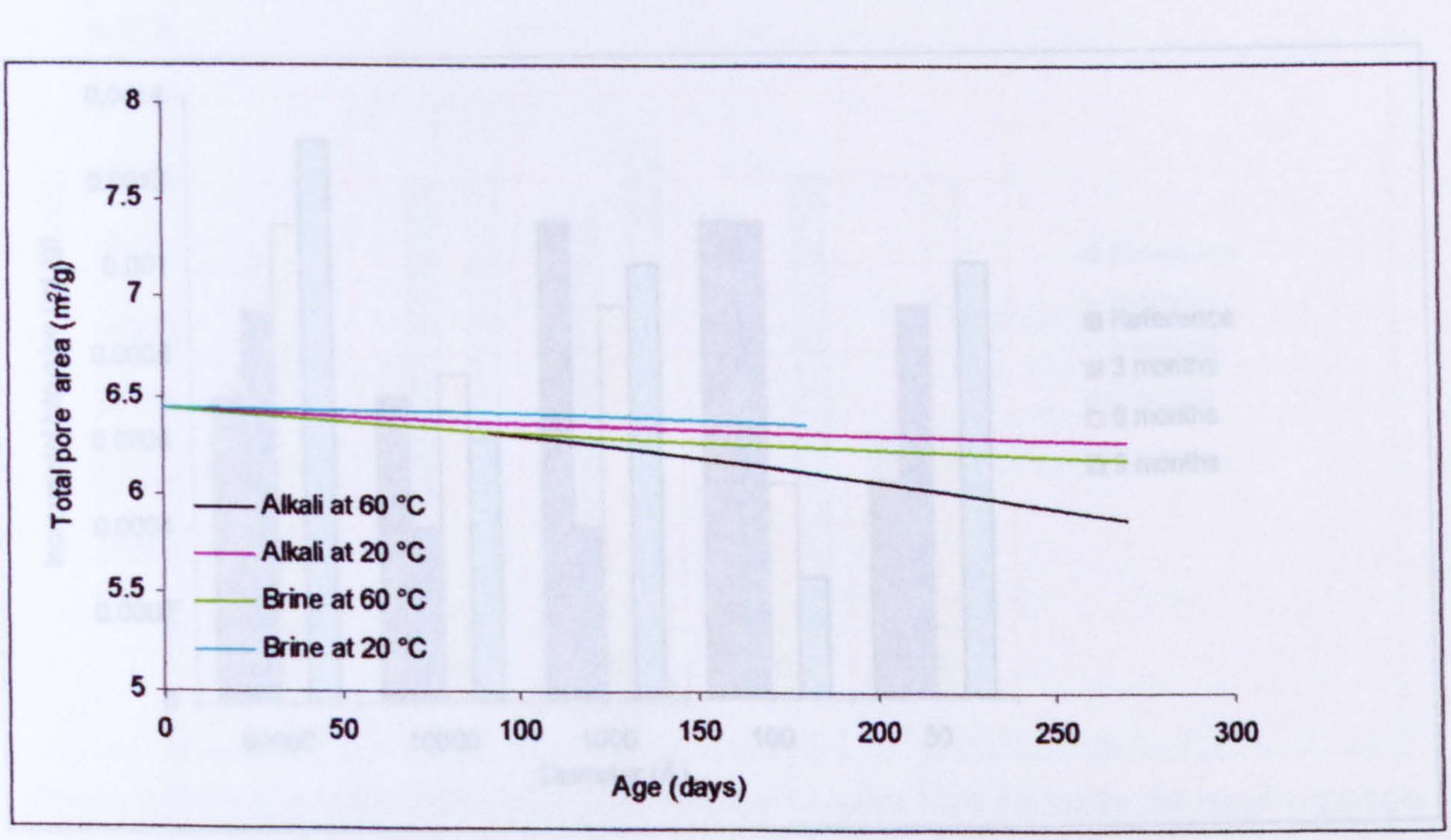

Figure 6.50: The effect of immersion period and temperature on the pore surface area in both alkaline and brine solutions

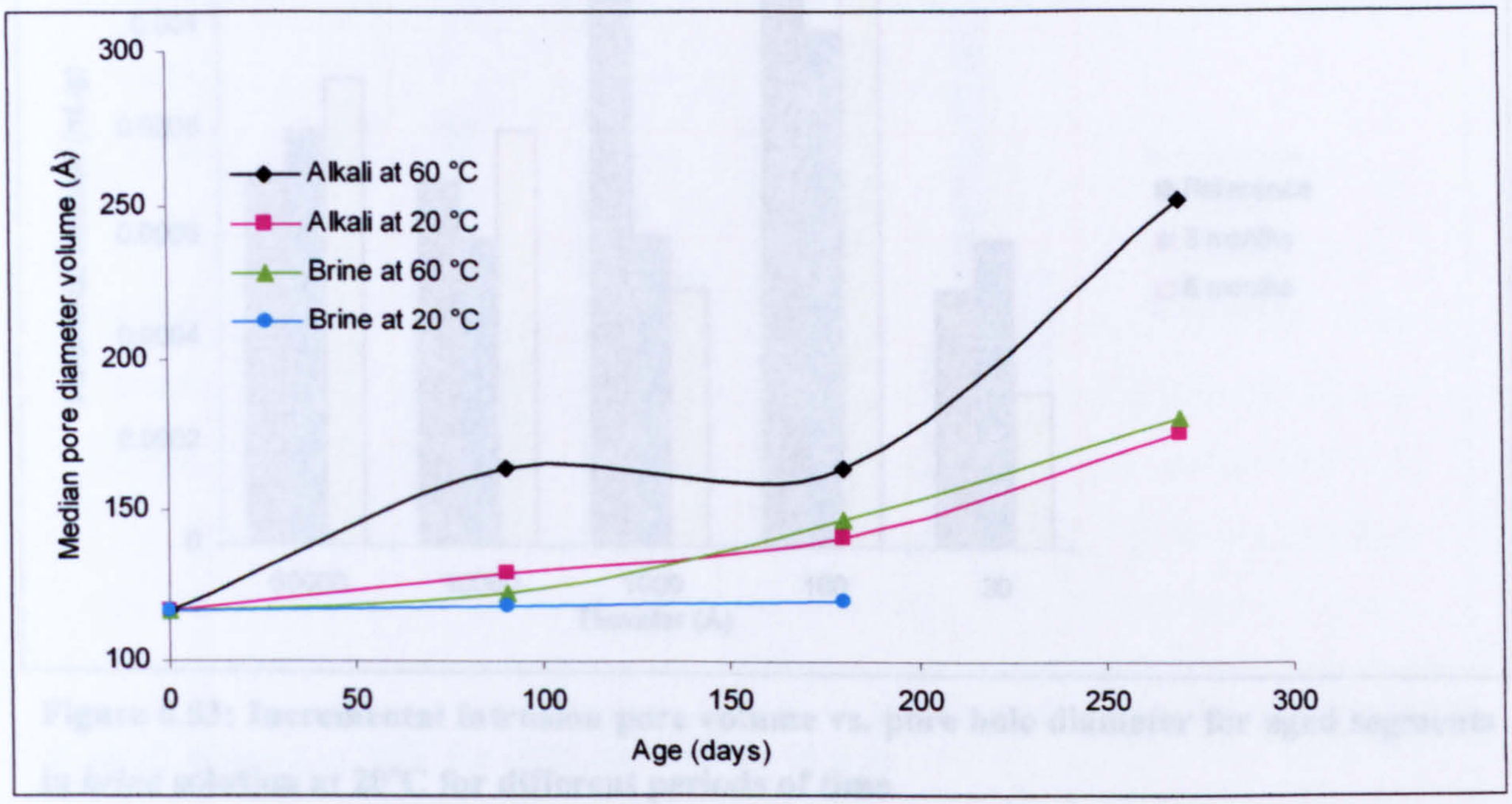

Figure 6.51: The effect of immersion period and temperature on the median pore diameter in both alkaline and brine solutions

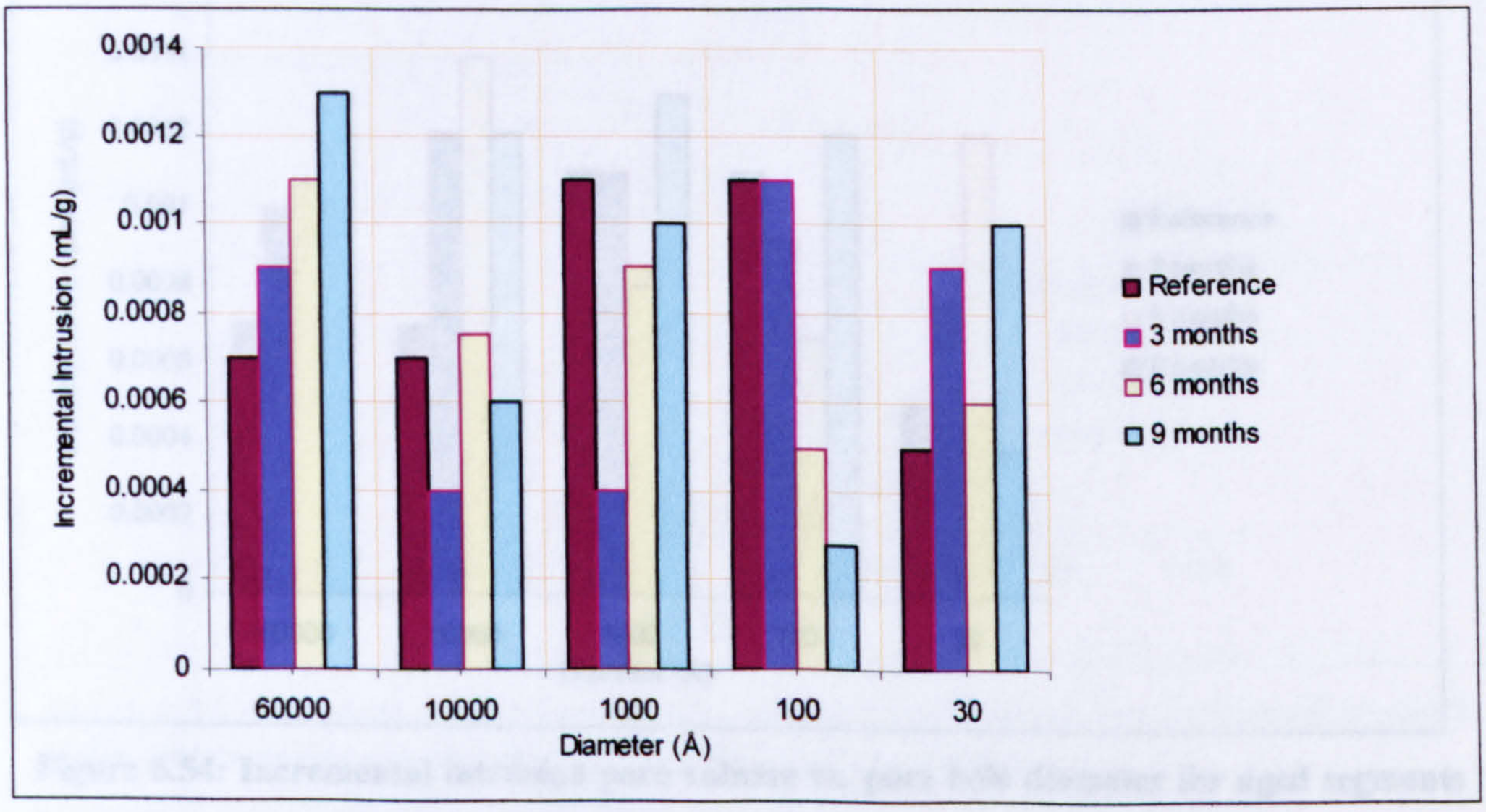

Figure 6.52: Incremental intrusion pore volume vs. pore hole diameter for aged segments in *brine* solution at 60°C for different periods of time

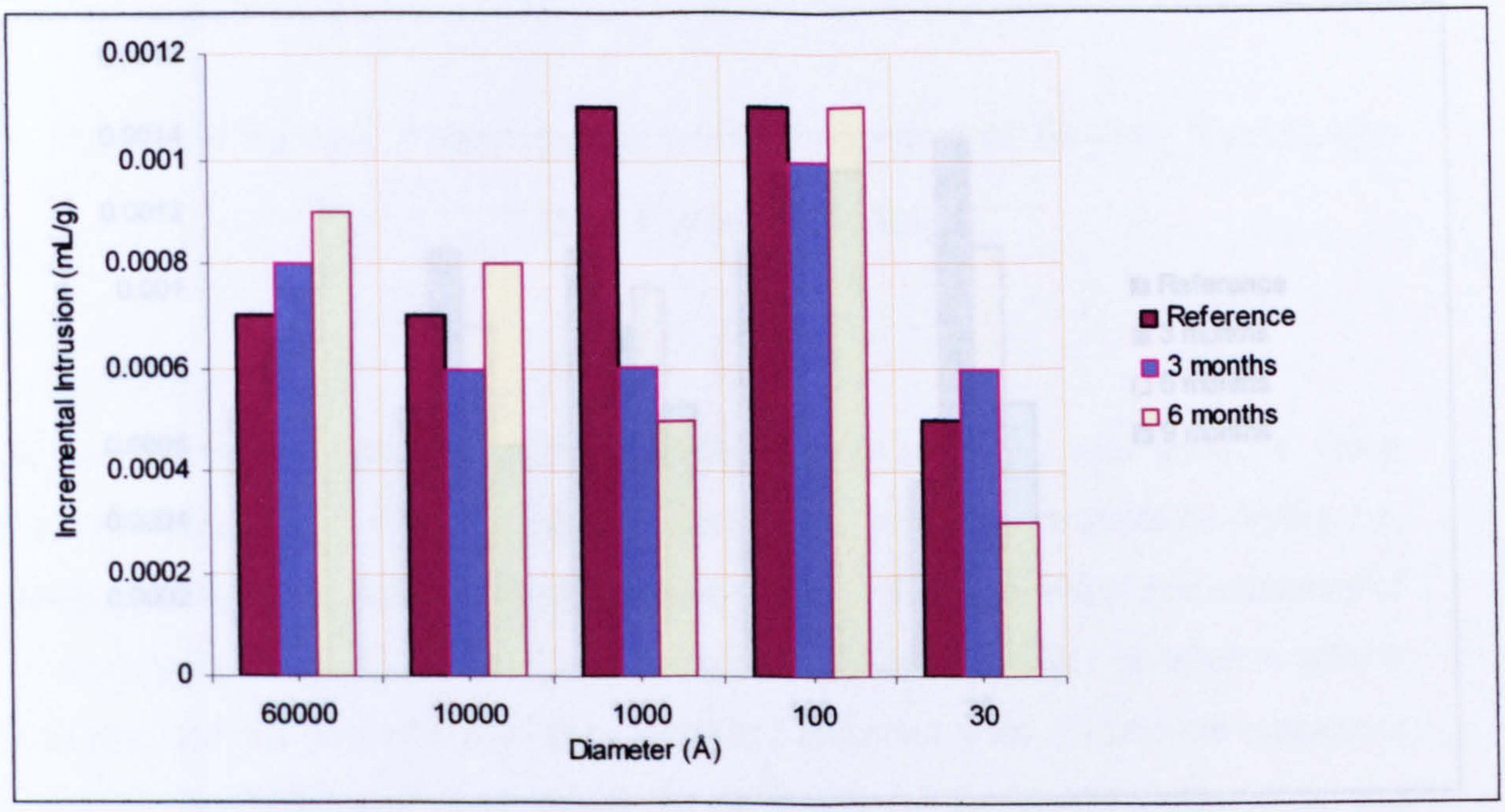

Figure 6.53: Incremental intrusion pore volume vs. pore hole diameter for aged segments in *brine* solution at 20°C for different periods of time

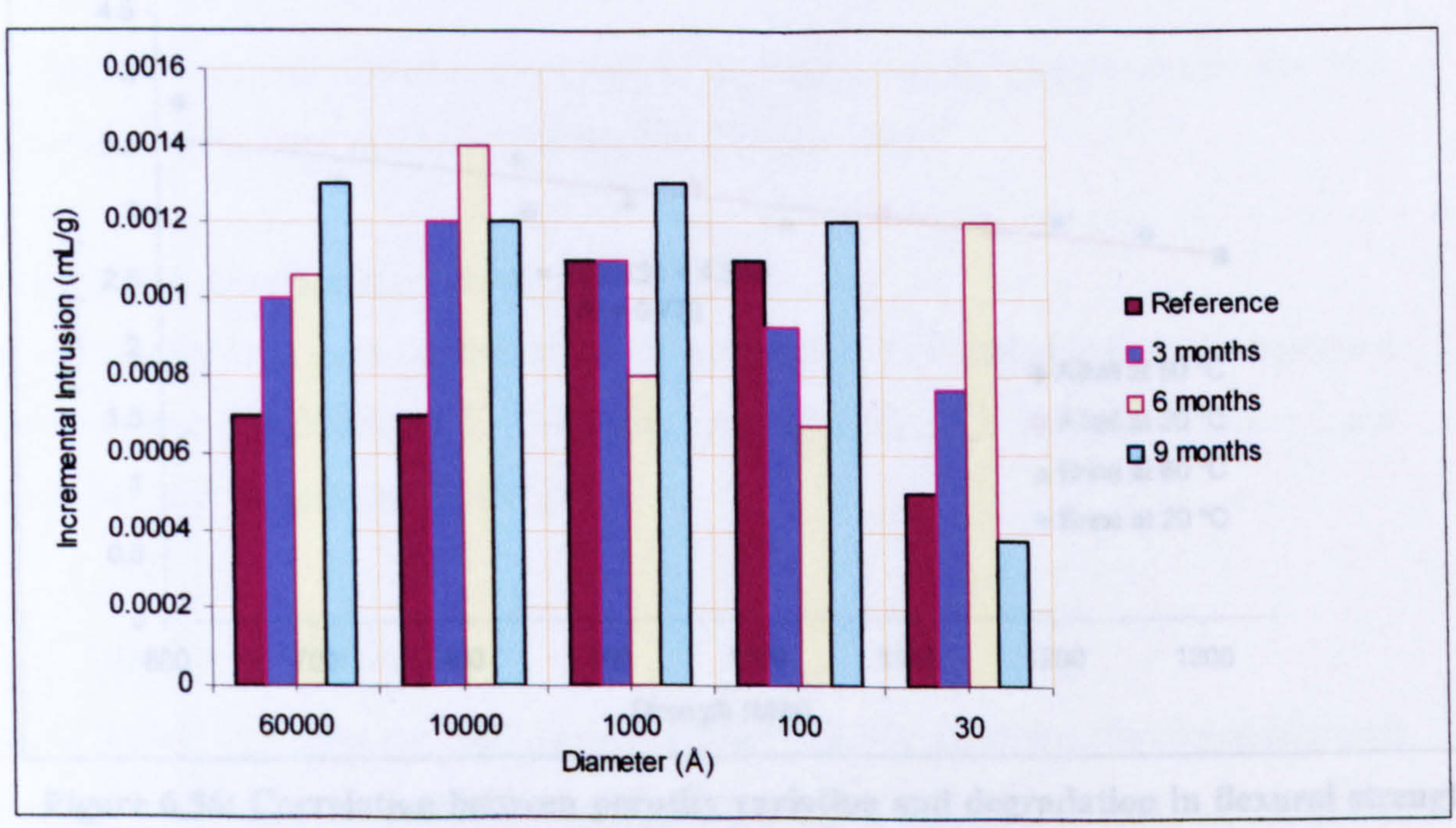

Figure 6.54: Incremental intrusion pore volume vs. pore hole diameter for aged segments in *alkali* solution at 60°C for different periods of time

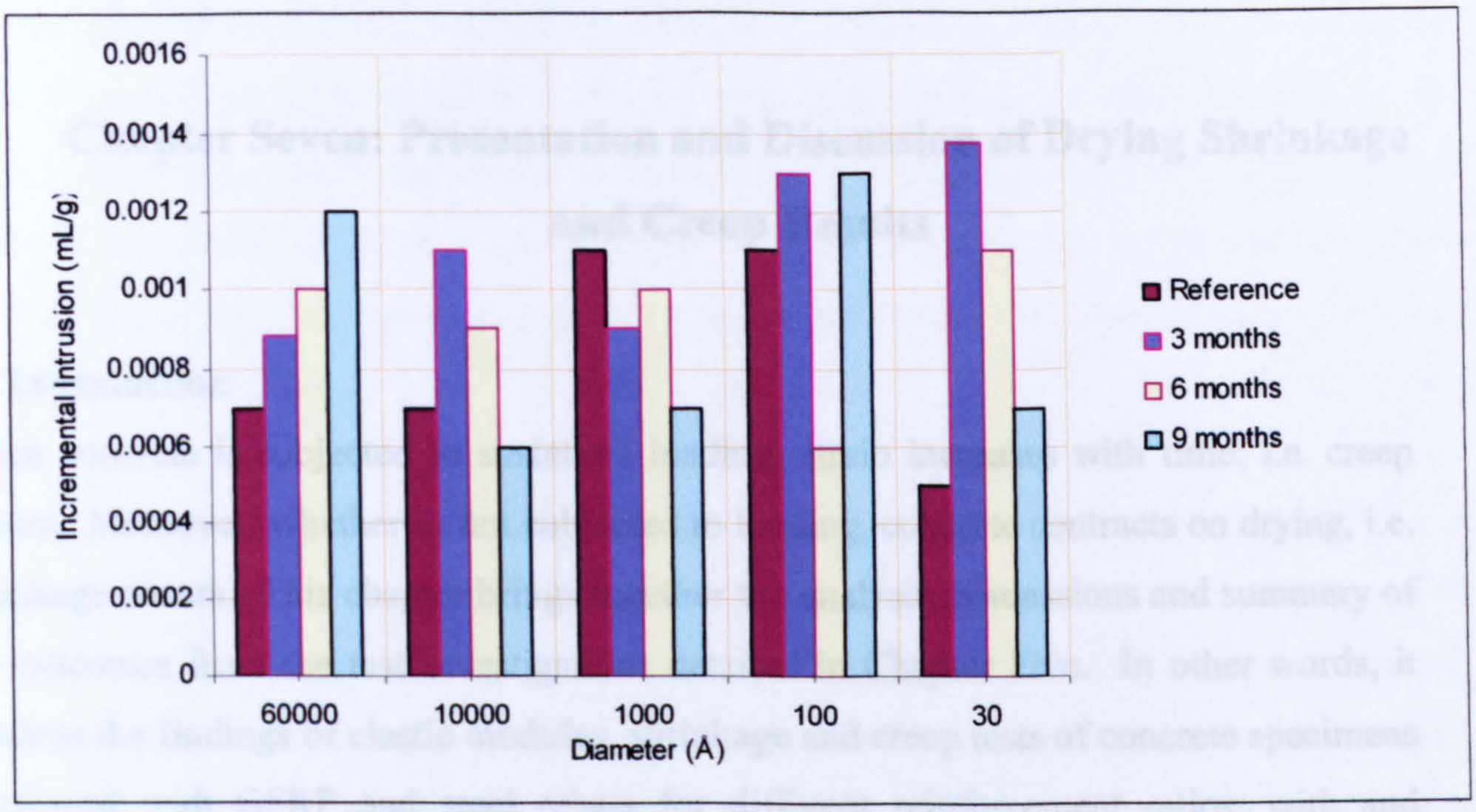

Figure 6.55: Incremental intrusion pore volume vs. pore hole diameter for aged segments in *alkali* solution at 20°C for different periods of time

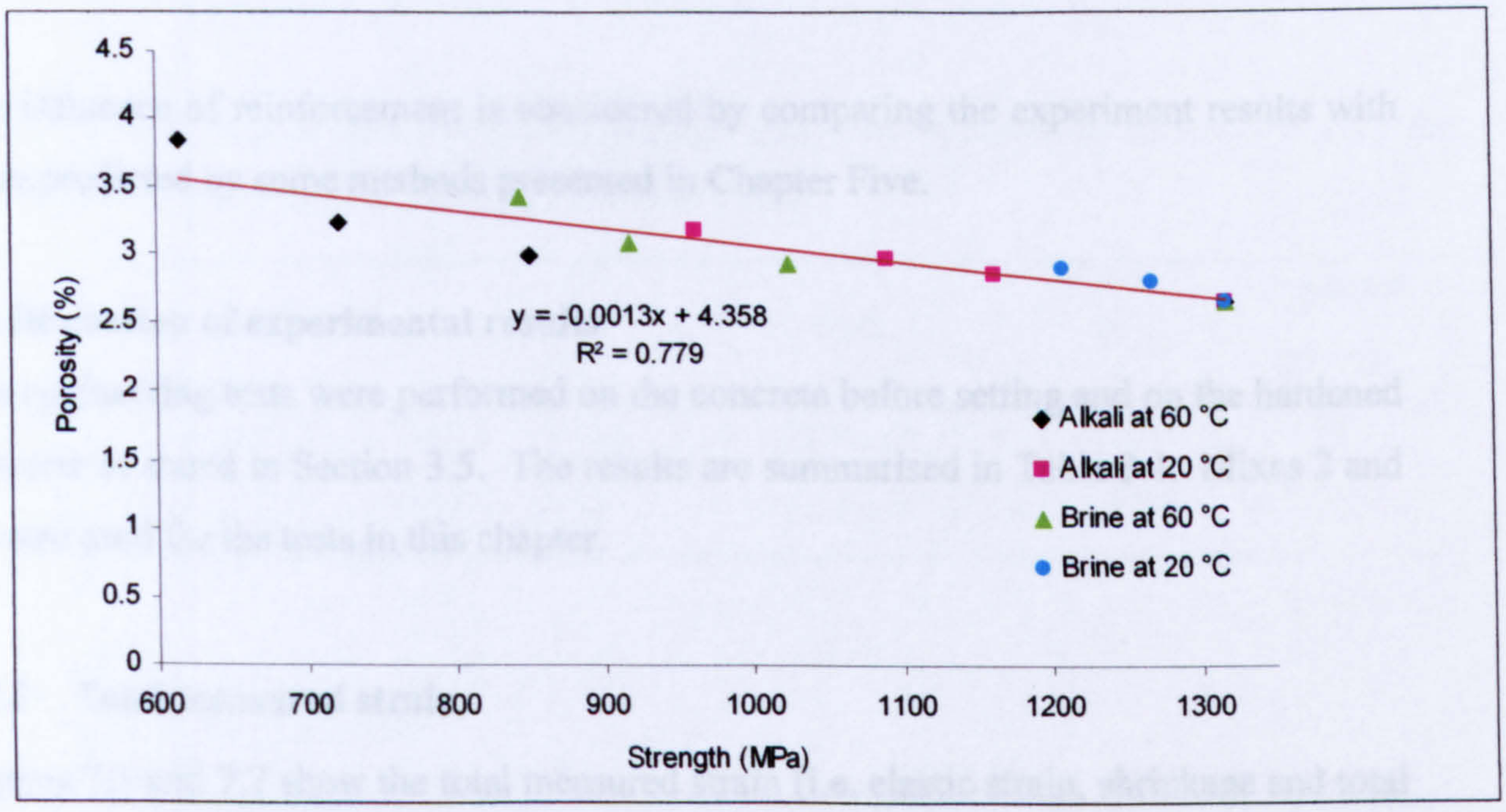

Figure 6.56: Correlation between porosity variation and degradation in flexural strength of GFRP specimens due to aging in different hostile conditions

Chapter Seven: Presentation and Discussion of Drying Shrinkage and Creep Results

7.1 Introduction

When concrete is subjected to sustained loading, strain increases with time, i.e. creep occurs. Moreover, whether or not subjected to loading, concrete contracts on drying, i.e. shrinkage occurs. This chapter brings together the analysis, discussions and summary of the outcomes from the test investigations detailed in Chapter Five. In other words, it presents the findings of elastic modulus, shrinkage and creep tests of concrete specimens reinforced with GFRP and steel rebars for different reinforcement ratios, with and without shrinkage reducing admixture (SRA), namely Eclipse®. All test results are compared to control concrete specimens, namely, non-reinforced ones that have similar mix design, curing environment, and drying and/or loading conditions.

The influence of reinforcement is considered by comparing the experiment results with those predicted by some methods presented in Chapter Five.

7.2 Discussion of experimental results

The engineering tests were performed on the concrete before setting and on the hardened concrete as stated in Section 3.5. The results are summarised in Table 3.4. Mixes 2 and 3, were used for the tests in this chapter.

7.2.1 Total measured strain

Figures 7.1 and 7.2 show the total measured strain (i.e. elastic strain, shrinkage and total creep) for the non-reinforced and reinforced specimens with GFRP and steel rebars at different reinforcement ratios for three months (94 days). The results also illustrate that, as volume of reinforcement to volume of concrete ratio increased, restraint of the concrete movement increased too (total strain decreased). Furthermore, the influence of steel reinforcement on the concrete's total strain reduction was higher than that of GFRP rebars. This was due to higher modulus of elasticity of steel compared to that of GFRP.

The effect of the shrinkage reducing admixture (SRA) on total strain was also examined. The amount of SRA added was 2% by weight of cement, (as recommended by the manufacturer). The tests were under the same conditions as those without SRA. Figures 7.3 and 7.4 show the total strain of non-reinforced and reinforced specimens with GFRP and steel rebars at different reinforcement ratios for three months of loading and drying (94 days).

Figures 7.5 and 7.6 present the total strain for all specimens (with and without SRA) at ninety four days. Total strain relationships for concrete specimens reinforced with GFRP and steel with different reinforcement ratios were established from these figures. These were then extrapolated to predict total strain of non-reinforced concrete and compared with the actual total strain of control concrete specimen. The latter is also shown in these figures. In addition, the slopes of these relationships are displayed too. The higher the modulus of elasticity of reinforcement, the higher the slopes of these relations. Table 7.1 presents these relationships.

Table 7.1: Total strain (10^{-6}) relationships and their correlation coefficients (R^2) for reinforced concrete specimens at 94 days of loading

SRA	GFRP	R^2	Steel	R^2	Measured (plain)
0	$\varepsilon = -9782.2\,\rho + 3169.7$	0.955	$\varepsilon = -21154\,\rho + 3034$	0.991	3201
2%	$\varepsilon = -4619.4\,\rho + 1884.7$	0.991	$\varepsilon = -8451.7\,\rho + 1615.6$	0.999	2070

Where

ε = total strain at loading.

ρ = reinforcement ratio.

The constants in these equations in the above table are the expected total strain readings of the control (non-reinforced) specimen, which can be compared with the actual (measured) total strain of the control specimen. In general, there is a close agreement between the measured and extrapolated values with a maximum error of 9% for concrete

specimens reinforced with GFRP rebars and 22% for concrete specimens reinforced with steel.

The SRA reduced the total time-dependent strain of non-reinforced concrete by 35% after three months of loading. Furthermore, the total strain of specimens reinforced with 4, 6 and 8 GFRP rebars (0.045, 0.068 and 0.091 of reinforcement/concrete ratio) was reduced by 39%, 36.3% and 36.2%, respectively. For specimens reinforced with 4, 6 and 8 steel rebars (0.036, 0.054 and 0.071 of reinforcement/concrete ratio) the reduction in total strain was 41.8%, 40% and 32.6%, respectively. From these scattered results, it seems that SRA has a similar influence of the reduction of total strain for all specimens.

7.2.2 Modulus of elasticity and effective modulus

Modulus of elasticity is the property which controls the load distribution of a combined system composed of two materials. In addition, it determines the stiffness of the material. In this part of the investigation, modulus of elasticity was measured by dividing the applied compressive stress (σ, MPa), which was 25% of concrete compressive strength, by the elastic strain (e_o), as shown in the following equation:

$$E(t_0) = \sigma / e_o \qquad (7.1)$$

Where

$E(t_0)$ = modulus of elasticity at the time of loading (28 days), (GPa).

Table 7.2 and both Figs. 7.7 and 7.8 summarise the results of elastic moduli for reinforced and non-reinforced (control) specimens.

Table 7.2: Elastic moduli (GPa) at loading of various concrete specimens

SRA	Control (№ of bars)	GFRP (№ of bars)			Steel (№ of bars)		
	(0)	(4)	(6)	(8)	(4)	(6)	(8)
0%	31.9	34.2	35.6	36.5	36.3	39.3	43.7
2%	27.4	28.5	29.5	30.8	34.8	37.8	42.4

It can be seen that there is a reduction in the elastic modulus of all the specimens when SRA was added. In fact, this was expected since it is mentioned in the data sheet of Eclipse® that its addition may cause a reduction in concrete compressive strength by a maximum of 15%. It is known that the modulus of elasticity increases or decreases with an increase or decrease in the compressive strength of concrete, respectively. According to the results of the 28-day compressive strength tests carried out on the concrete specimens with and without SRA, the compressive strength reduction was about 21.5%.

From Table 7.2 it can be seen that the modulus of elasticity of non-reinforced concrete and concrete specimens reinforced with GFRP rebars were affected most by the addition of the SRA, i.e. stiffness retention was around 84%. While other specimens reinforced with steel rebars had stiffness retention of about 95%. This could be due to the relatively high stiffness of steel rebars (200GPa) that would have compensated for the stiffness reduction of concrete. The modulus of elasticity of GFRP rebars in compression is about 48GPa.

Table 7.2 also highlights the effect of reinforcement ratio on the elastic moduli of the concrete specimens. For concrete specimens reinforced with GFRP rebars having reinforcement ratios of 0.045, 0.068 and 0.091, the elastic modulus rose by 7%, 11.5% and 14%, respectively. While, for concrete specimens reinforced with steel rebars having reinforcement ratios of 0.036, 0.054 and 0.071, the elastic modulus rose by 14%, 23% and 37%, respectively. Moreover, for concrete specimens contain SRA and reinforced with GFRP rebars having reinforcement ratios of 0.045, 0.068 and 0.091, the elastic modulus rose by 4%, 8% and 12%, respectively. While, for concrete specimens reinforced with steel rebars having reinforcement ratios of 0.036, 0.054 and 0.071, the elastic modulus rose by 27%, 38% and 55%, respectively.

Figures 7.9 and 7.10 illustrate relationships for the measured effective moduli of all specimens at 94 days of loading. These relations are obtained from the measurement of drying shrinkage deducted from the total strains of specimens and summarised bellow:

Table 7.3: Effective moduli (GPa) relationships and their correlation coefficients (R^2) for concrete specimens reinforced with GFRP and steel and control concrete specimen

SRA	GFRP	R^2	Steel	R^2	Measured (plain)
0	$\varepsilon = 50.1\,\rho + 9.5$	0.957	$\varepsilon = 191.2\,\rho + 7.0$	0.954	10.1
2%	$\varepsilon = 47.4\,\rho + 13.0$	0.992	$\varepsilon = 146.6\,\rho + 13.9$	0.997	12.3

The constants in these equations are the expected measured effective modulus of the control specimens extrapolated from these relations. By and large, the measured and extrapolated numbers are relatively close with a maximum error of 30% for steel and 6% for GFRP.

Comparing the results in Table 7.3, it is clear that SRA increased the effective modulus of the control specimens. This was due to the reduction in creep as will be seen in the following sections.

7.2.3 Drying shrinkage

Figures 7.11 and 7.12 compare drying shrinkage of non-reinforced and reinforced specimens with both GFRP and steel rebars, for three months (94 days). The figures show that drying shrinkage reduces with an increase in the amount of reinforcement. The reduction in drying shrinkage was greater when steel rebars were used due to the higher modulus of elasticity of steel compared with GFRP.

The lower stiffness of the GFRP reinforcement may be beneficial in terms of reducing internal tensile stresses in concrete and hence cracking, which develops due to the restraint of shrinkage by reinforcement. This was taken into account by Chen and Choi (2002) in their analytical model.

Figures 7.13 and 7.14 demonstrate the difference between shrinkage of non-reinforced and reinforced specimens with GFRP and steel rebars in concrete containing SRA, after three months of drying. SRA reduces the surface tension of pore water. With a reduced surface tension, the force pulling in on the walls of the pores is reduced, and the

resultant shrinkage strain is reduced. As before, the influence of steel reinforcement on the shrinkage reduction (shrinkage restraint) was higher than that of GFRP rebars due to the higher modulus of elasticity of steel compared with GFRP. Thus, less shrinkage cracking could be expected in specimens reinforced with GFRP rebars. It can be seen that shrinkage only started to take place for most specimens including the plain specimen after two days of drying and after 9 days for the specimen reinforced with 6 steel rebars and finally after 11 days for the specimen reinforced with 8 steel rebars. This is due to the addition of SRA which reduces the surface tension of pore water and hence could make more pore water in concrete behave like free water (i.e., its loss does not affect shrinkage). The first 40 days of drying for all specimens showed a rather abnormal shrinkage behaviour. Subsequently, all specimens yielded a similar rate of shrinkage.

Figures 7.15 and 7.16 illustrate drying shrinkage of all specimens after ninety four days. Drying shrinkage relationships for concrete specimens reinforced with GFRP and steel with different reinforcement ratios were established from these figures and extrapolated to predict drying shrinkage of non-reinforced concrete. Table 7.4 gives these relationships. The higher the modulus of elasticity of reinforcement, the higher the slopes of these relations.

Table 7.4: Drying shrinkage (10^{-6}) relationships and their correlation coefficients (R^2) for concrete specimens reinforced with GFRP and steel and control concrete specimen

SRA	GFRP	R^2	Steel	R^2	Measured (plain)
0	$\varepsilon = -1241\,\rho + 440.6$	0.998	$\varepsilon = -2783\,\rho + 367.7$	0.998	475
2%	$\varepsilon = -712\,\rho + 288.2$	0.993	$\varepsilon = -1707\,\rho + 251.2$	0.998	315

When the constants in these equations are compared with the actual (measured) shrinkage of the control specimens, generally, there is close agreement with maximum errors of 9% for concrete specimens reinforced with GFRP rebars and 23% for concrete specimens reinforced with steel rebars.

Comparing the drying shrinkage behaviour of specimens with and without SRA (i.e. Figs. 7.11 and 7.12, with Figs. 7.13 and 7.14) illustrates the effect of this admixture in reducing the rate of shrinkage of concrete significantly, although, for specimens containing SRA, it took a longer time for the shrinkage to level out. In other words, specimens with no SRA needed about 40 days (in the drying conditions of this investigation) for the shrinkage to be reduced significantly, while specimens with SRA needed more than three months for shrinkage to level out.

For non-reinforced specimens with SRA, the rate of shrinkage was about 7.7με/day for the first 20 days then 2.17 με/day until the end of the three months. That would, hopefully, give time for creep to relieve some tensile stresses in reinforced concrete due to shrinkage restraint, and therefore diminish shrinkage cracking. For specimens without SRA the rate of shrinkage was around 14.3με/day for the first 19 days, 4.6με/day for the next twenty days and 1.1 με/day up to the end of the three months period.

With regard to reinforced specimens, the rate of drying shrinkage is tabulated for specimens with and without SRA in Tables 7.5 and 7.6, respectively. It is important to stress that these rates are only an approximate guide to show the influence of SRA, and different reinforcement types and ratios.

Table 7.5: Rate of drying shrinkage (με/day) for reinforced concrete containing SRA

Days	GFRP (№ of bars)			Steel (№ of bars)		
	(4)	(6)	(8)	(4)	(6)	(8)
1 to 30	4.35	3.64	3.53	3.33	3.02	2.36
30 to 94	2.03	2.0.5	2.09	1.48	1.4	1.22

A summary of drying shrinkage after three months for all specimens is displayed in the following table:

Table 7.6: Rate of drying shrinkage (με/day) for reinforced concrete specimens without SRA

Days	GFRP (№ of bars)			Steel (№ of bars)		
	(4)	(6)	(8)	(4)	(6)	(8)
1 to 19	10.22	10	9.73	7.7	6.74	5.84
19 to 40	4.04	3.9	3.52	2.97	2.41	2.05
40 to 94	1.08	0.84	0.72	0.56	0.36	0.27

Table 7.7: Drying shrinkage (10^{-6}) of reinforced and non-reinforced specimens after thee months

SRA	Control (№ of bars)	GFRP (№ of bars)			Steel (№ of bars)		
	(0)	(4)	(6)	(8)	(4)	(6)	(8)
0%	475	383	357	327	269	216	170
2%	315	255	241	223	190	160	129

After three months, the drying shrinkage was reduced by 34% due to SRA for the non-reinforced concrete specimens. For concrete specimens reinforced with GFRP rebars, the average shrinkage reduction was 32%. While, for concrete specimens reinforced with steel rebars, the average shrinkage reduction was 26%. These values are in agreement with the manufacturer's data sheet for SRA, namely, the range of shrinkage reduction at a dosage of 2% by weight of cement is in the order of 25 to 50%.

Upon reviewing the percentage reductions of shrinkage for the SRA specimens, it was noticeable that as reinforcement stiffness increased the shrinkage reduction decreased slightly.

Table 7.7 also highlights the effect of reinforcement ratio on the drying shrinkage of the concrete specimens. For concrete specimens reinforced with GFRP rebars having reinforcement ratios of 0.045, 0.068 and 0.091, the drying shrinkage fell by 19%, 21% and 31%, respectively. While, for concrete specimens reinforced with steel rebars having reinforcement ratios of 0.036, 0.054 and 0.071, the drying shrinkage declined by 43%, 54% and 64%, respectively. Moreover, for concrete specimens containing SRA

and reinforced with GFRP rebars having reinforcement ratios of 0.045, 0.068 and 0.091, the drying shrinkage went down by 19%, 23% and 29%, respectively. While, for concrete specimens reinforced with steel rebars having reinforcement ratios of 0.036, 0.054 and 0.071, the drying shrinkage decreased by 40%, 50% and 60%, respectively. From these results, it can be seen that the shrinkage restraint by the same reinforcement type and ratio is almost not affected by the addition of SRA.

7.2.4 Creep

Figures 7.17 and 7.18 illustrate the development of total (basic plus drying) creep upon loading and drying of concrete specimens reinforced with GFRP and steel rebars, respectively, over a period of three months. The total creep was not measured directly, instead it was calculated as follows:

$$C = \varepsilon_{tot} - e_o - \varepsilon_{sh} \qquad (7.2)$$

Where

C = total creep (10^{-6}).

ε_{tot} = total measured strain (10^{-6}).

e_o = elastic strain (10^{-6}).

ε_{sh} = drying shrinkage (10^{-6}).

In general, the influences of reinforcement ratio and stiffness were clear in creep results, and similar to what happened in the case of the drying shrinkage. It is noted from Figs. 7.17 and 7.18 that the bond between concrete and reinforcement was enough to transfer some stresses developed in concrete, due to loading and drying, to the reinforcement. This was because reinforced specimens exhibited less creep and shrinkage than the non-reinforced ones.

Figures 7.19 and 7.20 show the corresponding creep coefficient of concrete specimens reinforced with GFRP and steel rebars, while, Figs. 7.21-7.24 reflect the effect of SRA on all specimens. Creep coefficient is defined as the ratio of creep to the initial elastic deformation. Creep coefficient results were used in this investigation to calculate the reduced moduli as shown in Equations (5.2) and (5.4), Section 5.4.2.

Table 7.8: Total creep (10^{-6}) of reinforced and non-reinforced specimens after three months

SRA	Control (№ of bars)	GFRP (№ of bars)			Steel (№ of bars)		
	(0)	(4)	(6)	(8)	(4)	(6)	(8)
0%	1861	1564	1314	1225	1228	1022	702
2%	965	667	586	546	504	429	373

After three months, the total creep of the SRA control mix was reduced by 48%. For concrete specimens reinforced with GFRP and steel rebars, the average total creep reduction was almost the same (i.e. 55%). It can be said, therefore, that the effect of SRA was similar in both reinforced and non-reinforced specimens.

Table 7.8 highlights the effect of reinforcement ratio on the total creep of the concrete specimens. For concrete reinforced with GFRP rebars having reinforcement ratios of 0.045, 0.068 and 0.091, the total creep decreased by 16%, 29% and 34%, respectively. While, for concrete specimens reinforced with steel rebars having reinforcement ratios of 0.036, 0.054 and 0.071, the total creep declined by 34%, 45% and 62%, respectively. Moreover, for concrete specimens containing SRA and reinforced with GFRP rebars having reinforcement ratios of 0.045, 0.068 and 0.091, the total creep decreased by 30%, 39% and 43%, respectively. While, for concrete specimens reinforced with steel rebars having reinforcement ratios of 0.036, 0.054 and 0.071, the total creep went down by 47.7%, 55.5% and 61%, respectively. SRA increased the influence of reinforcement ratio on restraining the creep in concrete, especially with the lower reinforcement ratio. Both SRA and reinforcement act to reduce creep strain although by different mechanisms. Steel rebars reduced creep more than GFRP ones, because the modular ratio of concrete reinforced with steel in this investigation, namely 5.6, was higher than that of concrete reinforced with GFRP, namely 1.3 (Brown 1997).

7.3 Prediction of elasticity, shrinkage and creep

Creep and shrinkage can be determined experimentally by conducting tests on in the particular test used. However, in absence of test data, the designer must refer to one of the existing methods for predicting creep and shrinkage. The remaining part of this chapter deals with the comparison of predicted and measured values of shrinkage, creep

and elasticity. The approach used is to consider, firstly, the influence of reinforcement is considered using the composite model developed in Chapter five. Secondly, the movements of non-reinforced (plain) concrete as estimated by some Codes of Practice, namely, British Standards (BS 5400-4 (1990), and BS 8110-2 (2001)), CEB-FIP (1990), ACI 209R-92 and the estimate by Gardner and Zhao (1993). Finally, the influence of reinforcement is considered using existing Code-type methods.

7.3.1 Applications of the proposed composite model

When the measured values of $E(t_0)$ for non-reinforced concrete are used in Equation (5.20) the results are shown in Table 7.9.

Table 7.9: Comparison between measured and predicted elastic moduli by the proposed composite model based on measured elastic modulus of plain concrete

Reinforcement Type	Without SRA			With SRA		
	Measured	Predicted		Measured	Predicted	
4-GFRP	34.2	32.6	(-5%)	28.5	28.3	(-0.7%)
6-GFRP	35.6	33.0	(-7%)	29.5	28.8	(-3%)
8-GFRP	36.5	33.3	(-9%)	30.8	29.2	(-5%)
4-Steel	36.3	37.9	(4%)	34.8	33.5	(-4%)
6-Steel	39.3	40.9	(4%)	37.8	36.6	(-3%)
8-Steel	43.7	43.9	(0.3%)	42.4	39.7	(-6%)

The accuracy (shown in parentheses) had a maximum error of 9%, with most of the predicted results being underestimated.

When measured values of the modulus of elasticity of non-reinforced concrete ($E(t_0)$) are used, the predictions of the effective modulus and the age-adjusted effective modulus are shown in Tables 7.10 and 7.11.

Table 7.10: Comparison of three-month measured and predicted reduced moduli (GPa) by composite model using measured elastic modulus of plain concrete for specimens reinforced with *GFRP*

SRA	Measured GFRP (№ of bars)			Predicted by EM GFRP (№ of bars)			Predicted by AAEM GFRP (№ of bars)		
	(4)	(6)	(8)	(4)	(6)	(8)	(4)	(6)	(8)
0%	11.6	13.2	13.9	11.8(2%)	12.7(-4%)	13.6(-2%)	13.2(14%)	14.0(6%)	14.8(6%)
2%	15.2	16.4	17.3	13.9(-8%)	14.7(-10%)	16.0(-7%)	15.2(0%)	15.6(-5%)	16.8(-2%)

Table 7.11: Comparison of three-month measured and predicted reduced moduli (GPa) by composite model using measured elastic modulus of plain concrete for specimens reinforced with *steel*

SRA	Measured steel (№ of bars)			Predicted by EM steel (№ of bars)			Predicted by AAEM steel (№ of bars)		
	(4)	(6)	(8)	(4)	(6)	(8)	(4)	(6)	(8)
0%	13.9	16.0	20.7	16.9(21%)	20.3(27%)	23.7(14%)	18.3(32%)	21.6(35%)	25.0(21%)
2%	19.2	21.6	24.5	19.0(-1%)	22.4(4%)	25.7(5%)	20.3(6%)	23.7(10%)	27.0(10%)

From the above tables, the composite model generally underestimates the measured reduced modulus for specimens reinforced with GFRP and overestimates the specimens reinforced with steel.

The proposed composite model was also used to predict the restrained shrinkage, namely, Equation (5.27). When both drying shrinkage (S_c) and elastic modulus (E_c) are provided from the measurements of the non-reinforced specimens, the results are shown in Tables 7.12 and 7.13.

Table 7.12: Comparison of three-month measured and predicted drying shrinkage for specimens reinforced with *GFRP* using measured shrinkage and elastic modulus of plain concrete

SRA	Measured GFRP (№ of bars)			Predicted by composite model GFRP (№ of bars)		
	(4)	(6)	(8)	(4)	(6)	(8)
0%	383	357	327	443(16%)	428(20%)	413(26%)
2%	255	241	223	291(14%)	279(16%)	268(20%)

Table 7.13: Comparison of three-month measured and predicted drying shrinkage for specimens reinforced with *steel* using measured shrinkage and elastic modulus of plain concrete

SRA	Measured steel (№ of bars)			Predicted by composite model Steel (№ of bars)		
	(4)	(6)	(8)	(4)	(6)	(8)
0%	269	216	170	386(43%)	351(63%)	321(89%)
2%	190	160	129	248(30%)	223(39%)	201(56%)

From the above tables, it is clear that the composite model overestimates the drying shrinkage of reinforced concrete most of the time. The accuracy of the results (shown in parentheses) for the cases where drying shrinkage and elastic modulus of non-reinforced concrete were estimated was higher than when they were measured in most cases. In the investigation, the reinforcement ratios were considered to make the effect of reinforcement properties more obvious. However, in practice the level of reinforcement

in the specimens reinforced with 6 and 8 rebars is greater than that recommended in the Codes.

A comparison between experimental results of concrete specimens reinforced with GFRP and steel and predictions of drying shrinkage by the composite model (Equation (5.27)), using the effective modulus (Equation (5.2)) is shown in Tables 7.14 and 7.15; and using the age-adjusted effective modulus (Equation (5.4)) is shown in Tables 7.16 and 7.17.

Table 7.14: Comparison of three-month measured and predicted drying shrinkage of specimens reinforced with *GFRP* using effective modulus EM

SRA	Measured GFRP (№ of bars)			Predicted by composite model GFRP (№ of bars)		
	(4)	(6)	(8)	(4)	(6)	(8)
0%	383	357	327	387(1%)	352(-1%)	322(-1.5%)
2%	255	241	223	266(4%)	245(1.6%)	227(1.7%)

Table 7.15: Comparison of three-month measured and predicted drying shrinkage of specimens reinforced with *steel* using effective modulus EM

SRA	Measured steel (№ of bars)			Predicted by composite model Steel (№ of bars)		
	(4)	(6)	(8)	(4)	(6)	(8)
0%	269	216	170	274(1.8%)	224(3.7%)	188(10%)
2%	190	160	129	197(3.7%)	164(2.5%)	140(8.5%)

There is hardly any difference between the measured and predicted values. The high accuracy of this method was due to the replacement of static modulus of elasticity by the effective modulus in the composite model equation (i.e. Equation (5.27)), which considers the time effect of creep.

Table 7.16: Comparison of three-month measured and predicted drying shrinkage of specimens reinforced with *GFRP* using age-adjusted effective modulus AAEM

SRA	Measured GFRP (№ of bars)			Predicted by composite model GFRP (№ of bars)		
	(4)	(6)	(8)	(4)	(6)	(8)
0%	383	357	327	396(3%)	363(1.6%)	335(2%)
2%	255	241	223	270(6%)	251(4%)	233(4%)

Table 7.17: Comparison of three-month measured and predicted drying shrinkage of specimens reinforced with *steel* using age-adjusted effective modulus AAEM

SRA	Measured Steel (№ of bars)			Predicted by composite model Steel (№ of bars)		
	(4)	(6)	(8)	(4)	(6)	(8)
0%	269	216	170	289(7%)	240(11%)	203(19%)
2%	190	160	129	204(7%)	172(7.5%)	148(15%)

Using the EM yielded more accurate results, although both the EM and AAEM produced highly accurate estimates of shrinkage.

For the whole period of testing, Figs. 7.25-7.28 compare experimental results of concrete specimens reinforced with GFRP and steel with predicted drying shrinkage by the composite model using the reduced modulus of non-reinforced concrete specimens. As can be seen in the figures, the prediction was more accurate on longer term as opposed to early period of drying. Because the proposed composite model for shrinkage prediction uses the measured drying shrinkage of non-reinforced specimens as one of the input data to predict the drying shrinkage of reinforced specimens. Moreover, the rate of shrinkage of both types of specimens (i.e. reinforced and non-reinforced specimens) was similar only in long term shrinkage. Therefore, the proposed composite model is expected to yield better results in long term shrinkage. Likewise for specimens made with SRA, the prediction of early age was relatively not very accurate but latter on towards 80 days of drying the accuracy of prediction improved.

In Table 7.18, the tensile stresses in reinforced concrete after three months due to shrinkage restraint by GFRP and steel rebars in accordance with the proposed composite model (Equation (5.15)). The shrinkage values used in this equation are measured from non-reinforced and reinforced concrete specimens. In addition, the reduced modulus of non-reinforced concrete was used.

Table 7.18: Tensile stress in reinforced concrete (MPa) after three months due to shrinkage restraint by reinforcement in accordance with the composite model

SRA	GFRP (№ of bars)			Steel (№ of bars)		
	(4)	(6)	(8)	(4)	(6)	(8)
0%	0.9	1.2	1.5	2.1	2.6	3.1
2%	0.7	0.9	1.1	1.5	1.9	2.3

7.3.2 Modulus of elasticity

All the Codes of Practice use the strength of concrete to estimate the modulus of elasticity. Predictions are compared with measured values of the two plain mixes in Table 7.19.

Table 7.19: Comparison between measured and predicted elastic moduli

SRA	Measured (GPa)	ACI 209 (GPa)	CEB-FIP (GPa)	BS8110 (GPa)	Gardner & Zhao (1993) (GPa)
0	32.8	37.0(13%)	39.5(20%)	32.4(-1%)	37.4(14%)
2%	27.3	32.8(20%)	36.4(33%)	29.7(9%)	33.5(23%)

From the above table, it is apparent that the prediction methods overestimate the measured modulus of elasticity except in BS8110 when there was no SRA. The accuracy of the methods, however, (shown in parentheses) was reasonable, with the BS8110 being the most accurate especially with the mix without SRA.

For the reinforced concrete specimens, estimate of elastic modulus was made by the composite model expressed by Equation (5.20). Predictions are compared with the

measured values in Table 7.20. The elastic modulus for non-reinforced concrete was estimated by BS8110. The British Standards method was used because it revealed more accuracy than the other methods presented in Table 7.19.

Table 7.20: Comparison between measured and predicted elastic moduli by the proposed composite model based on estimate elastic modulus of plain concrete

Reinforcement Type	Without SRA			With SRA		
	Measured	Predicted		Measured	Predicted	
4-GFRP	34.2	33.1	(-3%)	28.5	33.1	(16%)
6-GFRP	35.6	33.5	(-6%)	29.5	33.5	(13%)
8-GFRP	36.5	33.8	(-7%)	30.8	33.8	(10%)
4-Steel	36.3	35.8	(-1%)	34.8	35.8	(3%)
6-Steel	39.3	38.8	(-1%)	37.8	38.8	(3%)
8-Steel	43.7	41.9	(-4%)	42.4	41.9	(-1%)

The accuracy of the proposed composite model for modulus of elasticity, (shown in parentheses) was high with a maximum error of 16%. All of the predicted results for the concrete mix without SRA were underestimated. For the other mix, however, most of the results were overestimated.

7.3.3 Creep and effective modulus

Estimates of the 94-day creep of non-reinforced concrete are given in Table 7.21 in terms of creep coefficient. Shown in Table 7.22 are the reduced modulus values, which allow for creep, as calculated using Equations (5.2) and (5.4), i.e. the effective modulus (EM) and age adjusted effective modulus (AAEM). Those can be compared with the measured reduced moduli.

Table 7.21: Comparison between measured and predicted creep coefficient (ϕ) of non-reinforced concrete mixes after three months

SRA	Measured	BS 5400	BS 8110	ACI 209	CEB-FIP	Gardner and Zhao (1993)
0	2.15	1.82(-15%)	2.12(-2%)	1.02(-53%)	1.31(-39%)	1.10(-49%)
2%	1.22	(49%)	(74%)	(-17%)	1.48(21%)	1.67(37%)

Table 7.22: Comparison between measured and predicted reduced moduli by EM and AAEM methods of non-reinforced concrete mixes after three months

SRA	Measured		BS 8110		ACI 209		BS 5400		CEB-FIP		Gardner and Zhao(1993)	
	EM	AAEM	EM	AAEM	EM	AAEM	EM	AAEM	EM	AAEM	EM	AAEM
0	10.4	11.9	10.4 (0%)	11.8 (-1%)	18.3 (76%)	20.2 (70%)	11.5 (11%)	13.0 (9%)	17.1 (64%)	19.0 (60%)	17.8 (71%)	19.6 (65%)
2%	12.3	13.6	9.5 (-23%)	10.9 (-20%)	16.2 (32%)	17.9 (32%)	10.5 (-15%)	11.9 (-13%)	14.7 (20%)	16.5 (21%)	12.5 (2%)	14.1 (4%)

composite model to allow for reinforcement. The measured values are the applied stress divided by the drying shrinkage deducted from the total strain.

From Tables 7.24 and 7.25, it can be seen that specimens reinforced with GFRP were predicted fairly accurately with a maximum error of 26%. Similarly for specimens reinforced with steel the prediction error was relatively low, especially with SRA specimens. The maximum error was 44%.

7.3.4 Drying shrinkage

The amount of shrinkage of non-reinforced concrete was estimated by BS 5400-4:1990, BS 8110-2:1985, ACI 209R-92, CEB-FIP 90 and Gardner and Zhao (1993). In British Standards prediction k values for shrinkage are presented as graphs while these factors are given as formulae by Gilbert (1988) and Alexander (2002), respectively. All equations are presented in Section 5.4.1. Estimates of the 94-day drying shrinkage of non-reinforced concrete are given in Table 7.26. The accuracy in Table 7.26 (shown in parentheses) of BS 5400 and Gardner and Zhao (1993) was relatively good for predicting drying shrinkage of plain concrete especially for the SRA mix. BS 8110, CEB-FIP and ACI 209 showed reasonable accuracy for the SRA mix only.

Figure 7.29 illustrates the drying shrinkage of the non-reinforced concrete specimens (control) and specimens containing SRA and compares them with the BS methods. Both BS methods underestimated the drying shrinkage of the control concrete. BS 8110 initially overestimated drying shrinkage of specimen containing SRA and then underestimated it after 12 days of drying. BS 5400 overestimated the specimen with SRA, but in the long term (beyond 90 days of drying) BS 5400 may underestimate shrinkage. In general, both BS 5400 and BS 8110 predict the drying shrinkage of non-reinforced concrete specimens containing SRA reasonably well, and BS 5400 is better for non-reinforced specimens with and without SRA.

Table 7.24: Comparison of three-month measured and predicted reduced moduli (GPa) by composite model using estimated elastic modulus of plain concrete for specimens reinforced with *GFRP*

GFRP (№ of bars)	Measured		Predicted							
			BS 8110				BS 5400			
			EM		AAEM		EM		AAEM	
SRA	0	2%	0	2%	0	2%	0	2%	0	2%
(4)	11.6	15.2	12.1(4%)	11.3(-26%)	13.5(16%)	12.6(-17%)	13.1(13%)	12.2(-20%)	14.6(26%)	13.6(-11%)
(6)	13.2	16.4	13.0(-2%)	12.2(-26%)	14.3(8%)	13.4(-18%)	14.0(6%)	13.1(-20%)	15.4(17%)	14.4(-12%)
(8)	13.9	17.3	13.8(-1%)	13.0(-25%)	15.1(9%)	14.2(-18%)	14.8(6%)	13.9(-20%)	16.2(17%)	15.2(-12%)

Table 7.25: Comparison of three-month measured and predicted reduced moduli (GPa) by composite model using estimated elastic modulus of plain concrete for specimens reinforced with *steel*

Steel (№ of bars)	Measured		Predicted							
			BS 8110				BS 5400			
			EM		AAEM		EM		AAEM	
SRA	0	2%	0	2%	0	2%	0	2%	0	2%
(4)	13.9	19.2	17.2(23%)	16.3(-15%)	18.6(33%)	17.6(-8%)	18.2(31%)	17.3(-10%)	19.7(41%)	18.6(3%)
(6)	16.0	21.6	20.6(29%)	19.7(-9%)	21.9(37%)	21.0(-3%)	21.6(35%)	20.7(-4%)	23.0(44%)	22.0(2%)
(8)	20.7	24.5	24.0(16%)	23.2(-5%)	25.3(22%)	24.4(-0%)	25.0(21%)	24.1(-2%)	26.4(27%)	25.4(4%)

Table 7.26: Comparison between measured and predicted drying shrinkage of non-reinforced concrete mixes after three months

SRA	Measured	BS 5400	BS 8110	ACI 209	CEB FIP	Gardner and Zhao (1993)
0	475	304 (-36%)	237 (-50%)	225 (-53%)	263 (-45%)	300 (-37%)
2%	315	304 (-3%)	237 (-25%)	225 (-28%)	320 (2%)	339 (8%)

For concrete specimens that are symmetrically reinforced, Alexander (2002) and BS 8110 provide prediction formulae for restrained shrinkage, namely, Equations (5.6) and (5.7), respectively. BS 5400 did not provide such formula, but its predicted drying shrinkage for non-reinforced specimen was used in Alexander's formula that predicts drying shrinkage for reinforced specimens.

Figures 7.30-7.32 compare the experimental results of concrete specimens reinforced with GFRP with predictions. By and large, Alexander (2002) and BS 8110 underestimate the drying shrinkage for specimens reinforced with 4, 6 and 8 GFRP rebars. However, Alexander (2002) overestimates the drying shrinkage with SRA throughout the three month drying period. This is understandable, as Alexander (2002) does not account for SRA in his prediction method. BS 8110 initially overestimates shrinkage of concrete with SRA, and then underestimates shrinkage towards the end of the testing period. Generally, both Alexander (2002) and BS 8110 predict the drying shrinkage of concrete specimens reinforced with GFRP rebars and containing SRA reasonably well.

Figures 7.33-7.35 compare the experimental and predicted results of concrete specimens reinforced with 4, 6 and 8 steel rebars. Alexander (2002) predictions are in relatively close agreement especially concrete reinforced by 6 steel rebars. However, his method generally overestimates the drying shrinkage of specimens with SRA. BS 8110 estimates lie between specimens reinforced with steel and those reinforced with steel and containing SRA. Once again, this could be due to that both prediction methods do not consider the presence of admixtures in concrete.

The proposed composite model was used to predict the restrained shrinkage, namely, Equation (5.27). When both drying shrinkage (S_c) and elastic modulus (E_c) are provided from the estimates by BS 5400 and BS 8110, respectively, of the non-reinforced specimens, the results are shown in Tables 7.27 and 7.28.

Table 7.27: Comparison of three-month measured and predicted drying shrinkage for specimens reinforced with *GFRP* using estimated shrinkage and elastic modulus of plain concrete

SRA	Measured GFRP (№ of bars)			Predicted by composite model GFRP (№ of bars)		
	(4)	(6)	(8)	(4)	(6)	(8)
0%	383	357	327	283(-26%)	274(-23%)	264(-19%)
2%	255	241	223	282(11%)	271(12%)	261(17%)

Table 7.28: Comparison of three-month measured and predicted drying shrinkage for specimens reinforced with *steel* using estimated shrinkage and elastic modulus of plain concrete

SRA	Measured Steel (№ of bars)			Predicted by composite model steel (№ of bars)		
	(4)	(6)	(8)	(4)	(6)	(8)
0%	269	216	170	247(-8%)	225(4%)	206(21%)
2%	190	160	129	243(28%)	220(38%)	200(55%)

7.3.5 Tensile stress due to restraint

Figures 7.36 and 7.37 illustrate the development of tensile stress in concrete due to shrinkage restraint, caused by 4GFRP and 4steel rebars in accordance with Alexander (2002) (i.e. Equation (5.9)). Free shrinkage (un-restrained) strain (ε_{cs}) in this equation was either calculated from BS 5400 and BS 8110 (i.e. Equation (5.1)) or measured from non-reinforced specimens with and without SRA. Preference was made to BS 5400 method, because it yielded the nearest results when compared with the shrinkage strain measured from the non-reinforced specimens and substituted in Alexander's formula , namely Equation (5.9). For the BS 5400 method substituted in Equation (5.19), the tensile stresses of the specimens reinforced with GFRP and steel rebars were

underestimated. However, specimens reinforced with GFRP and steel rebars and containing SRA were initially overestimated, but later on towards the end of the investigation period the tensile stress readings coincided with the prediction results. From these figures it appeared that the prediction methods will finally underestimate all the specimens' tensile stress.

As can be seen in Table 7.29, the concrete tensile stress increased as shrinkage restraint increased. Shrinkage of non-reinforced specimens was used in Equation (5.9).

Table 7.29: Tensile stress in reinforced concrete (MPa) after three months due to shrinkage restraint by reinforcement in accordance with Alexander (2002)

SRA	GFRP (№ of bars)			Steel (№ of bars)		
	(4)	(6)	(8)	(4)	(6)	(8)
0%	1.0	1.5	2.0	2.9	4.0	5.1
2%	0.7	1.0	1.3	1.9	2.7	3.4

It has to be mentioned that these values are only estimates. The flexural strengths for concrete specimens with and without SRA are 5.13 and 5.93MPa, respectively. Therefore, there is a big risk of cracks developed in concrete specimens without SRA and reinforced with 6 and 8 steel rebars. It can be seen that SRA reduces the risk of cracks in concrete.

As can be seen, the results in Table 7.18 are lower than those in Table 7.29 due to mainly the allowance for creep relaxation.

7.4 Summary

7.4.1 Modulus of elasticity, creep and effective modulus

In this chapter, the influence of reinforcement ratio, reinforcement stiffness and the addition of SRA on the concrete's total strain (due to loading and drying) and the concrete's elastic modulus were considered.

The inclusion of SRA reduced the concrete's total time-dependent strain by an average of 37.3% after 94 days of loading and drying, regardless of the type and amount of reinforcement. Relationships between reinforcement ratio and total strain of reinforced concrete were derived from the results (Table 7.1), and the higher the modulus of elasticity of reinforcement the greatest the slopes of these relations.

The introduction of SRA in the concrete resulted in a reduction in the concrete compressive strength of about 21.5% and a reduction of 15% in modulus of elasticity. For concrete reinforced with GFRP and steel rebars the modulus of elasticity decreased by about 15% and 5%, respectively. The variation in stiffness reduction is due to the relatively high stiffness of steel (200 GPa) compared to that of GFRP rebars (48 GPa).

Relationships for the measured effective moduli of all the specimens after three months of loading were developed and summarised in Table 7.3. SRA caused an increase in the measured effective modulus due to a reduction in creep. There was a 17.3 percentage increase for the control specimen after three months of loading and drying.

Modulus of elasticity of non-reinforced concrete was estimated by a number of Codes of Practice and compared with the measured one. The results showed that the BS8110 was the most accurate especially with the mix without SRA.

Estimate of elastic modulus for reinforced concrete was made by the composite model and compared with the measured values in Table 7.10. The results reveal a relatively high accuracy.

In this investigation, the influence of reinforcement ratio, reinforcement stiffness and the addition of SRA on the concrete's total creep were considered. The influence of steel reinforcement on the total creep reduction was higher than that of GFRP rebars, this was due to the higher modulus of elasticity of steel compared to GFRP. SRA increased the influence of reinforcement ratio on restraining creep in concrete. Because both SRA and reinforcement act to reduce creep strain although by different mechanisms.

For concrete specimens reinforced with GFRP rebars, having different reinforcement ratios, the average total creep decreased by 26% for specimens without SRA and 37% for specimens with SRA. While, for concrete specimens reinforced with steel rebars the average total creep declined by 47% for specimens without SRA and 55% for specimens with SRA after 94 days of loading and drying.

The inclusion of SRA reduced the concrete's total creep by an average of 54% after 94 days of loading and drying (this includes non-reinforced and reinforced specimens). This total creep reduction was larger than the drying shrinkage reduction.

The 94-day creep in terms of creep coefficient of non-reinforced concrete was estimated by a number of Codes of Practice and compared with the measured one. Also the reduced modulus values, i.e. the effective modulus (EM) and age adjusted effective modulus (AAEM) were estimated and compared with the measured reduced moduli. Both BS 8110 and BS 5400 showed relatively high accuracy. Gardner and Zhao (1993) showed high accuracy for the SRA mix.

Estimates of effective modulus (EM) and age-adjusted effective modulus (AAEM) by the composite model (Equation (5.20)) are also considered. The BS 8110 and BS 5400 were used to predict modulus of elasticity of plain concrete, while EM and AAEM were used to allow for time-dependent strain (i.e. creep), and the composite model to allow for reinforcement. The accuracy of the results was increased by using the measured modulus of elasticity of non-reinforced concrete ($E(t_0)$) instead of the estimated elastic modulus by the Codes of Practice.

7.4.2 Drying shrinkage

The results illustrated how both ratio and stiffness of reinforcement combine to restrain the concrete movement. The use of lower stiffness reinforcement, namely GFRP, could help in reducing internal tensile stresses in concrete and therefore eliminating the risk of shrinkage cracking. But on the other hand there is more shrinkage than for steel.

Drying shrinkage relationships for concrete specimens reinforced with GFRP and steel with different reinforcement ratios were established and shown in Table 7.4. The higher the modulus of elasticity of reinforcement, the higher the slopes of these relations.

The influence of steel reinforcement on shrinkage reduction (shrinkage restraint) was greater than that observed with concrete reinforced with GFRP rebars. This was due to higher modulus of elasticity of steel compared with GFRP. Less shrinkage cracking is expected to be in specimens reinforced with GFRP composite.

From the results it was apparent that SRA significantly reduced the drying shrinkage of concrete specimens. The inclusion of SRA reduced the concrete's drying shrinkage by an average of 29.8% (this includes non-reinforced and reinforced specimens).

The amount of shrinkage of non-reinforced concrete was estimated by a number of Codes of Practice and compared with the measured ones. BS 5400 and Gardner and Zhao (1993) showed relatively good prediction especially for the SRA mix. BS 8110, CEB-FIP and ACI 209 showed reasonable accuracy for the SRA mix only.

Shrinkage of reinforced specimens was estimated by the proposed composite model. When the measured modulus of elasticity of non-reinforced concrete was used in the composite model, results were reasonably accurate for the mix without SRA. The accuracy was enhanced by using effective modulus and age-adjusted effective modulus of non-reinforced concrete instead of the modulus of elasticity.

7.4.3 Tensile stress due to restraint

The development of tensile stress in concrete due to shrinkage restraint, caused by GFRP and steel rebars in accordance with Alexander (2002) and the proposed composite model were considered in this investigation and summarised in Tables 7.28 and 7.29. According to Alexander (2002), the induced tensile stress by high values of steel reinforcement was almost equal to the tensile strength of concrete. But in fact the creep relaxation in concrete would help relieving some tensile stresses; this was clear in Table 7.29.

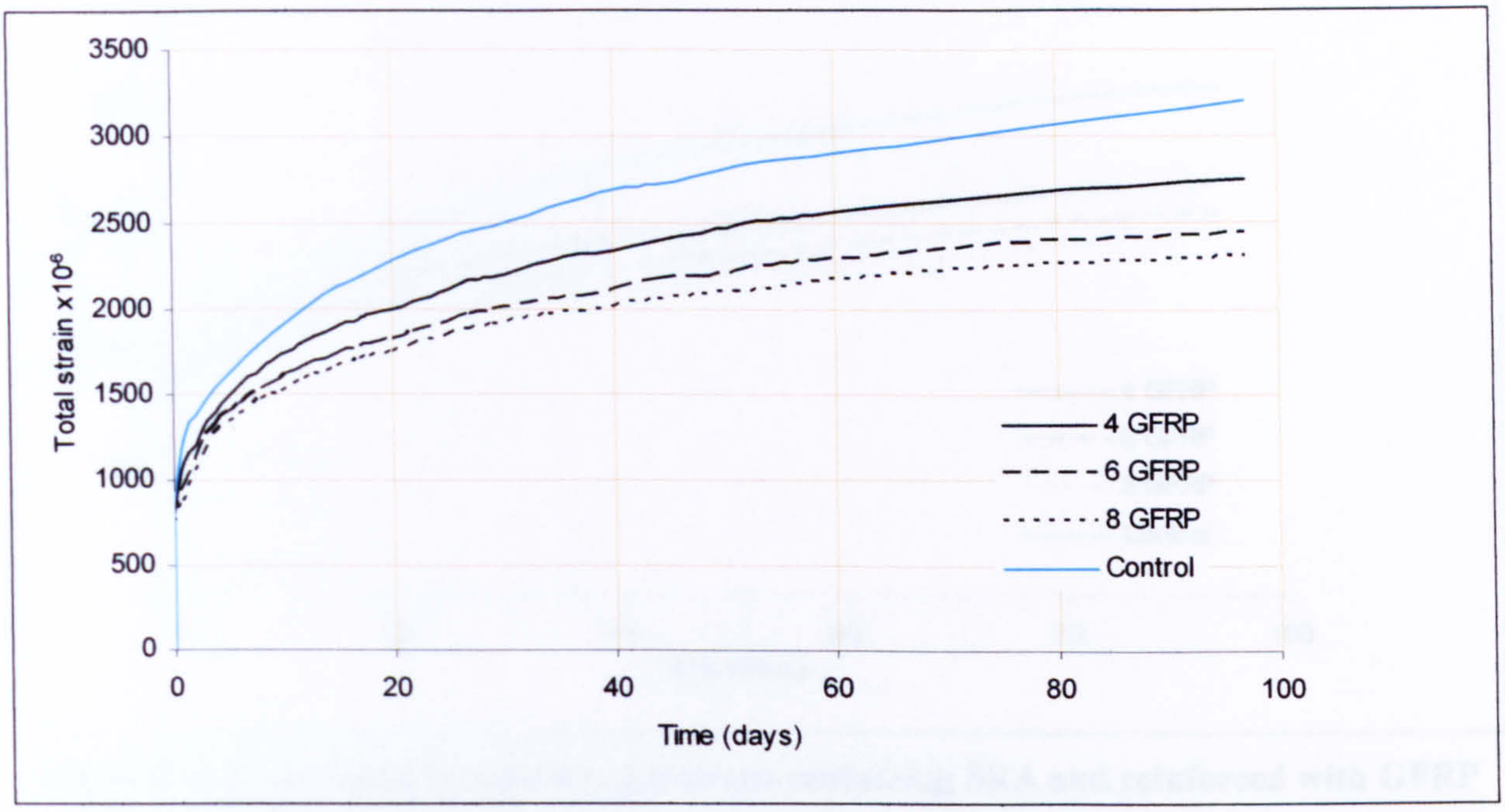

Figure 7.1: Total strain of concrete specimens reinforced with GFRP rebars with different reinforcement ratios and control concrete specimen

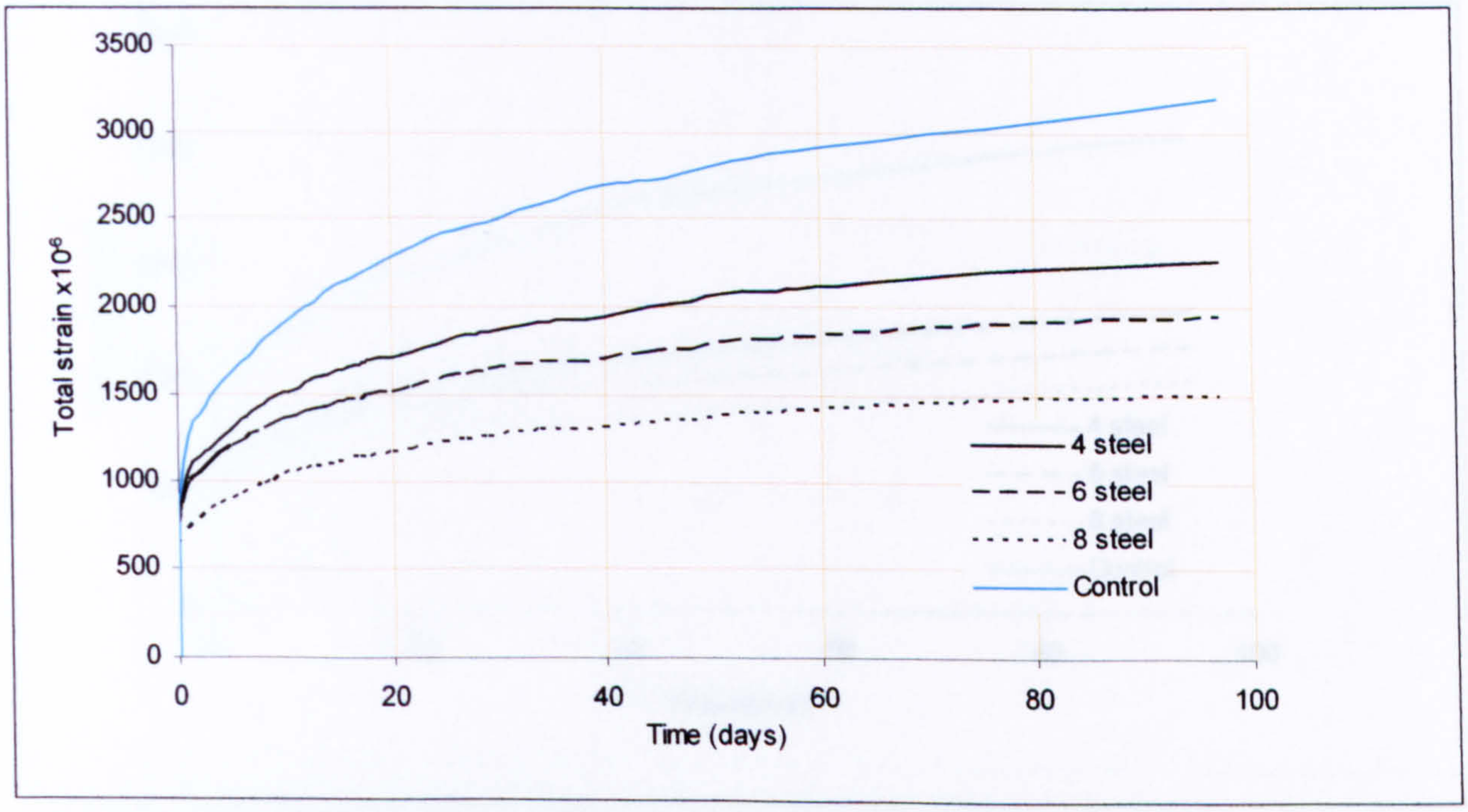

Figure 7.2: Total strain of concrete specimens reinforced with steel rebars with different reinforcement ratios and control concrete specimen

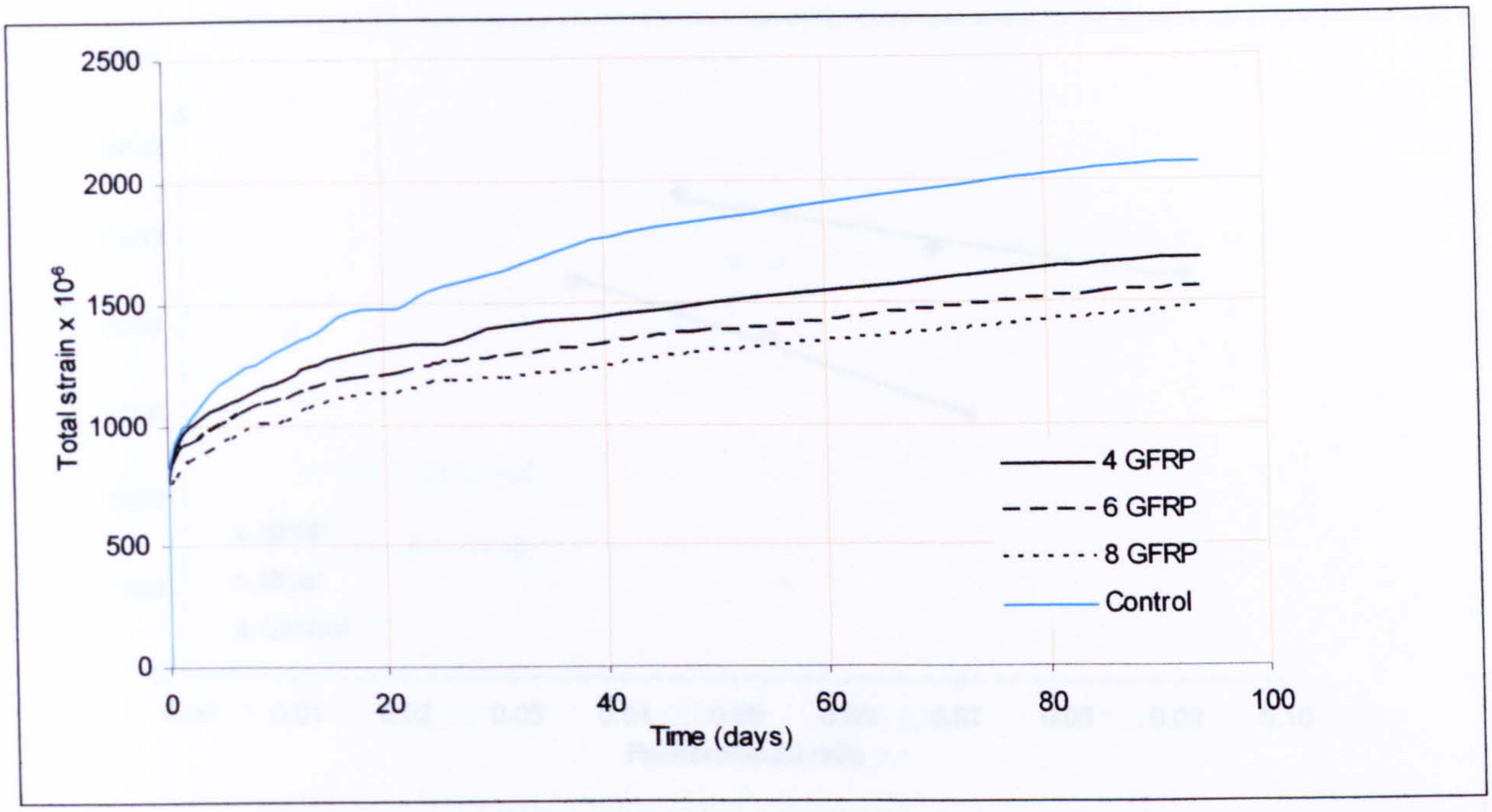

Figure 7.3: Total strain of concrete specimens containing SRA and reinforced with GFRP rebars with different reinforcement ratios and control concrete specimen

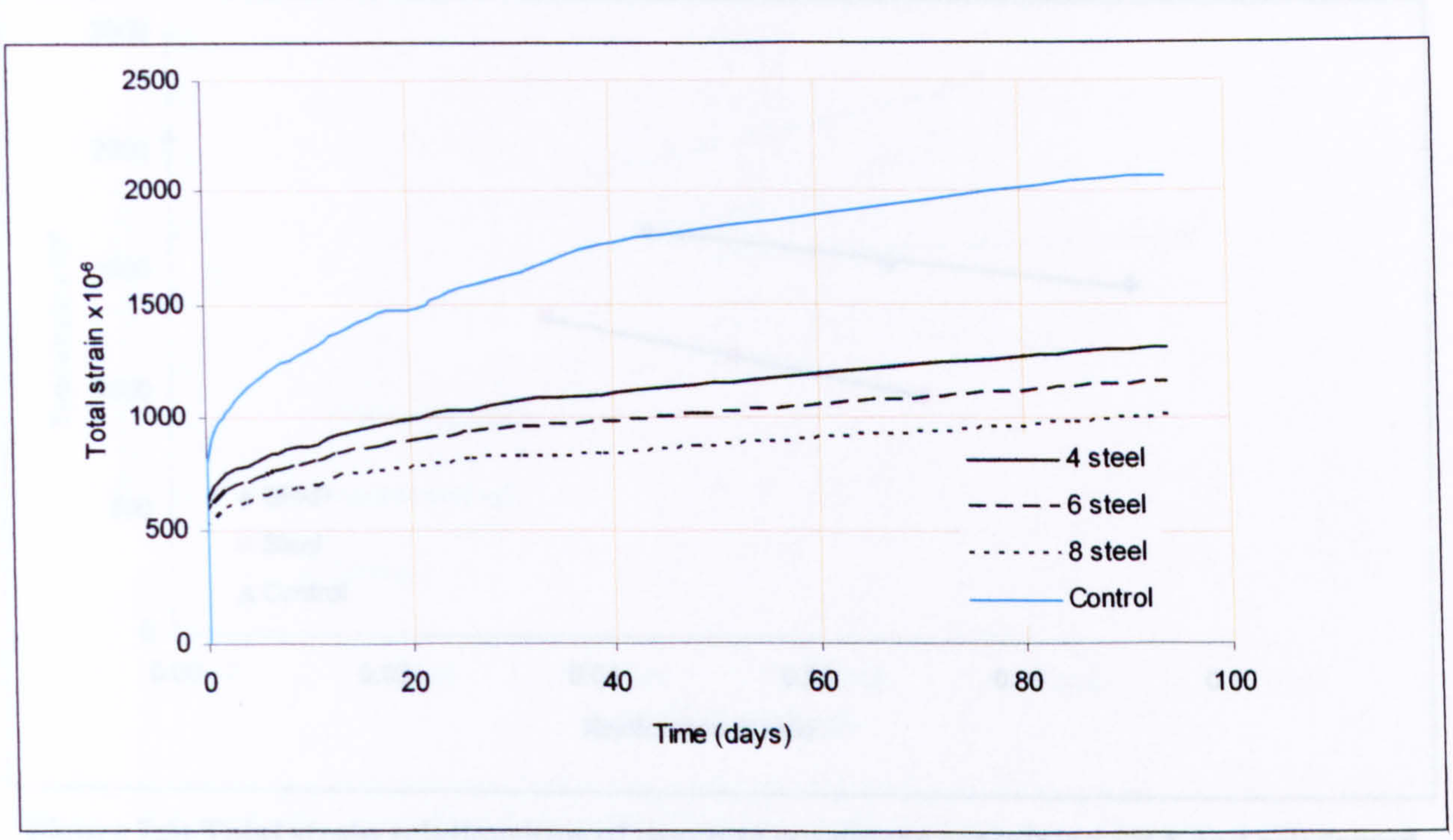

Figure 7.4: Total strain of concrete specimens containing SRA and reinforced with steel rebars with different reinforcement ratios and control concrete specimen

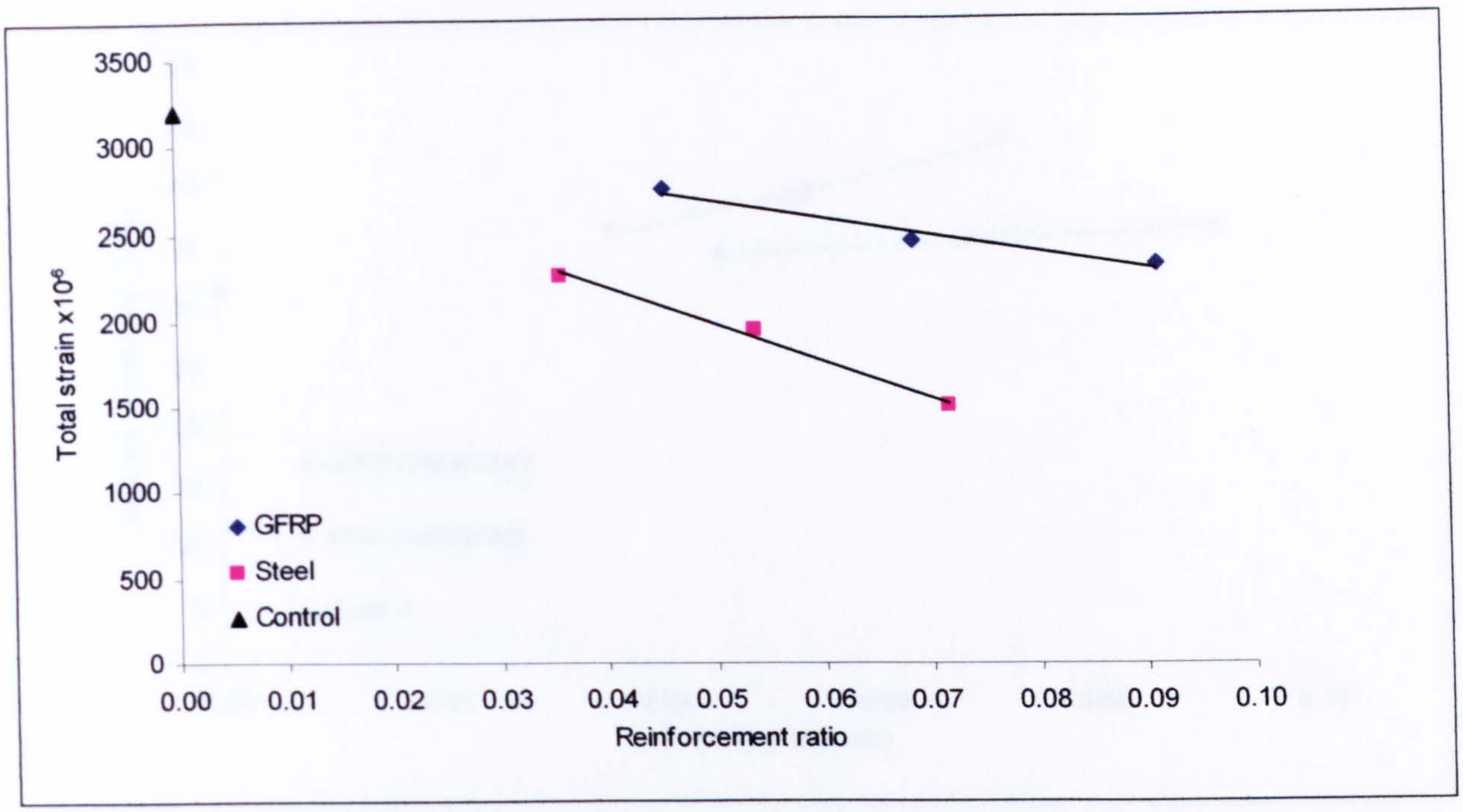

Figure 7.5: Total strain relationships for concrete specimens reinforced with GFRP and steel and control concrete specimen after ninety four days of loading

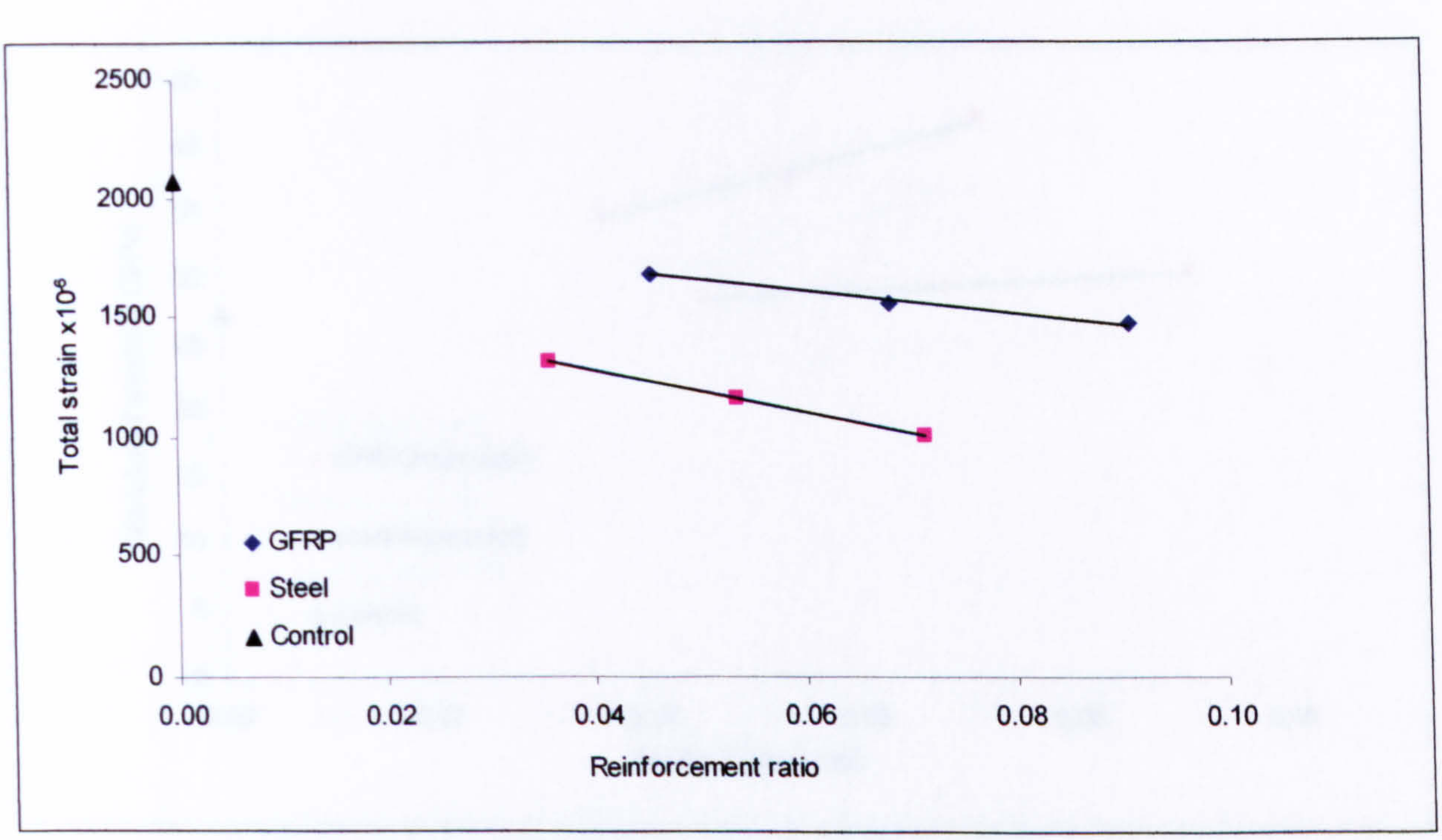

Figure 7.6: Total strain relationships of concrete specimens containing SRA and reinforced with GFRP and steel and control concrete specimen after ninety four days of loading

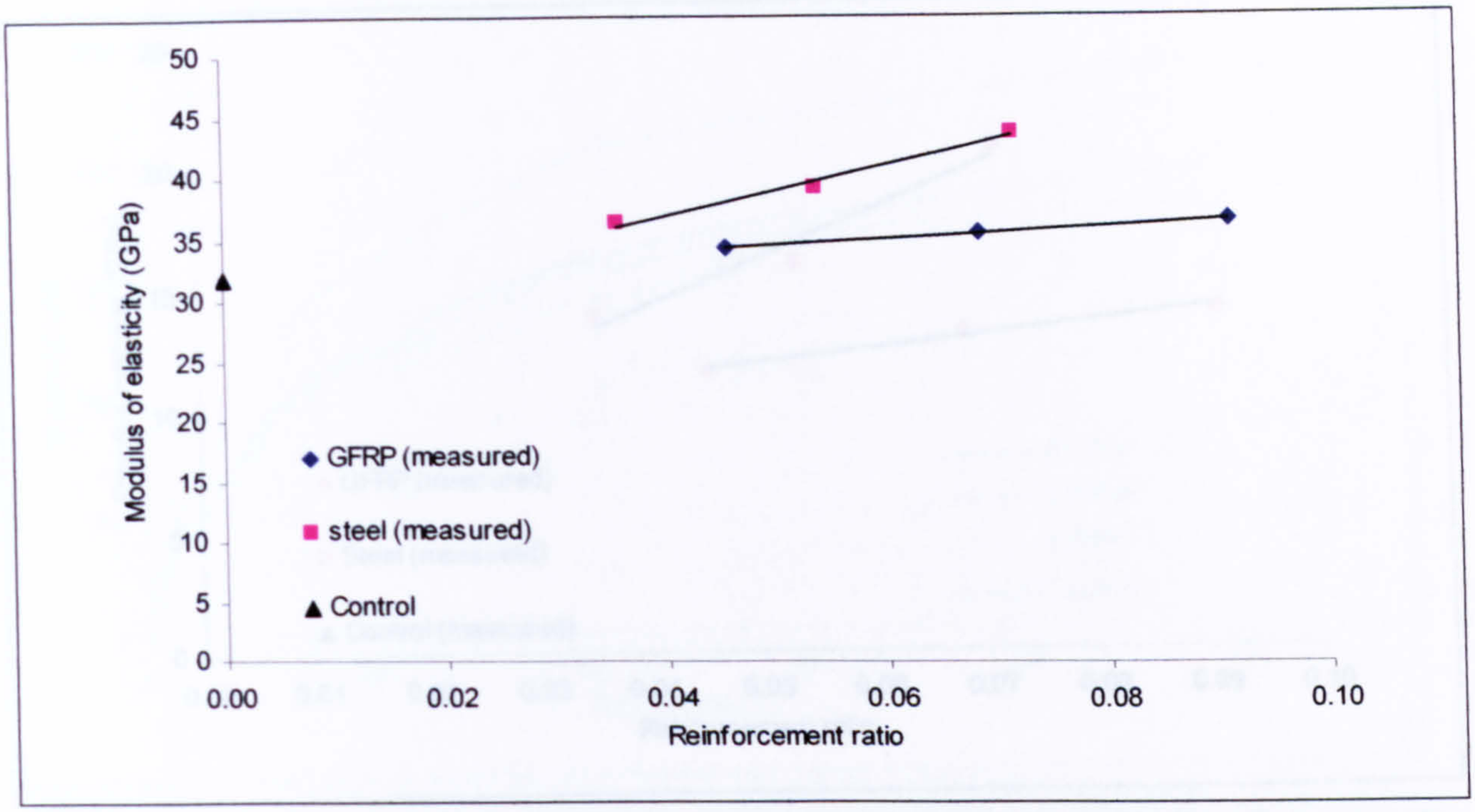

Figure 7.7: Elastic moduli relationships of concrete specimens reinforced with GFRP and steel with different reinforcement ratios and control concrete specimen

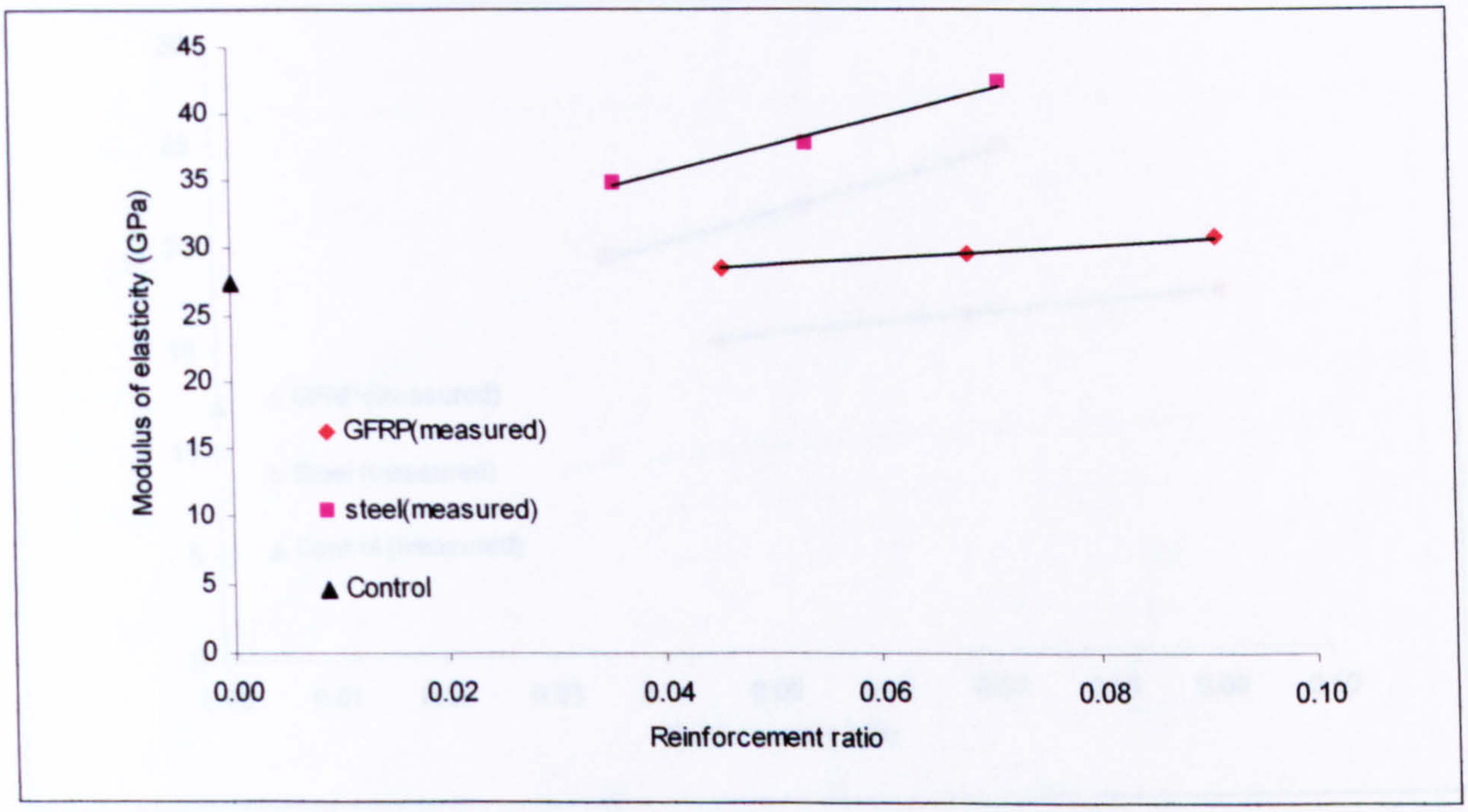

Figure 7.8: Elastic moduli relationships of concrete specimens containing SRA and reinforced with GFRP and steel with different reinforcement ratios and control concrete specimen

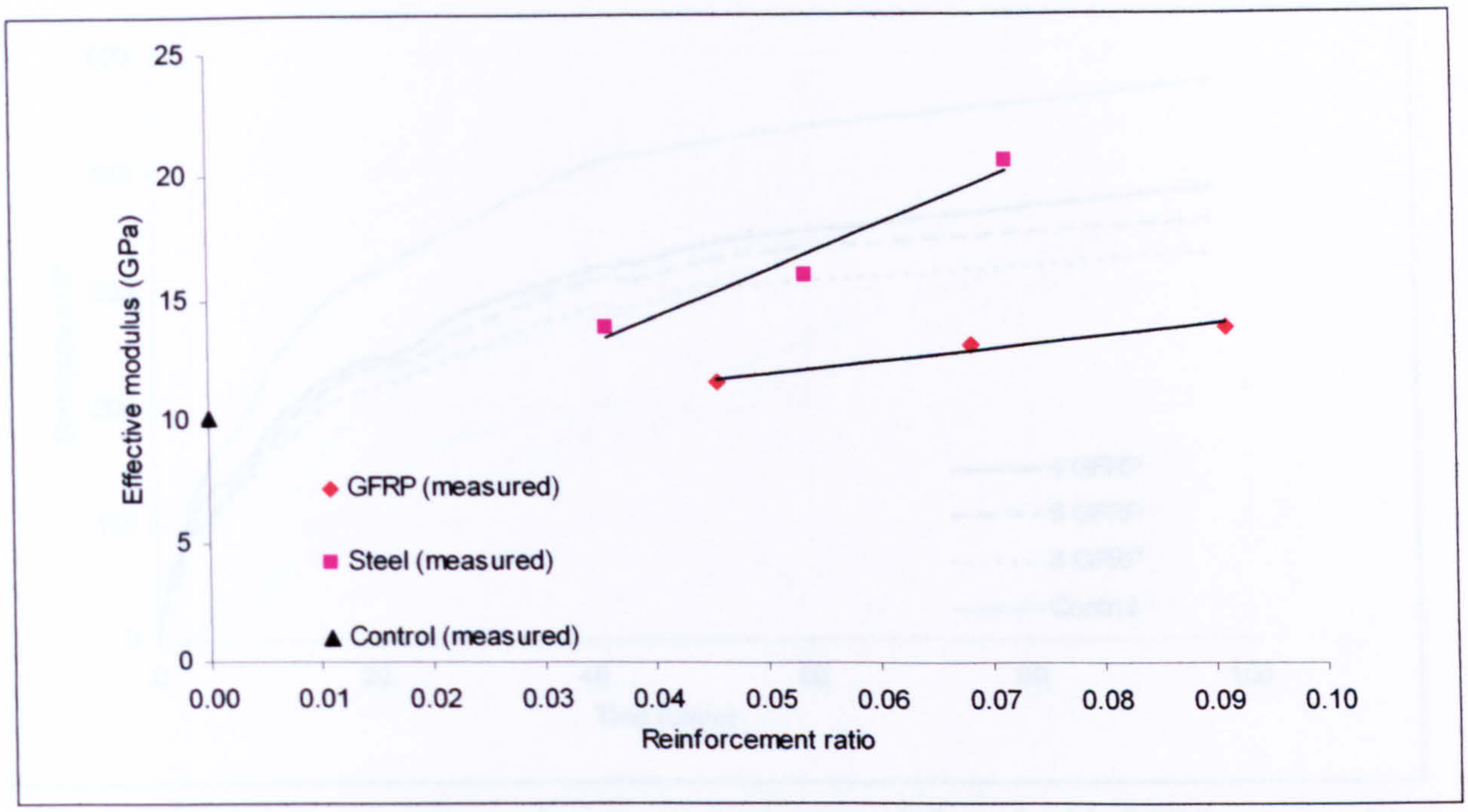

Figure 7.9: Effective moduli relationships after ninety four days loading for concrete specimens reinforced with GFRP and steel with different reinforcement ratios

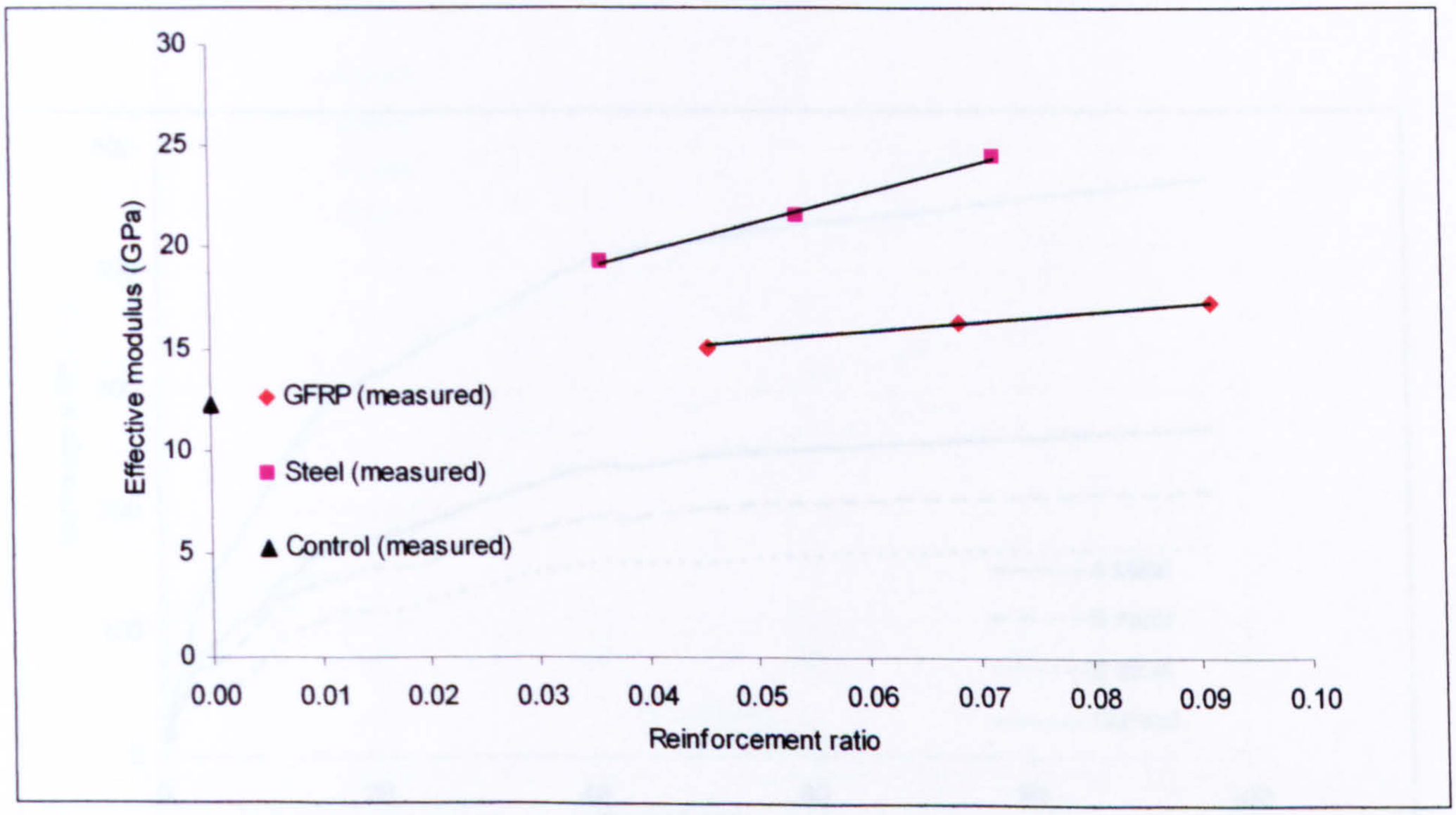

Figure 7.10: Effective moduli relationships after ninety four days loading for concrete specimens containing SRA and reinforced with GFRP and steel with different reinforcement ratios

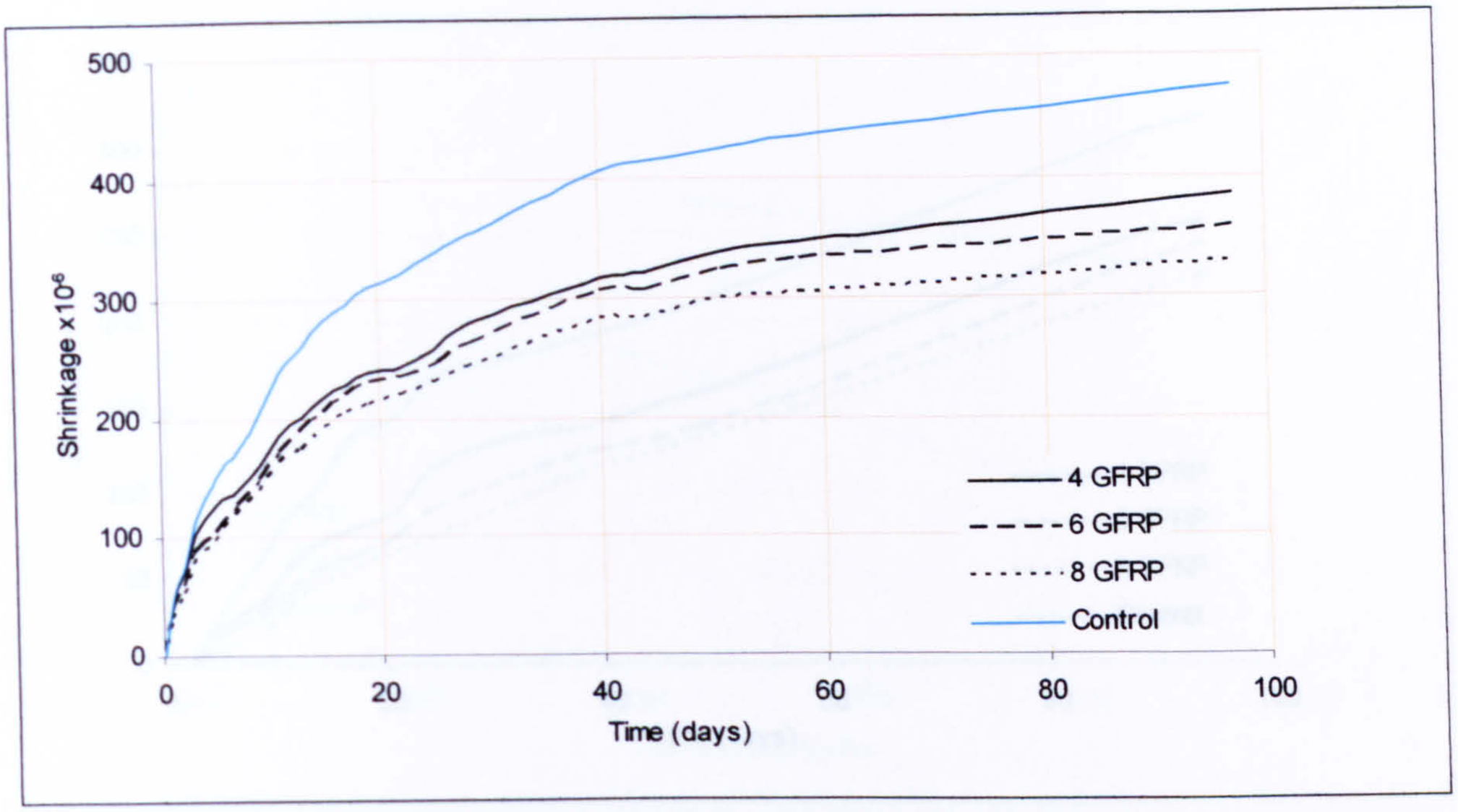

Figure 7.11: Drying shrinkage of concrete specimens reinforced with GFRP rebars with different reinforcement ratios

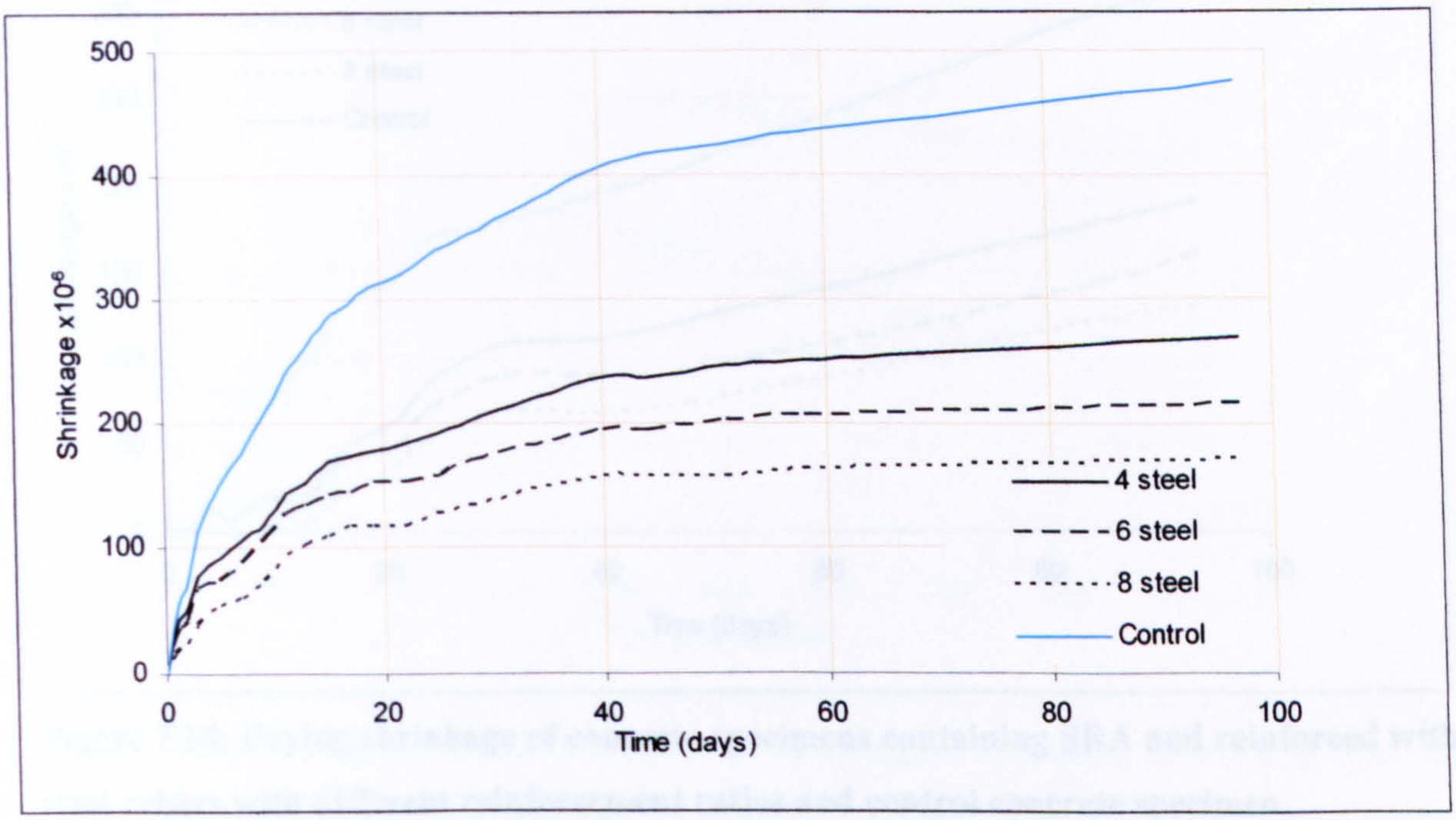

Figure 7.12: Drying shrinkage of concrete specimens reinforced with steel rebars with different reinforcement ratios

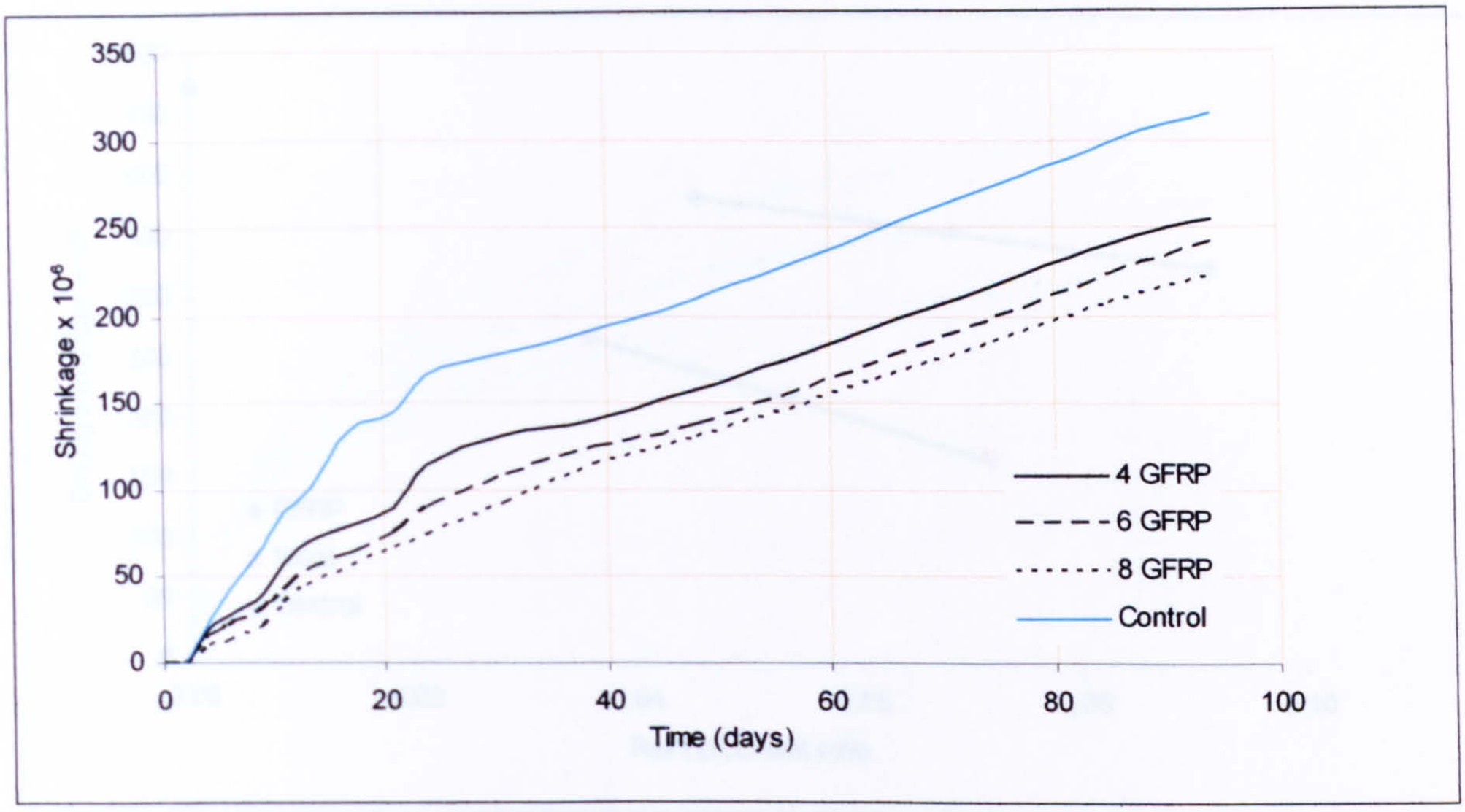

Figure 7.13: Drying shrinkage of concrete specimens containing SRA and reinforced with GFRP rebars with different reinforcement ratios and control concrete specimen

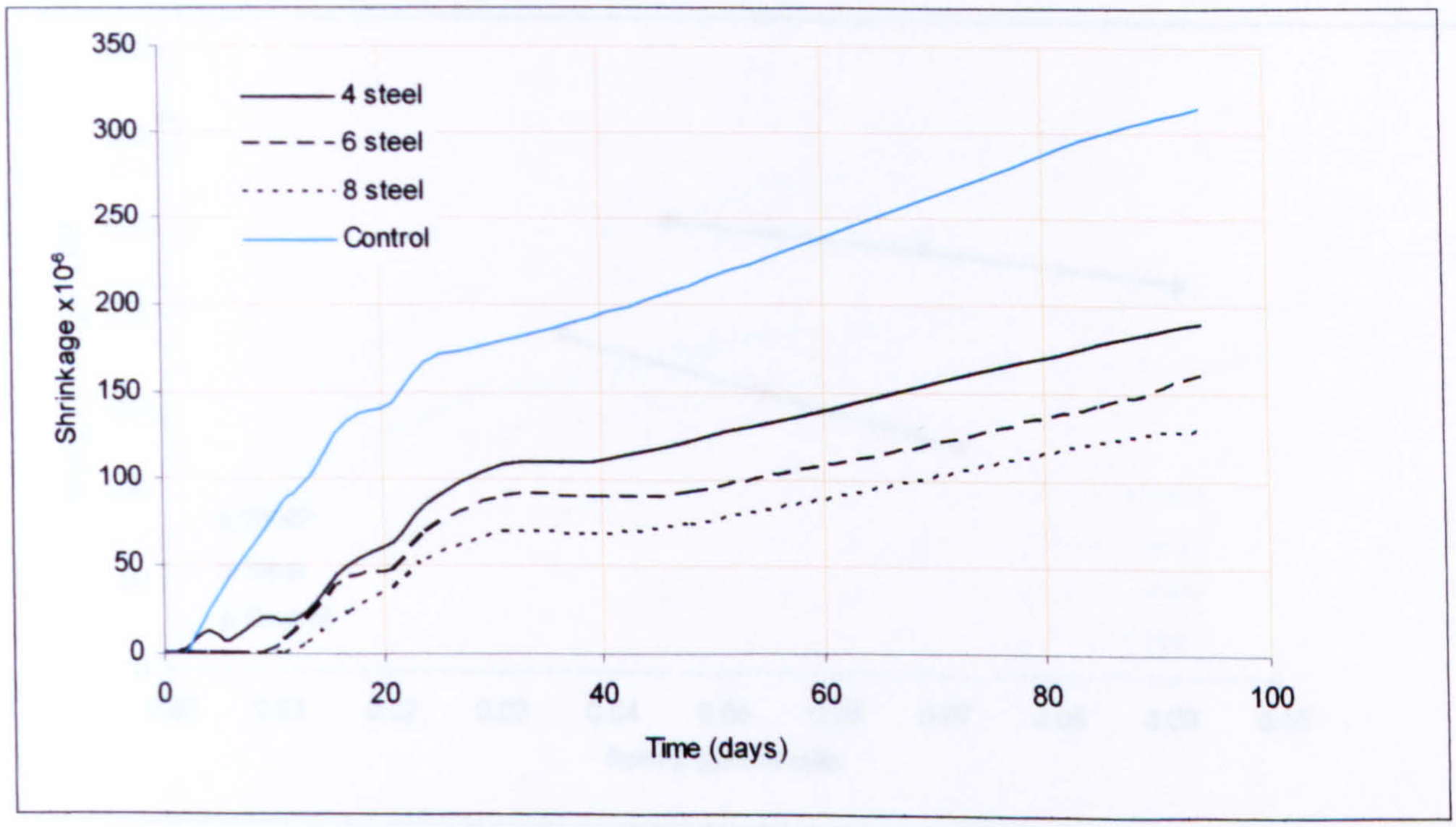

Figure 7.14: Drying shrinkage of concrete specimens containing SRA and reinforced with steel rebars with different reinforcement ratios and control concrete specimen

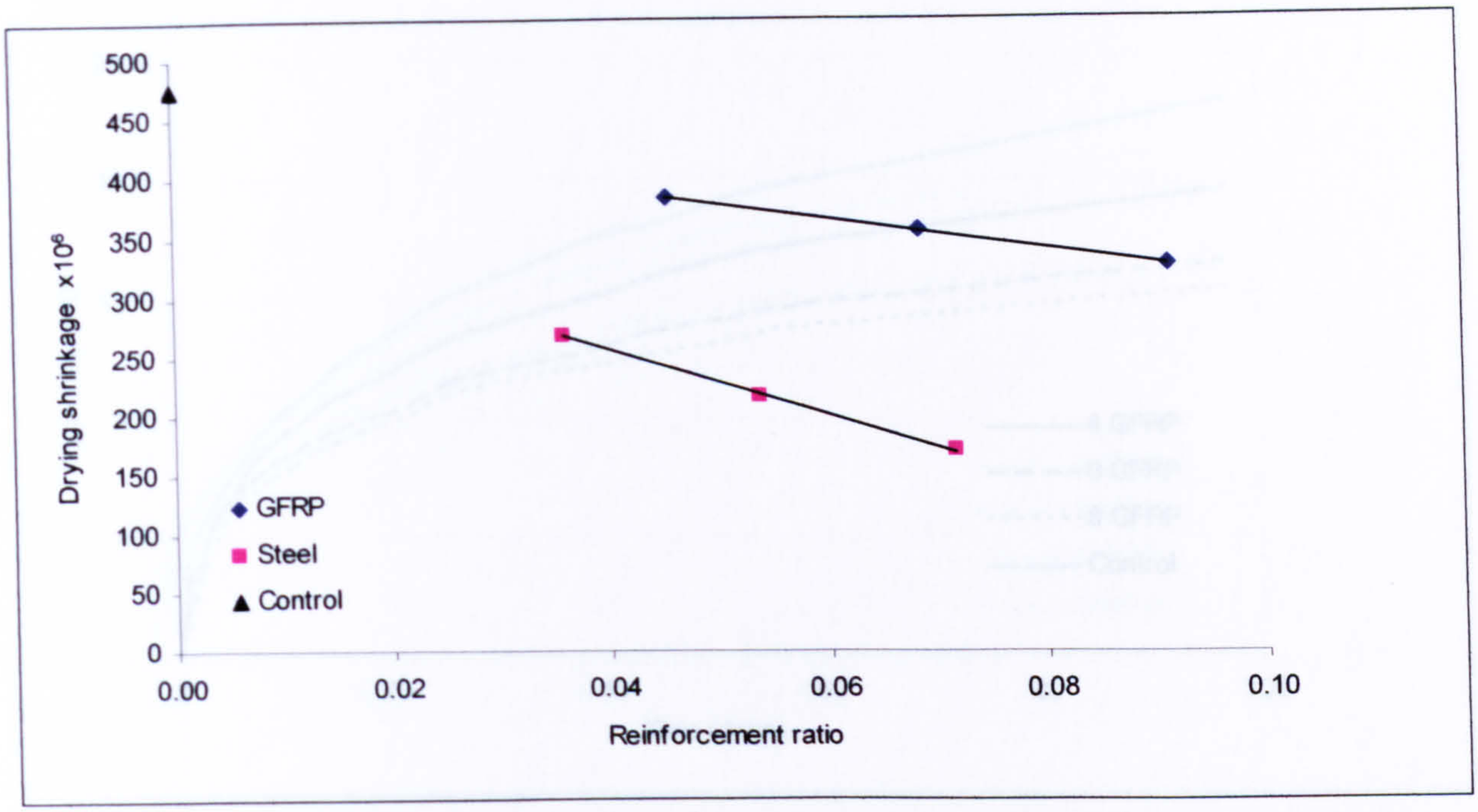

Figure 7.15: Drying shrinkage relationships for concrete specimens reinforced with GFRP and steel and control concrete specimen after ninety four days of drying

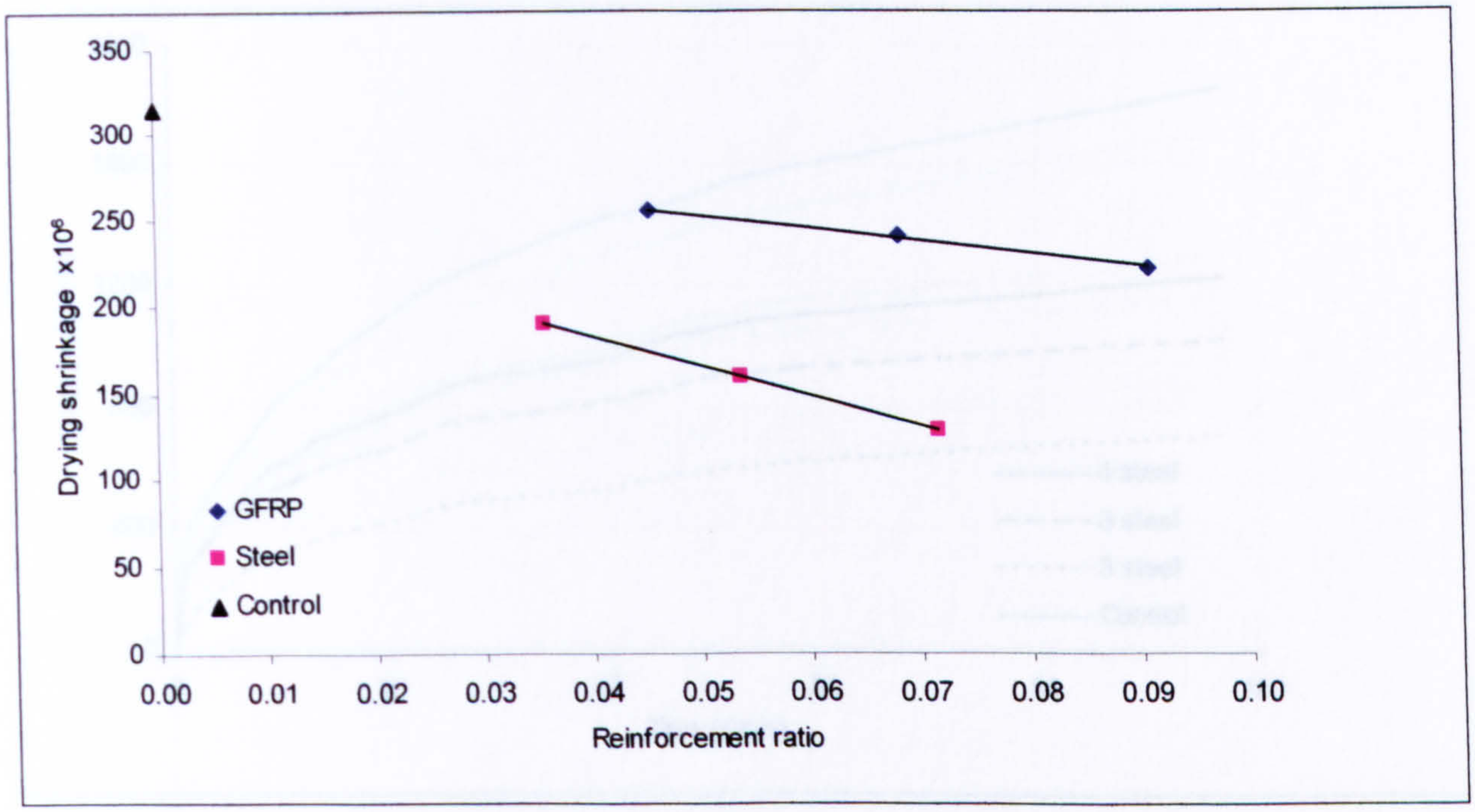

Figure 7.16: Drying shrinkage relationships of concrete specimens containing SRA and reinforced with GFRP and steel and control concrete specimen after ninety four days of drying

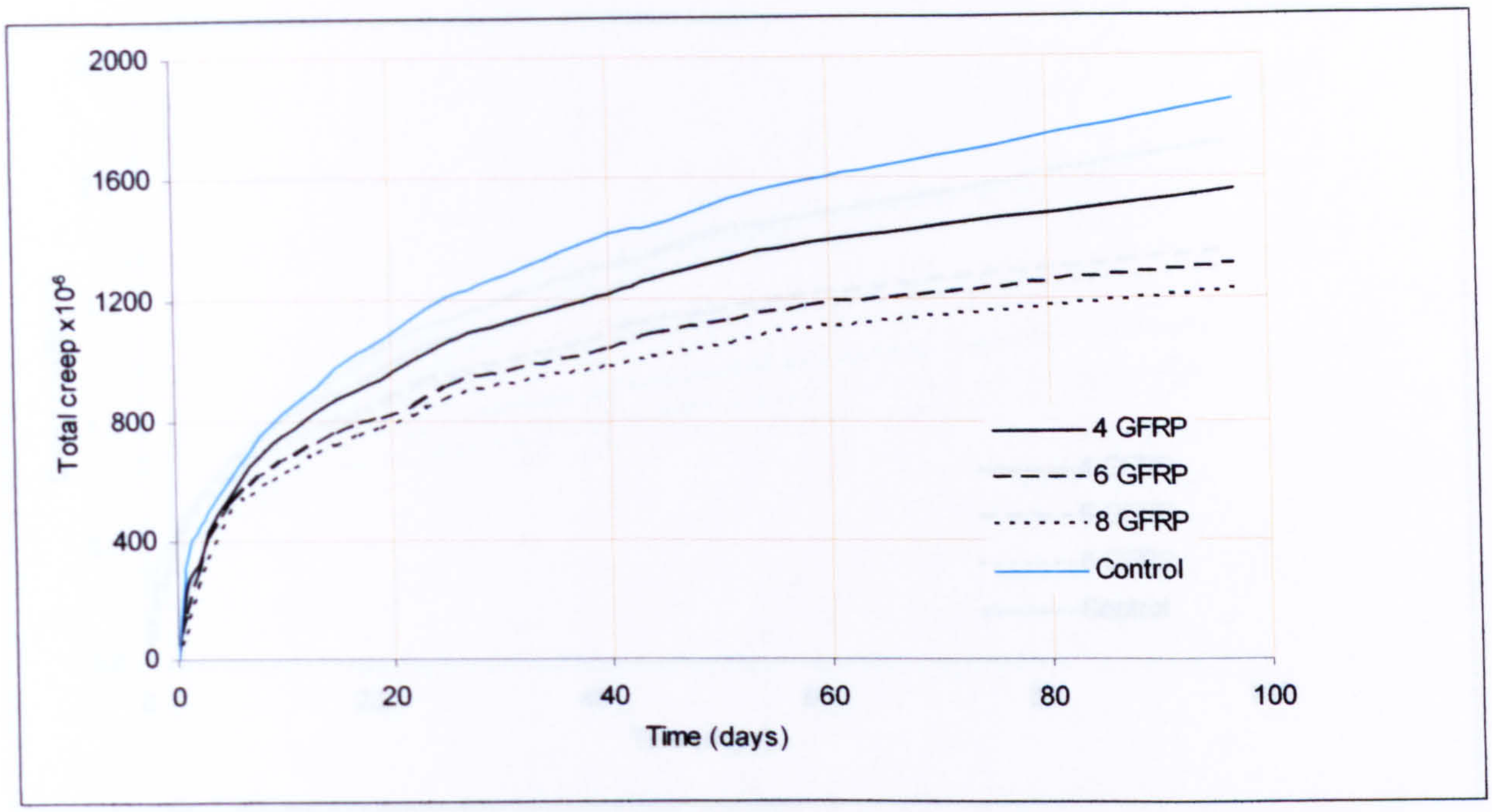

Figure 7.17: Total creep of concrete specimens reinforced with GFRP rebars with different reinforcement ratios, and control concrete specimen

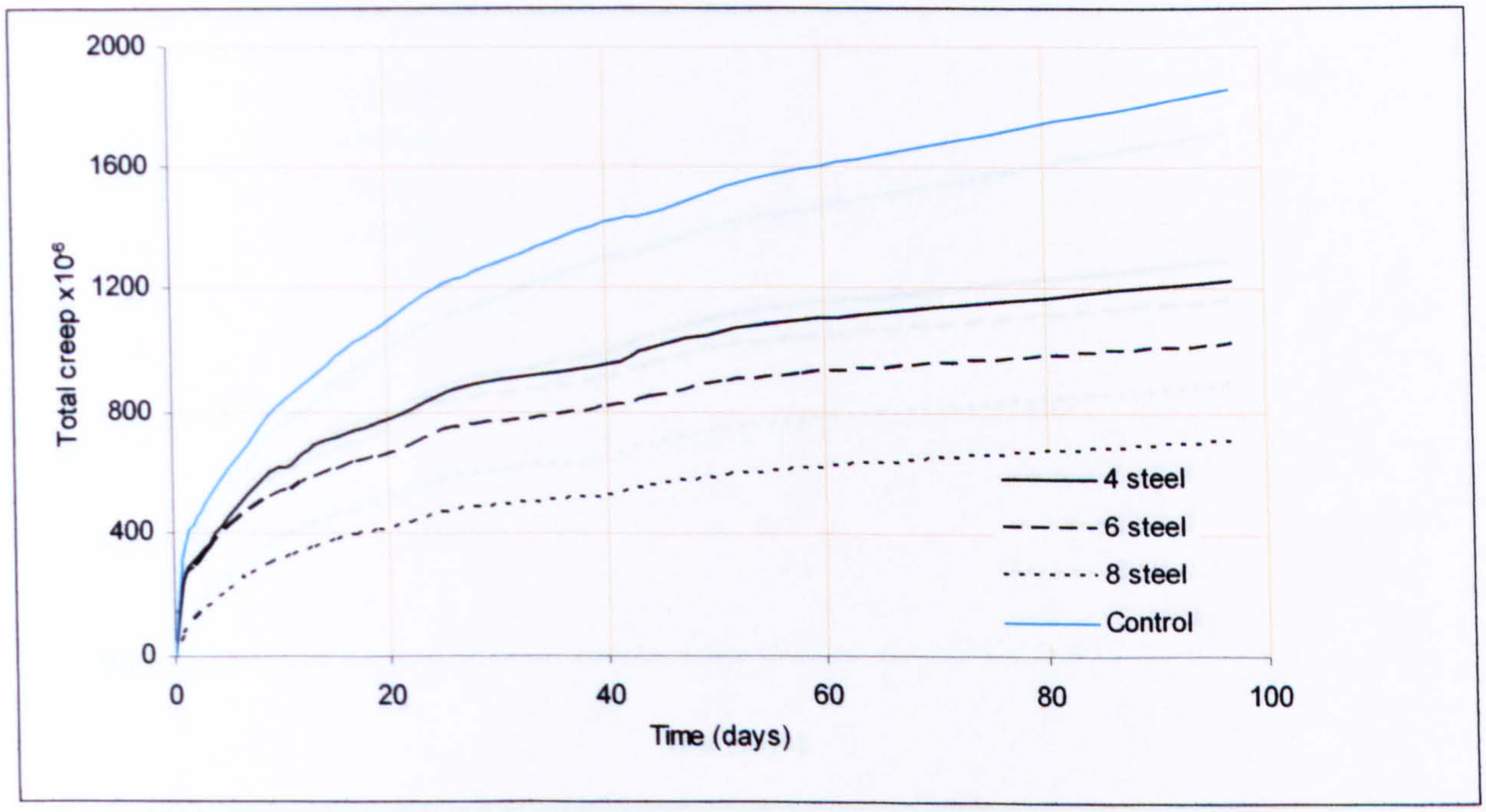

Figure 7.18: Total creep of concrete specimens reinforced with steel rebars with different reinforcement ratios, and control concrete specimen

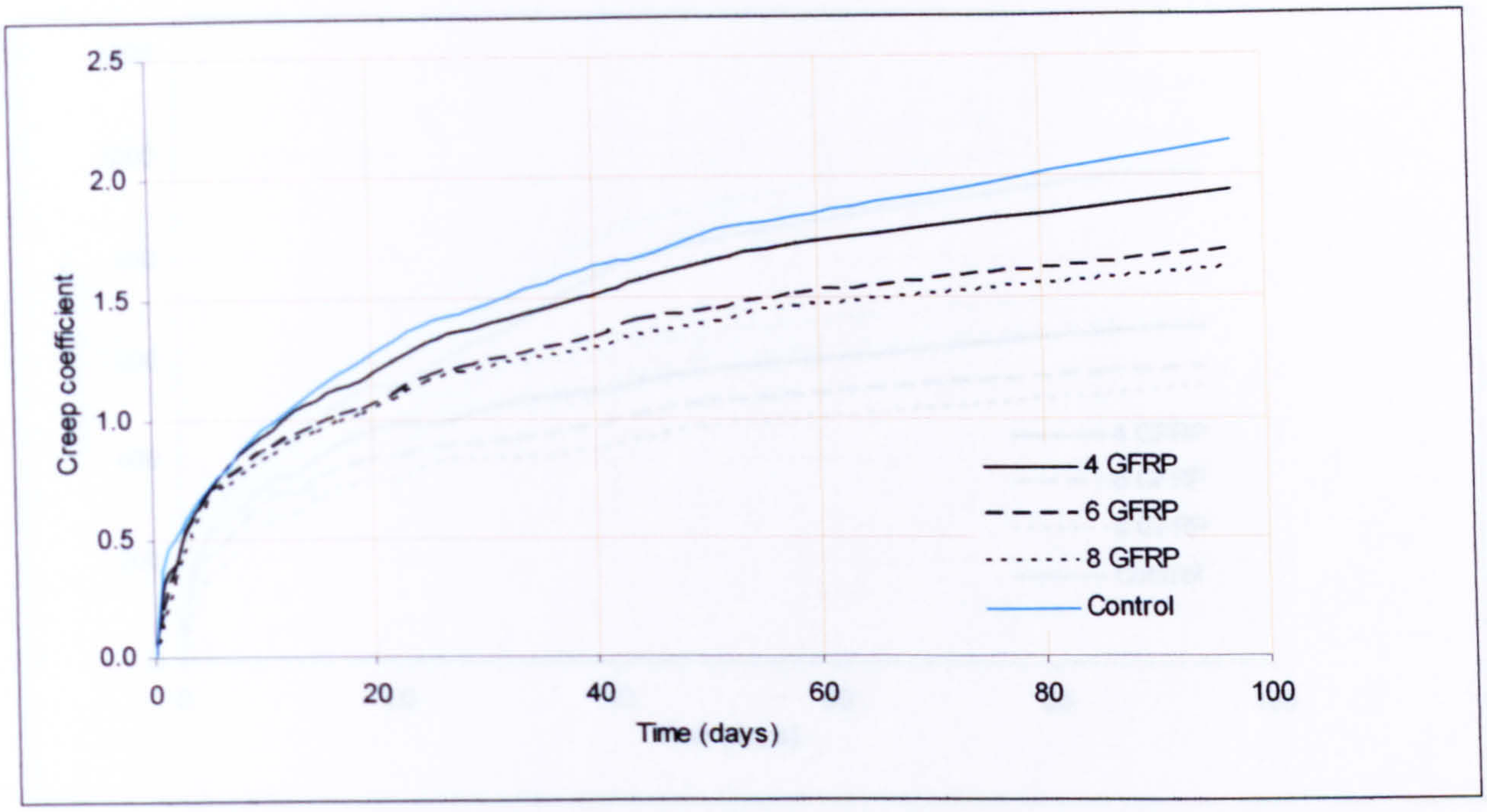

Figure 7.19: Creep coefficient of concrete specimens reinforced with GFRP rebars with different reinforcement ratios and control concrete specimen

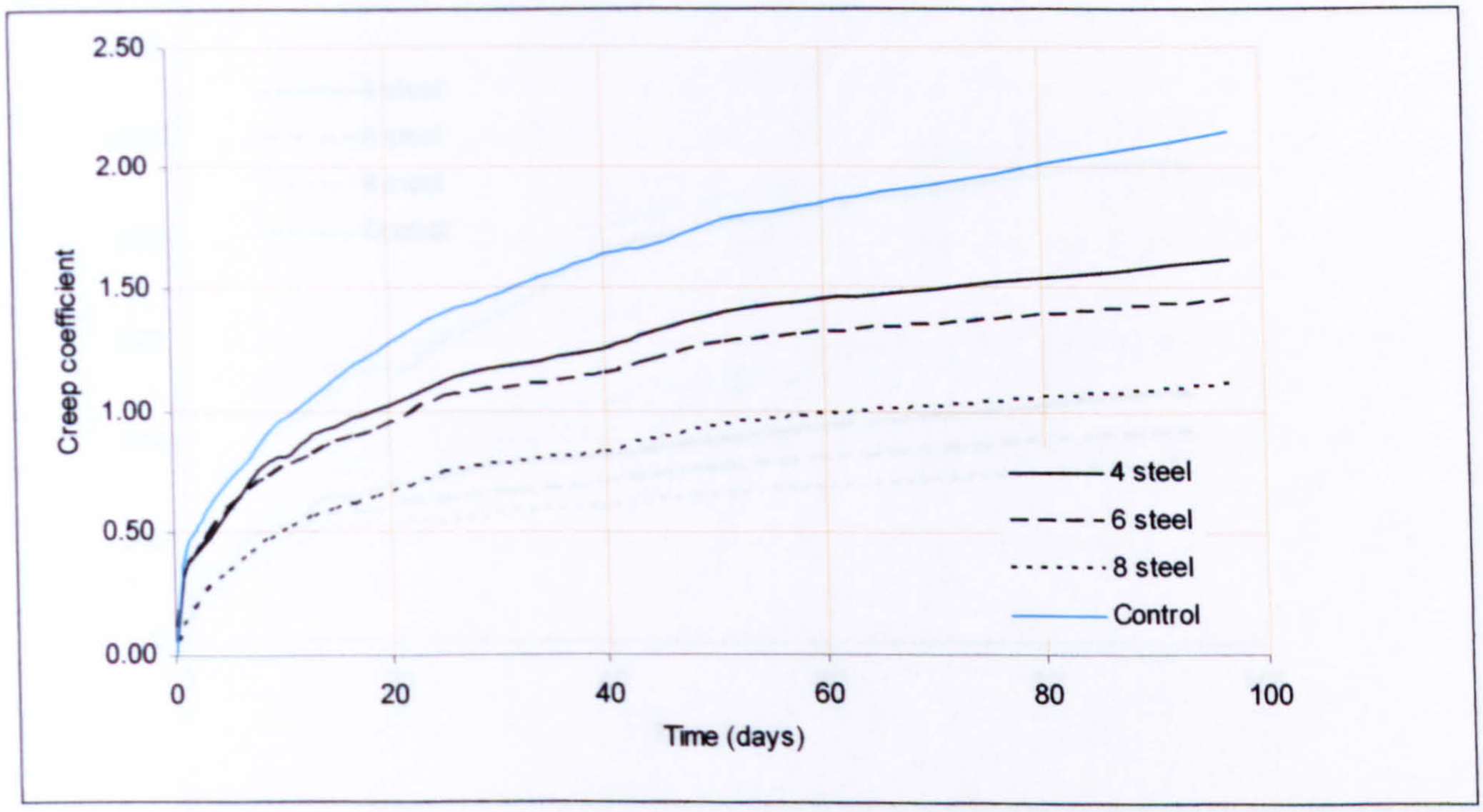

Figure 7.20: Creep coefficient of concrete specimens reinforced with steel rebars with different reinforcement ratios and control concrete specimen

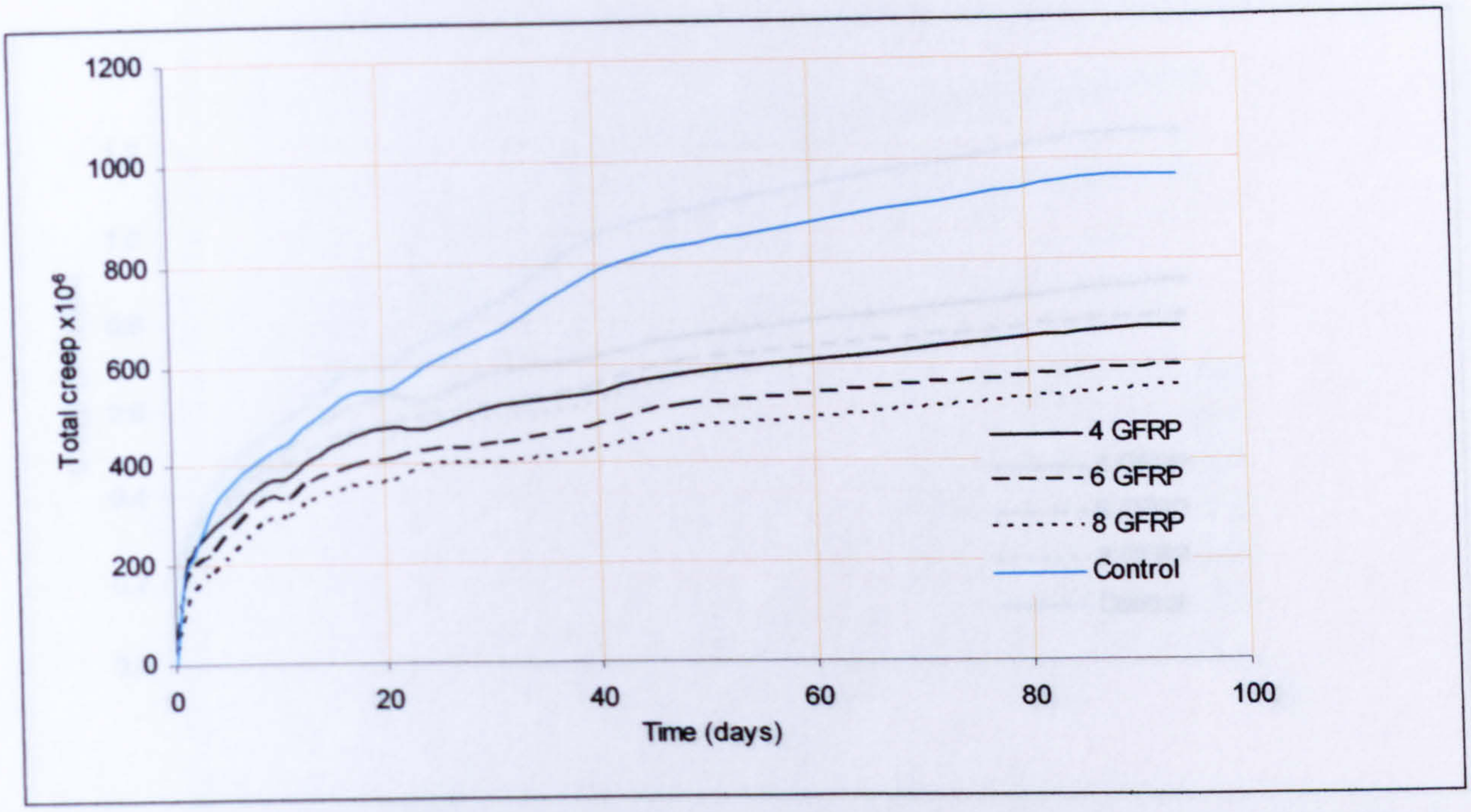

Figure 7.21: Total creep of concrete specimens including SRA and reinforced with GFRP rebars with different reinforcement ratios, and control concrete specimen

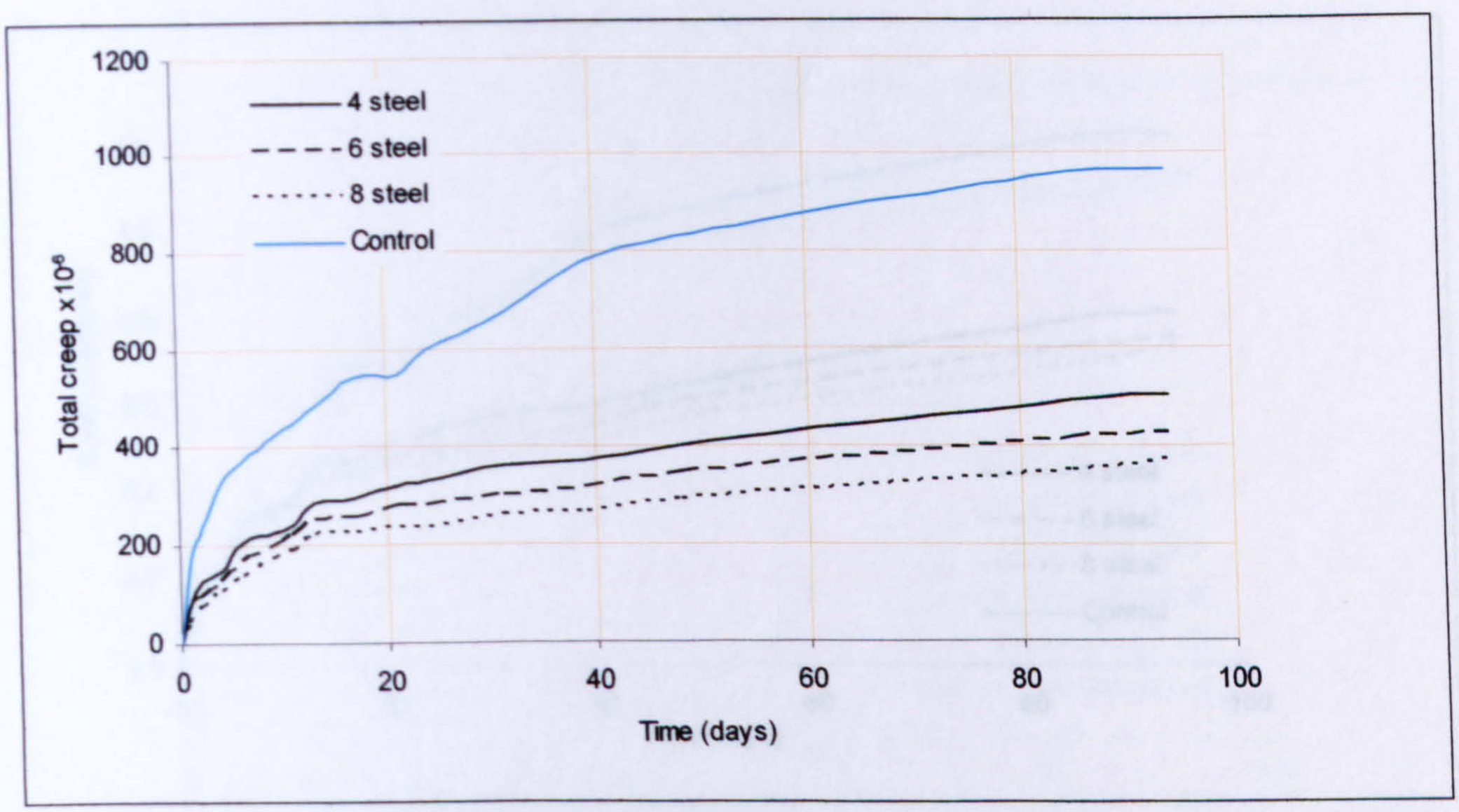

Figure 7.22: Total creep of concrete specimens including SRA and reinforced with steel rebars with different reinforcement ratios, and control concrete specimen

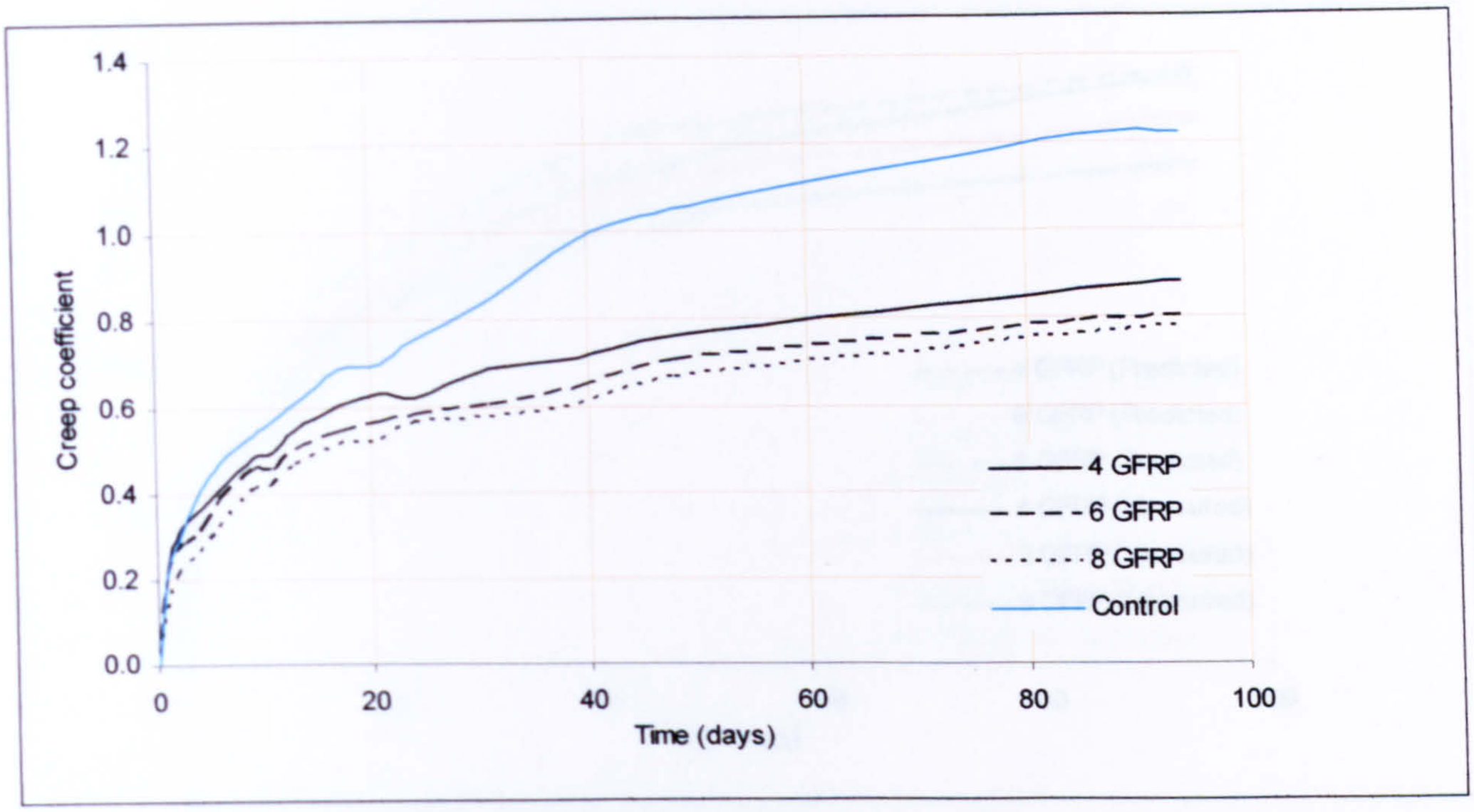

Figure 7.23: Creep coefficient of concrete specimens containing SRA and reinforced with GFRP rebars with different reinforcement ratios and control concrete specimen

Figure 7.24: Creep coefficient of concrete specimens containing SRA and reinforced with steel rebars with different reinforcement ratios and control concrete specimen

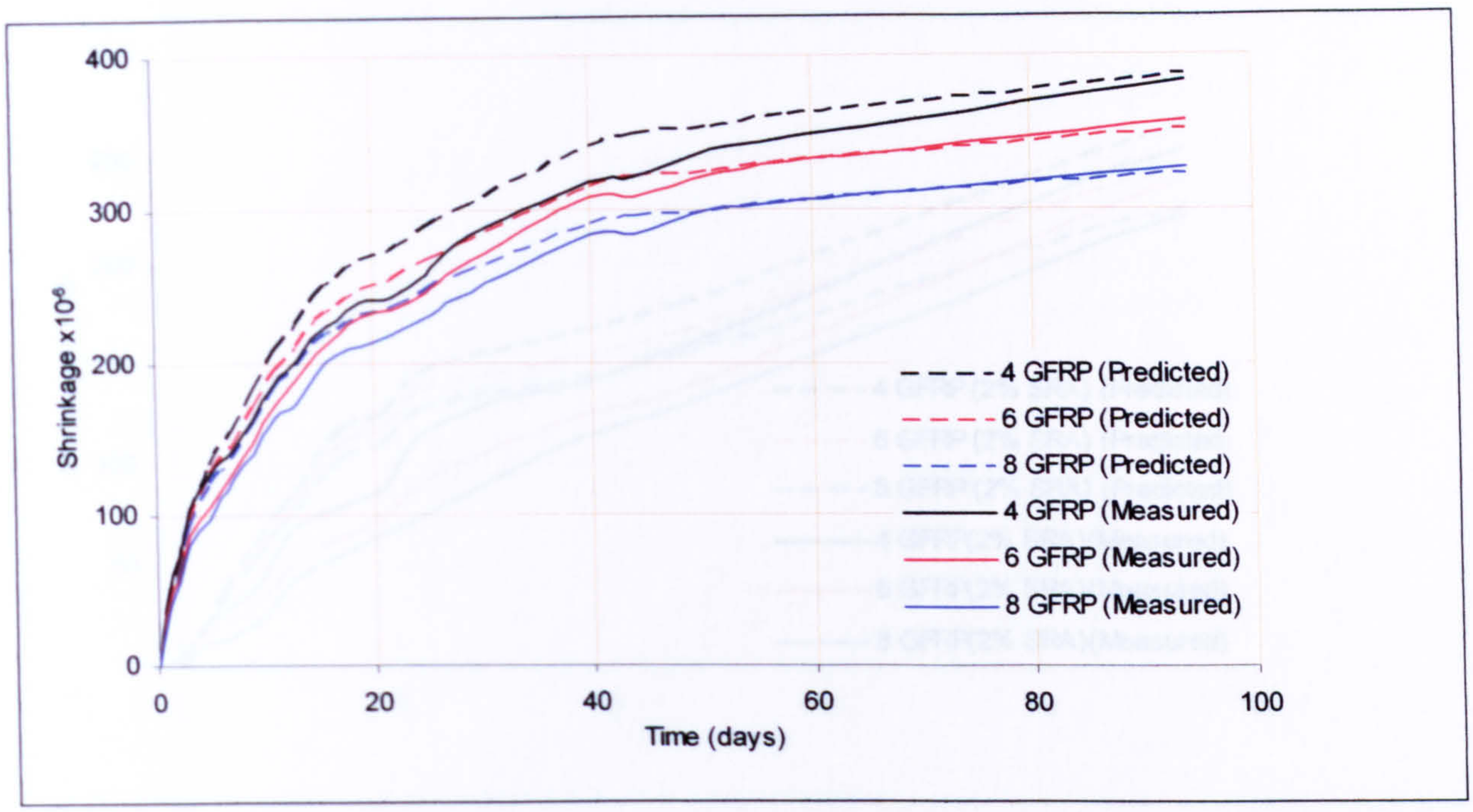

Figure 7.25: Drying shrinkage of concrete specimens reinforced with GFRP rebars, compared with composite model using the effective modulus

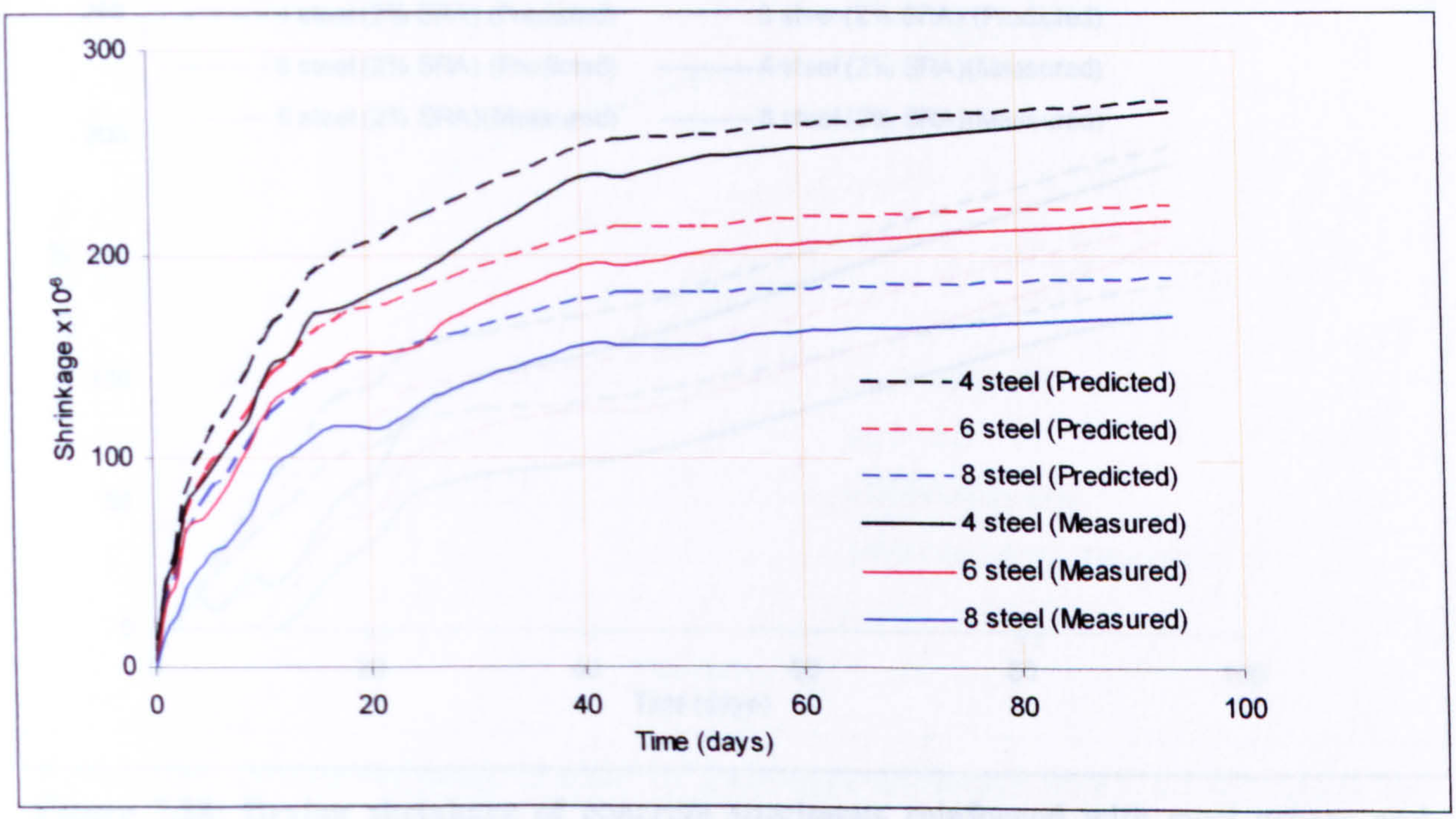

Figure 7.26: Drying shrinkage of concrete specimens reinforced with steel rebars, compared with composite modelling using the effective modulus

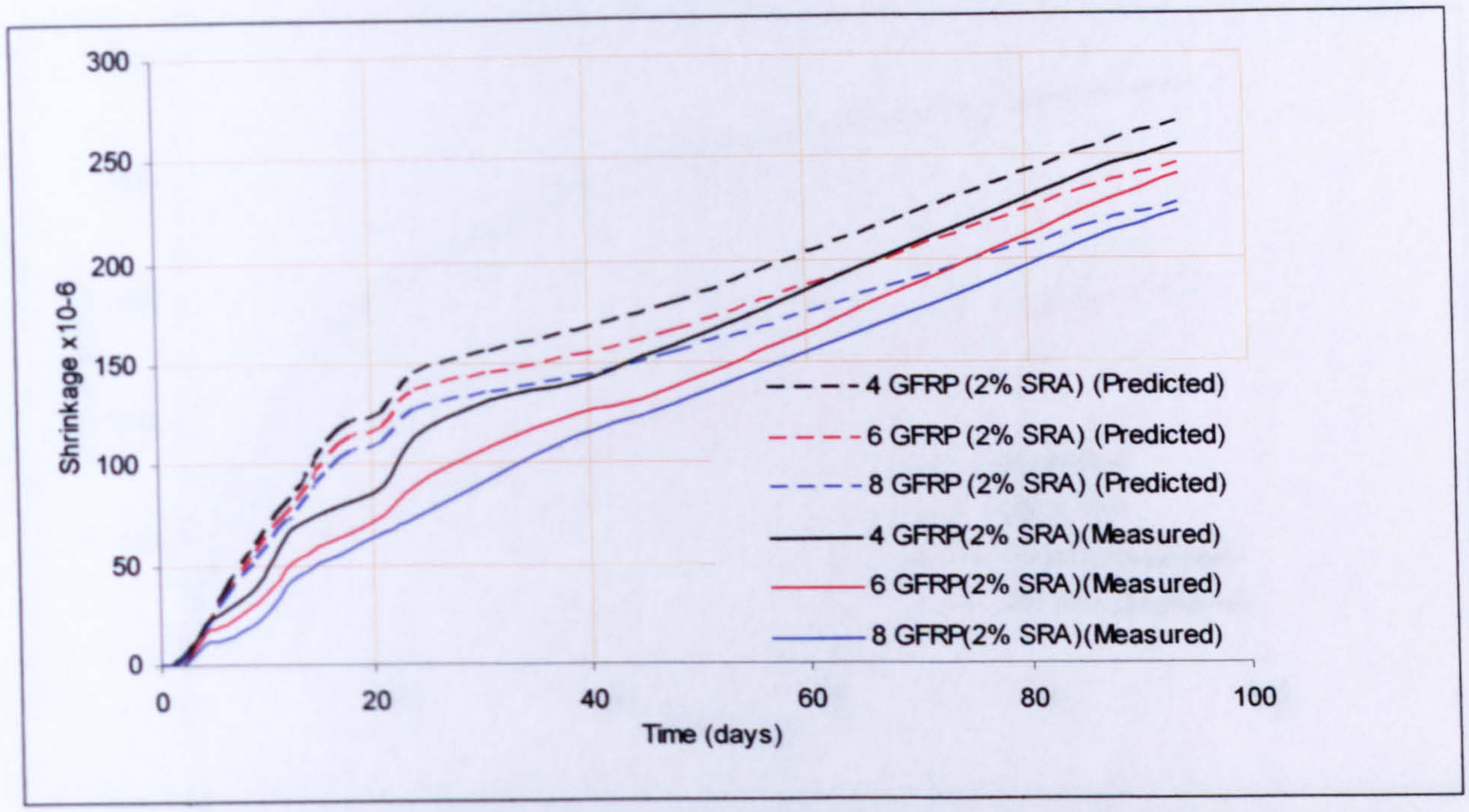

Figure 7.27: Drying shrinkage of concrete specimens reinforced with GFRP rebars and containing SRA, compared with composite modelling using the effective modulus

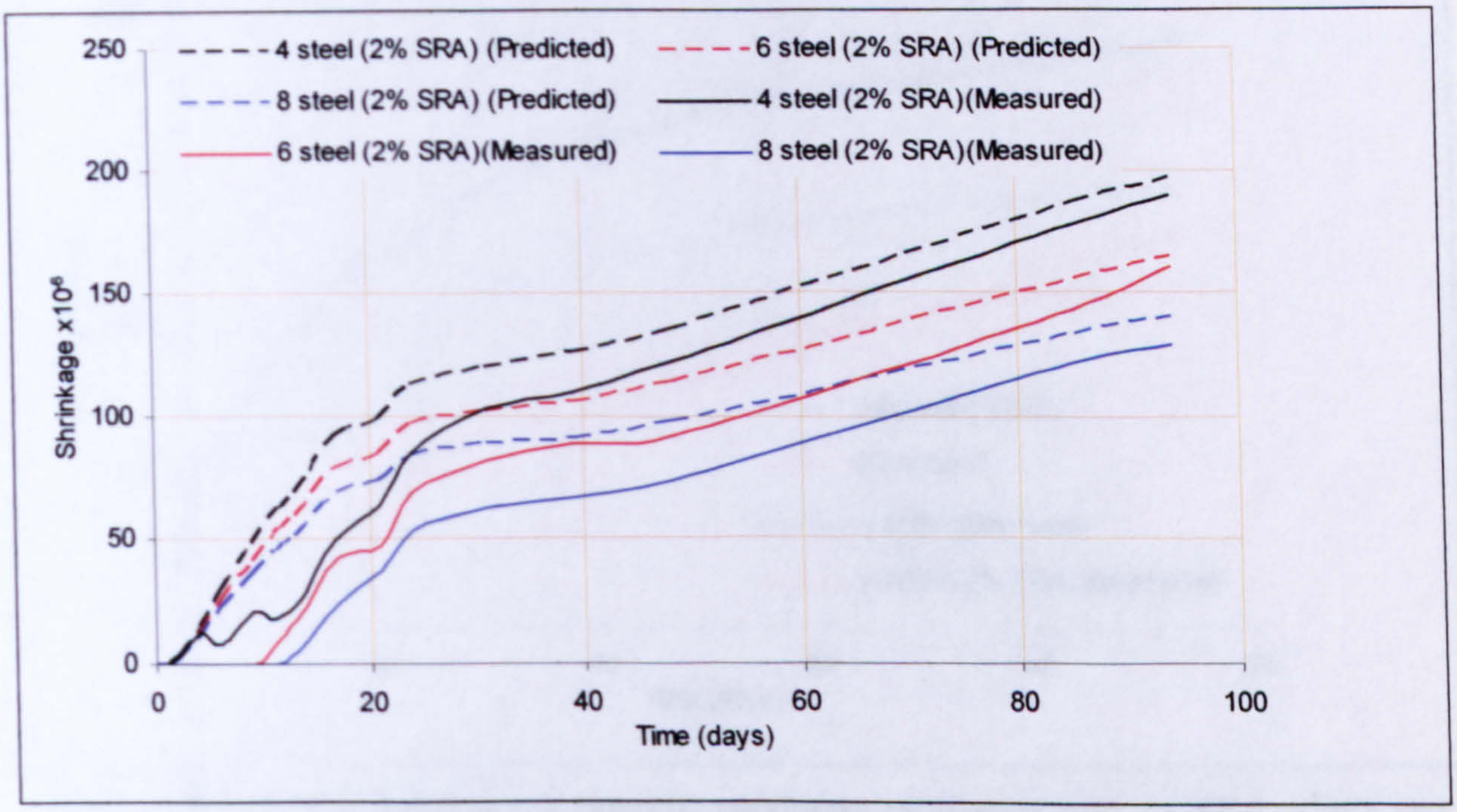

Figure 7.28: Drying shrinkage of concrete specimens reinforced with steel rebars and containing SRA, compared with composite modelling using the effective modulus

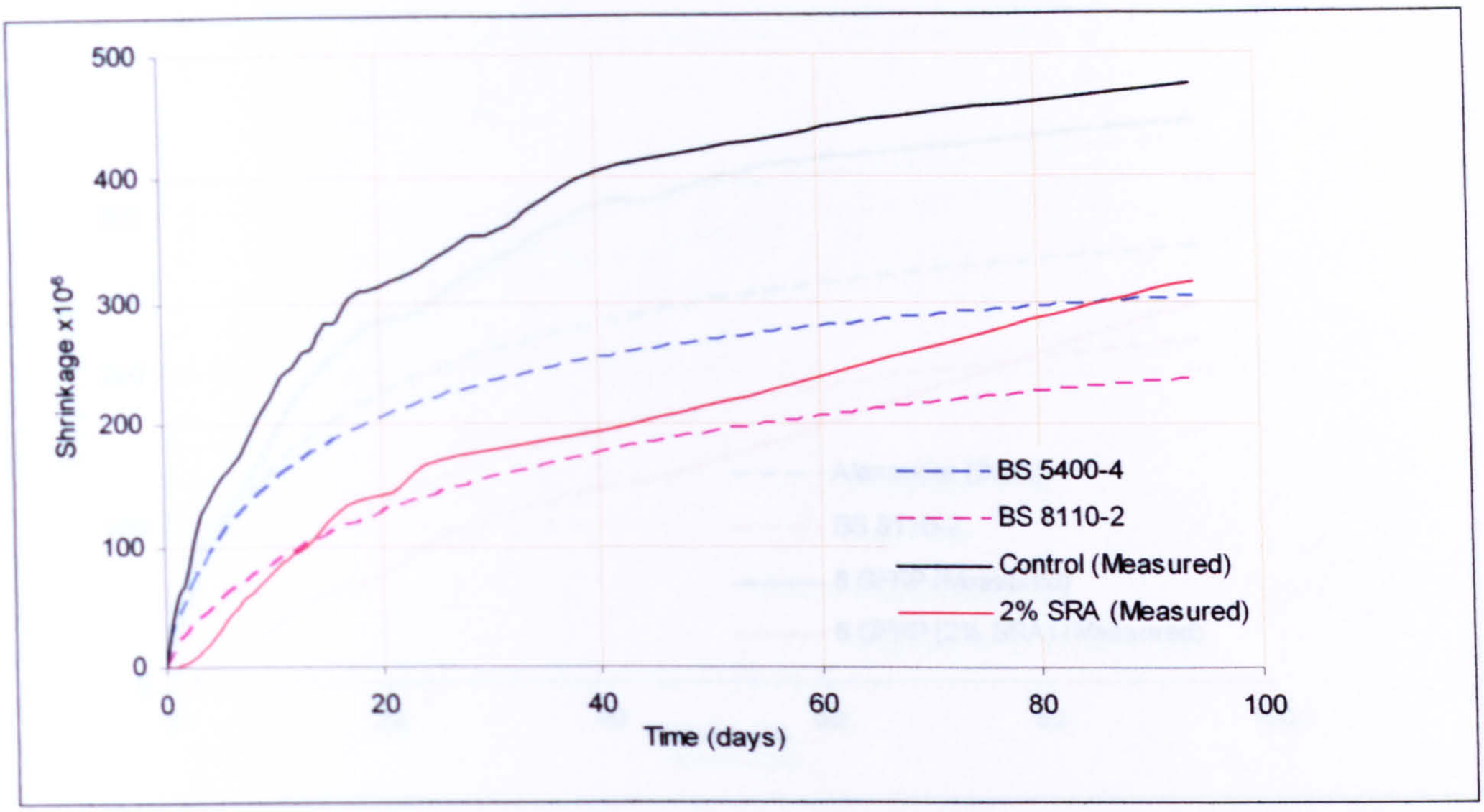

Figure 7.29: Drying shrinkage of non-reinforced concrete specimens and specimens containing SRA, compared with BS prediction methods

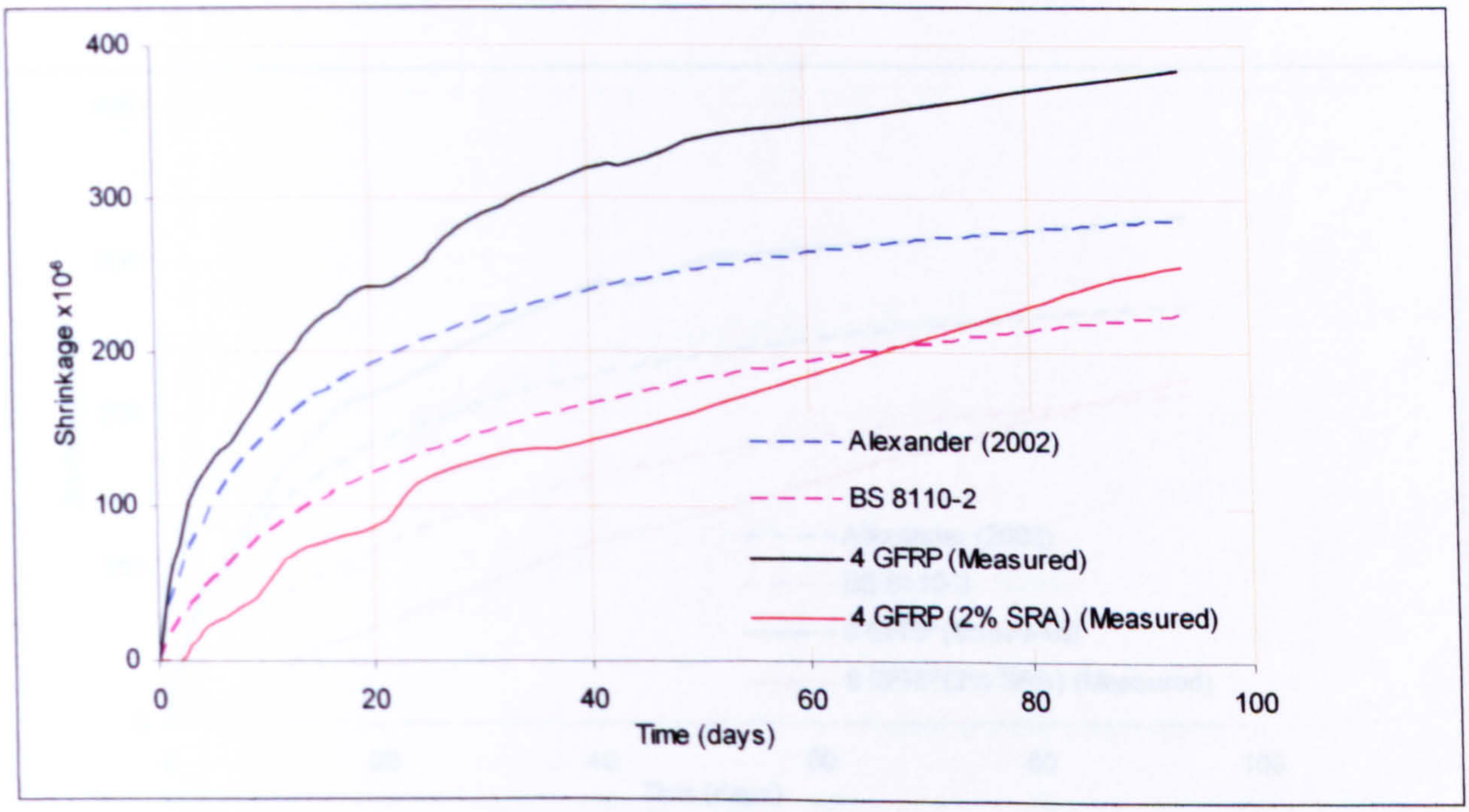

Figure 7.30: Drying shrinkage of concrete specimens reinforced with 4 GFRP rebars and specimens containing SRA, compared with BS 8110-2 and Alexander (2002) prediction methods

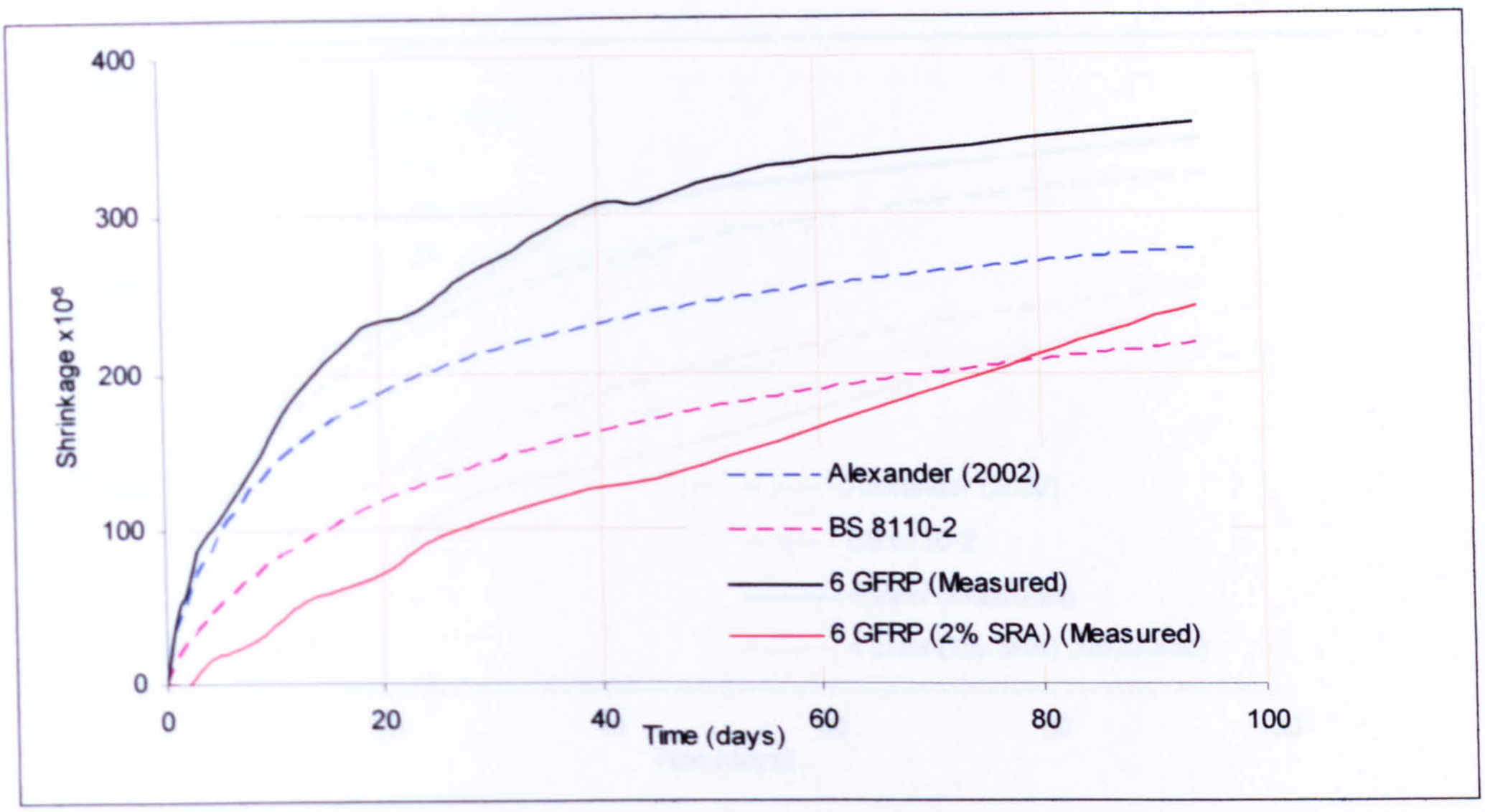

Figure 7.31: Drying shrinkage of concrete specimens reinforced with 6 GFRP rebars and specimens containing SRA, compared with BS 8110-2 and Alexander (2002) prediction methods

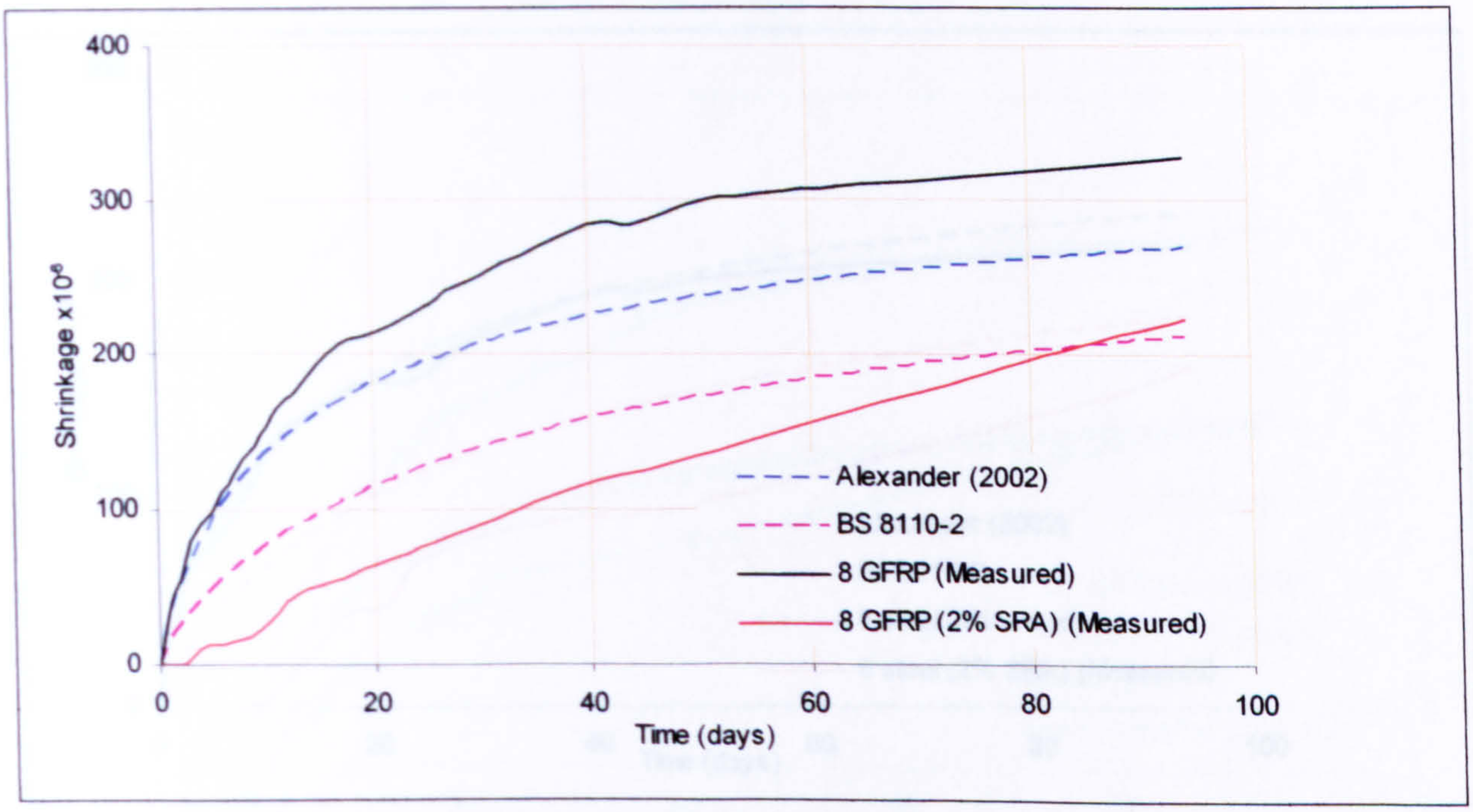

Figure 7.32: Drying shrinkage of concrete specimens reinforced with 8 GFRP rebars and specimens containing SRA, compared with BS 8110-2 and Alexander (2002) prediction methods

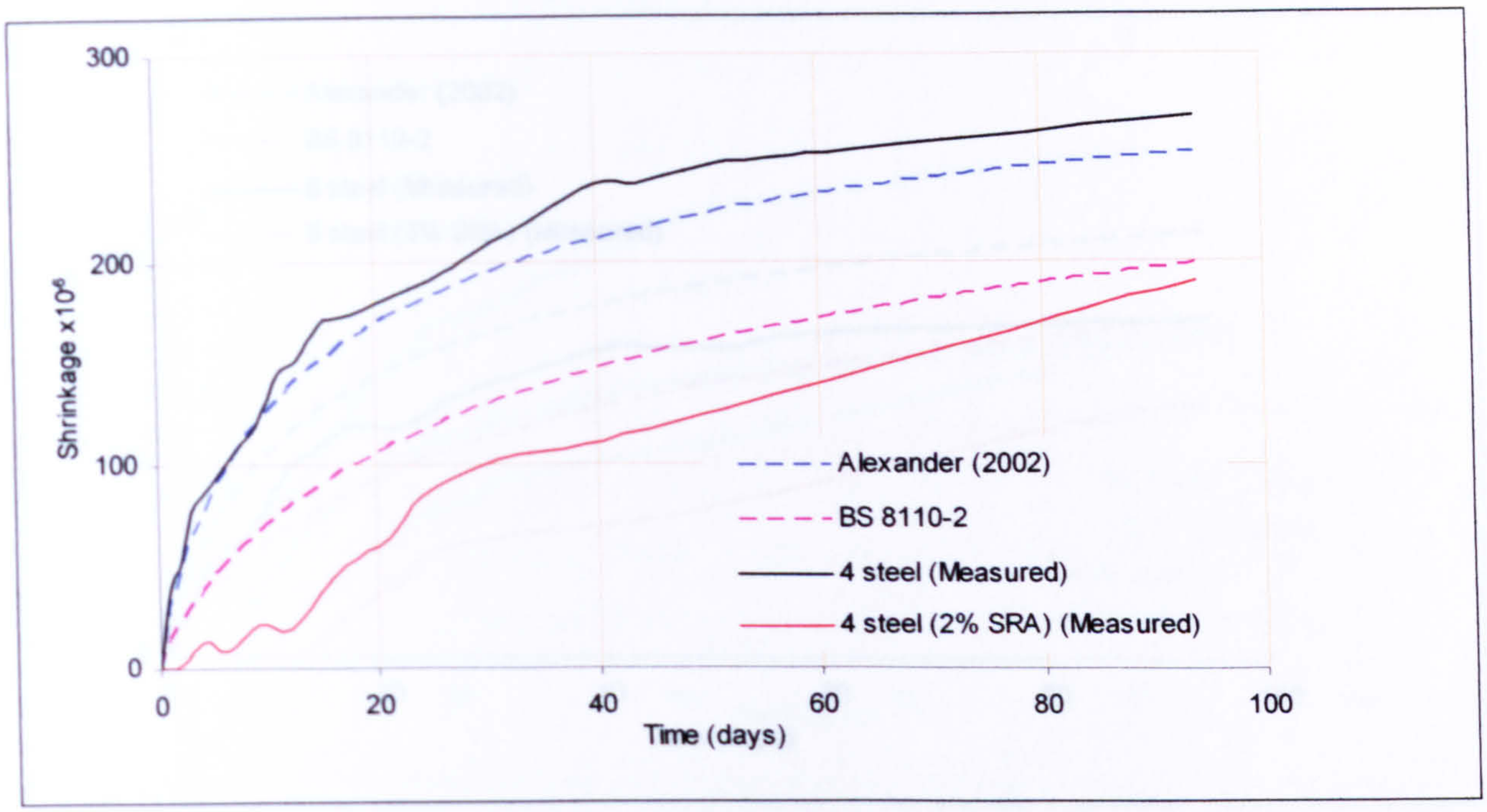

Figure 7.33: Drying shrinkage of concrete specimens reinforced with 4 steel rebars and specimens containing SRA, compared with BS 8110-2 and Alexander (2002) prediction methods

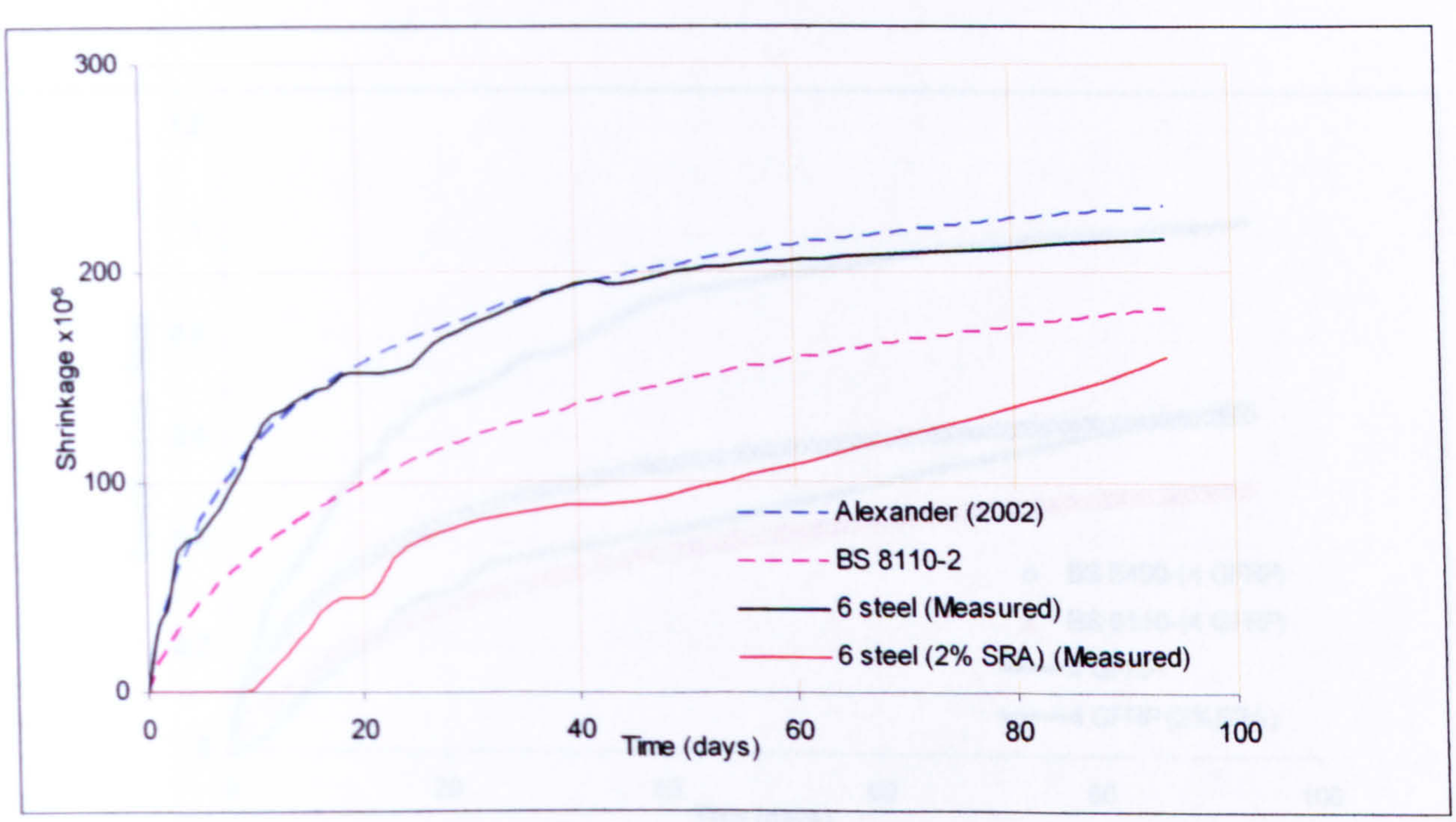

Figure 7.34: Drying shrinkage of concrete specimens reinforced with 6 steel rebars and specimens containing SRA, compared with BS 8110-2 and Alexander (2002) prediction methods

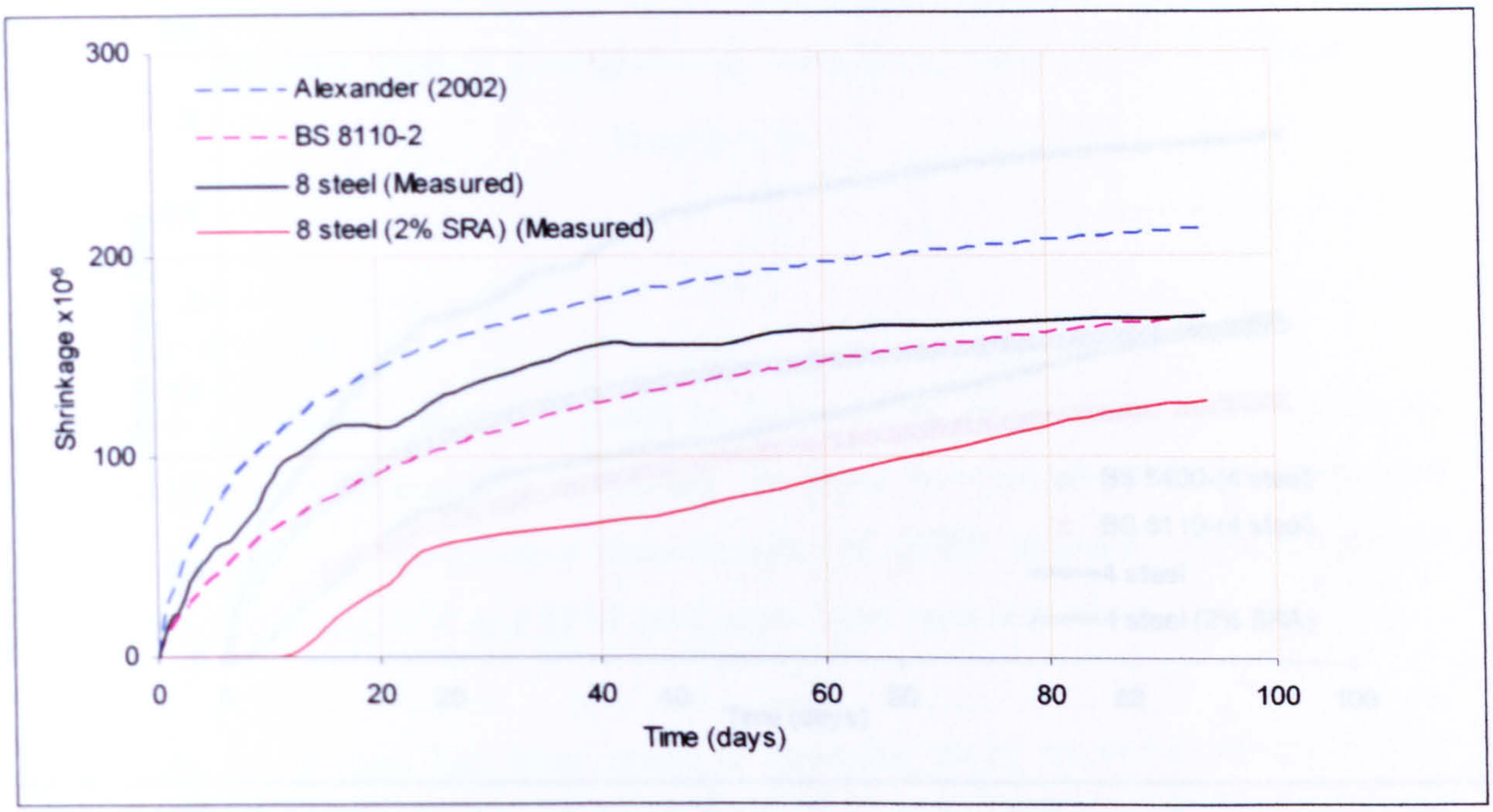

Figure 7.35: Drying shrinkage of concrete specimens reinforced with 8 steel rebars and specimens containing SRA, compared with BS 8110-2 and Alexander (2002) prediction methods

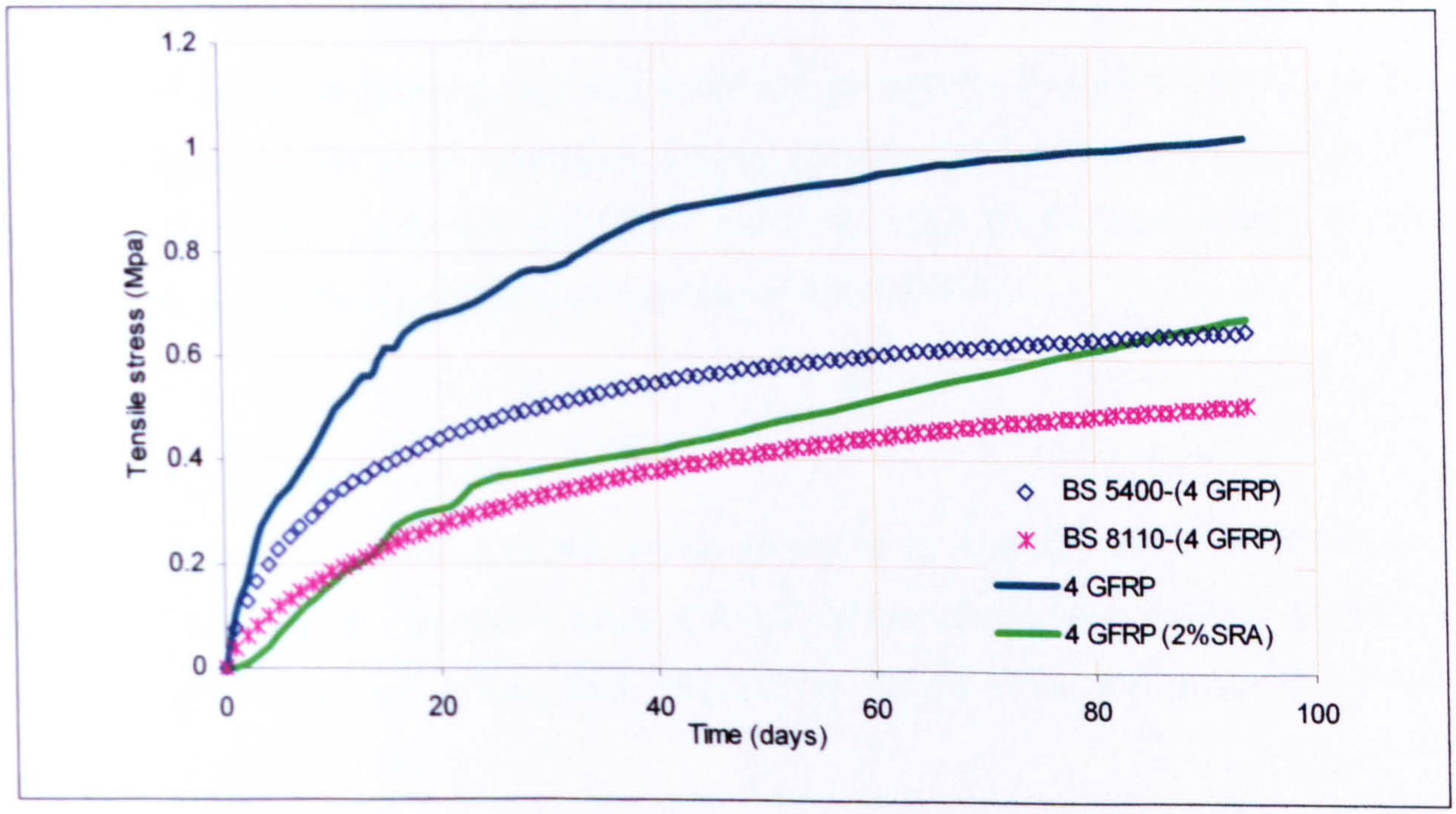

Figure 7.36: Development of tensile stress in concrete due to shrinkage restraint, caused by GFRP rebars in accordance with Alexander (2002)

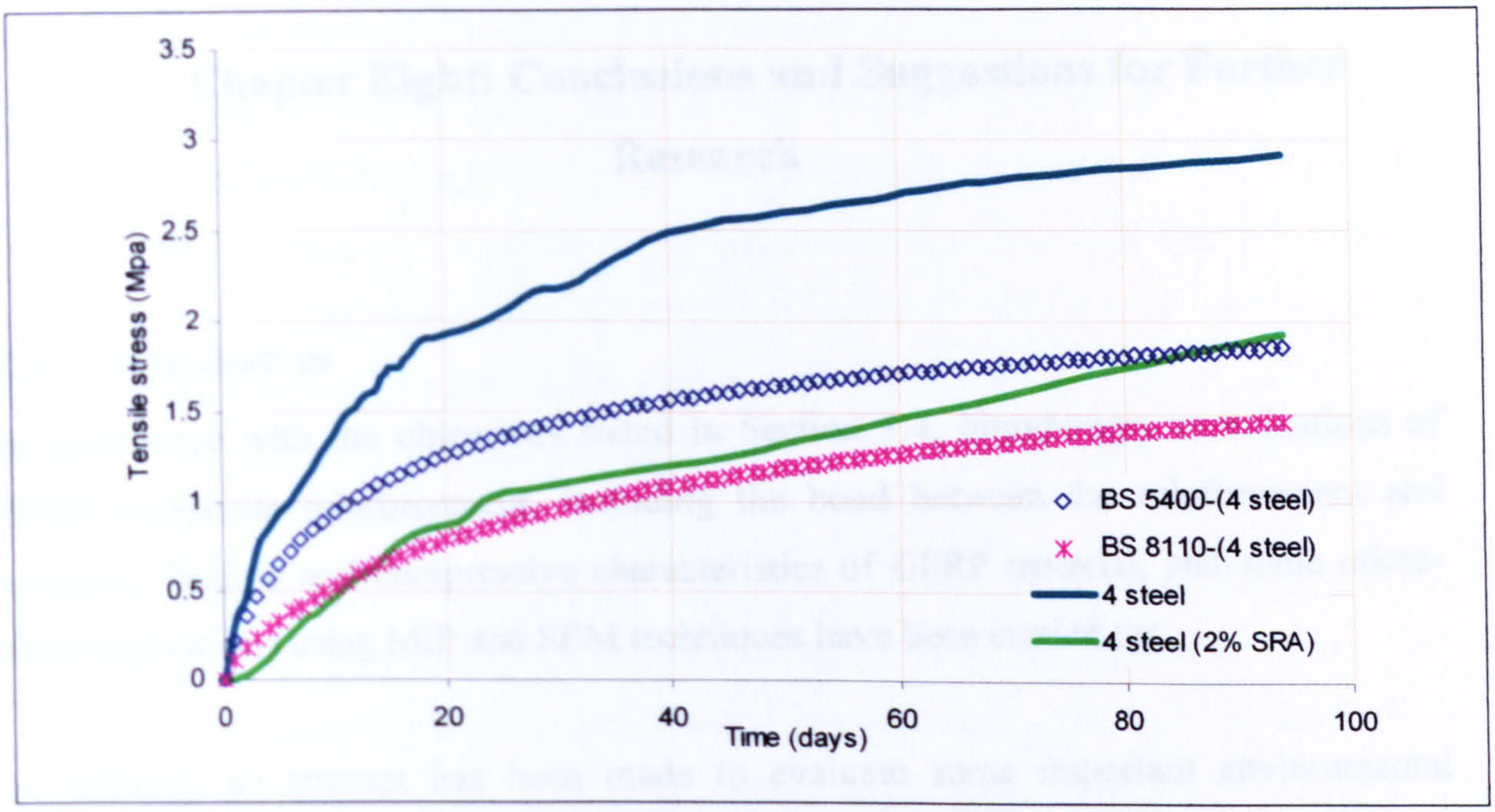

Figure 7.37: Development of tensile stress in concrete due to shrinkage restraint, caused by steel rebars in accordance with Alexander (2002)

Chapter Eight: Conclusions and Suggestions for Further Research

8.1 Introduction

In accordance with the objectives stated in Section 1.4, introductory examinations of GFRP composite reinforcement, including the bond between the reinforcement and concrete, flexural and compressive characteristics of GFRP material, and some micro-structural aspects using MIP and SEM techniques have been carried out.

In addition, an attempt has been made to evaluate some important environmental challenges of GFRP rebars in concrete by using some methods of monitoring the detrimental effects of both alkali and brine solutions on the composite rebars. The means of observing these effects include engineering tests for GFRP bars, namely flexural strength and pore structure analysis of the GFRP segments using MIP (on aged specimens).

Finally, an extensive experimental and analytical programme has been carried out in order to compare the elastic modulus, drying shrinkage and creep characteristics of concrete specimens reinforced with GFRP and steel rebars for different reinforcement ratios, with and without a shrinkage reducing admixture (SRA).

8.2 Conclusions

1. Glass fibre reinforced plastic rebars appear to be promising as a substitute for steel reinforcement in concrete in terms of durability (resistance against corrosion due to elevated pH levels and brine), high strength to weight ratio, low porosity of the composite reinforcement.

2. For the GFRP reinforcement, concrete with compressive strengths of 45 and 80MPa yielded bond strengths of 7.7 and 11.6MPa, respectively. The GFRP rebar

showed lower bond strength values than steel ones despite its greater strength. In this investigation, the effect of the concrete compressive strength on the bond capacity was clear when relatively high concrete strength (e.g. 80MPa) was used. For an increase in compressive strength of concrete of 1.78, the bond strength of GFRP reinforced concrete increased by 1.5 times. Therefore, it is recommended to use high-strength concrete when FRP reinforcements are utilised, especially that ACI 440 (2001) recommends the use of such concrete, because high-strength concrete allows for better use of high-strength properties of FRP rebars and can increase the stiffness of the cracked section.

3. The modulus of elasticity of GFRP in flexure was about 41GPa and in compression was 48GPa, which is approximately 25% of that of steel rebars. The variation in compression and flexural stiffness results was due to different methods of testing and the anisotropic nature of the GFRP composite. The lower modulus of elasticity of GFRP rebars has an effect on the increase in the deflection of beams reinforced by GFRP rebars, hence high concrete strength is recommended as the increased deflection would increase compressive loads on concrete. In addition, the brittleness of high strength concrete, in comparison to normal strength concrete, can reduce the deformability of the flexural member.

4. For the GFRP tested in this investigation, the average compressive strength was 602MPa with a maximum strain of 0.01358, and the average flexural strength was 1315MPa with a maximum strain of 0.034. Furthermore, the material exhibited elastic behaviour up to failure with no yielding as in steel. The yielding of the steel provides ductility and hence an early warning of failure in flexural concrete elements reinforced with steel. The non-ductile behaviour of GFRP reinforcement necessitates a reconsideration of the so-called under-reinforced flexural design philosophy. Anyhow, in order to compensate for the lack of ductility, a reinforced flexural concrete element should possess a higher margin of safety against failure than that used in steel reinforced concrete.

5. As GFRP is a composite material, its properties could be sensitive to any changes in the components. Therefore, the span to depth ratio (in the flexural test for FRP rebars) should not be taken from the standard tests directly, instead several attempts

should be carried out until the best one to achieve satisfactory failure mode is obtained; in this investigation the ratio was 24.

6. The MIP test showed the GFRP composite to have a low total porosity namely 2.641% and a cumulative intrusion of 0.0132 ml/g, which should provide protection to its core. The pore distribution was also uniform.

7. Developing SEM images could be added to the set of quality control tests to ensure that the composite materials satisfy the requirements, such as: fibres condition during manufacturing and whether or not the resin matrix provides protection to the fibres.

8. The alkali attack mechanism was similar to that of brine solution; however the former was more severe because alkalinity enhances fibre dissolution and matrix hydrolysis, followed by interface de-bonding. The flexural strength retention after 270 days for the composite aged in brine at 60°C and 20°C was about 64% and 85%, respectively. While in alkali solutions, the flexural strength retention after 270 days for the composite aged at 60°C was about 47%, and that at 20°C was around 73%.

9. The effect of higher temperatures was reflected in the increased rate of degradation. Although this effect on degradation was more pronounced at longer ages of exposure. For example, despite the big difference between the strength retention after 270 days, the degradation after 30 days was in close agreement, i.e. the strength reductions of 18% and 11% for aging at 60°C and 20°C in alkali solutions, respectively, were recorded.

10. In this investigation, aging in different solutions did not affect the failure mode of the GFRP rebars in the flexural test. Therefore, same span length was used for aged specimens as well. In addition, aged specimens continued to exhibit the elastic behaviour up to failure.

11. In all aging solutions, porosities for all specimens increased and flexural strength decreased but at different rates as a result of different susceptibilities of GFRP to different aggressive environments. An overall correlation between ultimate flexural

degradation and porosity for all detrimental environments investigated in this research was found (Equation (6.6)). In general, in all aging solutions, the longer the specimens were exposed, the more mechanical degradation occurred.

12. MIP examinations of aged specimens indicated an increase in larger pores at the expense of smaller ones. In turn, easier access by hostile ions to the load bearing component, i.e. glass fibres, could be expected.

13. Distortion of the pore structure of the composite material due to aging in alkali solutions was more pronounced than in the brine solutions for each set of temperatures (i.e., aging in alkali caused more micro-cracks and openings than in brine aging at 60°C, and 20°C). As a result, more strength degradation occurred with alkali aging than with brine solution.

14. Volume and stiffness of reinforcement influenced the movement characteristics of reinforced concrete. By and large, as the ratio and elastic modulus of reinforcement increase, the movement restraints increase. Similar effects can be stated for concrete specimens made with the SRA.

15. The lower stiffness of GFRP rebars reduces the degree of concrete restraint to movement, therefore less internal tensile stress in concrete is developed and less microcracks are expected.

16. The inclusion of SRA caused a reduction in the following concrete properties:

- Compressive strength of non-reinforced specimens by 21.5%.

- Elastic modulus by 14% for non-reinforced specimens, and for concrete specimens reinforced with GFRP rebars the reduction in elastic modulus was approximately 17%. For concrete specimens reinforced with steel rebars the reduction was approximately 3.5%.

- **Total time-dependent strain after three months, by an overall average of 37.3% after 94 days of loading and drying under the conditions of this investigation, for all types and amounts of reinforcement.**

- Drying shrinkage after three months, by 34% for non-reinforced specimens and for concrete specimens reinforced with GFRP rebars the average shrinkage reduction was 32%. For concrete specimens reinforced with steel rebars the reduction was approximately 26%. The average overall reduction is 29.8% (this includes non-reinforced and reinforced specimens).

- Total creep after three months, by 48% for non-reinforced concrete specimens. For concrete specimens reinforced with GFRP and steel rebars the average reduction was 55%. The total creep reduction was larger than the drying shrinkage reduction.

17. Several methods of prediction as given in Codes of Practice were used to compare estimated values with the experimental results. For predicting the modulus of elasticity of non-reinforced concrete with and without SRA, BS 8110 is recommended as it had a maximum error of 9%, although all other methods considered in this investigation yielded relatively high accuracy. For prediction of creep coefficient of non-reinforced concrete, both BS 8110 and BS 5400 were reliable for concrete mix without SRA. For the SRA mix, ACI 209 was more accurate. The accuracy of BS 5400 and Gardner and Zhao (1993) methods were relatively good for predicting drying shrinkage of plain concrete with and without SRA.

18. The accuracy of predicting the reduced moduli (to allow for creep) for non-reinforced concrete was very good for all methods especially those of BS 8110 and BS 5400 with a maximum error of 23% and 11% for mixes with and without SRA. The reduced moduli were given by EM and AAEM methods.

19. The accuracy of predicting the modulus of elasticity of reinforced concrete by the proposed composite model with $E(t_0)$ obtained from the BS8110 was the highest with a maximum error of 16%. When the measured values of $E(t_0)$ for non-reinforced

concrete were used in the proposed composite model, the effect on accuracy was an improvement.

20. Reduced moduli of reinforced concrete were estimated with the BS 8110 and BS 5400 methods (to predict modulus of elasticity of non-reinforced concrete), and the EM and AAEM by the proposed composite model. Estimates had a maximum error of 26% and 44% for specimens reinforced with GFRP and steel, respectively.

21. When measured values of the modulus of elasticity of non-reinforced concrete ($E(t_0)$) and measured EM and AAEM were used together with the proposed composite model, the accuracy improved considerably.

22. Using the proposed composite model to predict the restrained shrinkage of reinforced concrete with both drying shrinkage and elastic modulus being provided from the measurements of the non-reinforced specimens, yielded relatively high accuracy, but not for the SRA mix. However, when reduced modulus was used instead of elastic modulus, the accuracy improved considerably for both concrete mixes.

23. The development of tensile stress in concrete due to shrinkage restraint by steel rebars was greater than that for GFRP rebars.

8.3 Suggestions for further work

1. The bond capacity of FRP rebars in high strength concrete should be investigated further, especially when additives that contribute to the concrete strength are used.

2. Elevated temperatures increase the rate of degradation of GFRP in all aging solutions and that can have an adverse effect on determining the degradation progress. To avoid this, either tests at normal temperature should be performed or testing the aged specimens more frequently (with shorter intervals) to monitor the changes more clearly.

3. The adverse effects on the GFRP rebars due to the alkaline and brine solutions are higher than that of the actual cement paste because the ions are more mobile. In

addition, high temperatures increase the degradation of GFRP, because chemical reactions are enhanced at elevated temperatures. It is recommended, therefore, that more investigations are performed to correlate the results of direct exposure of composite rebars to chemical solutions to those embedded in concrete.

4. Specimens with SRA should undergo shrinkage and creep tests for longer periods of time than the three-month period as in this investigation, at least until the rate of movement becomes very small.

5. Existing structures reinforced with FRP should be investigated and the results correlated with those of laboratory specimens, especially since fibre optic strain sensors embedded in the FRP rebars have shown reliable strain monitoring (Kalamkarov *et al.*, 2000).

6. In this investigation, the measurements of creep, drying shrinkage and elastic modulus of concrete specimens were limited to one curing condition, namely 28 days in the fog room. Also the specimens were stored under one environmental condition, namely temperature at 20°C and relative humidity of 67% due to limitation of time and reinforcement material. Other curing conditions and storage conditions, such as wet/dry cycles, a hot-dry environment and aggressive solutions could be investigated.

7. The assumption that restraint by reinforcement is the same for creep and elastic strain, so that creep coefficient is independent of reinforcement, did not seem to be valid for this investigation. It is suggested that the assumption be re-examined by a thorough literature review and by experimental tests.

References

- ACI Committee 201, (1991). "Guide to Durable Concrete (ACI 201)", *ACI Material Journal*, Vol. 88, No. 5, 544-582.
- ACI Committee 209, (1982). "Prediction of Creep, Shrinkage, and Temperature Effects in Concrete Structures (ACI 209-82)", *American Concrete Institute*, Detroit, Michigan.
- ACI Committee 209, (1992). "Prediction of Creep, Shrinkage, and Temperature Effects in Concrete Structures (ACI 209R-92)", *American Concrete Institute*, Detroit, Michigan.
- ACI Committee 318, (1989). "Building Code Requirement for Reinforced Concrete (ACI 318M-89)", *American Concrete Institute*, Detroit, Michigan.
- ACI Committee 408, (1992). "State-of-the-Art Report on Bond Under Cyclic Loads (ACI 408-92)", *American Concrete Institute*, Detroit, Michigan.
- ACI Committee 440, (1996). "State-of-the-Art Report on Fibre Reinforced Plastic Reinforcement for Concrete Structure (ACI 440R-96)", *American Concrete Institute*, Farmington Hills, Michigan.
- ACI Committee 440, (2001). "Guide for the Design and Construction of Concrete Reinforced with FRP Bars (ACI 440.1R-01)", *American Concrete Institute*, Farmington Hills, Michigan.
- Adams, P.B., (1984). "Glass Corrosion. A Record of the Past? A predictor of the Future?", *Journal of Non-crystalline Solids, Vol. 67, No. 4*, 193-205.
- Adimi, M.R. and Boukhili, R. (1998). "Influence of Resin and Temperature on the Interlaminar Shear Fatigue of Glass Fibre Reinforced Composite Rods", *Durability of Fibre Reinforced Polymer (FRP) Composites for Construction, Proceedings of the First International Conference (CDCC'98), Sherbrook (Quebec) Canada,* August 5-7, 681-690.
- Al Cheikh, A. and Murat, M., (1988). "Kinetics of Non-congruent Dissolution of E-glass Fibre in Saturated Calcium Hydroxide", *Cement and Concrete Research, Vol. 18, No. 6*, 943-950.
- Alexander, S., (2002). "Understanding Shrinkage and its Effect: Part 1", *Concrete*, October, 61-63.
- Almusallam, T.H., Al- Salloum, Y.A., Alsayed, Y.A., and Amjad, M., (1997). "Behaviour of Concrete Beams Doubly Reinforced by FRP bars", *Proceedings of*

the Third International Symposium on Non-metallic (FRP) Reinforcement for Concrete Structures (FRPRCS-3), Japan Concrete Institute, Sapporo, Japan, Vol. 2, 471-478.

- Al-Salloum, Y.A., Alsayed, Y.A., Almusallam, S.H., (2000). "Deflection Model for Concrete Beams Reinforced by GFRP Bar", *Proceeding of the ACUN-2 International Composites Conference – Composites in the Transportation Industry*, Vol. 1, 78-83.
- Alsayed, S. and Alhozaimy, A. (1998). "Effect of High Temperature and Alkaline Solutions on the Durability of GFRP Bars", *Durability of Fibre Reinforced Polymer (FRP) Composites for Construction, Proceedings of the First International Conference (CDCC'98), Sherbrook (Quebec) Canada*, 623-634.
- Alsayed, S.H., (1998). "Flexural Behaviour of Concrete Beams Reinforced with GFRP Bars", *Cement and Concrete Composites*, Vol. 20, 1-11.
- Al-Zahrani, M.M., Al-Dulaijan, S.U., Nanni, A., Bakis, C.E., and Boothby, T.E., (1999). "Evaluation of Bond Using FRP Rods with Axisymmetric Deformations", Construction and Building Materials, Vol. 13, 299-309.
- Ananta, S, (1999). "Crystal Structural Microstructural Design of Perovskite Relaxor Ceramics", *Ph.D Thesis*, University of Leeds, U.K.
- Anderson, G.R., Munley, E., and Bank, L.C., (1994). "Durability of Concrete Reinforced with Pultruded Fibre Reinforced Plastic Grating", *Plastics in Building Construction*, Vol. 18, No. 8, 6-12.
- ASTM D 3916 (1998) "Standard Test Method for Tensile Properties of Pultruded Glass-fibre-reinforced Plastic Rod". *ASTM*, West Conshohocken, 502-505.
- ASTM D 3918 (1998). "Standard Definitions and Terminology of Terms Relating to Reinforced Plastic Pultruded Products". *ASTM*, West Conshohocken, 510-512.
- ASTM D 4476 (1997) "Standard Test Method for Flexural Properties of Fibre Reinforced Pultruded Plastic Rods". *ASTM*, West Conshohocken, 65-69.
- ASTM D 695 (1996) "Standard Test Method for Compression Properties of Rigid Plastics". *ASTM*, West Conshohocken, 77-83.
- Bajracharya, Y.M., (2001). "Engineering and Performance Properties of Metakaolin-OPC Concrete", *Ph.D. Thesis*, University of Leeds, UK.

- Bakis, C.E., Freimanis, A.J., Gremel, D., and Nanni, A., (1998). "Effect of Resin Material on Bond and Tensile Properties of Unconditioned and Conditioned FRP Reinforcement Rods" *Durability of Fibre Reinforced Polymer (FRP) Composites for Construction, Proceedings of the First International Conference (CDCC'98), Sherbrook (Quebec) Canada*, 525-535.
- Bank, L.C., Puterman, M., and Katz, A., (1998). "The Effect of Material Degradation on Bond Properties of Fibre Reinforced Plastic Reinforcing Bars in Concrete", *ACI Materials Journal*, Vol. 95, No. 3, 232-243.
- Barkatt, A. and Bank, L.C., (1995). "Environmental Degradation of Fibre Reinforced Plastics Materials in Neutral, Acidic and Basic Aqueous Solutions", *Corrosion 95, The NACE International Annual Conference and Corrosion Show,* NACE International, Houston, TX, Paper No. 138, 1-15.
- Bazant, Z.P., and Xi, Y., (1994). "Drying Creep of Concrete: Constitutive Model and New Experiments Separating its Mechanisms", *Materials and Structures*, Vol. 27, 3-14.
- Bedard, C., (1992). "Composite Reinforcing Bars: Assessing their Use in Construction", *Concrete International*, 55-59.
- Benmokrane, B., Chaallal, O., and Masmoudi, R., (1995). "Glass Fibre Reinforced Plastics (GFRP) Rebars for Concrete Structures", *Construction and Building Materials*, Vol. 9, No. 6, 353-364.
- Benmokrane, B., Rahman, H., Ton-That, M. and Robert, J., (1998). "Improvement of the Durability of FRP Reinforcement for Concrete Structures" *Durability of Fibre Reinforced Polymer (FRP) Composites for Construction, Proceedings of the First International Conference (CDCC'98), Sherbrook (Quebec) Canada*, 571-585.
- Benmokrane, B., Tighiouart, B., and Chaallal, O., (1996). "Bond Strength and Load Distribution of Composite GFRP Reinforcing Bars in Concrete", *ACI Materials Journal*, Vol. 93, No. 3, 246-253.
- British Standards Institution, (1983). "Method for Determination of Slump", *BSI*, London, BS 1881: Part 102.
- British Standards Institution, (1983). "Method for Determination of Flexural Strength of Concrete Beams", *BSI*, London, BS 1881: Part 118.
- British Standards Institution, (1983). "Method for Determination of Compressive Strength of Concrete Cubes", *BSI*, London, BS 1881: Part 116.

- British Standards Institution, (1983). "Method for Making Test Cubes from Fresh Concrete", *BSI*, London, BS 1881: Part 108.
- British Standards Institution, (1983). "Standard Apparatus for Compressive Strength Testing of Concrete", *BSI*, London, BS 1881: Part 117.
- British Standards Institution, (1984). "Method for Determination of Flow", *BSI*, London, BS 1881: Part 105.
- British Standards Institution, (1985). "Specification for Superplasticising Admixtures", *BSI*, London BS 5075: Part 3.
- British Standards Institution, (1990). "Steel, Concrete and Composite Bridges: Part 4-Code of Practice for Design of Concrete Bridges", *BSI*, London, BS 5400: Part 4.
- British Standards Institution, (1992). "Specification for Aggregates from Natural Sources for Concrete", *BSI*, London, BS 882.
- British Standards Institution, (1996). "Portland Cement", *BSI*, London, BS 12.
- British Standards Institution, (1998). "Fibre-reinforced Plastic Composites Determination of Flexural Properties", *BSI*, London, BS EN ISO 14125.
- British Standards Institution, (1998). "Glass Fibre Reinforced Plastics-Flexural Test-Three Point Bend Method", *BSI*, London, BS EN 2746.
- British Standards Institution, (2001). "Structural Use of Concrete: Part 2-Code of Practice for Special Circumstances", *BSI*, London, BS 8110: Part 2: 1985.
- Brooks, J.J., (1989). "Influence of Mix Proportions, Plasticisers and Superplasticisers on Creep and Drying Shrinkage of Concrete", *Magazine of Concrete Research*, Vol. 41, No. 148, 145-153.
- Brooks, J.J., and Neville, A.M., (1978). "Predicting Long-term Creep and Shrinkage from Short-term Tests", *Magazine of Concrete Research*, Vol. 30, No. 103, 51-61.
- Brooks, J.J., and Neville, A.M., (1975). "Estimating Long-term Creep and Shrinkage from Short-term Tests", *Magazine of Concrete Research*, Vol. 27, No. 90, 3-12.
- Broomfield, J.P. (1997). "Corrosion of Steel in Concrete Understanding Investigation and Repair", E & FN Spon an Imprint of Chapman & Hall, London.
- Brown, V.L., (1997). "Sustained Load Deflections in GFRP Reinforced Concrete Beams", *Proceedings of the Third International Symposium on Non-metallic (FRP) Reinforcement for Concrete Structures (FRPRCS-3)*, Japan Concrete Institute, Sapporo, Japan, Vol. 2, 495-502.

- Brown, V.L., and Bartholomew, C.L., (1993). "FRP Reinforcing Bars in Reinforced Concrete Members", *ACI Materials Journal*, Vol. 90, No. 1, 34-39.
- Burgoyne, C.J., (1993). "Should FRP be Bonded to Concrete", *Non-Metallic Reinforcement and Prestressing, American Concrete Institute, SP 138-23*, 367-380.
- Burgoyne, C.J., (1997). "Rational Use of Advanced Composites in Concrete", *Non-Metallic (FRP) Reinforcement for Concrete Structures, Proceeding of the Third International Symposium*, Vol. 1, 75-88.
- Burgoyne, C.J., and Head, P.R., (1993). "Aberfeldy Bridge – an Advanced textile Reinforced Footbridge", *TechTextil Symposium, Frankfort*, Paper No., 418.
- Cabrera, J.G., and Lynsdale, C.J., (1988). "Measurement of Chloride Permeability in Superplasticised Ordinary Portland Cement and Pozzolanic Cement Mortars", *International Conference on Measurements and Testing in Civil Engineering*, 279-291.
- Carter, H.G., and Kibler, K.G., (1978). "Langumir-Type Model for Anomalous Moisture Diffusion in Composite Resins", *Journal of Composite Materials*, Vol. 12, 118-131.
- Castro, F. P., and Carino, J.N., (1998). "Tensile and Non-destructive Testing of FRP Bars", *Journal of Composites for Construction*, Vol. 2, No. 1, 17-27.
- CEB-FIP Model Code 90 for Concrete Structures, (1990). "Evaluation for the Time Dependent Behaviour of Concrete", Bulletin d'Information No. 195, Comite European du Beton/Federation Internationale de la Precontrainte, Lausanne.
- Chaallal, O. and Benmokrane, B., (1996). "Fibre-reinforced Plastic Rebars for Concrete Applications", *Composites: Part B 27B*, 245-252.
- Chaallal, O., Benmokrane, B., and Masmoudi, R., (1992). "An Innovative Glass-Fibre Composite Rebar for Concrete Structures", *Advanced Composite Materials in Bridges and Structures*, Canadian Society for Civil Engineering, 169-177.
- Chakraborty, M., Das, D., Basu, S., and Paul, A., (1979). "Corrosion Behaviour of a ZrO_2-containing Glass in Aqueous and Alkaline Media and in a Hydrating cement Paste". *International Journal Cement Composition*, Vol. 1, No. 3, 103-109.
- Chen, R.H.L., and Choi, J.H., (2002). "Effects of GFRP Reinforcing Rebars on Shrinkage and Thermal Stresses in Concrete". *15th ASCE Engineering Mechanics Conference*, Columbia University, New York, 1-8.

- Chin, J.W., Nguyen, T., and Aouadi, K. (1997). "Effect of Environmental Exposure on Fibre-Reinforced Plastic (FRP) Materials Used in Construction", *Journal of Technology and Research*, JCTRER, Vol. 19, No. 4, 205-213.
- Chin, J.W., Haight, M.R., Hughes, W.L. and Nguyen, T., (1998). "Environmental Effects on Composite Matrix Resins Used in Construction", *Durability of Fibre Reinforced Polymer (FRP) Composites for Construction, Proceedings of the First International Conference (CDCC'98), Sherbrook (Quebec) Canada*, 229-241.
- Clarke, J., and Sheard, P., (1998). "Design Durable FRP Reinforced Concrete Structures", *Durability of Fibre Reinforced Polymer (FRP) Composites for Construction, Proceedings of the First International Conference (CDCC'98), Sherbrook (Quebec) Canada*, 13-24.
- Clarke, J.L. (1996). "Structural Design of Polymer Composites", Edited by Clarke, J.L., E & FN Spon, an Imprint of Chapman & Hall.
- Clarke, J.L. (1998). "Steeling Concrete with Fibre Reinforced Plastics", *Materials World*, Vol. 6, No. 2, 78-80.
- Clarke, J.L. (1999). "Fiber-reinforced Plastic Reinforcement for Concrete", *Concrete*, Current Practice Sheet No. 114, 15-16.
- Cook, R.A., and Hover, K.C., (1993)."Mercury Porosimetry of Cement-Based Materials and Associated Correction Factors", *ACI Materials Journal*, Vol. 90, No. 2, 152-161.
- Crank, J., (1986). "The Mathematics of Diffusion", Clarendon Press, Oxford 2nd edition.
- Daniel, I.M. and Ishai, O. (1994). "Engineering Mechanics of Composite Materials", Oxford University Press, Oxford.
- Devalapura, R.K., Gauchel, J.V., Greenwood, M.E., Hankin, A., and Humphrey, T., (1997). "Long-term Durability of Glass-fibre Reinforced Polymer Composites in Alkaline Environments", *Non-Metallic (FRP) Reinforcement for Concrete Structures, Proceedings of the 3rd International Symposium*, Vol. 2, 83-90.
- Diamant, Y., Marom, G., Broutman, L.J., (1981). "The Effect of Network Structure on Moisture Absorption of Epoxy Resins", *Journal of Applied Polymer Science*, Vol. 26, 3015-3025.
- Diamond, S., (1996). "Digital Images Publication for Backscatter SEM Micrographes", *Cement and Concrete Research*, Vol. 26, No. 1, 3-7.

- Dimbleby, V., and Turner, W.S., (1926). "The Relationship Between Chemical Composition and the Resistance of Glasses to the Action of Chemical Reagents. Part 1", *Journal Society Glass Technology*, Vol.10, 304-358.
- Dokun, O.D., Jacobs, L.J. and Haj-Ali, R.M. (2000). "Ultrasonic Monitoring of Material Degradation in FRP Composites", *Journal of Engineering Mechanics*, Vol. 126, No. 7, 704-710.
- Domone, P.L.J. (2001). "Construction Materials Their Nature and Behaviour", 3rd Edition, Spon Press London, Edited by Illston, J.M. and Domone, P.L.J.
- Doremus, R.H., Mehrota, Y., Lanford, W.A. and Burman, C., (1983). "Reaction of Water with Glass: Influence of Transformed Surface Layer", *Journal of Materials Science, Vol. 18, No. 2*, 612-622.
- Drzal, L.T., (2001). "Interfaces and Interphases", *ASM Handbook Volume 21 Composites*, Vol. 21, 169-179.
- Ehsani, M.R., (1993). "Glass-fibre Reinforced Bars", *Alternative Materials for the Reinforcement and Prestressing of Concrete*, Blackie Academic & professional an Imprint of Chapman & Hall, London. Edited by Clarke, J.L.
- Ehsani, M.R., Saadatmanesh, and Tao, S., (1997). "Bond Behaviour of Deformed GFRP Rebar", *Journal of Composite Materials*, Vol. 31, No. 14, 1413-1430.
- Ehsani, M.R., Saadatmanesh, and Tao, S., (1995). "Bond of Hooked Glass Fibre Reinforced Plastic (GFRP) Reinforcing Bars to Concrete". *ACI Materials Journal*, Vol. 92, No. 4, 391-400.
- Erik, M.A., and Rizkalla, S.H., (1993). "Anchorages for FRP Reinforcement", *Concrete International*, Vol. 15, No. 6, 54-59.
- Faza, S.S., and GangaRao, H.S., (1990). "Bending and Bond Behaviour of Concrete Beams Reinforced with Plastic rebars", *Transportation Research Record 1290*, 185-193.
- Faza, S.S., and GangaRao, H.S., (1993). "Glass FRP Reinforcing Bars for Concrete", *Fibre-reinforced Plastic (FRP) Reinforcement for Concrete Structures-properties and Applications*, edited by Nanni, A., Elsvier Science Publishing Co. Inc., New York, N.Y., 167-188.
- GangaRao, V.S., and Vijay, P.V., (1997). "Aging of Structural Composites Under Varying Environmental Conditions", *Non-metallic (FRP) Reinforcement for Concrete Structures, Proceedings of the 3rd International Symposium*, Vol. 2, 91-98.

- Gardener, N.J., and Zhao, J.W., (1993). "Creep and Shrinkage Revisited", ACI Materials Journal, Vol. 90, No. 3, 236-246.
- Gere, J.M., and Timoshinko, S.P. (1992). "Mechanics of Materials", Chapman & Hall, London, 3rd edition.
- Gilbert, R. (1988). "Time Effects in Concrete Structures", Elsevier, New York.
- Gilbert, R. and Gowripalan, N, (1993). "Long-Term Behaviour of Prestress Concrete Beams Using Nonmetallic Tendons", *Proceedings of Concrete 2000, University of Dundee*, 255-264.
- Gjorv, O.E., and Vennesland, O., (1976). "Sea Salts and Alkalinity of Concrete", *ACI Material Journal*, Vol. 73, No. 9, 512-516.
- Glaster, R.E., Moore, R.L., and Chiao, T.T., (1983). "Life Estimation of an S Glass/Epoxy Composite Under Sustained Tensile Loading", *Composite Technology Review*, Vol. 5, No. 21.
- Glaster, R.E., Moore, R.L., and Chiao, T.T., (1984). "Life Estimation of an S Glass/Epoxy Composite Under Sustained Tensile Loading", *Composite Technology Review*, Vol. 6, No. 26.
- Grace, N.F., Soliman, A.K., Abdel, G., and Saleh, K.R., (Nov, 1998). "Behaviour and Ductility of Simple and Continuous FRP Reinforced Beams", *Journal of Composites for Constructions*, Vol. 2, No., 4, 186-194.
- Gupta, V.B., Drzal, L.T., Lee, C.Y.C. and Rich, M.J., (1985). "The Temperature-dependence of Some Mechanical Properties of a Cured Epoxy resin System", *Polymer Engineering and Science*, Vol. 25, 812-823.
- Hall, T., and Ghali, A., (2000). "Long-term Deflection Prediction of Concrete Members Reinforced with Glass Fibre Reinforced Polymer Bars", *Canadian Journal of Civil Engineering (Canada)*, Vol. 27, No. 5, 890-898.
- Hassan, K.E., (1993). "Influence of Surface Treatments on Durability Performance of Concrete", *Ph.D. Thesis*, University of Leeds, UK.
- Hassan, K.E., Brooks, J.J., and Al-Alawi, L., (2001). "Compatibility of Repair Mortars with Concrete in a Hot-dry Environment", *Cement and Concrete Composites*, Vol. 23, 93-101.
- Hassan, K.E., Cabrera, J.G., and Head, M.K., (1998). "The Effect of Aggregate Type on the Properties of High Performance, High Strength Concrete", *International Conference on HPHSC*, Perth, Australia. Edited by Rangan, B.V., and Patnaik, A.K.

- Head, M.K., (2001). "Influence of the Interfacial Transition Zone (ITZ) on the Properties of Concrete", *Ph.D. Thesis*, University of Leeds, UK.
- Holte, L.E., Dolam, C.W., and Schamidt, R.J., (1993). "Epoxy Socketed Anchors for Non-metallic pressurising Tendons", *Fibre-Reinforced-Plastic Reinforcement for Concrete Structures- International Symposium ACI SP-138*, edited by Nanni, A. and Dolan, C.W., American Concrete Institute, Farmington Hills, Michigan, 381-400.
- Iyer, S.L., and Anigol, M., (1991). "Testing and Evaluating Fibreglass, Graphite and Steel Cables for Pretensioned Beams". *Advanced Composite Materials in Civil Engineering Structures, Proceedings of the Specialty Conference, ASCE, Las Vegas*, 44-56.
- Jones, R.F., (1998). "Guide to Short Fibre Reinforced Plastics", Hanser Publishers, Munich.
- Kachlakev, D.I., (2000). "Experimental and Analytical Study on Unidirectional and Off-axis GFRP Rebars in Concrete", *Composites: Part B Engineering*, Vol. 31, 569-575.
- Kachlakev, D.I., and Lundy, J.R., (1998). "Bond Strength Study of Hollow Composite Rebars with Different Micro Structure", *Proceedings of the Second International Conference on Composites in Infrastructure (ICCI-98)*, Tucson, Ariz., 1-14.
- Kachlakev, D.I., and Lundy, J.R., (1999). "Performance of Hollow Glass Fibre-Reinforced Polymer Rebars", *Journal of Composites for Construction*, Vol. 3 No. 2, 87-91.
- Kajorncheappunngam, S., Gupta, R.K., and GangaRao, H.V.S., (2002). "Effect of Aging Environment Degradation of Glass-reinforced Epoxy", *Journal of Composites for Construction*, Vol. 6, No. 1, 61-69.
- Kalamkarvo, A.L., MacDonald, D.O., Fitzgerald, S.B. and Georgiades, A.V., (2000). "Relaiability Assessment of Pultruded FRP Reinforcements with Embedded Fibre Optic Sensors", *Composite Structures*, Vol. 50, 69-78.
- Karbhari, V.M., Chin, J.W., and Reynaud, D., (2000). "Critical Gaps in Durability Data for FRP Composites in Civil Infrastructure", *Society for the Advancement of Materials and Process Engineering (SAMPE), 45th International SAMPE Symposium and Exhibitio, Long Beach, CA*, 549-563.

- Katsuki, F., and Uomoto, T., (1995). "Predection of Deterioration of FRP Rods due to Alkali Attack", *Non Metallic (FRP)Reinforcement for Concrete Structures, Proceedings of the 2nd International RILEM Symposium (FRPRCS-2)*, 82-89.
- Katz, A., (2000). "Bond to Concrete of FRP Rebars after Cyclic Loading", *Journal of Composites for Construction*, Vol. 4, No. 3, 137-144.
- Kobayashi, K., and Fujisaki, T., (1995), "Compressive Behaviour of FRP Reinforcement in Non-prestressed Concrete Members", *Proceedings of the Second International RILEM Symposium on Non-metallic (FRP) Reinforcement for Concrete Structures (FRPRCS-2), Ghent, Belgium*, 267-274.
- Kovler, K., (1999). "A New Look at the Problem of Drying Creep of Concrete under Tension", *Journal of Materials in Civil Engineering*, ASCE, Vol. 11, No. 1, 84-87.
- Kovler, K., (1995). "Interdependence of Creep and Shrinkage for Concrete under Tension", *Journal of Materials in Civil Engineering*, ASCE, Vol. 7, No. 2, 96-101.
- Kristiawan, S.A., (2002). "Restrained Shrinkage Cracking of Concrete", *Ph.D. Thesis*, University of Leeds, UK.
- Kumar, A., and Gupta, R.K., (1998). "Fundamentals of Polymers", McGraw-Hill, New York.
- Larner, L.J., Speakman, K., and Majumdar, A.J., (1976). " Chemical Interactions Between Glass Fibres and Cement", *Journal of Non-Crystalline Solids*, Vol. 20, 43-74.
- Larralde, J., and Silva-Rodriguez, R., (1993). "Bond and Slip of FRP Reinforcing Bars in Concrete", *Journal of Materials in Civil Engineering, ASCE*, Vol. 5, No. 1, 30-40.
- Lees, J.M., Gruffydd-Jone, B, and Burgoyne, C.J., (1995). "Expansive Cement Couplers: a Means of Pretensioning Fibre Reinforced Plastic Tendons", *Construction and Building Materials*, Vol. 9, No. 6, 413-423.
- Li, H., Burts, E., Sankarapandia, M., Robertson, M.A.F., Lesko, J.J. and Riffle, J.S. (1998). "Network Formation and Properties of Vinylester-Styrene Matrix Resins for Pultruded Composites, in Fibre Composites in Infrastructure", *Proceedings of the 2nd International Conference on Composites in Infrastructure (ICCI 98), Tucson, Arizona, USA*, Edited by Saadatmanesh, H. and Ehsani, M., Vol. 1, 35-44.

- Liszka, W.Z., (1972). "Accelerated Determination of creep of Lightweight Aggregate Concrete by the Use of Elevated Temperature", *Ph.D. Thesis*, University of Leeds, UK.
- Littles, J., Jacobs, L.J., Zureick, A.H. (1998a). "Single-sided Ultrasonic Technique to Characterise Thick FRP Composites", *Journal of Non-destructive Evaluation*, Vol.17, No. 4, 223-230.
- Littles, J., Jacobs, L.J., Zureick, A.H. (1998b). "Ultrasonic Techniques to Characterise Pultruded Composite Members", *Journal of Composites for Construction, ASCE*, Vol. 2, No. 3, 126-131.
- Majumdar, A.J., (1974). "The Role of the Interface in Glass Fibre Reinforced Cement". *Cement Concrete Research*, Vol. 4, No. 2, 247-266.
- Mallick, P.K., (1988). "Fibre Reinforced Composites, Materials, Manufacturing, and Design". Marcell Dekker, Inc., New York.
- Malvar, L.J., (1998). "Durability of Composites in Reinforced Concrete", *Durability of Fibre Reinforced Polymer (FRP) Composites for Construction, Proceedings of the First International Conference (CDCC'98), Sherbrook (Quebec) Canada*, 361-372.
- Malvar, L.J., (1995). "Tensile and Bond Properties of GFRP Reinforcing Bars", *ACI Materials Journal*, Vol. 92, No. 3, 276-285.
- Marshall, J.M., Marshall, G.P. and Pinzelli, R.F., (1982). "The Diffusion of Liquids into Resins and Composites" *Polymer Composites*, Vol. 3, No. 3, 131-137.
- Mehta, P.K. and Monteiro, Paulo J.M. (1993). "Concrete Structure, Properties, and Materials", Prentice Hall, Inc., New Jersey 2nd Edition.
- Micromeritics Combining Autopore 9220 Features for Speed and Accuracy, (1990). *The Micro Report*, Vol. 1, No. 3, 9-10.
- Micelli F.A., Naani, A., and La Tegola, A., (2001). "Effects of Conditioning Environment on GFRP Bars", *22nd SAMPE Europe International Conference: Making the Difference with Innovative Materials and Processes, CNIT, Paris*, 11-23.
- Nagataki, S. and Gomi, H., (1998). "Expansive Admixtures (Mainly Ettringite)", Cement and Concrete Composites, Vol. 20, 163-170.
- Nanni, A., AL-Zahrani, M., AL-Dulaijan, S., Bakis, C.E., and Boothby, T.E., (1995). "Bond of FRP Reinforcement to Concrete: Experimental Results", *Proceedings of the Second International RILEM Symposium on Non-Metallic FRP Reinforcement for Concrete Structures (FRPRCS-2), Ghent, Belgium*, 135-145.

- Nanni, A., Bakis, C.E., Mathew, J.A., (1998). "Acceleration of FRP Bond Degradation", *Durability of Fibre Reinforced Polymer (FRP) Composites for Construction, Proceedings of the First International Conference (CDCC'98), Sherbrook (Quebec) Canada*, 13-24.
- Nanni, A., (1993). "Flexural Behaviour and Design of Reinforced Concrete Using FRP Rods", *Journal of Structural Engineering*, Vol. 119, No. 11, 3344-3359.
- Nanni, A., (2001). "Relevant Field Applications of FRP Composites in Concrete Structures", *Proceedings Composites in Construction, CCC 2001, Porto, Portugal*, edited by Figueiras, J., Juvandes, L. and Furia R., 661-670.
- Neville, A., (1970). "Creep of Concrete: Plain, Reinforced and Prestressed", North-Holland Publishing Company, Amsterdam.
- Neville, A.M., (1998). "Properties of Concrete", Addison Wesley Longman Limited, Essex, 4th Edition.
- Neville, A.M., and Brooks, J.J., (1998). "Concrete Technology", Addison Wesley Longman Limited, Essex, 8th Edition.
- Neville, A.M., Dilger, W.H, and Brooks, J.J., (1983). "Creep of Plain and Structural Concrete", Longman Group Limited, Essex.
- Neville, A.M., (1959). "Tests on the Influence of the Properties of Cement on the Creep of Mortar", *RILEM Bull.*, No. 4, 5-17.
- Neville, A.M. and Liszka, W.Z., (1973). "Accelerated Determination of Creep of Lightweight Aggregate Concrete", *Civil Engineering*, Vol. 68, 515-519.
- Nishizaki, I. and Meiarashi, S., (2002). "Long-Term Deterioration of GFRP in Water and Moist Environment", *Journal of Composites for Construction*, Vol. 6, No. 1, 21-27.
- Nguyen, T., Aouadi, K., Alsheh, D. and Chin, J. (1997). "Effects of Civil Engineering Environments on Interfacial Properties of Polymer/Glass Fibre Composites", *4th International Conference on Composites Engineering (ICCE/4)*, Bi Island of Hawaii, Edited by David Hui. International Community for Composites Engineering and College of Engineering, University of New Orleans, 725-726.
- Nguyen, T., Byrd, E., Alsheh, D., Aouadi, K. and Chin, J. (1998). "Water at Polymer/Substrate Interface and its Role in the Durability of Polymer/Glass Fibre Composites", *Durability of Fibre Reinforced Polymer (FRP) Composites for*

Construction, Proceedings of the First International Conference (CDCC'98), Sherbrook (Quebec) Canada, 451-462.

- Nishimura, T., and Uomoto, T.; (1995). "Creep Fracture of Fibre Reinforced Plastic Rods", *Proceedings of Japan Concrete Institute*, Vol. 17, No. 1, 547-550.
- Oka, Y., Ricker, K.S., and Tomozawa, M., (1979). "Calcium Deposition on Glass Surface as an Inhibitor to Alkaline Attack", *Journal of the American Ceramic Society*, Vol. 62, 631-632.
- Pantuso, A., Spadea, G., Swamy, R.N., (1998). "An Experimental Study on the Durability of GFRP Bars" *Second International Conference on Composites in Infrastructure, Tucson, AZ*, Vol. 2, 476-487.
- Park, R., and Paulay, T., (1975). "Reinforced Concrete Structures", John Wiley & Sons, New York.
- Pepper, T., (2001). "Polyester Resins", *ASM Handbook Volume 21 Composites*, Vol. 21, 90-96.
- Perera, G., Doremus, R.H. and Lanford, W.A., (1991). "Dissolution Rates of Silicate Glasses in Water at pH 7", *Journal of the American Ceramic Society, Vol. 74, No. 6,* 1269-1274.
- Pickett, C., (1942). "The Effect of Change in Moisture-content on the Creep of Concrete Under a Sustained Load", *ACI Material Journal*, Vol. 38, 333-356.
- Pleimann, L.G., (1991). "Strength, Modulus of Elasticity, and Bond of Deformed FRP Rods", *Advanced Composites Materials in Civil Engineering Structures, Proceeding of the Specialty Conference, Materials Engineering Division, ASCE*, 99-110.
- Poh, K.W., (May 1998). "General Creep-Time Equation", *Journal of Materials in Civil Engineering*, Vol. 10, No. 2, 118-120.
- Porter, M.L. and Barnes, B.A., (1998). "Accelerated durability of FRP Reinforcement for Concrete Structures", *Durability of Fibre Reinforced Polymer (FRP) Composites for Construction, Proceedings of the First International Conference (CDCC'98), Sherbrook (Quebec) Canada*, 191-198.
- Porter, M.L., Mehus J., Young, K.A., O'Neil, E.F., and Barnes, B.A., (1997). "Aging for Fibre Reinforcement in Concrete", *Non-Metallic (FRP) Reinforcement for Concrete Structures, Proceedings of the 3rd International Symposium*, Vol. 2, 59-66.

- Prian, L. and Barkatt, A. (1999). "Degradation Mechanism of Fibre Reinforced Plastics and Its Implications to Prediction of Long-term Behaviour", *Journal of Materials Science*, Vol. 34, 3977-3989.
- Rahman, A.H., Kingsley, C.Y., Crimi, J., (1996). "Durability of a FRP Grid Reinforcement" *Advanced Composite Materials in Bridges and Structures, Second International Conference, Montreal, Quebec, Canada*, edited by Al-Badry, M.M., 681-690.
- Rahman, A.H., Taylor, D.A., and Kingsley, C.Y., (1993). "Evaluation of FRP as Reinforcement for Concrete Bridges", *Fibre-Reinforced-Plastic Reinforcement for Concrete Structures- International Symposium ACI SP-138*, edited by Nanni, A. and Dolan, C.W., American Concrete Institute, Farmington Hills, Michigan, 71-82.
- Rasheeduzzafar, Dakhil, F.H., Bader, M.A. and Khan, M.N., (1992). "Performance of Corrosion Resisting Steel in Chloride-bearing Concrete", *ACI Materials Journal*, Vol. 89, No. 5, 439-448.
- Richardson, (2001). "Electron Microscopy of Cement, in Structure and Performance of Cement", *Edited by Barnes, P and Bensted*, J, F and F. N. Spon.
- Riffle, J.S., Lesko, J.J. and Puckett, P.M. (1998). "Chemistry of Polymer Matrix Resins for Infrastructure, in Fibre Composites in Infrastructure", *Proceedings of the 2nd International Conference on Composites in Infrastructure (ICCI 98) Tucson, Arizona, USA*, Edited by Saadatmanesh, H. and Ehsani, M., Vol. 1, 23-35.
- RILEM CP 113, (1984). "Absorption of Water by Immersion Under Vacuum", *Materials and Structures, Research and Testing*, No. 101, 393-394.
- RILEM TC 107-GCS, (1996). "Short Form of Creep and Shrinkage Prediction Model B3 for Structures of Medium Sensitivity", Guidelines for the Formulation of Creep and Shrinkage Prediction Models, 587-593.
- RILEM/CEB/FIB, (1978). "Test of the Bond Strength of Reinforcement of Concrete: Test by Bending", *Recommendation RC.5*.
- Rixom, R., and Mailvaganam, N., (1999). "Chemical Admixtures for Concrete", E & FN Spon, an imprint of Routledge, London, 3rd edition.
- Ross, A.D., (1944). "Shape Size and Shrinkage", *Concrete and Constructional Engineering*, 193-199.

- Rubinsky, I.A., Rubinsky, A., (1954). "A Preliminary Investigation of the Use of Fibreglass for Prestressed Concrete", *Magazine of Concrete Research*, Vol. 6, No. 17, 71-78.
- Sanhdars, M.A.D., Oehlers, D.J., (2000). "Ductility Design of RC Beams with FR Bars", *Proceeding of the ACUN-2 International Composites Conference – Composites in the Transportation Industry*, Vol. 1, 210-215.
- Schultheisz, C.R., (1996). "Effect of Temperature and Fibre Coating on the Strength of E-glass Fibres and E-glass/Epoxy Interface for single Fibre Fragmentation Samples Immersed in Water", *Fibre, Matrix and Interface Properties, ASTM STP 1290, American Society for Testing of Material, Philadelphia,* 103-131.
- Schutte, C.L., (1994). "Environmental Durability of Glass-fibre Composites", *Material of Science Engineering*, Vol. 13, No. 7, 265-324.
- Seki, H., Sekijima, K., Konno, T.; (1997) "Test Method on Creep of Continuous Fibre Reinforcing Materials", *Non-metallic (FRP) Reinforcement for Concrete Structures; Proceedings of the 3rd International Symposium*, Vol. 2, 195-202.
- Sheard, P., Cleark, J., Dill, M., Hammersley, G., and Richardson, D., (1997). "Eurocrete-Taking Account of Durability for Design of FRP Reinforced Concrete Structure", *Non-Metallic (FRP) Reinforcement for Concrete Structures; Proceedings of the 3rd International Symposium*, Vol. 2, 75-82.
- Shen, C.H., and Springer, G.S., (1976). "Moisture Absorption and Desorption of Composite Materials", *Journal of Composite Materials*, Vol. 10, 2-20.
- Simhan, R.G., (1983). "Chemical Durability of ZrO_2 Containing Glasses", *Journal of Non-Crystalline Solids*, Vol. 54, 335-343.
- Sonawala, S.P., and Spontak, R.J., (1996). "Degradation Kinetics of Glass Reinforced Polyesters in Chemical Environments, Part 1: Aqueous Solutions", *Journal of Materials Science*, Vol. 31, 4745-4756.
- Soroka, I., (1993). "Concrete in Hot Environments" E & FN Spon, an imprint of Chapman & Hall, London.
- Springer,G.S., Sanders, B.A., Tung, R.W., (1981). "Environmental Effects on Glass Fibre Reinforced Polyester and Vinyl ester Composites", *Environmental Effects on Composite Materials, Technomic Publishing Co. Inc.*, Vol. 1,126-144.
- Sridharan, S. (1997). "Environmental Durability of E-glass/Vinyl ester Composites in Hot-moist Conditions", *Ph.D. Thesis*, Georgia Institute of Technology, Atlanta.

- Sumerak, J.E. and Martin, J.D., (2001). "Pultrusion", *ASM Handbook Volume 21 Composites*, Vol. 21, 550-564.
- Takewaka, K. and Khin, M. (1996). "Deterioration and Stress Rupture of FRP Rods in Alkaline Solution Simulating as Concrete Environment", *Proceedings of the Advanced Composite Materials in Bridges and Structures, CSCE*, 649-656.
- Tannous, F.E., and Saadatmanesh, H., (1998). "Environmental Effects on the Mechanical Properties of E-Glass FRP Rebars", *ACI Materials Journa*l, V. 95, No. 2, 87-100.
- Tannous, E., and Saadatmanesh,H., (1999). "Durability of AR Glass fibre Reinforced Plastic Bars", *Journal of Composites for Construction*, V. 3, No. 1, 12-19.
- Taylor, H.F.W., (1997). "Cement Chemistry", Thomas Telford, London, 2nd Edition.
- Theriault, M., and Benmokrane, B., (1998). "Effects of FRP Reinforcement Ratio and Concrete Strength on Flexural Behaviour of Concrete Beams", *Journal of Composites for Construction*, Vol. 2, No., 1, 7-16.
- Tighiouart, B, Benmokrane, B., and Gao, D., (1998). "Investigation of Bond in Concrete Member with Fibre Reinforced Polymer (FRP) bars", *Construction and Building Materials*, Vol. 12, 453-462.
- Uomoto, T., Nishimura, T., Ohga, H., (1995). "Static and Fatigue Strength of FRP Rods for Concrete Reinforcement", *Non Metallic (FRP) Reinforcement for Concrete Structures, Proceedings of the 2nd International RILEM Symposium (FRPRCS-2)*, 100-107.
- Uomoto, T., (2001). "Durability of FRP Reinforcement as Concrete Reinforcement", *FRP Composites in Civil Engineering, Proceedings of the International Conference on FRP Composites in Civil Engineering, 12-15 December, Hong Kong, China*, Edited by Teng, J.G., Vol. 1, 85-96.
- Uomoto, T., (2003). "Durability Design of GFRP Rods for Concrete Reinforcement" *Poceedings of the 6th International Symposium on Fibre Reinforced Plastics Reinforcing Concrete Structures FRPRCS-6, 8-10 July, Singapore*, Edited by Tan, K.H., Vol. 1, 37-50.
- Uomoto, T., Mutsuyoshi, H. and Sumida, A., (2001). "Alkali Resistance of Fibres, FRP Rods and Epoxy Resins", *Poceedings of the 5th International Conference on*

Fibre Reinforced Plastics for Reinforced Concrete Structures FRPRCS-5, 16-18 July, Cambridge, UK, Edited by Burgoyne, C.J., Vol. 1, 479-488.

- Vieth, W.R., (1991). "Diffusion in and Through Polymers", Hanser, New York.
- Vinson, J.R. and Sierakowski, R.L. (1986). "The Behaviour of Structures Composed of Composite Materials", Martinus Nijhoff Publishers, Dordrecht.
- Vijay, P.V. and GangaRao, H.V.S., (1999). "Accelerated and Natural Weathering of Glass Fibre Reinforced Plastic Bars", *Poceedings of the 4th International Fibre Reinforced Plastics Reinforcing Concrete Structures FRPRCS-4*, Baltimore, USA, 605-614.
- Wakabayashi, H. and Tomozawa, M., (1989). "Diffusion of Water into Silica Glass at Low Temperature", *Journal of the American Ceramic Society*, Vol. 72, No. 10, 1850-1855.
- Wallbank, E.J. (1989). "The Performance of Concrete in Bridges", HMSO, London, 96 PP.
- Washburn, E.W., (1921). "A Method of Determining the Distribution of Pore Sizes in a Porous Material", *Proceeding of the National Academy of Sciences*, Vol. 7, No. 115, 56-63.
- Weber, A.R., Luz, E.A. and Wagner, O., (1998). "Short and Long-term Performance of ComBAR® GRP Bars as a Structural Element for the Insulation of Thermal Bridges", *Durability of Fibre Reinforced Polymer (FRP) Composites for Construction, Proceedings of the First International Conference (CDCC'98), Sherbrook (Quebec) Canada*, 277-283.
- Winslow, D., and Diamond, S., (1970). "A Mercury Porosimetry Study of Evaluation of Porosity in Portland Cement", *Journal of Materials*, Vol. 5, 564-585.
- Winter, G., and Nilson, A.H., (1979)."Design of Concrete Structure", McGraw-Hill Book Company, London, 9th edition.
- Wittmann, F.H. and Roelfstra, P.E., (1980). "Total Deformation of Loaded Drying Concrete", *Cement and Concrete Research*, Vol. 10, 601-610.
- Wu, W.P., (1990). "Thermo-mechanical Properties of Fibre Reinforced Plastic bars", *Ph.D. Thesis*, West Virginia University, Morgantown.
- Yamaguchi, T., Kato, Y., Nishimura, T., and Uomoto, T.; (1997). "Creep Rupture of FRP Rods Made of Aramid, Carbon and Glass Fibre", *Non-metallic (FRP)*

Reinforcement for Concrete Structures; Proceedings of the 3rd International Symposium, Vol. 2, 179-186.

- Yilmaz, V.T. and Glasser, F.P., (1991). "Reaction of Alkali-Resistant Glass Fibres with Cement", *Glass Technology*, Vol. 32, No. 3, 91-98.
- Yilmaz, V.T., (1992). "Chemical Attack on Alkali-resistant Glass Fibres in a Hydrating Cement Matrix: Characterisation of Corrosion Products", *Journal of Non-crystalline Solids*, Vol. 151, 236-244.
- Yilmaz, V.T., Lachowski, E.E. and Glasser, F.P., (1991). "Chemical and Microstructural Changes at Alkali-Resistant Glass Fibre Cement Interfaces", *Journal of the American Ceramic Society*, Vol. 74, No. 12, 3054-3060.
- Zhang, S.Y., (1999). "Micro- and Macroscopic Characterizations of the Viscoelastic Fracture of Resin-based Fibre Composites", *Composites Science and Technology*, Vol. 59, 317-323.

Appendix

Table 1: Records of loads (by Instron) and their corresponding deflections (by LVDTs) for the joint-beam with average compressive strength of 45MPa and reinforced with steel rebar

Load (kN)	Deflection RHS(mm)	Deflection LHS(mm)
0.11	0	0
1.99	0.4876	0.4001
3.87	1.3651	0.6349
6.2	1.9462	1.4538
8.35	2.3850	2.0150
9.57	2.6106	2.3227
11.36	2.9260	2.5407
13.26	3.2426	2.7574
15.04	3.4291	3.1909
17.02	3.7252	3.5148

Table 2: Records of loads (by Instron) and their corresponding deflections (by LVDTs) for the joint-beam with average compressive strength of 80MPa and reinforced with steel rebar

Load (kN)	Deflection RHS(mm)	Deflection LHS(mm)
0	0	0
0.98	0.4854	0.4023
3.20	1.2552	1.1147
5.71	1.8437	1.6742
7.40	2.1854	1.8958
9.30	2.5088	2.1871
11.9	2.8102	2.6058
13.04	3.059	2.7144
15.04	3.2594	3.022
18.09	3.9011	3.5796
19.89	4.683	4.4484
20.01	6.9269	6.9363

Table 3: Records of loads (by Instron) and their corresponding deflections (by LVDTs) for the joint-beam with average compressive strength of 45MPa and reinforced with GFRP rebar

Load (kN)	Deflection RHS(mm)	Deflection LHS(mm)
0	0	0
3.96	0.8915	0.8901
7.94	1.8217	1.8477
11.89	2.8102	2.8283
15.88	4.3618	4.167
18.95	11.7859	11.6182
19.89	16.8031	16.28

Table 4: Records of loads (by Instron) and their corresponding deflections (by LVDTs) for the joint-beam with average compressive strength of 80MPa and reinforced with GFRP rebar

Load (kN)	Deflection RHS(mm)	Deflection LHS(mm)
0	0	0
4	0.8692	0.8549
7.98	1.6748	1.6108
11.96	2.6192	2.4559
15.95	3.5008	3.273
19.93	4.4416	4.1625
23.85	6.0368	5.7299
27.34	11.2275	11.1603
27.89	12.6074	12.7817

Table 5: Variation of flexural strength (σ_f) with immersion time for GFRP rebars at different temperatures

Condition	Sample 1		Sample 2		Sample 3		Sample 4		Sample 5	
	Strength (Mpa)	Max. strain	Strength (Mpa)	Max. strain	Strength (Mpa)	Max. strain	Strength (Mpa)	Max. strain	Strength (Mpa)	Max. strain
Control	1287	0.032	1293	0.035	1372	0.036	1317	0.034	1308	0.034
Alkali immersion for 30 days at 60°C	1074	0.030	1074	0.029	1074	0.028	1074	0.028	1074	0.027
Alkali immersion for 90 days at 60°C	827	0.021	875	0.021	839	0.021	863	0.021	849	0.021
Alkali immersion for 180 days at 60°C	684	0.017	767	0.019	704	0.018	751	0.019	720	0.018
Alkali immersion for 270 days at 60°C	678	0.022	553	0.016	584	0.017	647	0.020	636	0.018
Alkali immersion for 30 days at 20°C	1105	0.032	1230	0.035	1188	0.032	1193	0.034	1123	0.031
Alkali immersion for 90 days at 20°C	1094	0.028	1161	0.029	1111	0.028	1132	0.029	1140	0.029
Alkali immersion for 180 days at 20°C	1027	0.027	1155	0.031	1059	0.028	1123	0.030	1082	0.027
Alkali immersion for 270 days at 20°C	966	0.024	960	0.024	958	0.025	939	0.023	979	0.025
Saline immersion for 30 days at 60°C	1126	0.030	1089	0.030	1129	0.030	1098	0.030	1102	0.029
Saline immersion for 90 days at 60°C	995	0.024	1052	0.025	1009	0.024	1038	0.025	1030	0.024
Saline immersion for 180 days at 60°C	864	0.022	971	0.024	891	0.022	945	0.024	916	0.022
Saline immersion for 270 days at 60°C	896	0.021	795	0.021	870	0.021	837	0.021	828	0.020
Saline immersion for 30 days at 20°C	1303	0.037	1449	0.038	1335	0.037	1396	0.038	1394	0.037
Saline immersion for 90 days at 20°C	1218	0.032	1317	0.036	1243	0.033	1292	0.035	1272	0.035
Saline immersion for 180 days at 20°C	1283	0.033	1131	0.030	1184	0.030	1201	0.032	1233	0.031
Saline immersion for 270 days at 20°C	1040	0.026	1195	0.030	1079	0.027	1168	0.028	1110	0.028

Prediction of shrinkage and creep of concrete specimens

1.1 Creep:

1.1.1 ACI 209:

γ_{la} = 0.84
γ_{λ} = 0.82
γ_{vs} = 1.17
γ_{s} = 1.01
γ_{ψ} = 0.88

1.1.2 CEB-FIP

		SRA mix
ϕ_0 =	2.03	2.29
$\beta_c(t-t_0)$ =	0.65	
β_H =	307.3	
ϕ_{RH} =	1.99	
$\beta(f_{cm})$ =	2.13	2.4
$\beta(f_{t0})$ =	0.48	

1.1.3 BS:

	BS 5400	BS 8110
K_L	2.38	2.38
K_c	1.09	1.20
K_e	1.24	1.65
$K_{m(94)}$	0.69	0.68
$K_{j(94)}$	0.80	0.64

1.2 Shrinkage:

1.2.1 ACI 209:

γ_{la} = 0.86
γ_{λ} = 1.39
γ_{vs} = 1.10
γ_{s} = 1.01
γ_{ψ} = 0.31
γ_{c} = 0.98

1.2.2 CEB-FIP

		SRA mix
ε_{cso} =	325	395
$\varepsilon_s(f_{cm})$ =	300	365
β_{sc} =	5	

β_{RH} =	1.08
β_{sRH} =	0.699
$\beta_s(t-t_s)$ =	0.81

1.2.3 BS:

	BS 5400	BS 8110
K_L	291.259	336.7841
K_c	1.094258	1.201811
K_e	1.187969	0.905219
$K_{j(94)}$	0.801642	0.647515

1.2.4 Gardner and Zhao (1993)

	SRA mix	
V/S =	18.75	
K =	1	
$\beta(h)$ =	0.79	
$\beta(t)$ =	0.66	
ε_{shu} =	572	645